IMPACTS OF CLIMATE CHANGE ON HYDROLOGICAL REGIMES IN SOUTHERN SLOPES OF CENTRAL HIMALAYAS

A THESIS SUBMITTED TO THE

CENTRAL DEPARTMENT OF HYDROLOGY AND METEOROLOGY

INSTITUTE OF SCIENCE AND TECHNOLOGY

TRIBHUVAN UNIVERSITY, NEPAL

FOR THE AWARD OF

DOCTOR OF PHILOSOPHY

IN HYDROLOGY AND METEOROLOGY

BY

BHUMI RAJ BUDHATHOKI

SEPTEMBER 2023

IMPACTS OF CLIMATE CHANGE ON HYDROLOGICAL REGIMES IN SOUTHERN SLOPES OF CENTRAL HIMALAYAS

A THESIS SUBMITTED TO THE

CENTRAL DEPARTMENT OF HYDROLOGY AND METEOROLOGY

INSTITUTE OF SCIENCE AND TECHNOLOGY

TRIBHUVAN UNIVERSITY, NEPAL

FOR THE AWARD OF

DOCTOR OF PHILOSOPHY

IN HYDROLOGY AND METEOROLOGY

BY

BHUMI RAJ BUDHATHOKI

SEPTEMBER 2023

TRIBHUVAN UNIVERSITY

Institute of Science and Technology

DEAN'S OFFICE

Kirtipur, Kathmandu, Nepal

Reference No.:

Institute of Science & Technology
Dean's Office

EXAMINERS

The Title of Ph.D. Thesis: "Impacts of Climate Change on Hydrological Regimes in Southern Slopes of Central Himalayas "

Name of Candidate: Bhumi Raj Budhathoki

Internal Examiner:

Prof. Dr. Vishnu Prasad Pandey
Institute of Engineering
Tribhuvan University, NEPAL

External Examiners:

(1) Dr. Sudeep Thakuri
Mid-West University
Surkhet, NEPAL

(2) Dr. Suraj Mal
Jawaharlal Nehru University
Delhi, INDIA

(3) Prof. Dr. Jeffrey S. Owen
Hankuk University of Foreign Studies
Yongin, SOUTH KOREA

02 August, 2024

(Dr. Surendra Kumar Gautam)
Asst. Dean

DECLARATION

The thesis entitled **"Impacts of Climate Change on Hydrological Regimes in Southern Slopes of Central Himalayas"** is being submitted to the Central Department of Hydrology and Meteorology, Institute of Science and Technology (IOST), Tribhuvan University, Nepal for the award of the degree of Doctor of Philosophy (Ph.D.), is a research work carried out by the under the supervision of Emeritus Prof. Dr. Tirtha Adhikari of Central Department of Hydrology and Meteorology, Tribhuvan University and co-supervised by Dr. Suraj Shrestha of Central Department of Hydrology and Meteorology, Tribhuvan University.

This research is original and has not been submitted earlier in part or full in this or any other form to any university or institute, here or elsewhere, for the award of any degree.

.....

Bhumi Raj Budhathoki

RECOMMENDATION

This is to recommend that **Bhumi Raj Budhathoki** has carried out this research entitled **"Impacts of Climate Change on Hydrological Regimes in Southern Slopes of Central Himalayas"** for the award of Doctor of Philosophy (Ph.D.) in **Hydrology and Meteorology** under our supervision. To our knowledge, this work has not been submitted for any other degree.

He has fulfilled all requirements laid down by the Institute of Science and Technology (IOST), Tribhuvan University, Kirtipur for the submission of the thesis for the award of a Ph.D. degree.

.....

Tirtha Raj Adhikari, PhD

Supervisor

Emeritus Professor

Central Department of Hydrology and Meteorology

Tribhuvan University

Kirtipur, Kathmandu, Nepal

.....

Suraj Shrestha, PhD

Co-Supervisor

Visiting Faculty

Central Department of Hydrology and Meteorology

Tribhuvan University

Kirtipur, Kathmandu, Nepal

OCTOBER, 2023

Accredited by University Grants Commission (UGC), Nepal, (2021)
TRIBHUVAN UNIVERSITY
CENTRAL DEPARTMENT OF HYDROLOGY & METEOROLOGY
Kirtipur, Kathmandu, Nepal

Date:2080/10/07

LETTER OF APPROVAL

On the recommendation of Associate Prof. Dr. **Tirtha Raj Adhikari** and Dr. **Suraj Shrestha**, this PhD thesis Submitted by Bhumi Raj Budhathoki entitled **"Impacts of Climate Change on Hydrological Regimes in Southern Slopes of Central Himalayas"** is forward by the Central Department Research Committee (CDRC) to the Dean, IOST, T.U.

.....

Prof. Dr. Deepak Aryal
Professor
Head
Central Department of Hydrology and Meteorology,
Tribhuvan University
Kirtipur, Kathmandu
Nepal

Phone No.: 4-331418, 4-333887, Fax No.: 977-1-4331964

ACKNOWLEDGEMENTS

This dissertation entitled "**Impacts of Climate Change on Hydrological Regimes in Southern Slopes of Central Himalayas**" could not have been completed without the overwhelming cooperation and assistance of the following institutions and persons.

I am indebted to my respected supervisor, Dr. Tirtha Raj Adhikari, Emeritus Professor and Co-supervisor Dr. Suraj Shrestha, Central Department of Hydrology and Meteorology, Tribhuvan University, for providing numerous instructions and ideas throughout the period of my dissertation and research work. I would equally like to thank Prof. Dr. Deepak Aryal, Head of the Central Department of Hydrology and Meteorology for his meticulous motivation towards quality work. I would also like to special thanks to the Central Department of Hydrology and Meteorology and Institute of Science and Technology, Tribhuvan University for continuous cooperation and also remember the faculties, staffs and students of CDHM for their help. Also, i would like to thank Dr. Yam Prasad Dhital, Dr. Binod Dawadi, Ram Prasad Awasthi, and Somesh Thapa.

I heartily feel my duty to thank the University Grants Commission (UGC) for providing a PhD Fellowship and research grant for this research. I am also grateful to the Department of Hydrology and Meteorology (DHM) for the hydrological and meteorological data.

Finally, I would like to thank my mother Uma Budhathoki, father Prashuram Budhathoki, wife Apsara KC, baby Yisara Budhathoki, sister Hira Budhathoki, brother Late Bhojraj Budhathoki, Kuber Pandey, friends and relatives for continuous their love and support.

Bhumi Raj Budhathoki

September 2023

शोधसार

जलविज्ञान सम्वन्धी तथ्याङ्कहरुको नियमित पहुँचको सुनिश्चततालै जलस्रोत सम्वन्धी योजना, विकास र व्यवस्थापनलाई दिगो बनाउन महत्वपूर्ण भुमिका पुर्याउछ। यस अवधारणाभित्र रहेर विभिन्न किसिमका जलविज्ञान प्रारुपहरु जस्तै Spatial Process in HYdrology (SPHY), Hydrologiske Byrån avdeling for Vattenbalans (HBV), and Hydrologic Engineering Centre Hydrologic Modelling System (HEC HMS) को मूल्याङ्कनका दायराहरुको मेट्रिक्स प्रयोग गरी प्रभावकारिताको अध्ययन गरियो । उक्त मूल्याङ्कनका मेट्रिक्सहरुले मूख्यतयः Nash Sutcliffe Efficiency (NSE), Coefficient Correlation (r), Coefficient of Determination (R^2), Root Mean Square Error (RMSE), RMSE-observations Standard Deviation Ratio (RSR) and Volume Difference (P-Bias) लाइ समेटेको हुन्छ। तामाकोशी जलाधार अन्तर्गत बुस्ती र रस्नालु केन्द्रहरुबाट प्राप्त तथ्याङ्कको आधारमा तीन वटै जलविज्ञान प्रारुपहरुको दैनिक र मासिकरूपमा जलप्रवाह तथ्याङ्कको NSE मान ०.६२ भन्दा बढि भएको जाँच र प्रमाणीकरण सफलतापूर्वक सम्पन्न गरियो। अध्ययन गरिएका विभिन्न तथ्याङ्कीय सूचकाङ्कहरू मध्ये Coefficient of Determination सापेक्षिक रुपमा नजिक रहेको पाइयो ।

त्यसैगरी बेनीघाट जस्ता जलमापन केन्द्र नभएका स्थानहरुको जलप्रवाह पूर्वानुमान गर्न SPHY, HBV light and HEC HMS को प्रयोग गरी सम-जलधारको तथ्याङ्कन मिलान गरी जलप्रवाह अनुमान गरियो। ती पूर्वानुमानहरु दैनिक, मासिक, वार्षिक समय सीमाको लागि माथिल्लो जलाधारमा उपलव्ध जलमापन केन्द्रको तथ्याङ्मा आधारित रहेर गरियो । सुख्खायामको जलप्रवाह पूर्वानुमान उच्च जलप्रवाहको पूर्वानुमान भन्दा बढी प्रभावकारी देखियो भने जलप्रवाह पूर्वानुमानहरुको विसंगति बर्षाय़ाममा अधिक हुने देखियो । तथापि अनुकरणको क्रममा तीनवटै प्रारुपहरुले गैर जलमापन स्थानहरुमा उस्तै प्रकृतिको जलप्रवाह पूर्वानुमान देखियो । पूर्वानुमान अवधिमा गैर जलमापन स्थानहरुको जलप्रवाहको पूर्वानुमान नजिकका स्थानहरुको पूर्वानुमानको भन्दा बढी देखियो। गैर जलमापन प्रवाहको पूर्वानुमानका लागि एकल विधि भन्दा तलुनात्मक विधि बढी प्रभावकारी विकल्प देखिन्छ ।

तीनैवटा जलविज्ञान प्रारुपहरु मध्ये HBV light model द्वारा दैनिक निवेश परिसूचकहरु प्रयोग गरी तामाकोशी नदी जलाधारमा प्रभावकारी रुपमा जलप्रवाह अनुकरण गरियो । जलप्रवाहको विविधता यसका सम्भागहरुको सामयिक परिवर्तनमा भरपर्दछ। यस परिप्रेक्षमा तामाकोशी नदी जलाधारको बुस्ती जलमापन केन्दकोको हकमा आधार-अवधिमा वर्षा-बहावले मूख्यतः जलप्रवाहमा ६३% को योगदान पुर्याउदै हावी भएको देखियो, जसमा भूमिगत जलप्रवाह बहावको २०%, हिमनदी गलनबहाव १३%, र हिउँगलन बहावको ५% योगदान रहेको पाइयो। यस जलधार क्षेत्रमा उक्त आधार-अवधिमा जल सन्तुलनको भण्डारण क्षमतामा धनात्मक रहेको महत्वपूर्ण तथ्य पाइयो।

तामाकोशी नदी जलाधारको जलवायु परिवर्तन प्रभाव विश्लेषण गर्ने क्रममा यस अध्ययनले तापक्रम र वर्षाका आंकलनका लागि दुई वटा परिदृश्य सहितको Coupled Model Intercomparison Projects(CMIP 6) विश्लेषण प्रतिवेदनबाट चारवटा General Circulation Models (GCMs) लाई उपयोग गरिएको छ । दुवै परिदृश्यहरुको लागि तापक्रम र वर्षा साथसाथै बढ्दै जाने स्थिर प्रवृतिको चरित्र सवै GCMs ले प्रदर्शन गरेका छन्। विशेषतः SSP245 अन्तर्गतको NorESM2 MM

परिदृश्यले अपवादको रुपमा वर्षामा घटोत्तरी हुने देखाएको छ। अध्ययन क्षेत्रको लागि उक्त विश्लेषणले जलवायु परिवर्तन र जलचक्रको जल सन्तुलनका पक्षवीचको अनन्य विशिष्ट सम्वन्धलाई बुझ्न दिशा निर्देश गरेको छ। यसका अतिरक्त जल सन्तुलनका पक्षहरुलाई CMIP 6 को २ वटा GCMs लाई समाजिक-आर्थिक साझा पथपर्दशक (SSPs) परिदृश्यहरु (SSP245 र SSP585) मार्फत मूल्याङ्कन गरियो । उक्त विश्लेषणले वार्षिक, मासिक, ऋतुगत आधारमा आधार समयरेखा केन्द्रित, निकट-भविष्य, मध्य-भविष्य र सुदुर-भविष्य सहितको जलप्रवाह आंकलन समेटेको छ। २१औं शताब्दीको अन्तसम्ममा आधर समय भन्दा दुवै परिदृश्य अन्तर्गतका जलप्रवाहका घटकहरुः वर्षा, बहाव, वास्तविक बाष्पीवाष्पोत्सर्जन, वर्षा बहाव, हिमनदी गलनको प्रवृति बढ्ने तर भूमिगत बहाव र हिउँगलन घट्ने विश्लेषणको नतिजा रहेको छ, जसमा SSP585 प्रधान रुपमा महत्तम प्रभाव पार्ने देखिन्छ। मुख्यतया हिमनदी गलन बहाव जलवायु परिवर्तनको प्रभागकोरुपमा रहेको छ। यस वाहेक वर्षयामको वर्षा गर्मीयाममा तामाकोशी जल वहावको प्राथमिक कारकको रुपमा देखा पर्ने पाइएको छ।

यस अध्ययनले भविश्यको जलवायुको अवस्था आंकलन र जलबिज्ञान विधाका लागि महत्वपूर्ण घटकको रुपमा नदी बहावको भुमिकालाई स्पष्ट गर्न योगदान पुर्याउदछ। यसका साथै गैर-जलमापन क्षेत्र र तथ्याङ्क नभएका स्थानहरुका लागि आवश्यक तथ्याङ्क परिपुर्ति गर्न सन्दर्भ-सामग्रीको रुपमा दिशा निर्देश गर्नेछ। जलस्रोतको प्रभावकारी योजना, विकास र व्यवस्थापन र तामाकोशी नदी जलाधारको बहिर्गमन विन्दु वेनिघाटसम्म आवश्यक जलपामपन पूर्वानुमान गर्न पनि यो अध्ययनले सहायता पुर्याउने छ। साथै, जलवायु परिवर्तनको परिप्रेक्षमा जलस्रोत सम्वन्धी परियोजनाको लागि उपयुक्त प्रारुपहरुको विश्लेषण पहिचान गर्न तथा जल-उत्पन्न प्रकोप व्यवस्थापनमा यस अध्ययनले विशेष सहयोग पुर्याउनेछ।

मुख्य शब्दहरु: HBV light, SPHY, HEC HMS, Streamflow components, Water balance contribution, Climate change, Ungauged trans-boundary river, Tamakoshi river basin.

ABSTRACT

Ensuring the consistent accessibility of hydrological data highlights the sgnificance of careful planning, development and management of water resource projects. Within this framework, the effectiveness of diverse hydrological models, such as the Spatial Process in Hydrology (SPHY), Hydrologiske Byrån avdeling for Vattenbalans (HBV), and Hydrologic Engineering Centre Hydrologic Modelling System (HEC HMS) models, are assessed using a range of evaluation metrics. These metrics include the Nash Sutcliffe Efficiency (NSE), Coefficient Correlation (r), Coefficient of Determination (R^2), Root Mean Square Error (RMSE), RMSE-observations Standard Deviation Ratio (RSR) and Volume Difference (P-Bias). All three hydrological models were successfully calibrated and validated, demonstrating NSE values exceeding 0.62 for daily and monthly discharge data, based on observations from Busti and Rasnalu stations within the Tamakoshi river basin. Among the various statistical parameters assessed, the coefficient of determination showed a relatively close fit.

Similarly, continuous hydrological records for ungauged discharge predictions at locations like Benighat, are estimated using SPHY, HEC HMS, and HBV light models by leveraging data from donor catchments. These predictions span daily, monthly, and annual time frames, sourced from upstream gauged stations. It is significant to note that the accuracy of lowflow predictions surpasses that of high flow predictions, and discrepancies in flow predictions tend to emerge primarily during peak flow periods. Nevertheless, all three hydrological models exhibit similar flow patterns in simulating ungauged streamflow, with discharge at the ungauged receiver site exceeding that of the donor site during simulations. This comparative method proves to be a preferable alternative to individual methods for estimating ungauged discharge.

Among these three hydrological models, HBV light model effectively simulates streamflow components using daily input parameters in the Tamakoshi river basin. The variations in streamflow are dependent on the temporal changes in its components. In this context, it is observed that rain runoff predominantly dominates streamflow, constituting 62% of the contribution, with baseflow runoff accounting for 20%, glacier melt runoff for 13%, and snow melt runoff for 5% at the Busti gauge station during the baseline period. It is important to note that there was a positive change in storage within the water balance during the baseline period.

In order to evaluate climate change impacts, this study employs four General Circulation Models (GCMs) from the Coupled Model Intercomparison Projects (CMIP 6) Assessment Report 6, along with two scenarios for projecting temperature and precipitation in the Tamakoshi river basin. The findings of this study reveal a consistent trend among all GCMs, indicating a simultaneous increase in temperature and precipitation for both scenarios. Especially, the NorESM2 MM scenario under SSP245 stands as an exception, demonstrating a noteworthy decrease in precipitation. These assessments provide valuable insights into the complex interplay between climate change and the water balance components of the hydrological cycle in the specified region. Furthermore, water balance components are evaluated using an ensemble of two GCMs from CMIP 6, coupled with two Shared Socio-economic Pathways (SSPs) scenarios (SSP245 and SSP585). The assessment covers streamflow components on an annual, monthly, and seasonal basis, focusing on baseline, Near Future (NF), Middle Future (MF), and Far Future (FF) projections. It is worth noting that streamflow predominantly leads the Far Future (FF) projections. Among the streamflow components, precipitation, discharge, actual evapotranspiration, rain runoff, and glacier melt, results showed increase, while baseflow and snow melt runoff decreases by the end of the 21st century in comparison of baseline period under both scenarios, with SSP585 having a more pronounced effect. Particularly noteworthy is the substantial increase in glacier melt runoff attributable to climate change. Moreover, precipitation, governed by monsoons, emerges as the primary determinant of river discharge during the summer season in the Tamakoshi river basin.

This study contributes to projecting future climate conditions and the evolving role of streamflow components in hydrological regimes. Additionally, it provides valuable insights for future reference in generating streamflow data at ungauged sites and adderessing deficiencies in data records. This, in turn, facilitates effective planning, management, and development of water resource projects, extending from gauged stations to the outlet at Benighat within the Tamakoshi river basin. The findings also aid in the assessment of suitable models for water resource projects and water-induced disaster management, especially in the context of climate change.

Key Words: HBV light, SPHY, HEC HMS, Streamflow components, Water balance contribution, Climate change, Ungauged trans-boundary river, Tamakoshi river basin.

LIST OF ACRONYMS AND ABBREVIATIONS

ACCESS CM2	:Australian Community Climate and Earth System Simulator coupled model version 2
AET	:Actual Evapotranspiration
AG	:Calibration parameter (mm-1)
Alpha	:Non-linearity coefficient (-)
alphaGW	:Baseflow recession coefficient
AM	:Analogue Downscaling Method
amsl	:Average Mean Sea Level
AR3	:Third Assessment Report
AR5	:Fifth Assessment Report
AR6	:Sixth Assessment Report
BETA	:Parameter that determines the relative contribution to runoff from rain or snow melt (-)
CanESM5	:Canadian Earth System Model version 5
CCCM	:Canadian Climate Centre Model
CFGlacier	:Correction factor glacier
CFMAX	:Degree-Δt factor (mm oC-1 Δt-1)
CFR	:Refreezing coefficient (-)
CFSlope	:Correction factor slope (-)
CGCM3	:Coupled Global Climate Model
CHIRPS	:Climate Hazards Group Infrared precipitation with stations
CMFD	:China Meteorological Forcing Datasets
CMIP3	:Coupled Model Intercomparison Project Phase 3
CMIP5	:Coupled Model Intercomparison Project Phase 5
CMIP6	:Coupled Model Intercomparison Project Phase 6
CS	:Constant scaling
CWH	:Water holding capacity ·
DDFDG	:Degree Day Factor Debris-covered glacier
DDFG	:Degree Day Factor Debris-free glacier
DDFS	:Degree Day Factor for Snow
deltaGW	:Ground Water delay

DEM	:Digital Elevation Model
DHM	:Department of Hydrology and Meteorology
DJF	:December January February
dKG	:Maximum minus minimum outflow coefficient (t-1)
E	:Evaporation from the lake
EQM	:Empirical Quantile Mapping
ET	:Actual evapotranspiration
EVU	:Elevation Vegetation Unit
FC	:Maximum soil moisture storage (mm)
FDC	:Flow Duration Curve
FF	:Far Future
GCM	:General Circulation Model
GDM	:Glacier Degree Day Model
GlacF	:Glacier fraction
GLOF	:Glacial Lake Outburst Flood
GoN	:Government of Nepal
HadCM3	:Hadley Centre Coupled Model
HBV	:Hydrologiska Byråns Vattenbalansavdelning
HEC HMS	:Hydrologic Engineering Center - Hydrological Modeling System
HKH	:Hindu Kush Himalayan Region
HMA	:High Mountain Asia
ICIMOD	:International Center for Integrated Mountain Development
IPCC	:Intergovernmental Panel on Climate Change
JAMS	:Jena Adaptable Modelling System
JJAS	:June July August September
K	:Storage (or recession) coefficient (Δt-1)
K0	:Storage (or recession) coefficient (Δt-1)
K1	:Storage (or recession) coefficient (Δt-1)
K2	:Storage (or recession) coefficient (Δt-1)
KGmin	:Minimum outflow coefficient (t-1)
Ki	:Recession coefficient [1/Δt]
km2	:square kilometer
KSI	:Snow to Ice conversion factor (Δt-1)

KW	:Kinematic wave theory models
Kx	:Routing parameter recession coefficient
LOCI	:local intensity scaling
LP	:Soil moisture value above which AET reaches PET (-)
LULC	:land use and land cover
m	:meter
MAM	:March April May
MAXBAS	:Length of triangular weighting function (Δt)
MBC	:Monthly bias correction
MF	:Mid Future
mm	:millimeter
mm Day -1	:millimeter per day
mm y-1	:millimeter per year Day
mm/year	:Mili meter per year
MoFE	:Ministry of Forest and Environment
MPI ESM1 2HR	:Max Planck Institute for Meteorology Earth System Model version 1-2 HighResMIP
NBC	:Nested bias correction
NF	:Near Future
NorESM2 MM	:Norwegian Earth System Model version 2 1degree MM
NSE	:Nash-Sutcliffe Criterion of Efficiency
obs	:Observed
ON	:October November
P	:Precipitation in the lake
P	:Precipitation
P bias	:Percent of bias
PCALT	:Precipitation correction
PD	:Probability distributed models
PERC	:Threshold parameter (mm Δt-1)
PERC	:Maximum percolation to the lower zone [mm/Δt]
ppm	:part per million
PRECIS	:Providing Regional Climates for Impacts Studies
Q	:Outflow (mm Δt-1)

Q	:Discharge
Q_Base	:Baseflow runoff
Q_Glac	:Glacier melt runoff
Q_Rain	:Rain runoff
Q_Snow	:Snow melt runoff
Q_{bf}	:Discharge contributed by baseflow runoff
Q_{gm}	:Discharge contributed by glacier melt runoff
Qi	:Runoff component [mm/Δt]
QM	:Quantile mapping
Q_{rr}	:Discharge contributed by rain runoff,
QS	:Quantile scaling
Q_{sm}	:Discharge contributed by snow melt runoff,
Q_{Tot}	:Total contributed discharge,
RCM	:Regional Climate Model
RCPs	:Representative Concentration Pathways
RGI6	:Randolph Glaciers Inventory Version 6
RMSE	:Root Mean Square Error
RSR	:RMSE-observations standard deviation ratio
S	:Storage (mm)
SCA	:Snow Covered Area
SDSM	:Statistical Downscaling Model
SFCF	:Snowfall correction factor (-)
sim	:Simulated
SLZ	:Storage in lower zone [mm]
SMA	:Soil Moisture Accounting
SMHI	:Swedish Meteorological and Hydrological Institute
SNBC	:Simple nested bias correction
SnowSC	:Water storage capacity of Snow pack
SP	:Seasonal variability in degree-Δt factor (-)
SPHY	:Spatial Process in HYdrology
SRES	:Special Report on Emission Scenarios
SRM	:Snow Melt Runoff Model
SRTM	:Shuttle Radar Topography Mission

SSPs	:Shared Socio-economic Pathways
STZ	:Storage in top zone [mm]
SUZ	:Storage in upper zone [mm]
SWAT	:Soil and Water Assessment Tool
t	:Time (Δt)
TCALT	:Temperature correction
Tcrit	:Critical Temperature
Tmax	:Maximum Temperature
Tmean	:Mean Temperature
Tmin	:Minimum Temperature
TRMM	:Tropical Rainfall Measuring Mission
TT	:Threshold temperature (oC)
UH	:Unit hydrograph
UNFCCC	:United Nations Framework Convention on Climate Change
USACE	:United State Army Corps Engineers'
UZL	:Threshold parameter (mm)
UZL	:Maximum percolation to the upper zone [mm/Δt]
WECS	:Water Energy Commission Secreteriat
WMO	:World Meteorological Organization

LIST OF SYMBOLS

%	:Percentage
ΔS	:Change in storage
°C	:Degree Celsius
Δt	:Change in time
$\leq$	:Greater than or Equal
$\geq$	:Less than or Equal
*	:Astrik
r	:Coefficient correlation
R^2	:Coefficient of Determination

LIST OF TABLES

LIST OF FIGURES

TABLE OF CONTENTS

PAGE NO:.

CHAPTER 1

1. INTRODUCTION

1.1 Background

The future global climate and current local climate is uncertain and thus posses some risk in hydrological regimes as well as hydrological cycles. Changing climate impacts hydrological regimes in the hydrological cycle through the distinguished streamflow components. Streamflow possesses mainly two parts: surface flow and sub-surface flow. Surface flow consists of direct runoff from rain and snow-glacier melt while sub-surface flow is the infiltration of water from soil to subsoil. After 1960s, hydrological modeling systems were launched to simulate such hydrological processes. By now there are numerous hydrological models to estimate water balance and components by model parameterization. Firstly, Thornthwaite and Mather (1955) proposed their water balance model by continuous revision in their previous models. The water balance and hydrological regimes are affected by changing climate. Himalayas have a diverse climate, heterogeneous precipitation and hydrological regimes that cause water balance parameters including precipitation, runoff, evapotranspiration, soil moisture water deficit and temperature illustrate in-out flux hydrological system and water storage changes in temporal scale (Talchabhadel and Chhetri, 2023). The streamflow components contain different hydrological processes: rain-runoff contribution, groundwater-runoff contribution, snow melt and glacier melt-runoff contribution that is accumulated as the total river flow (Khanal *et al.*, 2021). The classification of streamflow components by different methods are divided into empirical or statistical methods and hydrological modeling methods. However, hydrological modeling is a robust approach to the separation of streamflow components (Wu *et al.*, 2021). The stochastic soil moisture water balance model suggests ways to partition precipitation into runoff and evaporation under different climate scenarios (Siegfried *et al.*, 2023). The effects of climate change on streamflow components are precipitation, discharge, baseflow, melting runoff and evapotranspiration that may vary in spatial and temporal scale (Bajracharya *et al.*, 2018). The knowledge of climate change impacts on hydrological regimes has greater importance which can contribute to sustainable water resources management in Himalayan regions (Nepal, 2016). The changing intensity and timing of precipitation will affect streamflow occurrence as floods or droughts.

Changing climate impacts on water resources and intensification of the global hydrological cycle as reported by the Third Assessment Report (AR3) of the Intergovernmental Panel of Climate Change (IPCC, 2001). A General Circulation Model (GCM) is a climate model that mathematically represents the general circulation of planetary atmosphere. These models are used to obtain reliable information regarding historical, current, and future climate trends (Gonzalez *et al.*, 2010) over long periods. Generally, using an ensemble of various GCMs in place of single GCM can represent a range of possible scenarios which provide a better idea about possible future climate (Pierce *et al.*, 2009). However, the spatial resolution of a GCM is not sufficient for countries with mountain regions, which makes it incompatible with local hydrological models. In practice a downscaling methods are used to fill this gap. Regional Climate Model (RCM) is available in relatively higher spatial resolutions than GCM. Furthermore, RCM can be placed within a given GCM to provide a more detailed simulation. RCM covers a smaller area with better resolution, which requires more intensive computation to run and is appropriate for areas with mountainous and coasts. The Coupled Model Inter-comparison Project Phase 5 (CMIP5) developed different climate change scenarios called Representative Concentration Pathways (RCPs) (Meinshausen *et al.*, 2011), which can project possible future climate scenarios. Studies have shown that RCP scenarios are an suitable approach in investigatiing future climatic conditions, and the results can be used to perform the impact analysis of climate change and plan future mitigation measures (Van Vuuren *et al.*, 2011).

The General Circulation Models (GCM) on future temperature and precipitation in the impact region and it's projections for future hydrological regime patterns differ widely based on data inputs and detailed studies to measeure impacts of such differences are acutely lacking. Consequently, the demand of intensive knowledge about future climate change projection is relatively higher. Main focus of the study is in temperature increases and changes to the hydrological cycle as the tendency that recent scientific knowledge supported by observed weather events results that extremes related to hydrological changes can be substantial though and the geographical and time-wise resolution of predicted changes is still low in many areas. This will produce frequent and intense rainfall events in consequent years which affects stream flow patterns on a basin scale, main focus of this study.

Hydrological models have a wide range of applications, including water resources planning, development and management, flood prediction, coupled systems modeling

including water quality, hydro-ecology and climate change projection, etc. However, due to the limitation of resources and the range of available measurement techniques, there are limitations to the availability of spatial-temporal data. Hence there exists a need to extrapolate spatial-temporal information from the available measurements. Moreover, there is a need to assess the possible hydrological impact of future system response. Hydrological models are often used to simulate future hydrological cycles and GCM-projected temperature and rainfall data are used to force these models. Hydrological modeling often plays a vital role in decision-making for water resources management and planning. Developed countries have always developed own their model as required but developing and under-developing countries have limited models (Souffront Alcantara *et al.,* 2019). Many conceptual hydrological models apply to water resource management (Nonki *et al.,* 2023). Several hydrological models were employed to simulate hydrological regimes in the Himalayas river basin. Hydrological models are commonly classified into two categories physically based and conceptually based (Singh *et al.*, 1995). Besides these two models, some other tools simulate semi-distributed nature. The models are also categorized into lumped, semi-distributed and distributed models.

Continuous hydrological records at the desired site with spatial and temporal coverage are required for the planning, development and management of applications of water. The spatial and temporal coverage of continuous hydrological records is usually not available. Discharge stations and observations are limited at transboundary Himalayan River basins mainly in under-developing countries due to continuous monitoring, maintenance and cost. Continuous modeling is suitable for instance and effective design simulations support ungauged sites (Grimaldi *et al.,* 2021). The ungauged simulation shall be linked to the runoff response from the routing process. Ungauged basins are partially or completely absent from the hydrological network those situations are unable to calibration. In the absence of flow records practitioners are using empirical approaches for discharge data and frequency analysis. Streamflow downstream is continuously changing due to climate change in Himalayan catchments (Adhikari *et al.*, 2022). The hydrological records require water resources project planning, development and management.

The crucial question and challenge are what will be the impact of climate change on hydrological regimes and what are the resulting temporal variations in hydrological regimes over the Tamakoshi river basin? This research evaluates the changes in

hydrological regimes resulting from the projected climate change by using CMIP6 datasets forced to the hydrological model. There are many regions where runoff and discharge will increase due to increasing precipitation but also many regions where there will be decreases. So, the individual basin and catchment may experience a significant impact of climate change in the whole hydrological regimes, locally and globally. The study is an overview of present hydrological regimes and their future prospective with respect to climate change which recognizes the fact that climate change impacts hydrological regimes in different ways volume of flow, timing of flow (discharge). This study aims to answer the questions related to the hydrological regime's expected increases and decreases due to climate change and water availability and the extent of such changes.

1.2 Rational of the study

The spatial and temporal coverage of river flow discharge data at a desired site is usually unavailable. Hydrological gauging stations installed across the basins are limited and not tolerable according to the norms and criteria of the World Meteorological Organization (WMO, 2008) in situ observations are limited due to the loss of gauging stations and the absence of a gauge reader, the continuous discharge data is a gap across the river basins in under development countries (Wongchuig-Correa et al., 2020). The availability of water from upstream to downstream in mountainous regions is changing and accurate hydrological predictions and information for the future supply are important (Lutz et al., 2016). Designing discharge data and transposing hydrological information at ungauged river basins is a significant task for water management (Seibert and Beven, 2009, Waseem et al., 2015).

However, the changing climate and hydrological regime might pose a risk to overall water resources management. Based on an ensemble of the GCMs under different SSPs scenarios, the GCMs data sets of CMIP6 implemented comprehensive climate change projections from local to global scale. CMIP6 data sets improve the knowledge to understand projections of climate change impacts on hydrological regimes for past, present and future (Lalande et al., 2021, Eyring et al., 2016).

This type of study ungauged streamflow simulation using hydrological models SPHY, HBV light and HEC HMS models investigate the ungauged flow simulation and HBV light model simulates climate change impacts on streamflow components viz; precipitation, actual evapotranspiration, water storage change, discharge from rain-

runoff, baseflow runoff, glacier melt runoff and snow melt runoff with CMIP6 GCMs data input still gap in trans boundary river basin. This study provides information about the climate change impacts on water balance components and its prospects which are helpful for future water-resource planning in hydropower, irrigation and drinking water as well as hydraulic infrastructure, etc. The results are also useful for water resources systems analysis, watershed hydrology, flood management, water sustainability, adaptation planning and sustainable management of water resources in other same circumstances in the Himalaya region. Thereafter now has great importance the utilization in the planning and design for water resource projects, early warning systems, dry season water management, climate foresight and inventory of water resources potentiality in local as well as regional scale.

1.3 Research questions

This study, the observed temperature and precipitation trend has been increasing in Himalayans basins resulting in the shrinking of snow and glacier areas in recent years. As a consequence, the runoff generation components and streamflow regime are affecting. The research questions raised in this study are as follows:

- What is the actual Catchment Area Ratio method for Ungauged basin?
- What are melt contributions to water balance?
- What is the temporal distribution of precipitation, temperature evapotranspiration, water storage change and discharges under SSPs?

1.4 Research objectives

The main aim of this research is to analyze the characteristics and variation of hydrological regimes under different climatic scenarios in high Himalayas Tamakoshi river basin. The specific objectives of this study are as follows.

- To compare and calibrate the discharge of different gauging stations by using hydrological models.
- To evaluate the melt contribution on water balance.
- To analyze of changes in precipitation, temperature, baseflow, rain runoff, snow-glacier melt, river discharge, evapotranspiration and water storage change between the baseline and future period by using climatic and hydrological model.

1.5 Limitations

The changes of climatological parameters in distances rapidly with the elevation in rugged mountainous regions effects temperature and precipitation patterns, Therefore the available hydro-meteorological stations could not covarage the complete basin area. Contineous data of precipitation, temperature and discharge data are records available at the limited stations mostly at lower elevations. So, the trend of the meteorological parameters at high elevations is rather complicated. Limited climate change 4 GCMs data were used and evaporation estimation using the Banley-Criddle equation, evaporation station not available in the study area.

1.6 Outline of the dissertation

The major body of the thesis is divided into six chapters, and it also has references and appendices. The thesis is summarized as follows.

Chapter 1: includes Introduction, research question, objectives, limitations and thesis outlines.

Chapter 2: includes Literature review on the Hydrological model, Stochastic model, Black box model, Deterministic model, Physically-based distributed model, Distributed model, Semi-distributed model, Lumped models physically based, Lumped model, Ungauged catchments, Climate change, Climate models, Scenarios and Bias correction.

Chapter 3: includes Materials and Methods, Study area, Hypsometric curve, Observed precipitation, discharge and temperature characteristics of Tamakoshi river basin, Input data availability, Climate change projection data, Hydrological modeling, Spatial Process in HYdrology (SPHY), Runoff routing, HBV-light, The applications HBV light model, HBV light Model routine, Snow routine, Parameters, Glacier routine, Parameters, Dynamic glacier, Response routine, Recession analysis, Soil moisture routine, Routing response, Model types, Three GW-boxes, STZ and SUZ distributed, Response routine, Model variants, Glacier, HEC HMS continuous simulation, Streamflow components, Water balance storage, Hydrological model calibration and validation, Evaluation methods, Bias correction of precipitation and temperature

Chapter 4: includes Model calibration and validation, comparison of model with statistical index, Flow simulation at ungauged site, Observed water balance components contribution on streamflow, Water balance storage, Climate change analysis, Bias correction, Projected impacts of GCMs, Projected precipitation, Projected temperature,

Climate change impacts on water balance components, Climate change impact on precipitation, Climate change impact on river discharge, Climate change impact on rain runoff, Climate change impact on baseflow runoff, Climate change impact on glacier melt runoff, Climate change impact on snow melt runoff, Climate change impact on actual evapotranspiration, Water balance storage changes

Chapter 5: Includes Conclusion and Recommendation

Chapter 6: Includes Summary

CHAPTER 2

2. LITERATURE REVIEW

2.1 Background

The extensive evaluation of the literature includes an analysis of how climate change is affecting hydrological patterns. This chapter provides a detailed explanation of this study, with particular attention to Hydrological Models and their all-encompassing overview, the difficulties presented by Ungauged Basins concerning climate change, taking into account a range of scenarios and correcting any biases that may exist. This analysis's sources are from reliable places, such as Google Scholar, official documents, and library materials, guaranteeing the inclusion of factual data. Building on the knowledge gained from the thorough literature evaluation, the research gap was established and used as the basis for the overall study design. This study aims to investigate the effects of climate change on water balance components in the Tamakoshi river basin through the simulation of ungauged hydrological processes. A key component of this research is the use of Climate Change Models (CCMs) datasets, which provide a thorough evaluation of the consequences. The significance of the data about ungauged basin records and climate change cannot be overstated in terms of planning, development, and management of water resources. The following subheadings are used in this chapter to present the literature review:

2.2 Hydrological model

In the fields of planning, catchment-scale development, and water resource management, hydrological models are essential instruments that are frequently utilized. These types were first developed in the 1960s and 1970s, and they have been in use for more than 50 years. In order to mimic catchment runoff, a number of very simple hydrological models were developed at this time, which resulted in the production of multiple conceptual models. These models use a small number of parameters to depict the complex and varied hydrological processes that occur within a catchment (Seibert and Bergström, 2022).

The signal that starts hydrological processes is precipitation. The amount of precipitation that eventually makes its way into streams is known as runoff or stream flow, and it captures the basin's overall response. A variety of factors are included in a

total runoff, including precipitation that falls directly onto a stream, groundwater or base flow, surface runoff, sub-surface runoff, and runoff from melting snow and glaciers. Stream flow data is crucial for hydrology and is needed for the design, management, and control of projects involving water resources.

By definition, simplified conceptual representations of particular hydrologic cycle components are what hydrological models are. Hydrological prediction and the understanding of hydrological processes are their two fundamental functions. These models find many uses, such as flood prediction, planning, development, and management of water resources, as well as coupled system modeling that includes hydro-ecology, water quality, and climate-related issues. However, due to a lack of resources and measurement methods, the availability of spatial-temporal data is frequently limited. As a result, extrapolating spatial-temporal information from the existing data becomes necessary. It also becomes crucial to evaluate the possible hydrological effects of future system responses, such as those brought about by changes in land management and climate (Pechlivanidis *et al.*, 2011).

There are many different types of hydrological models that fall into two categories: conceptual models and physically-based models. Depending on the features of the particular catchment, lumped, semi-distributed, or distributed models might be chosen. Numerous hydrological model concepts are shown in Figure 1, but a few main classification structures also stand out; these are discussed in the section that follows.

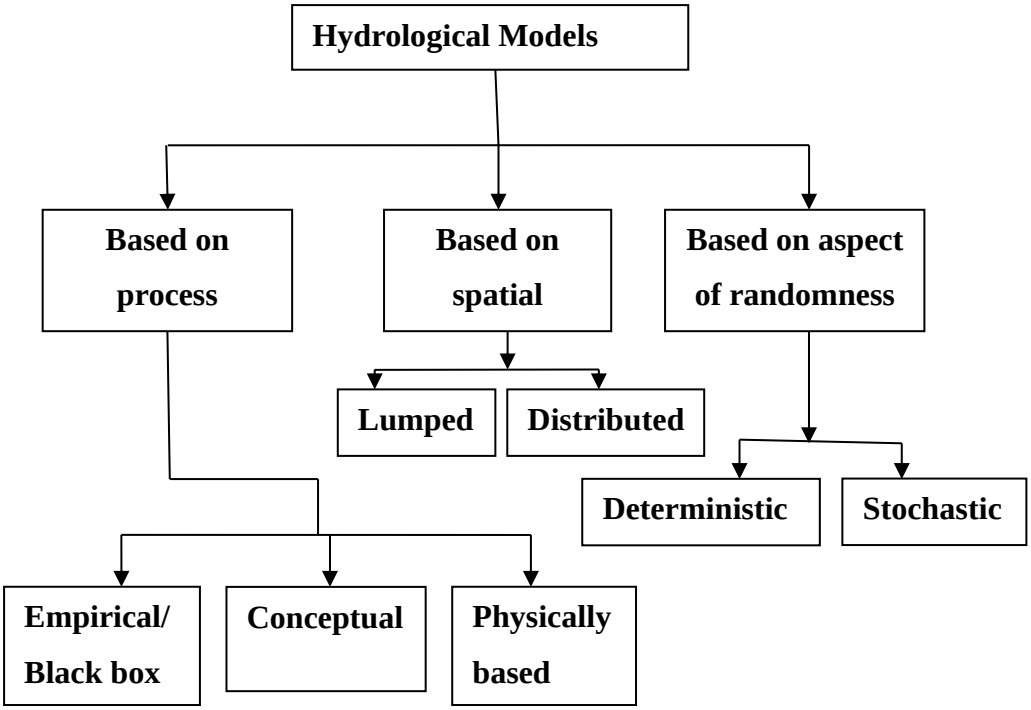

Figure 1: Classification of hydrological model

2.2.1 Stochastic model

These black-box models are data-driven systems that use statistical and mathematical principles to establish a connection between a given input (like rainfall) and the model's output (like runoff) (Cunderlik, 2003). Regression, transfer functions, neural networks, and system identification are often employed techniques. We refer to these models as stochastic hydrological models. The physical processes seen in the real world are attempted to be represented by these models. These models usually include channel flow, evapotranspiration, surface runoff, and subsurface flow.

2.2.2 Black box model

All that this model does is outline the functional connections between the inputs and outputs of the system (Pechlivanidis *et al.*, 2011). It follows that they are lumped parameter models. When compared to process parameters like mass or heat transfer coefficients, reaction kinetics, etc., the parameters of these functions have little physical importance. Compared to mechanistic models, black box models have this drawback. Nonetheless, the black box modeling approach is as successful if the goal is simply to properly depict specific trends in process behavior. Additionally, the cost of modeling is orders of magnitude lower than the expense of creating mechanistic models.

2.2.3 Deterministic model

A given input always yields the same output in a deterministic model, which does not take randomness into account. Equations are used in such a model to express the domain (Physics) of a system (Pechlivanidis *et al.*, 2011). Different combinations of lumped or distributed, empirical, conceptual, or physically based deterministic models are possible. Lumped, semi-distributed, and distributed models are the three basic types of deterministic hydrological models.

Deterministic hydrological models are the name given to these models. Deterministic hydrology models are further classified as continuous simulation models (which deal with modeling a system over time by a representation in which state variables change continuously with respect to time) and single-event models (single-event hydrological models will always be of uncertain value).

2.2.4 Physically based distributed model

One or more partial differential equations are used to represent processes in physically-based distributed models, where the equations and parameters are dispersed over space. A physically-based model, in contrast to lumped conceptual models, does not take into account that water flows in a region occur in a small number of storage units. Rather, the energy and water flows are computed directly from the governing continuum (partial differential) equations, like Boussinesq's equation for groundwater flow, Richard's equation for unsaturated zone flow, and the Saint Venant equations for overland and channel flow. Applications of distributed models include catchments with intricate channel networks, different land use and vegetation cover distributions in space, intricate subsurface aquifer systems, etc. These models enable the study of the interactions between surface water, groundwater, and the unsaturated zone, though flood modeling is the main area of interest. The spatiotemporal pattern of flood formation may be significantly influenced by the analysis of spatial variations in these interactions.

2.2.5 Distributed model

In contrast to lumped models, which average or disregard spatial variances, distributed models explicitly take these variations into account. In the Himalayan region, which is known for its high altitude and frigid temperatures, a distributed hydrological model is

essential for gaining important insights into the water cycle and cryosphere (Wang *et al.*, 2023).

The knowledge basis that underpins empirical, conceptual, and physically based models differs from one another. Physically based models describe each process's behavior using the laws of physics. Conceptual models are created when the behaviors used for the physically based models are drastically simplified. Rather than using physics, an empirical model is created via observations of the input and outcome.

Distributed model parameters are free to change in space at a resolution selected by the user. In order to assess the impact of this distribution on simulated precipitation-runoff behavior, the distributed modeling approach aims to integrate data regarding the spatial distribution of parameter variations with computational tools. Large volumes of data, which are frequently unavailable, are typically needed for parameterization in each grid cell of distributed models. The controlling physical processes, however, are meticulously modeled and, when used correctly, can yield the highest level of precision (Cunderlik, 2003).

The availability of spatially distributed data sets at relatively fine scales (such as remotely sensed data), information about physical catchment properties at small catchment scales, and the growing availability of powerful computer resources have all encouraged the use of distributed models. While rain gauge data is typically used by distributed models, remote sensing products have proven to be a useful substitute. Although it lacks the quantitative accuracy of rain-gauge networks, this type of data can provide good estimates of rainfall at precise geographical and temporal resolutions. In order to get around this issue, rain-gauge networks' point estimates of rainfall are typically used to calibrate remote sensed data (Pechlivanidis *et al.*, 2011).

Hydrological applications have long benefited from the use of distributed models for a variety of reasons, but problems with scale, parameter estimates, and calibration techniques arise. Distributed models are prone to becoming over-parameterized and hence ill-posed in relation to the available input-output data as the degree of spatial discretization grows. Accordingly, a typical issue is uncertainty in parameter estimations, which leads to ambiguity in model identification (Orlandini and Rosso, 1998, Madsen *et al.*, 2002), referenced in (Pechlivanidis *et al.*, 2011). Furthermore, the literature does not clearly show that distributed models are more accurate in terms of flow estimates at the catchment outlet than lumped models in terms of spatial resolution (Pechlivanidis *et al.*, 2011). This conclusion could be attributed to multiple sources of

uncertainty, including parameter estimation, data uncertainty, and model structure identifiability (Beven, 2009), as noted in (Pechlivanidis *et al.*, 2011).

Although the most important factor is often unclear because the results depend on the hydrological characteristics of the catchment, factors like the rainfall's spatial distribution, model parameters, and channel routing appear to make a distributed model more effective than a lumped model in some situations. Furthermore, rainfall and model spatial resolution appear to be related to distributed model efficiency. However, a number of causes of error and uncertainty, including rainfall, model structure, and model parameter uncertainty, should be taken into account and handled for improved model performance in distributed modeling. On the other hand, when a lumped model outperforms a dispersed model, the primary cause has been identified as the geographical variation of the model parameters (Pechlivanidis *et al.*, 2011).

2.2.6 Semi distributed model

By dividing a watershed into smaller subbasins, semi-distributed models—also referred to as simplified distributed models—allow for a partial geographic variation of parameters. Semi-distributed models fall into two main categories: conceptual models and physically based models.

Models like HEC HMS that are based on kinematic wave theory, also known as KW models, fall within the first group. The surface and subsurface flow equations used in more intricate distributed hydrologic models are represented more simply in these models.

Models of probability distribution, or PD models, fall within the second group. According to Cunderlik (2003), probability distributions of input parameters across the watershed are incorporated into PD models to account for geographical variances.

2.2.7 Physically based lumped model

In the 1960s, a novel set of models emerged, known as lumped models with a physically based approach. These models were designed to offer a more robust foundation for representing watershed processes. They consist of interconnected conceptual elements, with each element symbolizing a subsystem within the hydrologic cycle, such as evaporation, surface runoff under saturated conditions, and rill surface runoff. Nevertheless, despite the numerous parameters involved, the process descriptions

remain rather simplified. Consequently, there is minimal distinction between these models and the conventional lumped conceptual models.

In the 1970s, a fresh approach to hydrologic process modeling came into play. These models possess a flexible structure that adjusts to the system's inputs and outputs, earning them the label of "black box models." Among the initial iterations of these models were the autoregressive models, which were grounded in time series analysis. A more recent variant of this model, which allows for the incorporation of up-to-date data, is the artificial neural network model. While this model has yielded promising results in some cases, further research is essential to explore its full potential.

The criteria governing model structures still lack clarity, which poses challenges when applying these models in watersheds with insufficient data or when regionalizing parameters. Nevertheless, modern technology empowers us to attain comprehensive knowledge of specific variables with high spatial precision and efficiently handle substantial volumes of information. Consequently, it is reasonable to believe that a model incorporating the spatial distribution of variables will outperform a lumped model. Distributed models, in particular, excel in this regard by accurately representing the spatial variability of variables and faithfully replicating watershed processes, as opposed to lumped models.

Physically based distributed models delve into watershed processes with remarkable detail and can provide fine-resolution representations (typically at scales of 100-500 meters). These models solve equations for each individual unit (cell), and the outputs of neighboring cells are amalgamated. However, these sophisticated models necessitate extensive data and, thus far, have required extensive parameter calibration, if not the estimation of all variables from field data.

Presently, a middle ground is being explored between the two primary modeling approaches—lumped and distributed. This intermediate path is referred to as "models of distributed parameters." These models segment the watershed into smaller, more homogeneous units, to which lumped models are applied. The overall watershed response is an amalgamation of these unit-level responses. These models can be categorized based on the type of units used, which might include subwatersheds or artificial units defined by specific criteria. The application of lumped models to these

units is what characterizes them as "distributed models," although they retain a conceptual lumped nature.

Distributed hydrologic modeling is an evolving field, with various approaches, philosophies, and research directions. For instance, one category of distributed hydrologic models seeks to integrate these units in order to represent the spatial distribution of variables in a simplified manner.

2.2.8 Lumped model

Lumped hydrologic models have fixed parameters across a basin, focusing solely on the basin's outlet response without considering the individual subbasin responses explicitly. These models often lack representation of the physical characteristics of hydrologic processes, relying on empirical approximations to some extent. To address the impact of spatial parameter variability, methods like area-weighted averages are employed to calculate effective values for the entire basin. Lumped models are generally unsuitable for event-scale processes. However, when the primary concern is forecasting discharge, these models can offer simulations of comparable quality to more intricate distributed models (Cunderlik, 2003).

In conventional hydrological modeling, a prevalent approach involves the utilization of lumped models. These models depict a watershed as a unified entity and consider a single input of mean rainfall. The ensuing discharge at the outlet of the watershed is determined based on the overall system dynamics. Within this category, numerous hydrologic models are employed, typically hinging on the concept of the unit hydrograph (UH).

This concept operates effectively within a framework that assumes the watershed to be a linear, causative, and time-invariant system, where only a portion of the rainfall, known as rainfall excess, generates runoff. However, it is imperative to note that these models do not adequately account for the potential infiltration of surface runoff as it traverses a permeable riverbed. Consequently, they tend to underestimate the subsurface contribution to river flow.

Furthermore, identifying the unit hydrograph (UH) can be a complex undertaking. The derivation of the UH often necessitates solving the inverse problem using hydrological

information specific to the watershed, including rainfall and flow data. Unfortunately, such data may not always be readily available or of sufficient quality. Moreover, information regarding the spatial distribution of rainfall is often limited.

To mitigate these challenges, an alternative approach has been developed, wherein the watershed is conceptualized as a simplified system. This simplification enables the derivation of a single UH based on a limited set of parameters, which can be obtained through statistical techniques. These models are commonly referred to as lumped conceptual models.

Taking this concept a step further, efforts have been made to establish a relationship between the parameters of the unit hydrograph and the geomorphological characteristics of the watershed. This endeavor has given rise to the Geomorphologic Unit Hydrograph, which relies solely on the physical attributes of the watershed and does not rely on hydrological data for its formulation.

A number of models were later created for hydrological simulation after the hydrological model was initially presented on a computer in the late 1960s (Bergstrom, 2006). Although there are many uses for hydrological models, the simulation is limited in certain ways by the availability of geographical and temporal data. Hydrological models that have been verified and calibrated are used to assist basin and subbasin water resources planning management. According to Pechlivanidis *et al.* (2011), hydrological models evaluate the potential hydrological effects of potential system responses. According to basin characteristics, internal hydrological processes, data availability, and basin parameterizations, hydrological models are primarily divided into lumped, semi-distributed, and fully distributed models (Cunderlik, 2003, McDonnell *et al.*, 2007). The measured streamflow gauge station data at the basin is frequently used to calibrate and validate hydrological models (Dembélé *et al.*, 2020, Zhang *et al.*, 2023).

Streamflow in river basins is primarily influenced by precipitation in the basin areas. The characteristics of precipitation in complex river basins exhibit variations, often attributed to orographic effects (Shrestha *et al.*, 2019a). The attributes of rainfall are of great significance as they impact runoff and the functioning of hydrological systems in the central Himalayas region. Precipitation serves as the source of river discharge, which is composed of rain runoff, snow and glacier melting, and groundwater runoff

(Raghunath, 2006). River discharge plays a pivotal role in the hydrological cycle, a fact emphasized by Shiklomanov *et al.* in 2006.

The hydrological cycle itself is subject to profound alterations brought about by shifting climate patterns and modifications in water resource structures. Therefore, comprehending the past and prospective trends in hydrological occurrences is crucial (Cong *et al.*, 2009). Timely and accurate data on river discharge is the cornerstone for responding to the interplay of land surface and atmospheric forces. The livelihoods of human communities are heavily reliant on the availability of water from streams and rivers. In history, civilizations thrived along riverbanks primarily due to the dependable water supply (Spencer *et al.*, 1978). However, the changing climate and human activities have led to changes in river hydrology. Over the past two decades, there has been a substantial decrease in the annual discharge of 22% of the world's rivers and a significant increase in the annual discharge of 9% of the world's rivers (Walling and Fang, 2003). It is important to recognize that river discharge is not uniform across global to local scales; it evolves with both time and space. Mainly, river discharge tends to increase in high-altitude river basins (Manabe *et al.*, 2004, Peterson *et al.*, 2002).

In underdeveloped countries situated in the Himalayan River basin, there is a limitation in the number of discharge gauging stations, primarily due to cost and accessibility constraints (Wongchuig-Correa *et al.*, 2020). In the absence of regular ground station gauge data, remote sensing data can be effectively employed in conjunction with hydrological models to generate discharge data at both gauged and ungauged sites (Kite and Pietroniro, 1996). While developed countries possess hydrological models tailored to their specific needs, developing nations often grapple with limited hydrological models, necessitating the testing of multiple models as required (Souffront Alcantara *et al.*, 2019). The simulation of discharge and hydrological phenomena through various hydrological models is contingent upon the performance of the models (Nash and Sutcliffe, 1970). It is important to acknowledge that the performance of hydrological models is intricately linked to the characteristics of catchments and the quality of input data.

Among the diverse hydrological models, Spatial Process in HYdrology (SPHY) is a spatially distributed model capable of simulating terrestrial hydrology at various climatic scenarios on a basin-to-subbasin scale (Terink *et al.*, 2015). The SPHY model has found successful application in several river basins within the High Mountain Asia (HMA) region (Khanal *et al.*, 2021). Furthermore, the HBV model, a semi-distributed

conceptual model, has proven effective in modeling snow and glacier-fed river basins in Nepal (Adhikari, 2014, Adhikari *et al.*, 2022). In evaluating model components, the response of a catchment to the model's operation is crucial (Jansen *et al.*, 2021). These components encompass snow, soil moisture, and response and routing routines, which include parameters for lakes and glaciers. They are applied to generate discharge data at the outlet of catchments in HBV models (Seibert, 2005).

In situations where data is scarce or insufficient, precise model calibration and validation are indispensable, particularly for rainfall-runoff models. These models play a pivotal role in early warning systems and the development of surface and subsurface hydrological models (Teng *et al.*, 2017). Selecting the most appropriate model for simulating streamflow data in specific watersheds can be a daunting task due to the diverse objectives of researchers and the unique characteristics of each watershed (Golmohammadi *et al.*, 2014).

Many studies have been conducted to under the temperature and precipitation changes (Dahal et al., 2018; Thakuri et al., 2019), hydrological behaviors of rivers of Nepal using hydrological models / tools, like SWAT (e.g. Neupane et al., 2014; Neupane et al., 2015; Shrestha et al., 2017; Neupane et al., 2022; Neupane et al., 2017; Neupane and Pandey, 2021; Lamichhane et al., 2024), J2000 (Nepal et al., 2015; Nepal et al., 2017; Eeckman et al., 2015). Commonly used some of the available computation models, HBV model (Bergström, 1976, Bergstrom, 1992), GDM model (Kayastha *et al.*, 2020), SPHY model (Terink *et al.*, 2015), SWAT model (Arnold *et al.*, 1998), Mike 11 model (Célleri *et al.*, 2003), JAMS J2000 model (Krause, 2002), HEC HMS (USACE) etc. investigates the water balance and streamflow components in basin to sub-basin scales in Himalayas river basin.

A range of hydrological models, including those by Khanal *et al.* in 2021, Nepal *et al.* in 2014, Bharati *et al.* in 2014, Kaini *et al.* in 2021, Bajracharya *et al.* in 2018, Devkota and Gyawali in 2015, Adhikari *et al.* in 2022, Khadka *et al.* in 2014, and others, are designed to simulate the impacts of climate change in the Central Himalayas region. Notably, the HEC HMS model, developed by the Hydrological Engineering Center (HEC) of the US Army Corps of Engineers (USACE), delves into rainfall-runoff and routing processes, encompassing both natural and controlled elements (Feldman, 2000). The Spatial Process in Hydrology (SPHY) model, conceived by Terink *et al.* in 2015, has found successful application in a spectrum of tasks, including real-time soil moisture projections in low-lying areas, irrigation management, assessments of climate

change impacts on snow and glacier-fed river basins, and operational flow forecasting in Himalayan catchments. The Hydrologiska Byråns Vattenbalans avdelning (HBV) model is instrumental in estimating water balance components within the Himalaya river system, and it has been effectively applied in the context of Nepalese Himalayan rain runoff, snow, and glacier-fed river basins(Adhikari *et al.*, 2022, Bhattarai *et al.*, 2018, Thapa *et al.*, 2017, Shrestha and Alfredsen, 2011, Normand *et al.*, 2010).

Hydrological models, in general, play a pivotal role in simulating streamflow components and their contribution to river discharge in mountainous regions. Their utility in water resources research is steadily on the rise (Huang *et al.*, 2022). These models are instrumental in partitioning water into evaporation, runoff, and infiltration, serving as valuable tools for understanding and managing water resources (Lian *et al.*, 2021, Porporato and Yin, 2022). Therefore, the need for hydrological models capable of simulating streamflow at both the basin and sub-basin scales is paramount in this endeavor.

2.3 Ungauged catchment

Hydrological records play an indispensable role in the planning, development, and management of water resources projects. However, the availability of river flow discharge data at specific locations is often lacking both in terms of spatial and temporal coverage. The installation of hydrological gauging stations across river basins is limited, falling short of the standards set by the World Meteorological Organization (WMO, 2008). In many cases, on-site observations are constrained due to the loss of gauging stations and the absence of gauge readers, resulting in significant gaps in continuous discharge data, particularly in underdeveloped countries (Wongchuig-Correa *et al.*, 2020). The dynamic nature of water availability from upstream to downstream in mountainous regions is subject to change. Therefore, the provision of accurate hydrological predictions and information for future supply is of paramount importance (Lutz *et al.*, 2016). Transposing discharge data and hydrological information to ungauged river basins is a formidable task essential for effective water management (Seibert and Beven, 2009, Waseem *et al.*, 2015). Streamflow downstream is subject to continuous fluctuations driven by climate change within Himalayan catchments (Adhikari *et al.*, 2022).

Various methods have been employed to simulate discharge at both gauged and ungauged sites. Among these, the drainage area ratio method is a simple, linear, and

straightforward approach used to estimate discharge at ungauged sites within single-stream networks. A river basin typically consists of one or more sub-basins and the transposition of flow data to ungauged sites is achieved through different methodologies. These include the regionalization of parameters using nearest neighbors, the donor technique, and regional averaging, often accomplished through hydrological simulation using multiple modeling approaches (Razavi and Coulibaly, 2016, Van Liew and Mittelstet, 2018).

Flow forecasting, involving the transfer of data from gauged stations to ungauged ones through parameter transfer, is a more refined technique compared to the basic drainage area ratio method, especially when it comes to transfer of flow data upstream to downstream and vice versa (Li *et al.,* 2019). By combining the drainage area ratio method with parameter transfers facilitated by a hydrological model, the estimation of discharge at ungauged basins becomes independent (Swain and Patra, 2017). Hydrological modeling presents a pragmatic alternative for predicting streamflow data and calibrating it at ungauged sites (Bergstrom, 2006). Fully distributed hydrological models are applicable for flow forecasting in areas where data is scarce and challenging to obtain, particularly in mountainous regions (Kayastha *et al.*, 2020, Terink *et al.*, 2015, Waseem *et al.*, 2015).

An ensemble approach combining the drainage area ratio, the inverse distance weighted method, and regional regression methods is more robust and effective than relying on a single traditional method (Waseem *et al.*, 2015). In cases where in-situ ground discharge stations are lacking, satellite products have been used to estimate time series discharge at ungauged river basins (Sichangi *et al.*, 2018). Additionally, precipitation estimates have been derived from satellite data (Talchabhadel *et al.,* 2021). Satellite altimetry, which provides data on daily river stage, longitudinal channel slope, and river width, has enabled the estimation of river discharge at poorly gauged and ungauged sites when coupled with hydrological models (Birkinshaw et al., 2014) (Huang et al., 2020). The prediction of runoff remains a significant challenge due to the heterogeneous topography of mountainous catchments, with varying catchment characteristics from gauged to ungauged sites (Zhang and Han, 2017). The average precipitation, slope, channel length and elevations are the main parameters for the estimation of ungauged catchments (WECS/DHM, 1990, Li *et al.*, 2019, DHM, 2004).

To address the limited availability of discharge gauge data, various areal precipitation products, such as the China Meteorological Forcing Datasets (CMFD), Climate Hazards

Group Infrared precipitation with stations (CHIRPS), and the Tropical Rainfall Measuring Mission (TRMM), have been utilized to simulate streamflow. However, uncertainty remains in streamflow predictions (Wu *et al.*, 2019). The flow duration curve, which estimates the magnitude and frequency of river flow based on limited data samples, is a reliable tool for regional and long-term analysis of flow duration at ungauged sites (Castellarin *et al.*, 2004). Parameter regionalization and hydrological model simulations have proven effective in predicting ungauged stream flow (Kim and Kaluarachchi, 2008, Panthi *et al.*, 2021). Radar-based rainfall estimates have been employed for flood forecasting and early warning systems using fully distributed models at both gauged and ungauged sites (Cole and Moore, 2009).

In the context of Himalayan River basins, it is essential to acknowledge the critical role of precipitation in streamflow contribution. Precipitation serves as the primary driver of hydrological regimes, significantly impacting water resource availability. This is especially evident in the Himalayan region (Raghunath, 2006). The variations in flow regimes, particularly during the summer season, are predominantly influenced by precipitation and temperature responses on discharge within Himalayan river basins.

The characteristics of rainfall are integral to watershed and drainage management, exerting a profound influence on hydrological systems in the central Himalayas. In the monsoon season, precipitation increases with elevation due to orographic effects and the rain shadow (Shrestha *et al.*, 2019a). Moreover, precipitation exhibits distinctive patterns in the middle mountain areas of the western and central high Himalayas, with increased precipitation in the lowland regions during the pre-monsoon season in the central Himalayas (Karki *et al.*, 2017, Shrestha *et al.*, 2019b).

The spatial and temporal patterns of precipitation have a direct impact on downstream discharges. Changes in the timing of water availability have far-reaching consequences for mountainous communities, downstream agriculture, hydropower, and ecosystems (Khanal *et al.*, 2021). Accurate prediction of climate change impacts in the Himalayas region is crucial, particularly with regard to its effects on water availability for downstream populations (Khadka *et al.*, 2014). In the 21st century, climate change continues to present ongoing challenges (Shrestha *et al.*, 2016). The reduction in glacier ice volume and variations in snow-glacier melt runoff contribute significantly to shifts in water resource availability within the Himalayan River basin. The diminishing glacier ice volume and the changes in snow-glacier melt runoff are substantial factors in this regard (Singh *et al.*, 2021).

Continuous and comprehensive hydrological flow information is imperative for present and future planning and management. Effective hydrological planning and management policies are essential for safeguarding human communities and facilitating the development of physical infrastructure.

2.4 Climate change

The warming of the Earth's climate system is not uniform, with both the atmosphere and ocean experiencing a temperature rise. Additionally, there has been a reduction in the amounts of snow and glaciers, leading to a rise in sea levels. This increase in temperatures has been documented, with the Earth's temperature rising by 0.85°C between 1981 and 2012 over the past three decades. Furthermore, each successive decade has been warmer than the preceding one, as reported in the Fifth Assessment Report of the Intergovernmental Panel on Climate Change (IPCC, 2014a). In accordance with the more recent AR6 Sixth Assessment Report from the IPCC, the global average temperature increased by 1.10°C during the decade from 2011 to 2020. Projections based on low and high-emission scenarios suggest that the temperature could increase by approximately 1.3°C to 5.7°C by the end of the century in 2100 (IPCC, 2021).

The Tibetan Plateau and High Mountain Asia are often referred to as the "Asian Water Tower" due to their substantial freshwater storage in the cryosphere, surpassing that of polar ice sheets (Immerzeel *et al.*, 2010, Yao *et al.*, 2012, Yao *et al.*, 2019). Climate change and intensified human activities have significant impacts on the Tibetan Plateau region (Yao *et al.*, 2019). Numerous studies have indicated a rising trend in temperatures within the Himalayan basins (Qi *et al.*, 2013, Hu *et al.*, 2012, Shrestha *et al.*, 1999). Recent research anticipates a temperature increase of 5.8°C in Nepal by the year 2100, with more pronounced warming at higher altitudes (Bartlett *et al.*, 2010).

The Himalayan region boasts the third-largest store of ice and snow globally, following only Antarctica and the Arctic. This region is highly vulnerable to global warming, as a substantial portion of the Himalayan River basins is covered by snow and glaciers. Therefore, it is particularly susceptible to the effects of climate change (Maskey *et al.*, 2011).

The climate, weather, and hydrology of the Hindu Kush Himalaya region have been subject to continuous change from the past to the future (Lutz *et al.*, 2016, Lutz and Immerzeel, 2013, Immerzeel *et al.*, 2010). Climate change's potential impact on glacier

and snow melt runoff is particularly evident in the Himalayan region (Immerzeel *et al.*, 2013, Lutz *et al.*, 2014). Climate change evaluations have been carried out considering both historical and future projections, using various scenarios and datasets to estimate surface air temperature, snow cover extent, and precipitation in High Mountain Asia, including the Tibetan Plateau (Lalande *et al.*, 2021). The IPCC has identified a series of Representative Concentration Pathways (RCPs) for climate change future projections by the end of the century, based on the Coupled Model Intercomparison Project Phase 5 (CMIP5) dataset (Van Vuuren *et al.*, 2011).

Many studies have investigated historical and projected climate change impacts on melting and streamflow components in the Himalayan region, at various scales from basin to sub-basin, and using a range of methodologies (Immerzeel and Droogers, 2008, Immerzeel *et al.*, 2013, Lutz *et al.*, 2016, Nepal, 2016). High Mountain Asia serves as a critical water reservoir, storing substantial quantities of snow and glaciers (Immerzeel *et al.*, 2010, Kandel *et al.*, 2021). The impacts of climatic change on regional hydrological systems in semi-arid Central Asia are expected to be significant (Sorg *et al.*, 2012, Unger-Shayesteh *et al.*, 2013, Su *et al.*, 2022, Siegfried *et al.*, 2012, Li *et al.*, 2020, Gulakhmadov *et al.*, 2020, Zhang *et al.*, 2020, Khanal *et al.*, 2021). A comprehensive understanding of the effects of atmospheric warming on land ice and snow cover dynamics in Central Asian high mountain areas has been achieved through recent research and innovative data sources (Rounce *et al.*, 2020, Hugonnet *et al.*, 2021, Immerzeel *et al.*, 2020, Huss and Hock, 2018). The impacts of climate change on catchment-scale hydrological processes can significantly affect streamflow (Huang *et al.*, 2020b). Significant plan modifications are required on current policy and strategy for river basin management according to the climate change scenarios (Dahri *et al.*, 2021). The climate projections are constrained by high variability and large spread and dispersion of the General Circulation model outcomes (Kraaijenbrink *et al.*, 2017, Lutz *et al.*, 2016). Climate change poses numerous challenges to water resources, infrastructure development, agriculture and livelihood of South Asia evaluated by using 13 GCMs of CMIP6 datasets projected a warmer 3-5^{0}C and wetter by 13-30% climate by the end of 21st century (Mishra *et al.*, 2020). The vegetation change distribution will be difficult to observe and quantify. They play an important role in the partitioning of available water to evaporation, runoff and infiltration (Lian *et al.*, 2021, Porporato *et al.*, 2004, Porporato and Yin, 2022).

Hydrological modeling plays a key role in assessing the short and long-term hydrological response to climate change in the Himalayan River basin. These calibrated hydrological models generate projections of future streamflow under various scenarios (Adhikari *et al.*, 2022). Climate change impacts hydrological responses in mountainous river basins on temporal and spatial scales, ranging from catchment to large river basin scales and from sub-daily to century-long timescales (Khanal *et al.*, 2021). Predicting the impacts of climate change in the Himalayas is of utmost importance due to its effects on water availability for downstream populations (Khadka *et al.*, 2014, Khanal *et al.*, 2021).

Projections indicate an increase in the annual mean temperature (1.7-3.6 ^{0}C) and precipitation (11-23%) by the end of the century (MoFE, 2019). According to the Department of Hydrology and Meteorology (DHM), the annual maximum temperature trend is 0.056 ^{0}C per year and minimum temperature trend is 0.02 0C per year during monsoon season and the precipitation trend is increasing trend in monsoon and pre-monsoon seasons (DHM, 2017). The Pre-monsoon precipitation is increasing in the low land and central Himalayas region while monsoonal precipitation is increasing in the middle mountain in the western and central high Himalayas region (Shrestha *et al.*, 2019b, Karki *et al.*, 2017).

Temporal variations in water availability in rivers are expected to impact downstream populations, even if the overall change in mean streamflow is not prominently noticeable in most basins (WECS, 2011). The flow regimes vary seasonally, particularly in summer, due to the influence of temperature and precipitation on discharge in the Himalayan basin (Adhikari *et al.*, 2022, Adhikari, 2014). Water resources in the Hindu Kush Himalaya region are strongly influenced by climate change, and the region's abundance of water, combined with its topography, makes it highly suitable for hydropower generation (Shrestha *et al.*, 2016). Although the average water availability is not anticipated to pose a significant challenge due to climate change, temporal variations are expected to increase in the future (Devkota and Gyawali, 2015). Precipitation patterns vary, with maximum precipitation occurring during the monsoon and post-monsoon seasons, while minimum precipitation is observed during winter. However, increased precipitation and runoff are expected during all seasons in trans-mountain Himalayan regions, leading to an increase in average streamflow in the Koshi river basin (Bharati *et al.*, 2014, Kaini *et al.*, 2021). The predicted increase in future precipitation and temperature will likely impact river discharge in Nepalese river basins

(Khadka *et al.*, 2014, Bajracharya *et al.*, 2018, Dahal *et al.*, 2020, Pandey *et al.*, 2020). Evapotranspiration, the process of transferring water from land surface and water bodies to the atmosphere, plays a crucial role in the partitioning of available water into evaporation, runoff, and infiltration (Rajib *et al.*, 2018, Shah *et al.*, 2021, Zhang *et al.*, 2020).

In conclusion, climate change significantly influences catchment-scale hydrological processes, particularly impacting streamflow. Hydrological modeling is an essential tool for assessing the short- and long-term hydrological responses to climate change in the Himalayan River basin. These models generate future streamflow projections, which are vital for understanding and adapting to the changing hydrological landscape in the region.

2.4.1 Climate model

Global climate models (GCMs) serve as the fundamental mathematical framework underpinning our understanding of Earth's climate system. These models are rooted in the principles of physics, specifically the conservation of mass, energy, and momentum, which govern the intricate interactions among various components of the climate system. By utilizing these fundamental relationships, GCMs enable us to simulate crucial aspects of Earth's climate, encompassing large-scale temperature and precipitation patterns.

In the realm of future climate projections, there are two primary categories of models: General Circulation Models (GCMs) and Regional Climate Models (RCMs). GCMs provide a comprehensive representation of the physical processes taking place within the land, ocean, atmosphere, and cryosphere. However, GCM datasets are characterized by their relatively coarse spatial resolution. Conversely, RCMs extend the capabilities of GCMs by incorporating the same physical processes while offering higher spatial resolution over smaller geographic regions. Nevertheless, it is important to note that RCMs contend with similar uncertainties as GCMs, even when operating at higher resolutions.

To bridge the spatial resolution gap, GCMs often employ statistical downscaling methods to refine their outputs, making them more relevant at regional scales. On the other hand, RCMs employ a technique known as dynamical downscaling, wherein climate models are nested within one another at varying resolutions. This nesting allows RCMs to achieve finer spatial resolutions within a domain already defined by a GCM.

While GCMs typically operate at spatial resolutions ranging from 100 to 250 kilometers, RCMs create nested domains within the GCM's framework, affording spatial resolutions that span from 10 to 50 kilometers. Both GCMs and RCMs, despite their distinctions, serve as valuable and effective tools for projecting future climate scenarios, contributing significantly to our understanding and prediction of climate trends.

2.4.2 Climate projection scenarios

Global Climate Models (GCMs) datasets are utilized in climate research to understand and project future climate conditions. These datasets are organized under the framework of the Coupled Model Intercomparison Project (CMIP) and encompass various phases, such as CMIP3 (Phase 3), CMIP5 (Phase 5), and CMIP6 (Phase 6). They serve as crucial components of the Intergovernmental Panel on Climate Change (IPCC) Assessment Reports, denoted as AR4, AR5, and AR6.

This CMIP3 released scenarios from the IPCC's Special Report on Emissions Scenarios (SRES) (AR4), CMIP5 uses Representative Concentration Pathways (RCP) (AR5) and CMIP6 (AR6) considers the impacts of socio-economy on greenhouse gas (GHG) emissions by linking with RCPs to SSPs (Shared Socioeconomic Pathways). The four Shared Socio-economic Pathways (SSPs) and Representative Concentration Pathways (RCPs) scenarios are investigated by SSP1 RCP2.6, SSP2 RCP4.5, SSP3 RCP6.5 and SSP5 RCP8.5 (Van Vuuren *et al*., 2011, Riahi *et al.*, 2017) that refer to the SSP126, SSP245, SSP370 and SSP585 scenarios. Scenarios generated by the Intergovernmental Panel on Climate Change (IPCC) Special Report on Emissions Scenarios (Nakicenovic and Swart, 2000) formed on the basis for climate model projections in Phase 3 of the Coupled Model Intercomparison Project (Meehl *et al.*, 2007) and their assessment in the IPCC AR4 Working Group I (IPCC, 2007c) and were used to model impacts on societies and ecosystems (IPCC, 2007a, IPCC, 2014a, IPCC, 2014b) and mitigation strategies (IPCC, 2001, IPCC, 2007b, IPCC, 2014c). In 2007, an expert meeting at Noordwijkerhout agreed on a process for the development of new climatic scenarios (Moss *et al*., 2010, Moss *et al.,* 2008). That process began with the identification of the Representative Concentration Pathways (Van Vuuren *et al.,* 2011), a set of four pathways of land use and emissions of air pollutants and greenhouse gases that spanned a wide range of future outcomes through 2100. The RCPs were the basis for climate model projections in CMIP5 (Taylor *et al*., 2012) and their assessment in the IPCC AR5

(IPCC, 2013). The initial design for CMIP 6 was published in 2014 and is open for new comments from scientific societies as well as the community (Meehl *et al.*, 2014**).** Climate change impacts on a basin scale future water availability requires humans, industries and irrigation (IPCC, 2022a). The applications of GCMs increasing rapidly to climate change study context AR6 based on ocean and cryosphere changes (IPCC, 2022b). CMIP 6 is the latest physical science working group WG1 report of climate change projections released in 2021 (IPCC, 2021) and Summary for Policymakers to Climate Change a Synthesis Report Contributed by Working Groups I, II and III released (IPCC, 2023).

CMIP3 (AR4) incorporated scenarios derived from the IPCC's Special Report on Emissions Scenarios (SRES). These scenarios were based on considerations of demography, technology, and socio-economic developments. The SRES scenarios were categorized into four groups: A1, A2, B1, and B2, serving as the basis for climate model projections. These scenarios included A2 and B2, used with the HADCM3 model, and A2 and A1B with the CGCM3 model. A1B represented a future with rapid economic growth, a declining global population, and the adoption of efficient technologies, maintaining a balance between fossil and non-fossil energy sources. A2 depicted a heterogeneous evolution with regional emphasis, slower technological advancement, and steady population growth. B2 highlighted local and regional governance solutions, with intermediate economic growth, a focus on environmental protection, and social equity at regional and local levels (IPCC, 2000).

CMIP5 (AR5) introduced the concept of Representative Concentration Pathways (RCPs) to serve as the foundation for long-term and near-term climate modeling experiments (Van Vuuren *et al.*, 2011). These four RCPs encompassed a range of radiative forcing values for the year 2100, from 2.6 to 8.5 W/m^2. Climate modelers employed these RCPs to produce climate scenarios, enabling parallel experiments in tandem with the development of emission and socio-economic scenarios (Moss *et al.*, 2010). The four selected RCPs were considered to be representative of the literature and included one mitigation scenario (RCP2.6), two medium stabilization scenarios (RCP4.5/RCP6) and one very high baseline emission scenario (RCP8.5) (Van Vuuren *et al.*, 2011). RCPs 8.5 stands for rising radiative forcing pathways leading to 8.5 W/m^2 (1370 ppm CO_2 eq) by 2100, RCPs 6 stands for stabilization without overshoot pathway to 6 W/m^2 (850 ppm CO_2 eq) at stabilization after 2100, RCPs 4.5 stands for stabilization without overshoot pathway to 4.5 W/m^2 (650 ppm CO_2 eq) at stabilization after 2100,

RCPs 2.6 stands for peak in radiative forcing at 3 W/m^2 (490 ppm CO_2 eq) before 2100 then declines (the selected pathways decline to 2.6 W/m^2 by 2100.

CMIP6 (AR6) further expanded the scenario framework by introducing five Shared Socio-economic Pathways (SSPs), which were linked to the RCPs. The SSPs addressed different challenges for mitigation, resource efficiency, adaptation, and development. For instance, SSP1 emphasized low challenges for mitigation, resource efficiency, and rapid development, while SSP3 posed high challenges for mitigation, regionalized energy and land policies, and slow development. SSP4 featured low mitigation challenges but a global high technology economy, alongside regional low technology economy adaptations, while SSP5 involved high challenges for mitigation, resource and fossil fuel-intensive development, and low adaptation to rapid development. SSP5 stands for fossil fuel development, SSP4 for Inequality, SSP3 for Regional Rivalry, SSP2 for Middle of the road and SSP1 for Sustainability (O'Neill *et al.*, 2016).

These scenarios have been instrumental in climate studies conducted in various regions, such as the Himalayas River basin. Researchers have utilized SRES scenarios in their work, as demonstrated by Khadka *et al.* in 2014, Devkota and Gyawali in 2015, and others. Additionally, RCP scenarios have been employed in research, including studies by Bajracharya *et al.* in 2018, Adhikari *et al.* in 2022, and others. Furthermore, SSP scenarios have found application in research, exemplified by works from Lalande *et al.* in 2021, Mishra *et al.* in 2020, and Balu *et al.* in 2023. The evolution from SRES to RCP and subsequently to SSP scenarios reflects the dynamic nature of climate modeling and projections. These scenarios have become increasingly integral to the latest climate research, offering valuable insights into the diverse facets of climate change. Notably, the three generations of CMIP models, namely CMIP 1, 2, and 3, emphasize the importance of these scenarios and their correlations (Tian and Dong, 2020).

2.4.3 Bias correction

General Circulation Models (GCMs) frequently exhibit multiple biases in hydro-meteorological analysis, necessitating the application of bias correction methods. These methods typically employ statistical techniques and measurements, utilizing observed and simulated datasets of hydro-meteorological parameters to rectify projections in model runs. The selection of bias correction methods can be challenging due to their varying strengths and weaknesses, with their effectiveness hinging on the specific

objectives of the study, including parameters such as rainfall, temperature, runoff, and the chosen time period (daily, monthly, seasonal, or annual).

Several bias correction techniques are available, including linear scaling, local intensity scaling, power transformation, distribution mapping, and the delta change approach. GCMs consistently exhibit the most biases (Wilby and Harris, 2006, Nóbrega *et al.*, 2011) in precipitation (Dibike and Coulibaly, 2005), attributed to incomplete knowledge of global geophysical processes and scenario uncertainties related to future projections (Ghosh and Mujumdar, 2007, Themeßl *et al.*, 2012). A multitude of bias correction methods exists, ranging from scaling factors (Lenderink *et al.*, 2007, Chen *et al.*, 2011) to more complex non-parametric methods (Ghosh and Mujumdar, 2007), probability mapping (Teutschbein and Seibert, 2010), and imprecise mapping. The Delta change approach, Mean bias correction, and Quantile Mapping are commonly employed bias correction methods for climate change analysis (Maraun, 2016, Maraun and Widmann, 2018, Teutschbein and Seibert, 2013).

For the correction of daily temperature and precipitation data, the Mean bias correction method has been widely utilized (Mahmood and Babel, 2013). However, GCMs face significant challenges in minimizing biases in hydro-meteorological analysis, necessitating the identification of their sources and the quantification, mixing, and tracking of data analysis uncertainties (Themeßl *et al.*, 2012). Bias correction methods serve to mitigate systematic errors in climatic models, thereby improving their accuracy (Teutschbein and Seibert, 2010). Commonly employed bias correction methods for GCM rainfall scenarios include constant scaling (CS), quantile scaling (QS), quantile mapping (QM), monthly bias correction (MBC), simple nested bias correction (SNBC), and nested bias correction (NBC) (Johnson and Sharma, 2012). These methods are particularly useful for correcting daily rainfall data used to simulate runoff, thereby reducing biases in the process (Christensen and Lettenmaier, 2007). Extensive research has been conducted to address bias correction in GCMs for hydrological simulations. Nonetheless, the impact of climate change on hydrological regimes using GCM CMIP6 data remains largely unknown in the Tamakoshi river basin. The temporal variation of climate change on water balance components is not uniform across the entire basin, affecting the contributions of snow and glacier melt, rain runoff, and baseflow, which vary based on physiographic zones. Consequently, the flow regime of rivers and their connected stream networks in the basin remains uncertain.

This study aims to assess the performance of the SPHY, HBV , and HEC HMS models in the complex river system of the Tamakoshi river basin, taking into account river discharge, melt contributions, and ungauged simulations. Furthermore, the research investigates the impacts of climate change on the hydrological regimes of water balance components. In the context of a trans-boundary river system in the southern slopes of the central Himalayas, hydrological simulations are imperative due to the absence of adequate climate and discharge monitoring stations. The evolving climate, hydrological structures, and infrastructure development have profound effects on river discharge, its perennial flow, and water availability. This research contributes to a better understanding of the characteristics and variations in streamflow, aiding in the planning, development, and management of water resource projects.

CHAPTER 3

3. MATERIALS AND METHODS

3.1 Study area

Tamakoshi river is a transboundary Himalayan River basin which is one of the main tributaries of the Koshi river basin system located in the southern slope of central Himalayas in eastern Nepal. Tamakoshi river basin is a transboundary Himalaya River basin where 1444.57 km^2 areas lie in Chinese territory. Tamakoshi river basin geographically lies in the Dolakha and Ramechhap districts on the political boundary of Nepal. The basin occupies 2933.29 km^2 at Busti gauging station. Tamakoshi river basin is located at $27^0 20^{'}$ N to $28^0 20^{'}$ N and $85^0 40^{'}$ E to $86^0 40^{'}$ E elevation at Busti gauging station ranging from 849 masl to 6945 masl. This basin runoff and water balance is dominated by the monsoon rainfall. The geographical location of the research area is shown in Figure 2 with hydro-meteorological stations.

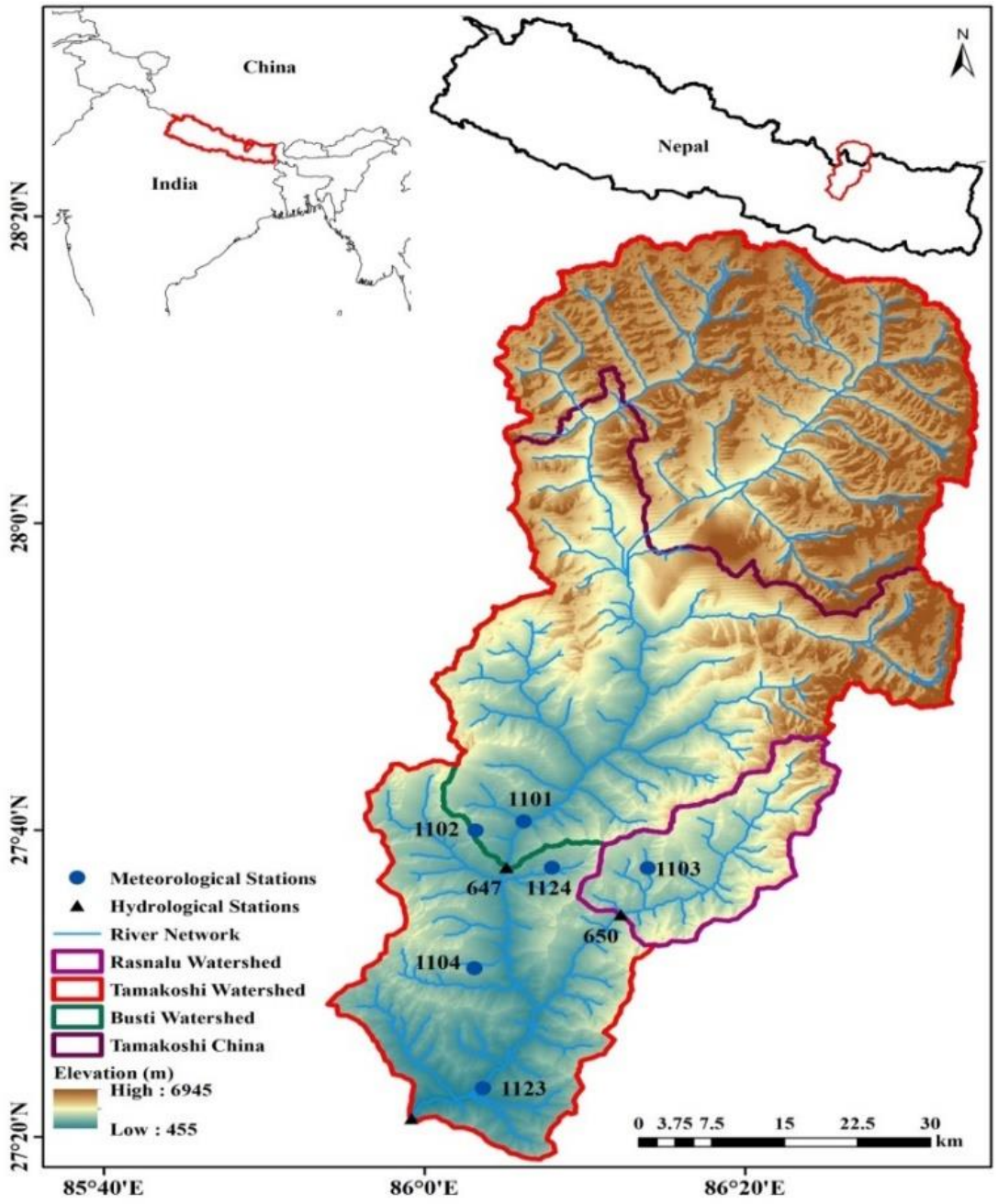

Figure 2: Study area with hydro-meteorological stations in Tamakoshi river basin.

3.2 Hypsometric curve

The aspect, elevation and area required to model simulation in non-vegetation glaciated and vegetation non-glaciated regions. The basin area is categorized into 13 and 14 elevation zones at 500 m high intervals at the catchment setting. Characteristics of precipitation (Rain or Snow) depend on the elevation and the threshold air temperature. The temperature and precipitation need to be corrected factor as PCALT 10-25 % and TCALT 6.5 ^{0}C/km accordingly elevation increment factor of HBV model. The area

elevation distribution hypsometric curve is shown in Figure 3 showed the total area to aspect wise East-west horizontal is 1327.85 km^2, North oriented area occupied 618.64 km^2 and South oriented area occupied in 901.62 km^2 among them 253.59 km^2 area covered by the glacier in Tamakoshi river basin.

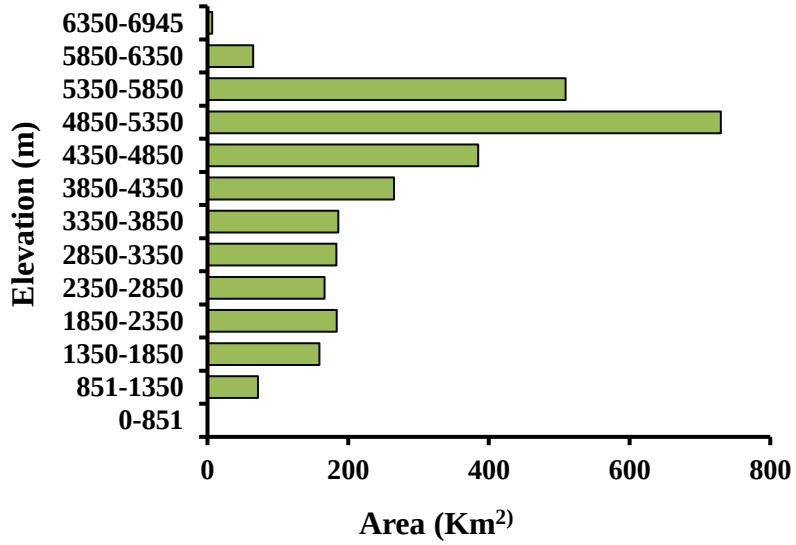

Figure 3: Hypsometric curve of the Tamakoshi river basin.

3.3 Observed precipitation, discharge and temperature characteristics of Tamakoshi river basin

An extensive analysis of observed data, encompassing precipitation, discharge, and temperature, was conducted on both an annual and monthly basis spanning the period from 1991 to 2020. This analysis was based on data collected from various meteorological and hydrological stations within the Tamakoshi river basin, which were made available by the Department of Hydrology and Meteorology (DHM), a division of the Government of Nepal.

Figure 2 presents a comprehensive overview of the station network, which comprises six meteorological stations and two hydrological station. Within this basin, the average annual precipitation stands at 1610 mm, while the average annual discharge amounts to 1542 mm. A more detailed breakdown reveals the following annual precipitation figure 4B showed at specific stations: Station 1103 recorded the highest with 2479 mm, followed by Station 1102 at 2148 mm, Station 1124 at 2056 mm, Station 1101 at 1218 mm, Station 1123 at 902 mm, and the lowest annual precipitation was observed at Station 1104 with 859 mm, as illustrated.

Examining the monthly variations, it is observed that Figure 4A showed the month of March consistently receives the lowest discharge, while August consistently registers the highest discharge levels. Notably, figure 4A showed the month of July experiences the highest levels of precipitation, while December consistently exhibits the lowest levels of precipitation within the Tamakoshi river basin.

Furthermore, the analysis of temperature data reveals that the mean temperature in January consistently exhibits the lowest values, while the mean temperature in June consistently reaches its peak. These observations were recorded at Station 1103 within the Tamakoshi river basin, as illustrated in Figure 4C.

It is essential to recognize that the climate in this basin exhibits a diverse range of characteristics. It is subtropical at lower elevations, transitioning to tundra conditions at higher elevations, indicating the dynamic climatic variability within this region (Karki *et al.*, 2016).

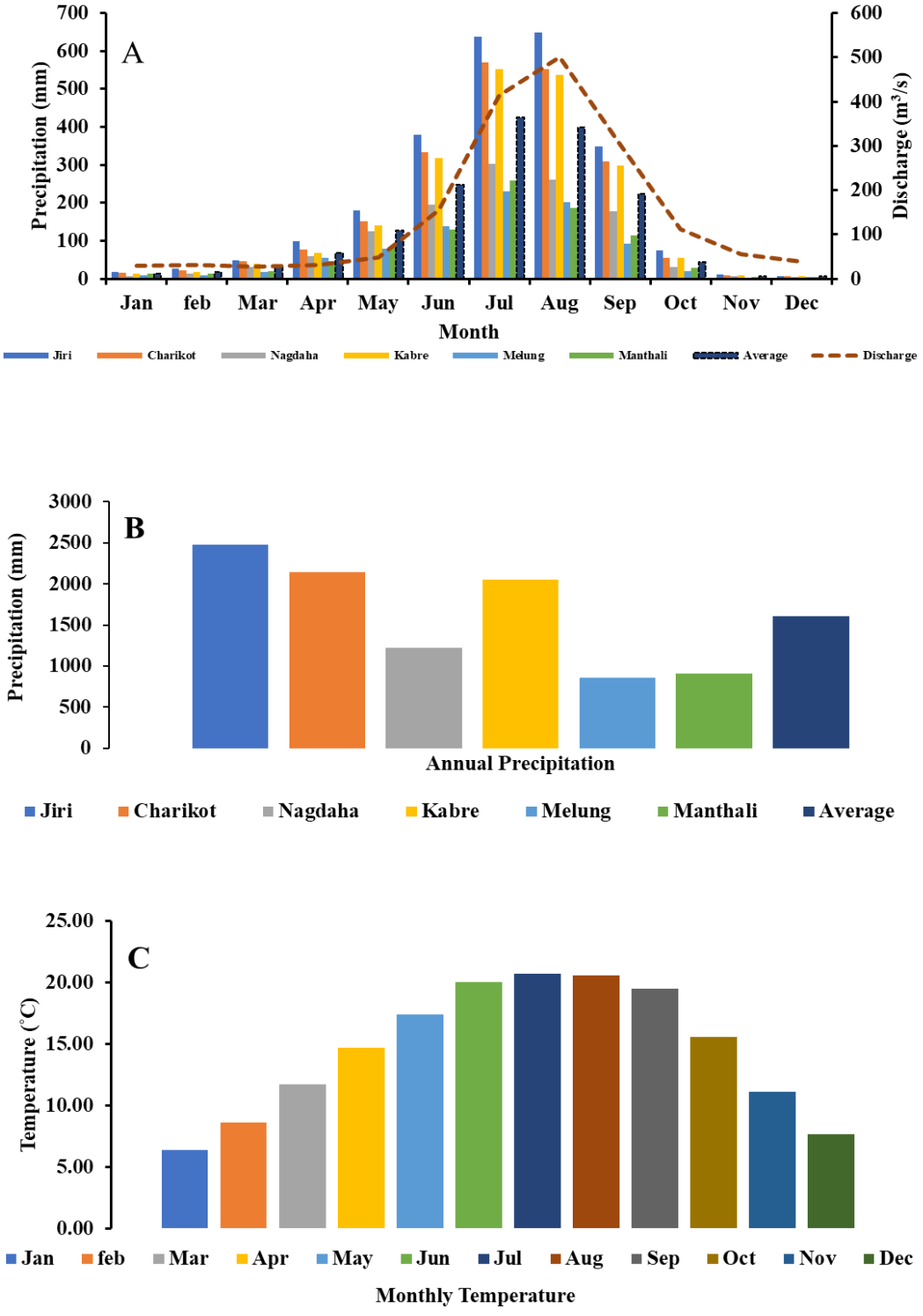

Figure 4: A) observed stations and average area monthly precipitation and discharge, B) stations average annual precipitation and C) monthly mean temperature of Tamakoshi river

3.4 Input data availability

The SPHY, HBV light and HEC HMS models predominantly rely on two categories of data layers i.e. static and dynamic datasets. The static datasets encompass land use/land cover (LULC) maps, soil maps, and digital elevation models, while the dynamic datasets consist of meteorological parameters such as precipitation, temperature (average, minimum, and maximum), and discharge. The Globecover dataset for the year 2009, which is openly accessible at http://due.esrin.esa.int/page_globcover.php, is employed as a static resource. Additionally, the digital elevation model (DEM) sourced from the Shuttle Radar Topographic Mission (SRTM) with a spatial resolution of 3 arc seconds and hydrologically conditioned data, available at http://hydrosheds.cr.usgs.gov/, is integrated into the model, as indicated in Appendix (Table A1). To further enhance the model's accuracy, the outlines of glaciers are obtained from the RGI 6.0 South Asia East dataset (Consortium, 2017). The dynamic component of the models relies on observational data, specifically precipitation and discharge records obtained from ground station datasets, meticulously collected by the Department of Hydrology and Meteorology (DHM). For the purpose of data filling, a normal ratio method is employed for the rainfall data. In addition to the existing six stations, an extra three stations are included in the analysis. To ensure the temperature data is appropriately adjusted, a temperature lapse rate is applied. Furthermore, evapotranspiration datasets are generated using the Blaney–Criddle equation, utilizing the mean monthly temperature data from Jiri. The climatic and hydrological data, as outlined in Appendix (Table A2), play a pivotal role in this research. The geographical locations corresponding to these datasets are depicted in Figure 2 for reference.

3.5 Climate change projection data

The future climate remains uncertain, contingent upon anthropogenic activities, socioeconomic development, and technologies aimed at mitigating greenhouse gas emissions in the Earth's atmosphere. This uncertainty necessitates the use of daily bias-corrected data for precipitation, maximum and minimum temperatures at a spatial resolution of 0.25°. This data is crucial for South Asian countries, including India, Pakistan, Bangladesh, Nepal, Bhutan, and Sri Lanka, as well as for 18 river basins within the Indian subcontinent.

The development of this bias-corrected dataset involved the application of Empirical Quantile Mapping (EQM) to both historical (1951-2014) and projected (2015-2100)

climate data. These projections encompass four climatic scenarios, namely SSP126, SSP245, SSP370, and SSP585, utilizing output from CMIP6-GCMs datasets, as detailed by Mishra *et al.* in 2020. The accuracy of this bias-corrected dataset was assessed by comparing it with observations, both for mean values and extremes of precipitation, maximum and minimum temperatures.

These bias-corrected projections derived from CMIP6-GCMs datasets hold considerable potential for climate change impact analyses in South Asian countries and hydrological impact assessments in the river basins of the Indian subcontinent in South Asia. The data encompasses spatial and temporal projections from ACCESS CM2, CanESM5, MPI ESM1 2HR, and NorESM MM spanning three scenarios, including historical references for bias correction, SSP2-4.5 (a medium stabilization scenario without an overshoot pathway to 4.5 W/m²), and SSP5-8.5 (an extreme emission scenario with a rising radiative forcing pathway of 8.5 W/m²). These projections have wide-ranging effects on local topography and global climatic conditions.

The daily precipitation and maximum and minimum temperatures were sourced from CMIP6-GCMs datasets, available via https://esgf-node.llnl.gov/search/cmip6/. These variables and scenarios were exclusively accessible from these GCMs datasets, and the scope of bias correction was consequently limited to these models. The spatial resolutions of these datasets are provided in the Appendix (Table A3). These variables were selected for the historical period (1850-2014), SSP245 scenario (2015-2100), and SSP585 scenario (2015-2100) under the r1i1p1f1 initial condition in daily time series. The scenarios in CMIP6 combine Shared Socioeconomic Pathways (SSP) with target radiative forcing levels after the 21st century. To ensure consistency, CMIP6 GCMs re-gridded all variables to a spatial resolution of 1°. The effect of this re-gridding, achieved through bilinear interpolation, was verified by comparing the gridded datasets against raw data, focusing on the all-India mean values of precipitation, maximum, and minimum temperatures.

It is well-acknowledged that outputs from various atmospheric parameters, including maximum and minimum temperatures and precipitation, acquired from GCMs often exhibit systematic biases. To produce reliable estimates for climate change impact assessments at regional and local scales, bias correction is essential. This correction involves employing statistical transformations to establish a function that maps the model output to a new distribution, aligning it with observations, a concept elucidated by Piani *et al.* in 2010.

For the Tamakoshi river basin, four Coupled Climate Model (CCM) datasets spanning 1991-2014 were employed as reference data. These were used to facilitate bias correction for near-future projections covering 2025-2049, mid future projections spanning 2050-2074, and far-future projections extending to 2075-2099. This approach aids in assessing the potential impact of climate change over various timeframes within the Tamakoshi river basin.

3.6 Hydrological modelling

3.6.1 Spatial Process in HYdrology (SPHY)

The Spatial Process in HYdrology (SPHY) model, as conceptualized by Terink *et al.* in 2015, is a dynamic glacier-based module that operates as a fully distributed hydrological model. It is designed to simulate hydrological processes across a broad range of spatial scales, encompassing large-scale basins, sub basins, and regional hydrology. This model employs a leaky bucket type water balance framework and effectively captures the intricacies of cryospheric hydrology, which includes integrated processes such as rainfall runoff, cryospheric interactions, evaporation, and soil hydrology. Importantly, the SPHY model operates with a high degree of flexibility, allowing it to adapt to different scales and conditions.

In the SPHY model, daily input parameters are employed to calculate the total runoff for each grid cell individually. This approach ensures a comprehensive evaluation of hydrological processes within the model's domain. The model maintains distinct storage components for soil water, dynamic snow, and groundwater in each grid cell. Specifically, it calculates snow melt runoff from snow covered grid cells, designating the runoff from glacier surfaces as glacier melt runoff. To compute snow melt and glacier melt runoff, a degree day approach calibrated for melt rates is employed. Snow melt is systematically calculated and subtracted from the snow storage during each time step. The model also addresses the refreezing of meltwater within the snowpack. When the accumulated snow melt surpasses a predefined storage threshold, snow melt runoff is generated.

Rainfall runoff within the SPHY model is determined by summing the contributions of surface runoff from rainfall and lateral flow from the soil water storage layer. Surface runoff calculation relies on saturation excess runoff principles. The resulting soil moisture, contingent on soil properties, is subject to processes like evapotranspiration,

capillary rise, and the land use type. Any remaining moisture contributes to river discharge through lateral flow or surface runoff, as part of the model's comprehensive hydrological representation.

Furthermore, the model accounts for groundwater storage and its gradual release as baseflow runoff. To ensure efficient routing of runoff, each runoff component is directed downstream using a straightforward recession coefficient. Meteorological stations and outlets are strategically positioned within the delineated watersheds of the cloned Digital Elevation Model (DEM). To interpolate meteorological data, bilinear interpolation methods are employed for station locations. Outlets must be placed within each subbasin and positioned on the river network to facilitate the model's accurate functioning. Accuflux, a function integrated into the SPHY model, serves the critical role of determining flow accumulation, particularly with regard to the total discharge, at the outlets situated within the river network. This feature enhances the model's ability to accurately assess flow dynamics and discharge patterns.

In summary, the SPHY model serves as a versatile and comprehensive hydrological tool that excels in simulating a wide range of hydrological processes at varying spatial scales. It incorporates sound principles and approaches to replicate the complexities of cryospheric hydrology, rainfall-runoff, and related phenomena. The model's efficiency in routing runoff and its integration of meteorological data and outlet locations ensure its utility in assessing flow dynamics within delineated watersheds. Accuflux, as a crucial component, contributes to the model's accuracy in determining flow accumulation and total discharge at specific outlets along the river network.

3.6.1a Runoff routing

The routing of streamflow deals with the transportation of water over a network of connected open-channel systems. Because flow in open channels is unstable, streamflow routing often requires the use of complex partial differential equations. Inside the SPHY model, the calculation is figuring out the total amount of water that leaves each cell, one after the other downstream.

For each cell under consideration, the SPHY model uses an integrated function within PCRaster called "accuflux" to quantify the cumulative runoff originating from upstream cells. This calculation includes the particular runoff produced inside the cell. Furthermore, a flow recession coefficient, represented by the symbol "kx(–)," is

included in the SPHY model to account for flow travel time that is impacted by channel friction. River flow in the context of the SPHY model is determined by applying the flow recession coefficient (Kx), which is controlled by the following three equations 1,2 and 3.

$$Q_{tot*} = \frac{Q_{Tot}.0.001.A}{24.3600} \quad (1)$$

$$Qaccu, t = accuflux(Fdir, Qtot*) \quad (2)$$

$$Qrout, t = (1 - Kx).Qaccu, t + kx.Qrout, t - 1 \quad (3)$$

where, Q_{tot*} (m^3/s) the specific runoff on day t, QTot the specific runoff in mm on day t, A (m^2) the grid-cell area, Qaccu;t (m^3/s) the accumulated streamflow on day t without flow delay taken into account, Qrout;t (m^3/s) the routed streamflow on day t, Qrout;t-1 (m^3/s) the routed streamflow on day t-1, F the flow direction network, and kx (–) the flow recession coefficient. kx has values ranging between 0 and 1, where values close to 0 correspond to a fast-responding catchment, and values approaching 1 correspond to a slow-responding catchment.

3.6.2 HBV light

The HBV (Hydrologiske Byrån avdeling for Vattenbalans) precipitation-runoff hydrological model, developed by the Swedish Meteorological and Hydrological Institute (SMHI) in Sweden, has a notable history. First introduced in the 1970s at SMHI, the HBV model found its initial application in Norway for runoff forecasting in 1974. Over the past half-century, the HBV model has served as a cornerstone for catchment-based hydrological modeling (Seibert and Bergström, 2022). Built upon a conceptual framework, the HBV model focuses on simulating basin hydrology, with a particular emphasis on estimating snow melt and glacier melt, employing the degree-day model approach.

The HBV model, a semi-distributed conceptual model, typically operates on daily timesteps. Its functioning revolves around the utilization of evaporation, temperature, and precipitation data inputs to simulate streamflow (Vormoor *et al.*, 2018). Within this modeling system, the HBV model effectively captures and represents various hydrological processes, including snow accumulation, glacier melt, snow melt, as well as the storage of moisture in soil and groundwater. Furthermore, it models runoff at both basin and sub-basin scales.

The components of the HBV model encompass distinct routines, each designed to address specific aspects of hydrology. These include the snow routine, glacier routine, routing routine, response routine, and soil moisture routine. The degree-day approach is employed to simulate snow melt and glacier melt. Soil water dynamics and evaporation are accounted for, along with groundwater, described using three linear reservoir equations. Channel routing is achieved through a triangular weighting function (Seibert, 1997). The HBV model has established a strong track record of success, having been applied globally to assess various hydrological phenomena and to investigate the impacts of climate change on river hydrology. It offers a reliable and straightforward framework for capturing runoff-generating processes and, notably, does not demand an extensive array of data inputs. This versatility has made the HBV model an effective tool for hydrological research in the Himalayan regions.

In the context of the HBV model, calibration and sensitivity analysis of selected model parameters are essential. Parameter values are initially estimated and subsequently fine-tuned through calibration. Within the model, the only physical features that require specification are the mean catchment elevation and the elevations of precipitation and temperature stations. Among the different variants of the HBV model, this research employs HBV light 4.0, as presented by Seibert and Vis in 2012, for streamflow simulation.

The model setup for the HBV model is applied at two specific locations: the Busti gauging station and Benighat. It simulates daily streamflow using daily data for rainfall, temperature, and potential evapotranspiration (PET) as input variables. At both locations, the HBV model is configured with elevation zones, featuring 13 zones at the Busti gauging station and 14 zones at Benighat. These zones are separated by 500-meter elevation differences, and a contributing area approach is employed in the soil routing routine when the model operates in distributed mode. Incorporating height increment correction factors denoted as PCALT (10%) and TCALT (0.00065/m), is essential for adjusting temperature and precipitation data. These correction factors ensure the accuracy of model outputs. Moreover, the HBV model can effectively simulate discharge at both glacierized and non glacierized zones, allowing for differentiation based on elevation and orientation within the basin area. The HBV model offers a robust and accessible tool for understanding and simulating the dynamics of streamflow, contributing to the analysis of hydrological processes in various contexts. The general

structure of the HBV model is visually depicted in Figure 5, alongside the relevant model parameters.

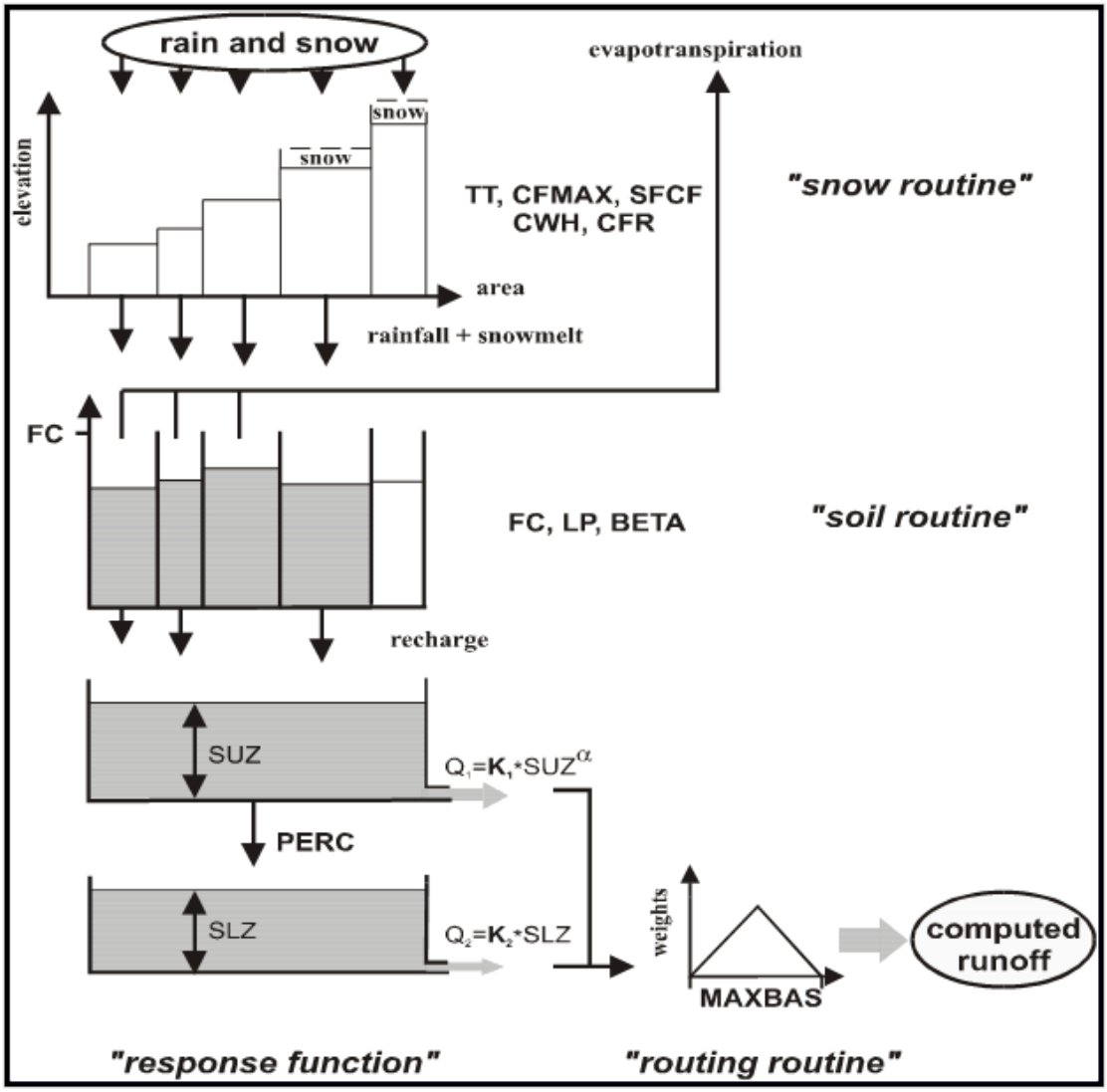

Figure 5: General structural overview of HBV model.

The applications HBV model

- To generate the runoff time from the metrological data (precipitation, air temperature)
- To determine the effect of the changes in the catchment.
- To generate continuous time series discharge data (or fill missing records)
- To study water balance components.
- To compute design floods for projects
- To simulate discharge with climate change scenarios
- Generation of the synthetic data runs for civil engineering work and
- other applications.

3.6.3 HBV model routine

The glacier, snow routine, response routine, routing routine, and soil moisture routines are among the model routines included in the HBV model. The model procedures that generate runoff are liable for the corresponding parameters. The following section presents the detailed HBV model structures:

3.6.3a Snow routine

The accumulation of snow occurs when temperatures drop below the threshold temperature (TT), which is typically close to 0°C. Snow melt commences when temperatures rise above TT, and this is calculated using a simple degree day method, denoted as degree-Δt for non-daily time steps. The rate of snow melt, denoted as meltwater, can be determined by the formula equation 4 follows:

$$meltwater = CFMAX(T - TT)(mm\Delta^{-1}) \quad (4)$$

Here, CFMAX varies normally between 1.5 and 4 mm $^{o}C^{-1}$ day^{-1} (in Sweden), with lower values for forested areas. As an approximation, the values 2 and 3.5 can be used for CFMAX in forested and open landscapes respectively. The snowpack retains meltwater until it reaches a specific threshold, denoted as CWH, which is typically set at 0.1 times the water equivalent of the snowpack. When temperatures drop below TT, the previously melted water refreezes. This refreezing of meltwater can be calculated using equation 5 the formula:

$$refreezing\ meltwater = CFR * CFMAX(TT - T) \quad (5)$$

The degree-Δt factor, represented by SP, plays a pivotal role in this process. When SP is set to 0, it indicates a constant degree-Δt factor. Values of SP greater than 0 correspond to a seasonal variation of the degree-Δt factor, with its peak occurring during the summer in the Northern Hemisphere. Conversely, values smaller than 0 results in a seasonal variation of the degree-Δt factor, with the optimum during the summer in the Southern Hemisphere. For a value of 1 (or -1), the degree-Δt factor varies between 0 in winter and 2 times CFMAX in summer, maintaining an average degree-Δt factor equal to CFMAX. Furthermore, all precipitation that is simulated as snow is subject to adjustment using a correction factor denoted as SFCF. These calculations are conducted

individually for each elevation and vegetation zone. To summarize, the key parameters involved in this snow melt and refreezing process are as follows:

CFMAX = degree-Δt factor (mm $^{o}C^{-1}$ Δt^{-1})
TT = threshold temperature (^{o}C)
SP = Seasonal variability in degree-Δt factor (-)
SFCF = snowfall correction factor (-)
CWH = water holding capacity (-)
CFR = refreezing coefficient (-)

3.6.3b Glacier routine

The computation of glacier melt employs the degree-day model concept approach, and the resultant meltwater is added to the glacier's water content. During each time step, a minor fraction denoted as KSI, of the simulated snow storage, is transformed into glacier ice. The parameter SP, with values ranging from less than 0 to larger than 0, governs the seasonal variation in the degree-Δt factor. When SP equals 0, a constant degree-Δt factor is assumed. Values of SP greater than 0 correspond to a seasonally varying degree-Δt factor with its peak in the summer in the Northern Hemisphere, while values smaller than 0 lead to a seasonally varying degree-Δt factor with its maximum in the summer in the Southern Hemisphere. When SP equals 1 (or -1), the degree-Δt factor oscillates between 0 in winter and 2 times CFMAX in summer, resulting in an average degree-Δt factor equal to CFMAX. The degree-day factor, CFMAX, is modified by a glacier correction factor (CFGlacier) and further multiplied or divided by a slope correction factor (CFSlope) depending on whether the slope is oriented to the north or south, respectively. These calculations are performed independently for each elevation and vegetation zone. The relationship between glacier water content and outflow varies over time to reflect the seasonal evolution of the subglacial drainage system (Stahl *et al.*, 2008). In the glacier routine module, the following parameters play a key role in determining glacier melt equation 6 and outflow:

$$Q_g = (KG_{min} + dKG * e^{(-AG*SWE)}) * S \qquad (6)$$

Here, SWE represents the water equivalent of the snowpack on top of the glacier, and S signifies the liquid water content of the glacier. The critical parameters governing the glacier model include:

CFMAX= degree-Δt factor (mm ^{0}C-1 Δt-1)

TT = threshold temperature (^{o}C)

SP = Seasonal variability in degree-Δt factor (-)

CFGlacier = Correction factor glacier (-)

CFSlope = Correction factor slope (-)

KGmin = Minimum outflow coefficient (t-1)

KSI = Snow to Ice conversion factor (Δt-1)

AG = Calibration parameter (mm-1)

dKG = Maximum minus minimum outflow coefficient (t-1)

Dynamic glacier

For simulating glacier melt, the HBV model provides a Glacier Profile file. Throughout the simulation period, the extent of the glaciers will be changed. Prior to the commencement of the actual model run, a lookup table is constructed using the Δt-parameterization method as described in (Huss *et al.*, 2010), based on the Glacier Profile file. Wideness scaling is added to the Δt-parameterization approach in order to reduce the glacier area of the distinct elevation bands (as indicated in the glacier profile) with decreasing thickness. Throughout the real model simulation, this lookup table is utilized. Every hydrological year, the corresponding glacier areas are chosen from the lookup database and applied to the various elevation zones depending on the percentage of glacier volume compared to the initial glacier volume (Seibert *et al.*, 2018). The spatial distribution of the glacier is contained in the Glacier Profile file, which is also utilized to create a lookup table that discusses the relationship between glacier area and glacier mass balance. The Glacier Routine uses the lookup table to update the glacier extent based on the simulated change in glacier mass balance after each hydrological year.

3.6.3c Response routine

The model of a single linear reservoir is a simple description of a catchment where the discharge runoff Q(t) at time t is supposed to be proportional to the water storage S(t). Figure 6 represents the response routine with a single linear reservoir.

PERC = threshold parameter (mm Δt^{-1})

UZL = threshold parameter (mm)

Alpha = non-linearity coefficient (-)

K2 = storage (or recession) coefficient (Δt^{-1})

K1 = storage (or recession) coefficient (Δt^{-1})

K0 = storage (or recession) coefficient (Δt^{-1})

Figure 6: A response routine with single linear reservoir with outlet.

Q = outflow (mm Δt-1)

S = storage (mm)

K = storage (or recession) coefficient (Δt-1)

t = time (Δt)

A realization of a single linear reservoir is a box with a porous outlets, thus obtaining Equation (7) from Darcy's law.

Water balance of the catchment in HBV using equation (8) as follows:

$$P(t) = E(t) + Q(t) + \frac{d*S(t)}{dt} \quad (8)$$

Ignoring precipitation and evapotranspiration gives

$$0 = Q(t) + \frac{d*S(t)}{dt} \quad (9)$$

and together with (7) the differential equation

$$0 = \frac{d}{dt}\frac{Q(t)}{k} + Q(t) \quad (10)$$

with the solution function

$$Q(t) = Q(t_0) * e^{(t_0 - t)k} \quad (11)$$

Recession Analysis:

If ln Q is plotted in Figure 7 against time during a dry period, the slopes of the hydrograph at different runoff values provide good firstly estimates of the response-function parameter

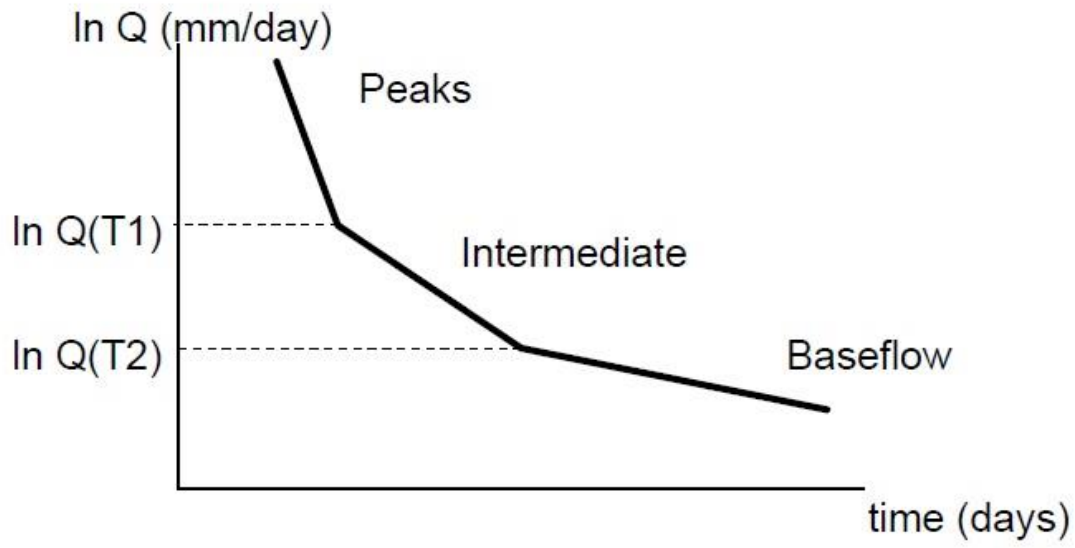

Figure 7: Schematic representation of recession of response function parameters.

Slope of the recession:

Intermediate: K1 + K2

Peaks: K0 + K1 + K2

Baseflow: K2

Thresholds:

Q(T2): PERC

Q(T1): PERC+K1·UZL

3.6.3d Soil moisture routine

The soil's capacity to retain moisture, as depicted in Figure 8, is determined by the field capacity (FC) parameter, which can be either at its maximum or minimum value. Infiltration into the soil is contingent upon the ratio between the current soil moisture level (Soil Moisture) and the field capacity (FC), and this relationship is governed by a non-linear function. The distinctive infiltration characteristics of various soil types are influenced by the BETA parameter, which plays a key role in determining how much water is allowed to pass through to subsequent stages, even when the soil moisture is considerably less than the field capacity. The actual evaporation process is calculated within the soil moisture management routine and is dependent on the LP values, which

define the fraction of FC above which the actual evaporation equates to the potential evaporation. When the actual soil moisture (Soil Moisture) falls below the LP value but remains above FC, a linear reduction of potential evaporation commences.

To clarify the terms used:

FC = maximum soil moisture storage (mm)

BETA= parameter that determines the relative contribution to runoff from rain or snow melt (-)

LP = soil moisture value above which AET reaches PET (-)

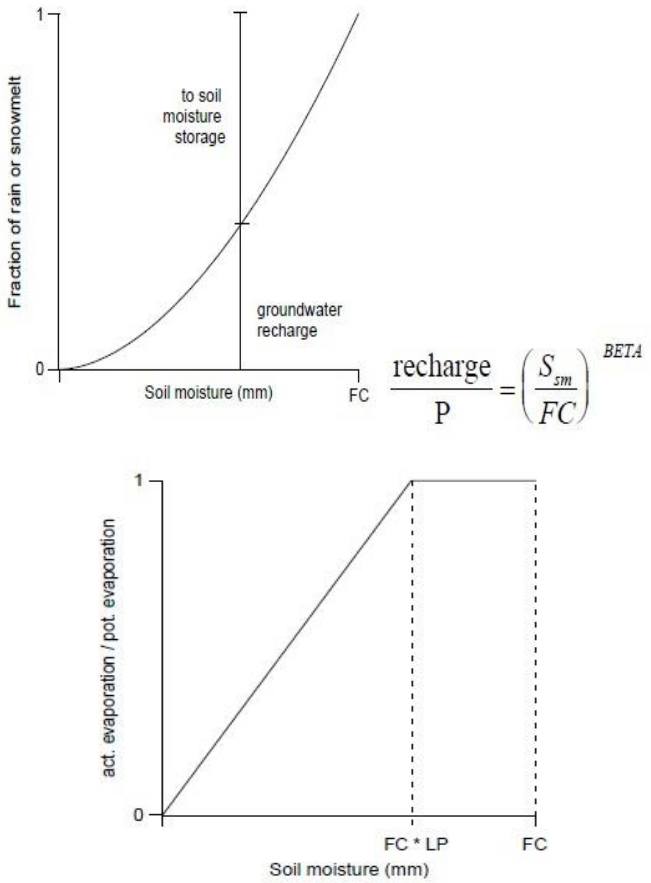

Figure 8: Soil moisture routine of HBV model.

FC is the field capacity of the model parameter and that does not necessarily equal measured values of the 'field capacity'.

3.6.3e Routing routine

By solving for and presuming the conservation of mass principle, discharge can be represented as an exponential function. The higher groundwater box SUZ (mm)

receives an addition of groundwater recharge. The maximum rate of percolation from the upper layer to the lower layer groundwater box SLZ (mm) is defined by PERC (mm/day). The computation of runoff from the groundwater boxes involves summing up two or three linear outflow equations, depending on whether the SUZ value exceeds the threshold value, UZL (mm). The modeled runoff (mm/day) is ultimately obtained by utilizing a triangle weighting function in (Figure 9) that is defined by the parameter MAXBAS. Plotted in the figure is the streamflow transformation function of the HBV model's routing response.

MAXBAS = Length of triangular weighting function (Δt)

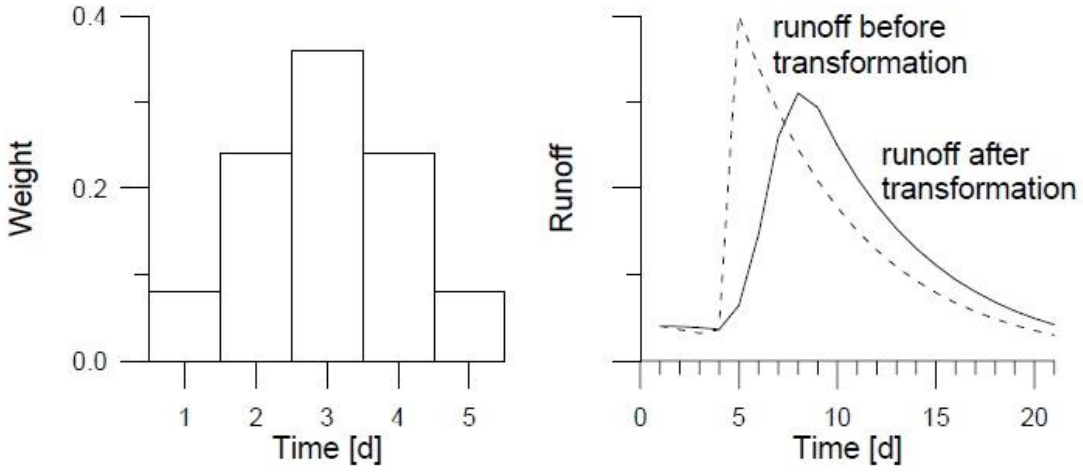

Figure 9: Transformation function of routing Response of HBV model.

3.6.3f Model types

Three GW-boxes, STZ and SUZ distributed

Response routine

Compared to the normal model variant, a third box named STZ is used on top of the other boxes, which is used in place of the two outflows from the upper groundwater box. STZ and SUZ boxes are distributed types, meaning that separate boxes are utilized for every height vegetation unit. A single linear outflow is determined by taking the water level and each box's constant (K0, K1, and K2 for STZ, SUZ, and SLZ, respectively). Using PERC, the flow from SUZ to SLZ is computed as before. The calculation of the flow from STZ to SUZ follows the same formula, with the maximum flow rate denoted by UZL (mm/Δt). Figure 3.9 shows the response function and response routine schematically.

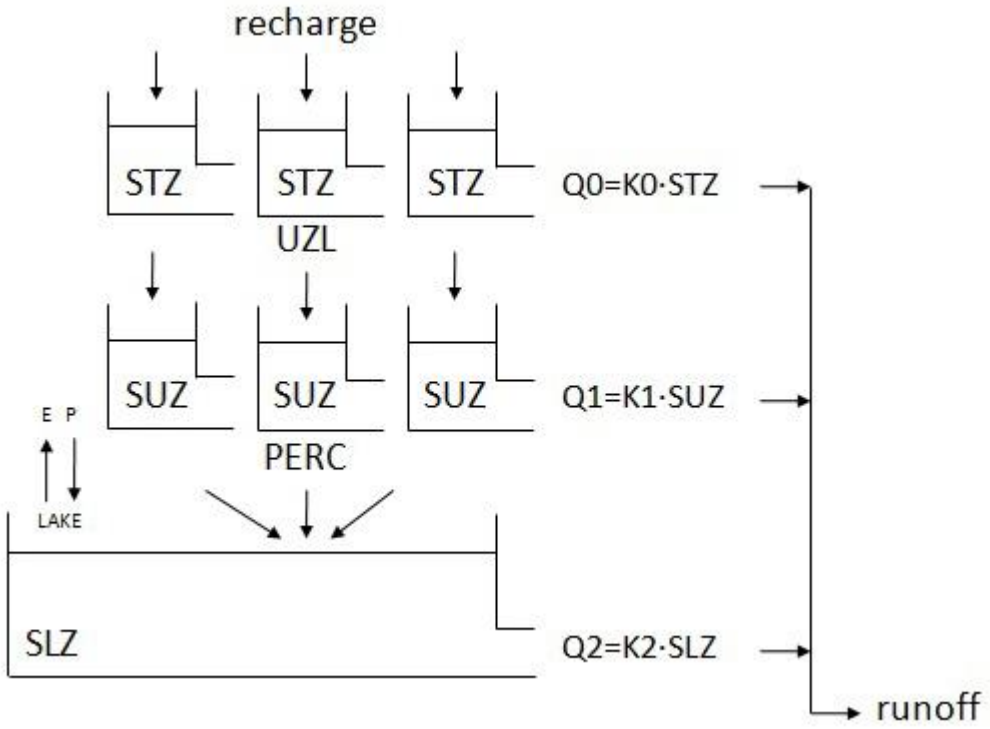

Figure 10: Response routine and Response function of HBV model.

SUZ = Storage in upper zone [mm]

STZ = Storage in top zone [mm]

SLZ = Storage in lower zone [mm]

PERC = Maximum percolation to the lower zone [mm/Δt]

UZL = Maximum percolation to the upper zone [mm/Δt]

P = Precipitation into the lake

E = Evaporation from the lake

Qi = Runoff component [mm/Δt]

Ki = Recession coefficient [1/Δt]

recharge = Input from soil routine [mm/Δt]

runoff = Total amount of generated runoff [mm/Δt]

3.6.3g Model variants

Glacier

When Elevation Vegetation Units (EVUs) are categorized into three primary groups based on their orientation: East/West oriented, South oriented, and North orientated.

This helps in choosing the glacier model variation for a model run. Every EVU can also be divided between areas with and without glaciers.

Two correction factors, a glacier correction factor (CFGlacier) and a slope correction factor (CFSlope), are defined for each vegetative zone. For south-oriented slopes, the degree day factor CFMAX's value is multiplied by CFSlope; for north-oriented slopes, it is divided by CFSlope. For slopes oriented east/west, CFMAX does not apply a correction factor. Between the soil routine, the glacier routine and the snow routine is applied, particularly to EVUs classified as glacier areas. This process is in charge of figuring out how much snow melts and turns into ice on the glacier. For these computations, the degree day factor is the CFMAX value multiplied by CFGlacier.

3.6.4 HEC HMS continuous simulation

The continuous modeling of river flow was conducted using HEC HMS version 4.9, developed by the U.S. Army Corps of Engineers in Davis, California. This versatile version serves multiple purposes, offering the capability to integrate with other software systems for a wide range of studies encompassing water resource assessment, urban drainage analysis, flow conveyance, flow forecasting, assessment of urbanization's future impact, design of reservoir spillways, flood damage mitigation, regulation of floodplains, and management of water systems. The outcomes of these modeling efforts are securely stored within the HEC-DSS data storage system.

In the course of this modeling endeavor, a user-friendly graphical interface (GUI) was harnessed within the HEC HMS model to construct basin and sub-basin configurations based on terrain data. The HEC hydrological modeling system effectively replicates the intricate hydrologic processes within the watershed. The simulation of key parameters within this model encompasses considerations such as the initial flow, recession ratio, and threshold flow.

Furthermore, the model's parameterization encompasses a breakdown into subbasins (10), junctions (9), reaches (10), sinks (1), along with components like the simple canopy model, deficit and constant loss methodology, simple surface model, monthly baseflow dynamics, wet and dry evapotranspiration periods, and the application of the Clark Unit Hydrograph transformation method. These settings within the HEC HMS model are primarily tailored for continuous simulations. The rainfall input is managed in such a way that all precipitation is initially intercepted and retained until the canopy's

storage capacity is reached. Once this threshold is met, any surplus precipitation flows onto the soil surface following the canopy's saturation. The surface method, as defined in the HEC HMS settings, emulates the ground's topography and accounts for the depressions where water accumulates subsequent to soil pores reaching their field capacity. Accumulated water within these depressions remains until runoff initiation, which occurs when the precipitation rate surpasses the soil's infiltration capacity, and the depression storage attains full capacity.

The values pertaining to canopy and surface storage were acquired through an analysis of Land Use and Digital Elevation Maps (DEM) derived from the Tamakoshi river basin. Additionally, to account for infiltration losses, the Soil Moisture Accounting (SMA) Loss Method, a component integrated within HEC HMS , was employed in conjunction with the canopy and surface methods. This comprehensive approach ensures a robust representation of hydrological processes within the studied watershed.

3.7 Streamflow components

The HBV light model is employed to simulate the parameters governing streamflow contributions within the Tamakoshi river basin. These contributions primarily comprise four components: accumulated runoff from rain, runoff resulting from snow melt, runoff derived from glacier melting, and baseflow runoff. The process of snow formation hinges on critical temperature thresholds coinciding with precipitation events. The contribution from snow and glaciers melting is determined using degree-day factor methodologies. In the case of the hydrological station at Busti, the HBV model calculates the streamflow contribution, denoted as Q_{Tot}, using the following equation 12:

$$Q_{Tot} = Q_{rr} + Q_{sm} + Q_{gm} + Q_{bf} \quad (12)$$

Here, Q_{bf} is discharge contributed by baseflow, Q_{rr} is discharge contributed by rain, Q_{gm} is discharge contributed by glacier melt, Q_{sm} is discharge contributed by snow melt and Q_{Tot} is total contributed discharge.

3.8 Water storage change

The water balance was evaluated by hydrological cycle components using HBV model. The water balance estimated at Busti gauging station is based on the principle of water mass conservation i. e. entering and discharging of water **(**Milly, 1994**).** The water availability storage is changing spatially and temporally. The water balance accounts

for changes in water storage. Water balance components simulated by the model are discharge Q_{sim}, observed discharge, Q_{obs}, Precipitation, Actual Evaporation and Potential Evaporation. The changing of water storage to calculated using equation 13.

$$\Delta S = P - Q - ET \quad (13)$$

Where, P is Precipitation, ΔS is change in storage, Q is discharge and ET is actual evapotranspiration.

Hydrological regimes categorized in this study into P is Precipitation, Q is discharge and AET is actual evaporation, where Q discharge includes total discharge that summation of contributed discharge (Q_rr+Q_sm+Q_gm+Q_bf), Q_{rr} is discharge contributed by rain runoff, Q_{sm} is discharge contributed by snow melt runoff, Q_{gm} is discharge contributed by glacier melt runoff and Q_{bf} is discharge contributed by baseflow runoff.

3.9 Hydrological model calibration and validation

Three distinct models, namely SPHY, HBV light, and HEC HMS, were utilized for simulating streamflow data. The calibration of these models was conducted either manually or through a trial-and-error methodology. The study focused on the Tamakoshi river basin, a river system primarily fed by snow and glaciers, encompassing multiple tributaries. Among these tributaries, Khimti is the most significant as it is rain-fed. The hydrological models incorporated a combination of static datasets, including latitude maps, land use land cover (LULC), Digital Elevation Model (DEM), and the Randolph Glacier Inventory version 6 (RGI 6). Additionally, dynamic datasets were employed, consisting of daily time series data from ground stations for key meteorological parameters, such as maximum temperature, minimum temperature, mean temperature and precipitation. Calibration of the simulated discharge data was executed using observed discharge data obtained from the Busti discharge station with station ID 647 and the Rasnalu discharge station with station ID 650. This calibration period spanned from 2004 to 2008 and was consistently applied to all models. Furthermore, in the case of the SPHY model, calibration was performed at the Rasnalu discharge station in Khimtikhola and validation at the Busti discharge station within the Tamakoshi river basin, and vice versa. The Tamakoshi river basin is equipped with two-gauge stations, specifically the Busti discharge station with ID 647 located at Tamakoshi and the Rasnalu discharge station with ID 650 situated at Khimti. The evaluation of model performance was carried out using the Nash-Sutcliffe Efficiency

(NSE), a commonly used metric for assessing model accuracy. In addition to NSE, the simulated discharge data were evaluated based on other statistical parameters, including the coefficient of determination (R^2) and the volume difference. The latter was assessed using the P bias, which measures the relative difference in volume between simulated and observed discharge data.

3.10 Evaluation metrices

The overall methods are presented in Figure 11. The performance of the hydrological model in the Tamakoshi river basin for hydrological simulation is evaluated by the Nash Sutcliffe Efficiency (NSE) (Nash and Sutcliffe, 1970) calculated by equation 14. NSE ranges from -∞-1, the observed mean is the better predictor than the model is closer to 1 is an excellent fit with observed discharge and simulated discharge.

$$\mathrm{NSE} = 1 - \frac{\sum_{i=1}^{n}(O_i - S_i)^2}{\sum_{i=1}^{n}(O_i - \bar{O})^2} \qquad (14)$$

The total variation of simulated discharge by a hydrological model with observed discharge is evaluated by coefficient of determination (R^2) in equation 15. The range of coefficient of determination ($R^{2)}$ is 0-1, closer to 1 is the best fit between observed discharge and simulated discharge.

$$R^2 = \left(\frac{\sum_{i=1}^{n}(O_i - \overline{O})(S_i - \overline{S})}{\sqrt{\sum_{i=1}^{n}(O_i - \overline{O})^2}\sqrt{\sum_{i=1}^{n}(S_i - \overline{S})^2}} \right)^2 \qquad (15)$$

Root Mean Square Error (RMSE) equation 16 measures the error between observed and simulated discharge values it equals 0 (zero) is a perfectly fit, with increasing RMSE values indicating an increasingly poorly fit, and RMSE values less than half the standard deviation of the observed (measured) data might be considered low and indicative of a good model simulation.

$$RMSE = \sqrt{\sum_{i=1}^{n} \frac{(S_i - O_i)^2}{n}} \qquad (16)$$

The RMSE-observations standard deviation ratio (RSR) is calculated using equation 17 as the ratio of the RMSE and standard deviation of measured discharge data. RSR varies

from the optimal value of 0 to a large positive value. The lower the RSR, the lower the RMSE and the better the model simulation.

$$RSR = \frac{\sum_{i=1}^{n}(S_i - O_i)^2}{\sqrt{\sum_{i=1}^{n}(O_i - \bar{O})^2}} \quad (17)$$

The goodness of fit between simulated and observed discharge was calculated using equation 18 the percent of bias (P bias).

$$Pbias\ or\ PEV\ = 100 \times \left[\frac{O_i - S_i}{O_i}\right] \quad (18)$$

where, O_i is measured observed discharge, S_i is simulated discharge, O is observed average discharge and S is simulated average discharge.

The degree of relation the pearson correlation between simulated and observed discharge was calculated using equation 19 as follows.

$$r = \frac{n(\sum os) - (\sum o)(\sum s)}{[n\sum o^2 - (\sum o)^2][n\sum s^2 - (\sum s)^2]} \quad (19)$$

Where r is correlation coefficient which is closer to 1 is best correlation of observed and simulated discharge, o is observed discharge and s is simulated discharge.

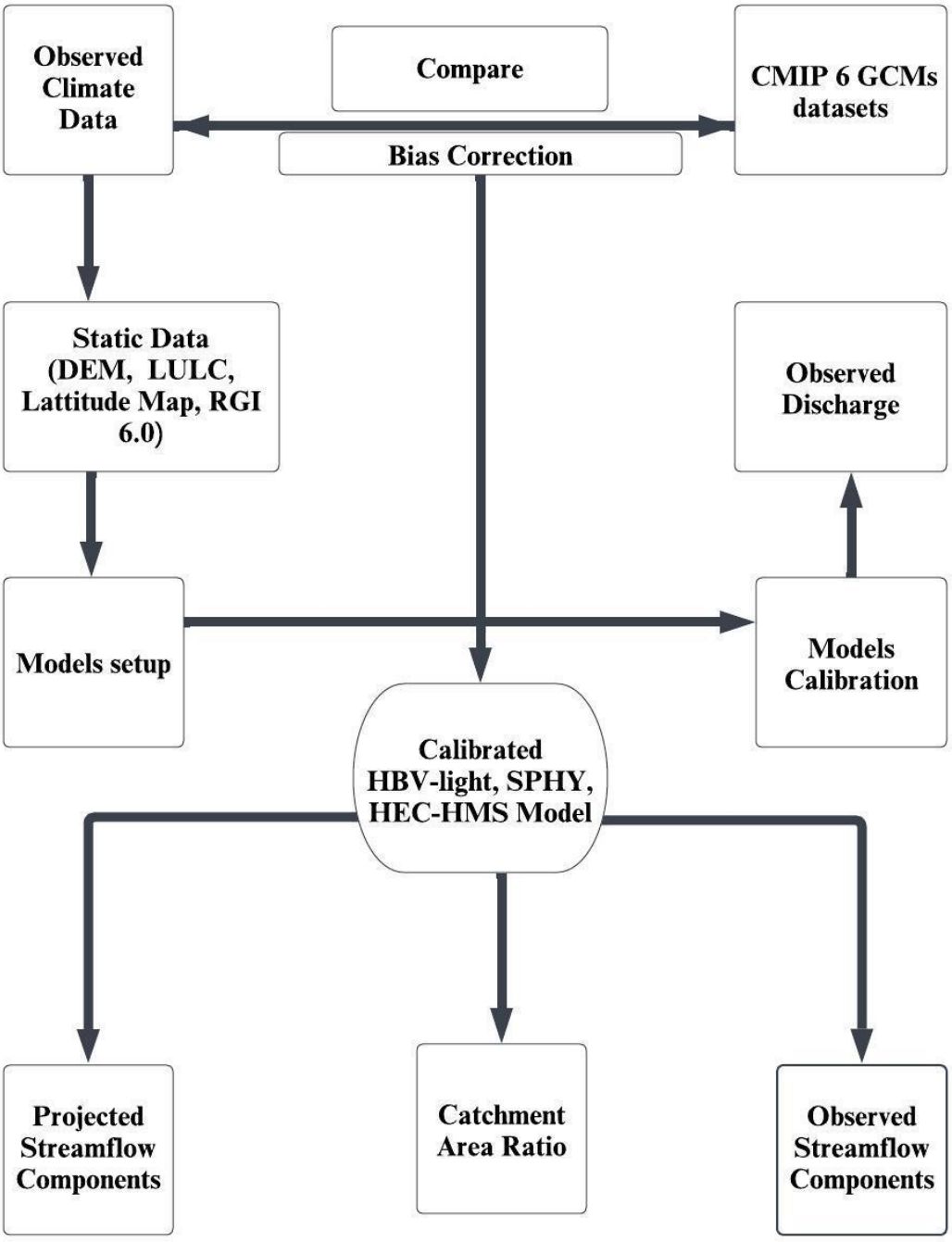

Figure 11: Schematic flow chart and overview of methodology.

3.11 Bias correction of precipitation and temperature

The study compares the downscale CMIP6, 4 GCM datasets of precipitation and temperature data with observed data bias correction required to both temperature and precipitation data due to the basin characteristics and spatial averaging. The numerous

sources of biases in hydroclimatic data analysis using GCMs are due to GCMs selection and ensembles, choice of the projection scenarios, downscaling techniques and modeling. Therefore, the downscaling of GCMs on a smaller scale requires hydrological modeling. In this research equations 20 and 21. are used to bias correction daily precipitation and temperature data (Mahmood and Babel, 2013).

$$P_{bdT=}P_{gcm} \times \left(\frac{P_{obsMM}}{P_{gcmMM}}\right) \quad (20)$$

$$T_{bdT} = T_{gcm} - \left(T_{gcmMM} - T_{obsMM}\right) \quad (21)$$

where, P_{bdP} and T_{bdT} are bias-corrected daily precipitation and temperature respectively. P_{gcm} and T_{gcm} are daily precipitation and temperature obtained from downscale data. P_{gcmMM} and T_{gcmMM} are long-term monthly mean of observed precipitation and temperature respectively, while and P_{obsMM} and T_{obsMM} are long-term monthly mean of precipitation and temperature simulated using GCMs for observed period.

CHAPTER 4

4. RESULTS AND DISCUSSION

4.1 Model calibration and validation

Hydrological models were used to calibrate and validate the Tamakoshi river at discharge station ID 647 as Busti and Khimti Khola at Station ID 650 Rasnalu. The calibration of the model took place between 2004 and 2008 in Busti while the validation occurred in Rasnalu during the period. This was due, to the distributed features of the model (Terink *et al.*, 2015 Terink *et al.*, 2017). Additionally, both HBV light and HEC HMS models were calibrated between 2004 and 2008 in Busti. Validated from 2011-2012 at the station. Daily discharge data was utilized for calibration and validation purposes across all models. The performance of these models was assessed on a monthly basis demonstrating good results. Please refer to Table 1 for daily and 2 for monthly details regarding their performance and statistical indexes in.

At the Busti gauging station, the SPHY model performed well, as evidenced by its 0.62 Nash Sutcliffe Efficiency (NSE), 0.76 coefficient of determination (R^2) for both simulated and actual discharge, and 26% simulated volume bias (P bias). The model got an NSE of 0.76, an R^2 of 0.76, and a P bias of 4% when it was verified at the Rasnalu station. Upon comparing the model's performance in the validation and calibration periods, we found that although the R^2 was relatively constant, the NSE and volume differences (P bias) increased. It is important to note, too, that as Figure 12A illustrates, the hydrographs of calibrated discharge overestimated peak discharge during rainy months. The disparity may be ascribed to multiple elements, including but not limited to data quality, model assumptions, local circumstances, input data uncertainty, and restricted data during extreme occurrences (Tigabu *et al.*, 2023). The calibrated and validated hydrographs at the Busti station are shown in Figure 12, along with the corresponding scatter plots.

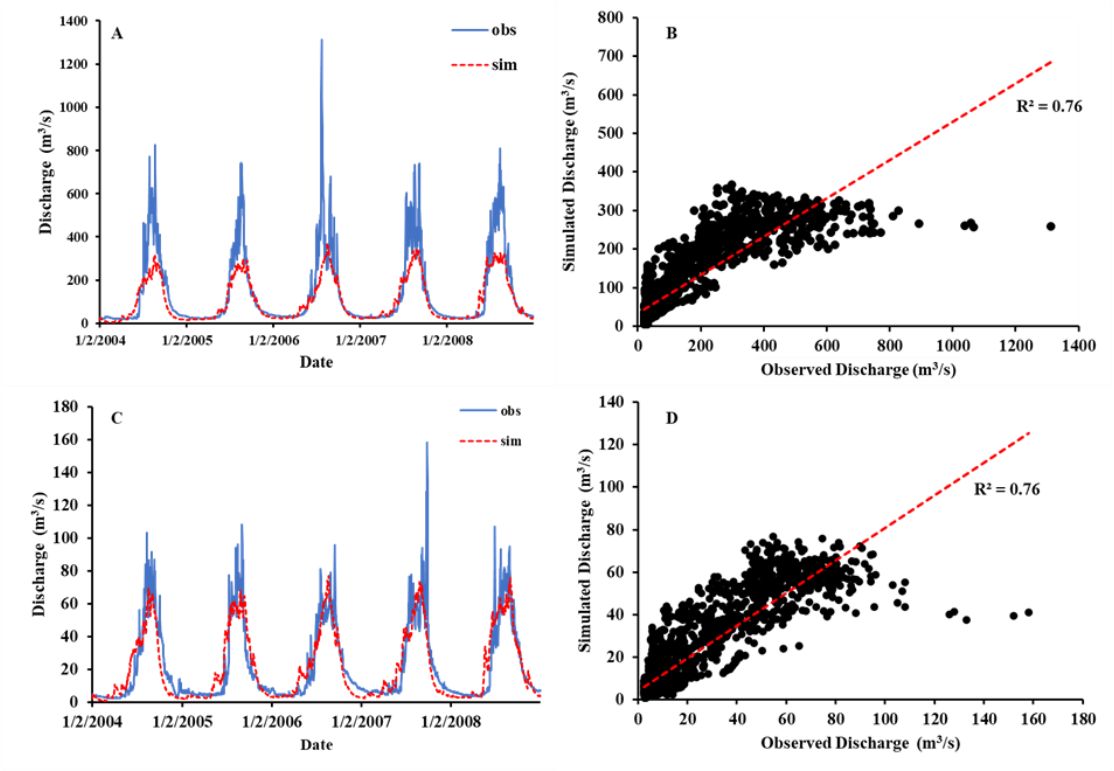

Figure 12: SPHY model daily calibration at Butsi A, scatter plot B and validation at Rasnalu C, Scatter plot D.

When the SPHY model was calibrated at the Rasnalu station, it performed fairly well. The bias between the simulated and observed volumes (P bias) was just 4%, the NSE was 0.79, and the R^2 comparing the simulated and observed discharge was 0.79. Not as positive were the outcomes of the model's validation at the Busti station, where the P bias increased to 26% and the NSE decreased to 0.61. The hydrograph demonstrated how the model miscalculated the peak discharges that occur during the wet season. This can be the result of problems with the model's assumptions about the input data or regional circumstances (Tigabu *et al.*, 2023, Nguyen *et al.*, 2022, Abbaspour *et al.*, 2019). It appears that low flows are better simulated by the SPHY model than large flows. Remarkably, when it came to simulating low-flow settings, the SPHY model outperformed the high-flow conditions in accuracy. It is noteworthy that, as Tables 1 and 2 show, the model's efficiency as indicated by NSE, R^2, and P bias seemed to be higher during the calibration period than during the validation period for the Rasnalu station. In Figure 13, the results are shown graphically with the hydrographs for the Rasnalu station that have been calibrated and validated together with corresponding scatter plots. Finally, when this comparative evaluation was made, the Rasnalu gauging station showed more resilient performance from the SPHY model than the Busti station.

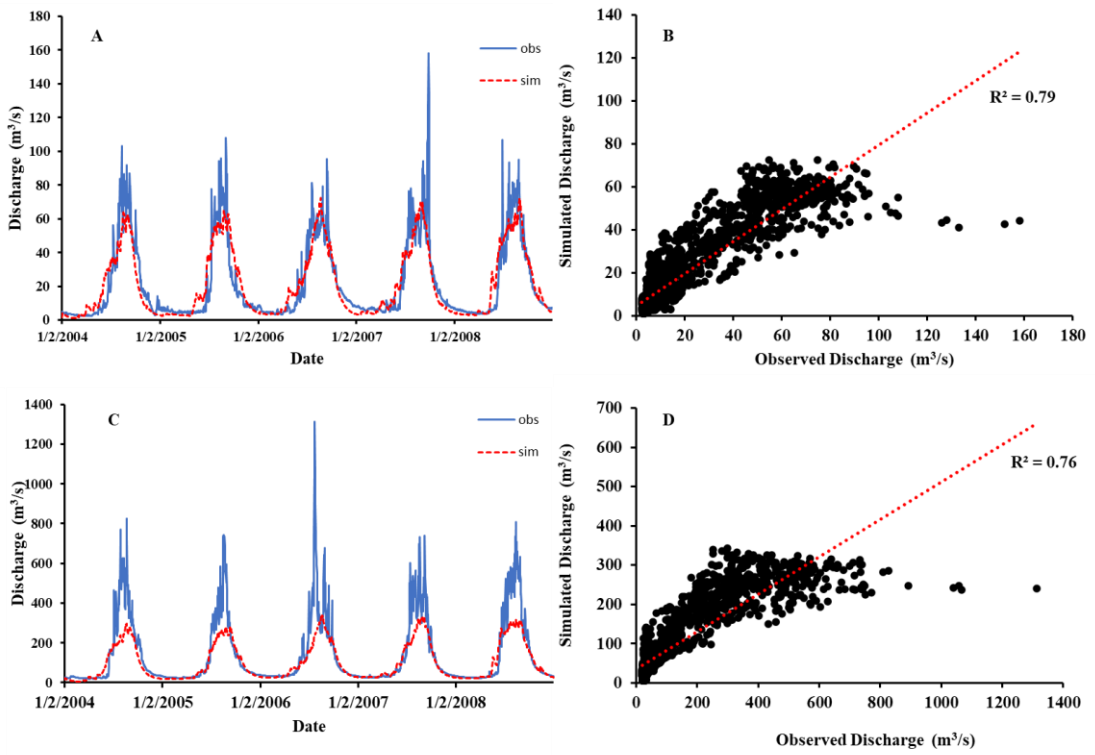

Figure 13: SPHY model daily calibration at Rasnalu A, scatter plot B and validation at Busti C, Scatter plot D.

The SPHY model's assessment of peak discharge at the Busti station fell short of accurate prediction. The reason for the discrepancy in estimation could be because the DHM's assessment of the discharge data, which is categorized as poor, fair, or good, places the statistics of both discharge stations in the 'fair' category. Furthermore, it's possible that the weather stations in the Busti watershed do not accurately reflect the real conditions throughout the watershed. The Himalayan basin has been witnessing a recurrent cascading nature hazard (Adhikari *et al.*, 2023; Talchabhadel *et al.*, 2023), mainly because of extreme events that obstruct the flow of water through the network of rivers. In order to overcome these obstacles, the parameters were calibrated and validated with values quantified in Appendix (Table A4). Remarkably, during the calibration, the groundwater parameters delta GW and alpha GW as well as the routing parameter recession coefficient (Kx) showed up as especially sensitive parameters in the basin.

The HEC HMS model was calibrated using observed river discharge data for the periods 2004-2008 and 2011-2012 for validation at the Busti discharge station ID 647 along the Tamakoshi river. The model's calibration results showed that its simulated

volume bias (P bias) was -2%, its Nash Sutcliffe Efficiency (NSE) was 0.78, and its coefficient of determination (R^2) between the simulated and observed discharge was 0.79. The NSE of 0.77, the R^2 of 0.78 for both simulated and observed discharge and the simulated volume bias (P bias) of 0.26% were found in the validation findings for 2011–2012. These model parameters were established using the values listed in Appendix (Table A5). Figure 14 displays hydrographs and scatter plots as a visual depiction of the calibration and validation performance of the HEC HMS model.

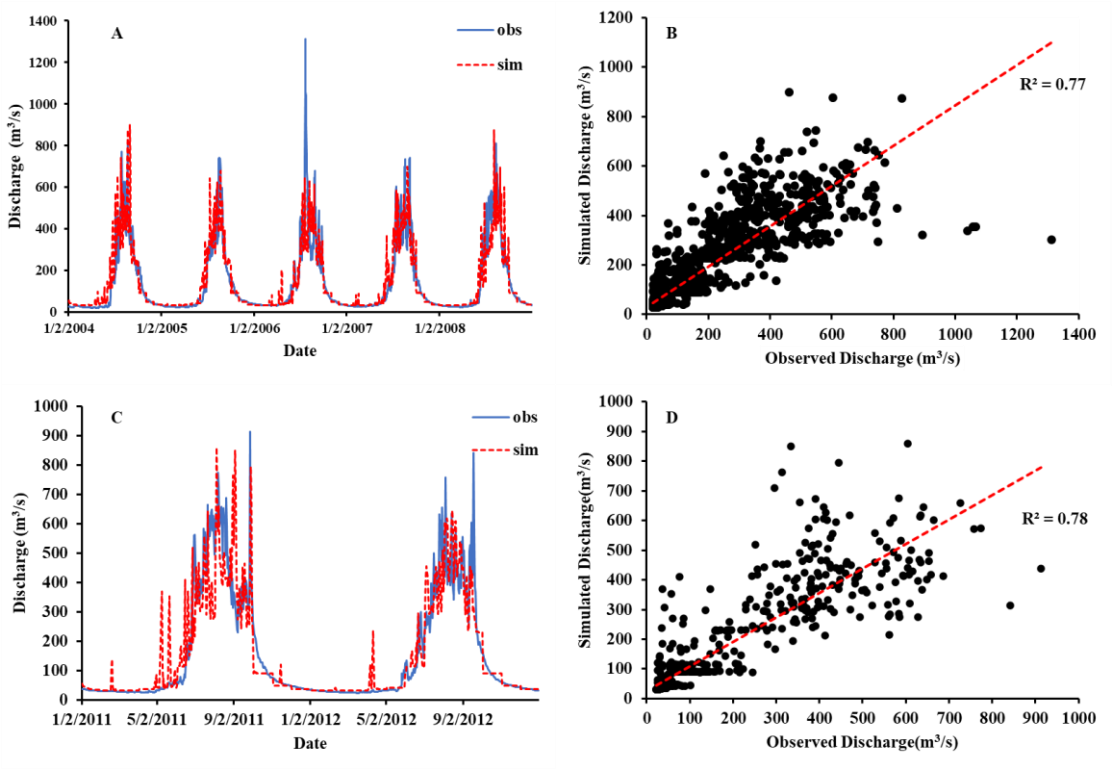

Figure 14: HEC HMS model daily calibration at Butsi A, scatter plot B and validation at Busti C, Scatter plot D.

When the HBV light model was run at the Busti location, the result was an NSE value of 0.77. The simulated volume difference (P bias) had a negative bias of -3%, and the Coefficient of Determination (R^2) between the simulated and observed data was also 0.77. Likewise, while evaluating the model's validation performance, the simulated volume difference (P-bias) revealed a bias of -21%, the NSE was 0.82, and the R^2 for the observed and simulated discharge was 0.87. Figure 15 shows the calibration and validation findings of the HBV light model graphically. Furthermore, Appendix (Table A6) provides comprehensive details about the calibrated and validated model parameters.

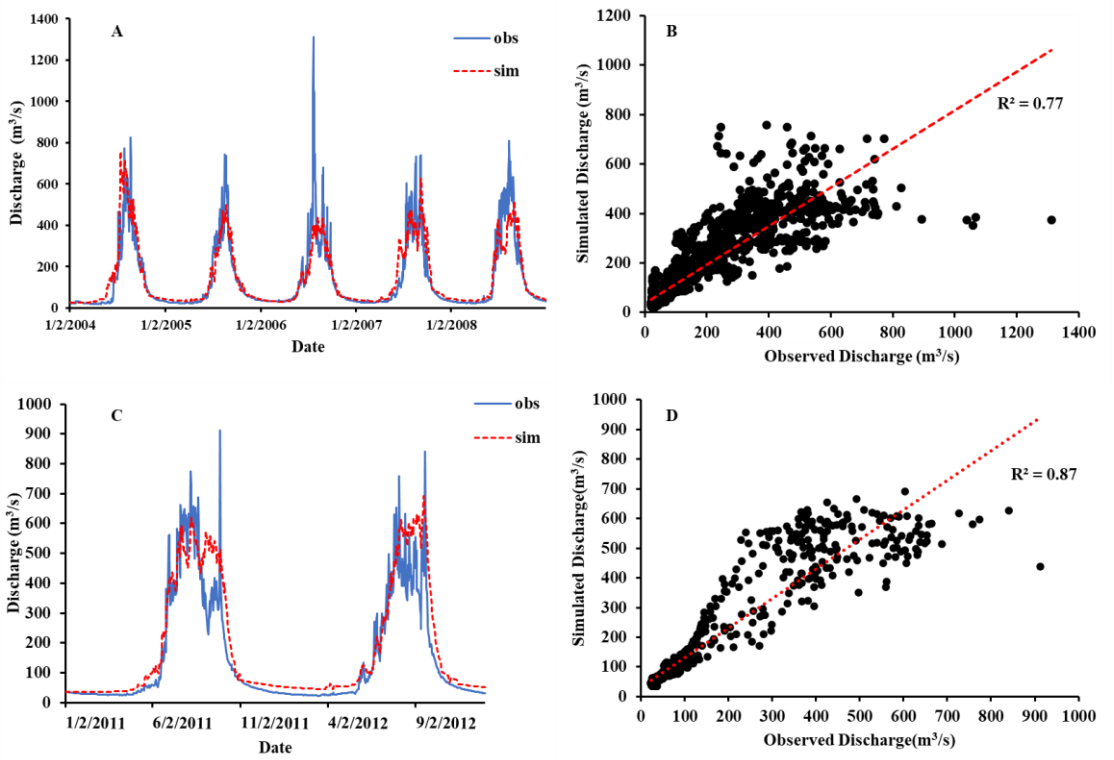

Figure 15: HBV model daily calibration at Butsi A, scatter plot B and validation at Busti C, Scatter plot D.

4.2 Comparison of model with statistical index

During both the calibration and validation periods, the model's simulated streamflow data was thoroughly assessed using statistical parameters. It should be noted that compared to the monthly calibration, the calibration procedure for the continuous daily simulation was more difficult. After evaluation, the statistical parameters showed that physically based, fully distributed models such as SHPY and semi-distributed models like HBV light and HEC HMS performed better in the validation phase than in the calibration phase. The model performance of fully distributed NSE values categorized to fully distributed models are Insufficient 0-0.2, Sufficient 0.2-0.4, Good 0.4-0.6, Very good 0.6-.0.8 and Excellent >0.8 (Foglia *et al.*, 2009) and the model performance NSE values categorized to semi-distributed models are unsatisfactory 0-0.50, Satisfactory 0.50-0.70, Good 0.70-0.80, Very good 0.80-1.00.

Various statistical indices showed that these three models performed well overall when compared to one another. Prominently, the assessed statistical indices (r, R^2, and RSR) were shown in Tables 1 and 2, which demonstrated similar daily simulation performance across the calibration. In terms of all statistical characteristics, such as r,

R^2, RMSE, and RSR, the HBV light and HEC HMS models showed similarities. Additionally, a similar pattern was seen in the model performance for HBV light and HEC HMS when assessed using NSE. During the simulation's calibration phase, the HBV light and HEC HMS models exhibited a volume differential (P bias) that significantly understated the actual discharge.

The validation phase revealed a similar trend to the calibration phase for all three models. Crucially, the simulation of the hydrological model showed that monthly calibration performed better than daily calibration (Table 1). The HBV light, HEC HMS and SPHY models were ranked based on their performance when compared to each other, and the models collectively showcased their distinct characteristics. On the basis of calibration and validation, the comparison of statistical indexes in table 1 HBV light model performed better than SPHY and HEC HMS in Tamakoshi river basin. The model performance mainly depends on the types of models and included parameters (Nonki *et al.,* 2021; Ouyang *et al.,* 2014). Generally, physically based distributed models are more reliable than conceptual and lumped modeling system (Tran *et al.,* 2018). Lumped models always exhibits better than physically based models (Das *et al.,* 2008) due to available functions of models' parameters but physically based distributed models are more reliable.

Table 1: Statistical indexes of daily calibration and validation of hydrological models

Models	**Calibration**						
	NSE	**R^2**	**P-bias**	**r**	**RMSE**	**RSR**	**Period**
SPHY	0.62	0.76	26.16	0.87	2.48	0.01	2004-2008
HBV	0.77	0.77	-3.54	0.88	1.92	0.01	2004-2008
HEC HMS	0.77	0.77	-2.71	0.88	1.93	0.01	2004-2008
Models	**Validation**						
	NSE	**R^2**	**P-bias**	**r**	**RMSE**	**RSR**	**Period**
SPHY	0.76	0.76	3.82	0.87	0.27	0.01	2004-2008
HBV	0.82	0.87	-21.17	0.93	49.03	0.27	2011-2012
HEC HMS	0.77	0.78	0.26	0.88	86.89	0.47	2011-2012

Table 2: Statistical indexes of monthly calibration and validation of hydrological models

Models	Calibration						
	NSE	**R^2**	**P-bias**	**r**	**RMSE**	**RSR**	**Period**
SPHY	0.71	0.86	25.98	0.93	15.57	0.09	2004-2008
HBV	0.86	0.86	-3.76	0.93	10.61	0.07	2004-2008
HEC HMS	0.93	0.94	-2.86	0.97	7.34	0.05	2004-2008
Models	**Validation**						
	NSE	**R^2**	**P-bias**	**r**	**RMSE**	**RSR**	**Period**
SPHY	0.87	0.87	3.80	0.94	1.44	0.06	2004-2008
HBV	0.88	0.93	-21.36	0.97	6.81	0.04	2011-2012
HEC HMS	0.95	0.95	0.15	0.97	4.50	0.03	2011-2012

4.3 Flow simulation at an ungauged site

At Rasnalu and the Busti station, the annual mean discharge from the contributing catchments was 21.88 m^3/s and 138.72 m^3/s, respectively. The Benighat receiving basin's annual mean discharge was estimated using a variety of hydrological models. The annual mean discharges were estimated from Busti station using the HBV light model, HEC HMS model, and SPHY model to be 201.55 m^3/s, 175.03 m^3/s, and 164.35 m^3/s, respectively. Likewise, the SPHY model from Rasnalu station estimated a discharge of 164.18 m^3/s.

The daily estimated streamflow data is shown in Figure 16A, which shows a good agreement between the daily flows obtained from the two calibrated sites and the ungauged site. The flow patterns match up nicely, however, because of the unpredictable nature of the rainfall, it is difficult to simulate the daily flow continuously at the ungauged site.

Monthly estimated streamflow data is shown in Figure 16B, showing lower flow rates in March based on the HBV light and HEC HMS simulations and lower flow rates in February based on the SPHY model. It is clear that the biggest flows are predicted by all models for August.

In addition, Figure 16C presents the yearly average streamflow simulation results for the years 2005 and 2006, demonstrating a consistent pattern in all models. For the ungauged site, Benighat, however, the HBV light model yields greater values than the SPHY and HEC HMS models. This disparity is explained by variations in the model's parameterization throughout the calibration process, which is a separate procedure for every model variation. An overview of the annual streamflow is also shown in Figure 16C, which shows that all hydrological models produce meaningful findings during low flow times, while the simulated estimated streamflow varies during high flow periods.

The application of ensemble modeling resulted in the uniformity and dependability of streamflow simulation throughout the basin. Utilizing the SPHY, HEC HMS, and HBV light models, the estimated discharge at Benighat demonstrated an annual average of 175.03 m^3/s, with monthly averages varying from 36.82 m^3/s in February to 526.97 m^3/s in September. The remaining months, from January to December, showed values of 39.88 m^3/s, 38.68 m^3/s, 52.96 m^3/s, 89.01 m^3/s, 235.26 m^3/s, 423.27 m^3/s, 385.74 m^3/s, 154.45 m^3/s, 73.29 m^3/s, and 48.60 m^3/s. Two different multi-modeling strategies were used in this work to simulate streamflow at ungauged sites. Streamflow from gauged stations to ungauged places was simulated in the first method, while calibrated models within the basin from the head donor catchment to the downstream receiver basin were used in the second. When used in conjunction with ensemble streamflow modeling, this creative method of using numerous models for streamflow estimation at ungauged locations constitutes a useful and comparative tool.

The different approaches to calculating ungauged streamflow could not simulate similar discharge (Van Liew and Mittelstet, 2018). When observational data is lacking, hydrological models can be used without the necessity for calibration as they can function well both inside and outside of gauged basins (Bergstrom, 2006). These hydrological models' special features and the characteristics of the catchments have an impact on how well they operate, as the calibration and validation procedures have shown. Notably, depending on their special characteristics, the SPHY, HBV light, and HEC HMS models display different performances. Each model could not simulate similar flow due to parameterization of model during calibration (Myes et al., 2021). The process of parameterization is independent accordingly model variants (Refsgaard et al., 1997). Hydrological models are independent to streamflow simulation at the ungauged site. The performance of the hydrological models varied based on their

features and the characteristics of the catchments, as revealed by the results of the calibration and validation process (Pechlivanidis et al., 2011; Refsgaard et al., 1997).

After calibration and validation, the SPHY model reliably models the streamflow transfer from the upstream catchments of Rasnalu and Busti to the downstream catchment of Benighat. On the other hand, streamflow from Busti to Benighat is transposed in both the HBV light and HEC HMS models. Particularly, Benighat is the basin that receives water from the Tamakoshi river basin, while Rasnalu and Busti are the main catchments that supply water to them. Using these calibrated models, the streamflow at Benighat is approximated.

For its daily flow simulation at Benighat, the SPHY model uses a spatially distributed modeling system and two different approaches: one simulates flow from the Busti station, and the other from the Rasnalu station. There is a strong correlation and close alignment between these daily streamflow simulations from Rasnalu and Busti at Benighat. In contrast to other models, the HBV light model typically produces greater daily, monthly, and yearly streamflow numbers. Simulating peak daily discharge is where the HEC HMS model shines, especially during high-flow seasons.

The total discharge from the upstream gauging stations of Busti and Rasnalu is less than the total streamflow at Benighat, according to all of these hydrological simulation results. This difference can be explained by the stream network's contribution to runoff, which raises the discharge downstream. As the last outflow of the Tamakoshi river basin, Busti and Rasnalu, as upstream donor catchments, direct their flow into the downstream receiver basin at Benighat.

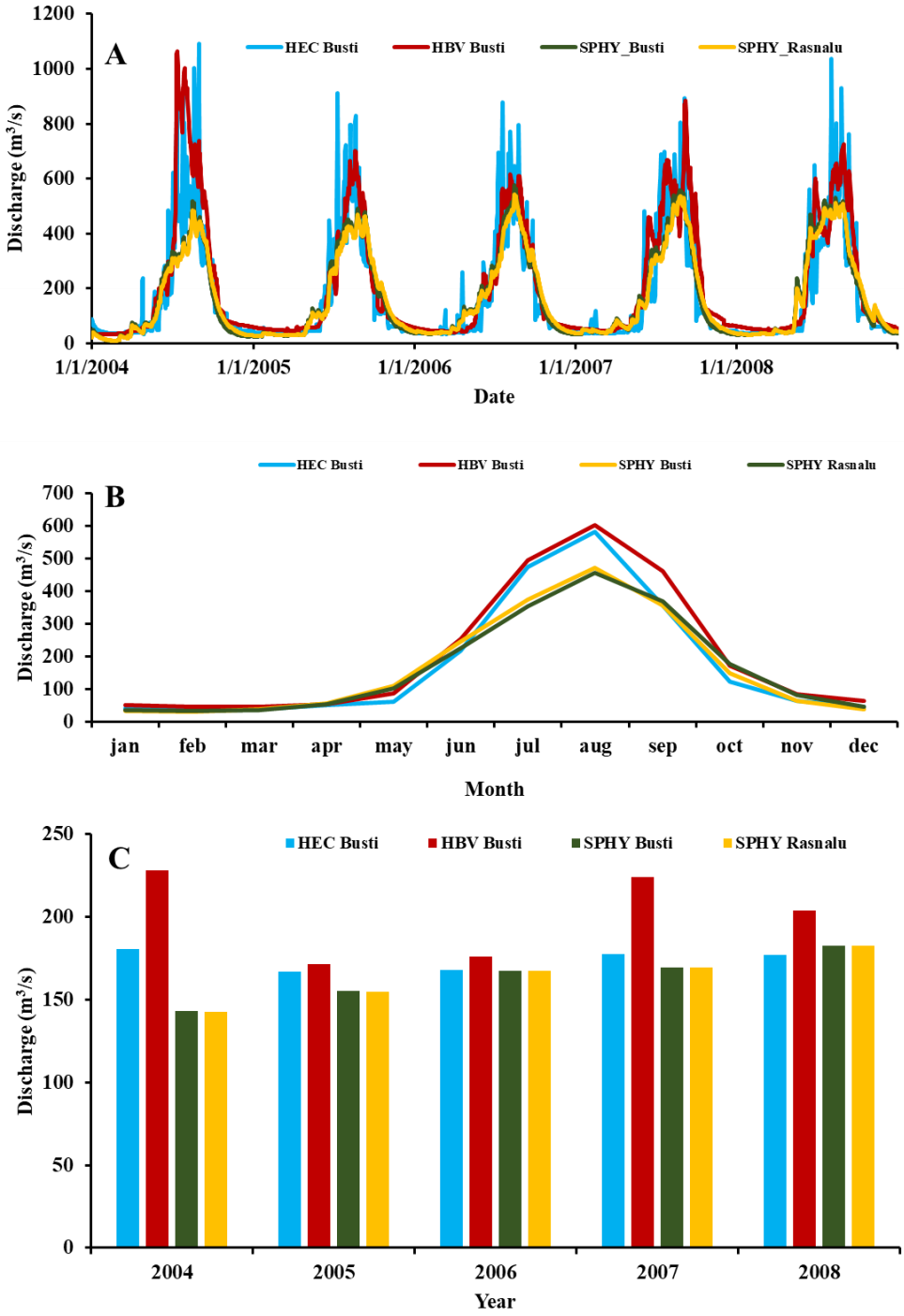

Figure 16: Comparison of ungauged discharge daily (A), monthly (B) and annual (C).

4.4 Observed water balance components' contribution to streamflow

The different streamflow components have been divided into discrete groups in this study. These components primarily include precipitation in the form of rain or snow, which depends on the critical temperature, as well as evapotranspiration, rain-runoff, baseflow runoff, snow melt runoff, and glacier melt runoff. The HBV light model was

used to simulate these streamflow components because it has outperformed other models that are currently available in glacier simulation.

The purpose of the study is to evaluate how much various streamflow components contribute to the river flow at the Busti Station over a thirty year period, from 1991 to 2020 (Figure 17B). The streamflow components that are specifically examined include the snow-glacier melt and rain-baseflow, both of which are important to the hydrological cyclic processes at the Busti discharge station. It is significant to note that these streamflow components are responsible for the yearly, seasonal, monthly, and daily temporal variations in the river discharge at the Busti hydrological station.

In the Tamakoshi river watershed, the monthly average streamflow contributions vary significantly; they are between 58.05 mm and 2.75 mm for glacier melt, 27.78 mm and 0.88 mm for snow melt, 41.55 mm and 35.40 mm for baseflow, and 601.05 mm and 45.01 mm for rain runoff. The combined effect of these various contributions is a total discharge that varies from 601.05 mm to 45.01 mm.

The Tamakoshi river basin's monthly, seasonal, and yearly relative percentages of streamflow contributions are shown in Figures 18A, 18B, and 18C. Remarkably, August exhibits the largest monthly contributions to streamflow, mostly due to precipitation runoff. On the other hand, baseflow makes a major contribution in October, and snow melt makes a considerable contribution in July. Conversely, streamflow in August is greatly impacted by glacier melt.

On the other hand, snow melt, baseflow, and glacier melt account for the lowest monthly streamflow contributions; these events mostly take place in February, with March serving as an exception because that month's lowest contributor is rain runoff. August records the largest total streamflow, while February records the lowest total discharge. The monthly analysis of relative streamflow contributions by runoff components, as shown in Figure 18A, reveals that baseflow dominates the remaining months from November to May, forming the overall streamflow's character. Rainfall runoff dominates from June to October.

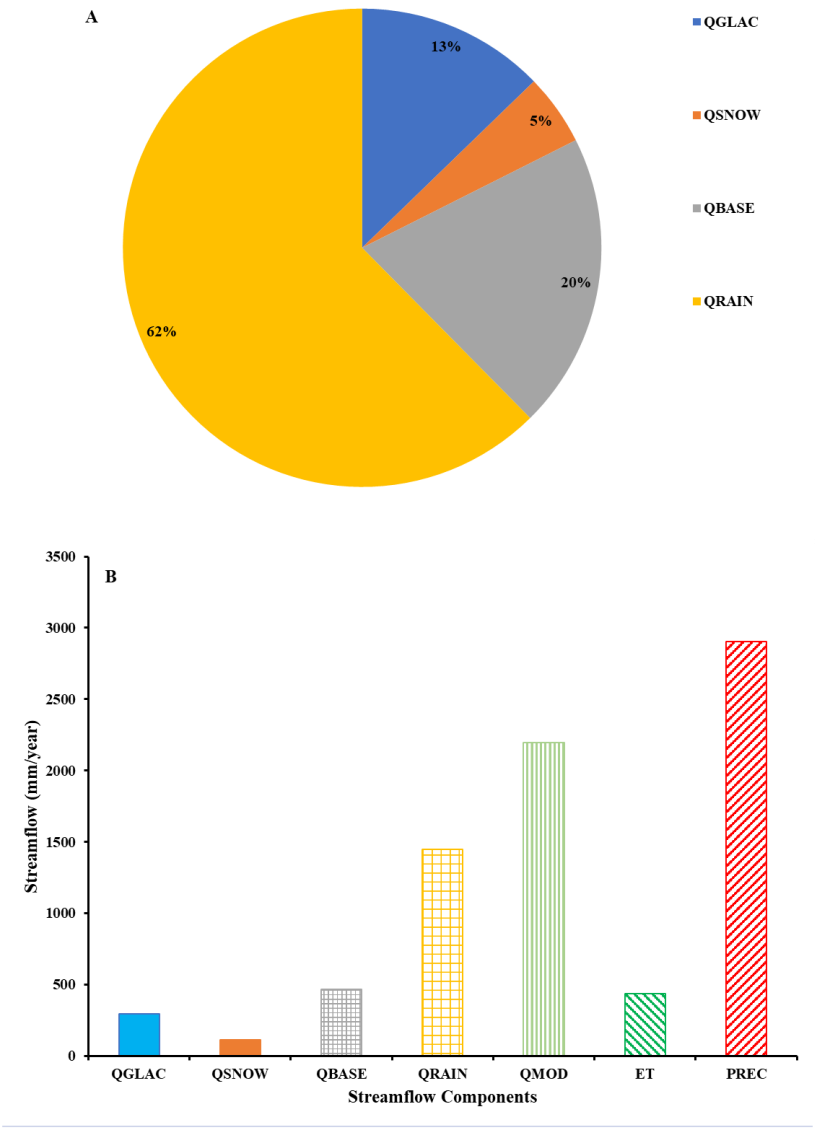

Figure 17: Annual water balance contribution (1991-2020).

The results show that, on average, the proportion of streamflow components peaks in the summer (June to September), while their contributions to streamflow are lowest in the winter (December to February) and pre-monsoon (March to May). In addition, the data shows that snow melt contributes the least to overall streamflow, whereas rain runoff contributes the most.

Specifically, the monsoon season records the lowest streamflow contribution, at 6.96%, while the winter season records the highest share, at 73.88%. The contribution of baseflow is mostly observed during the post-monsoon season.

Please refer to Figure 18B for an illustration of the seasonal fluctuations in the contributions of the streamflow component to riverine flow.

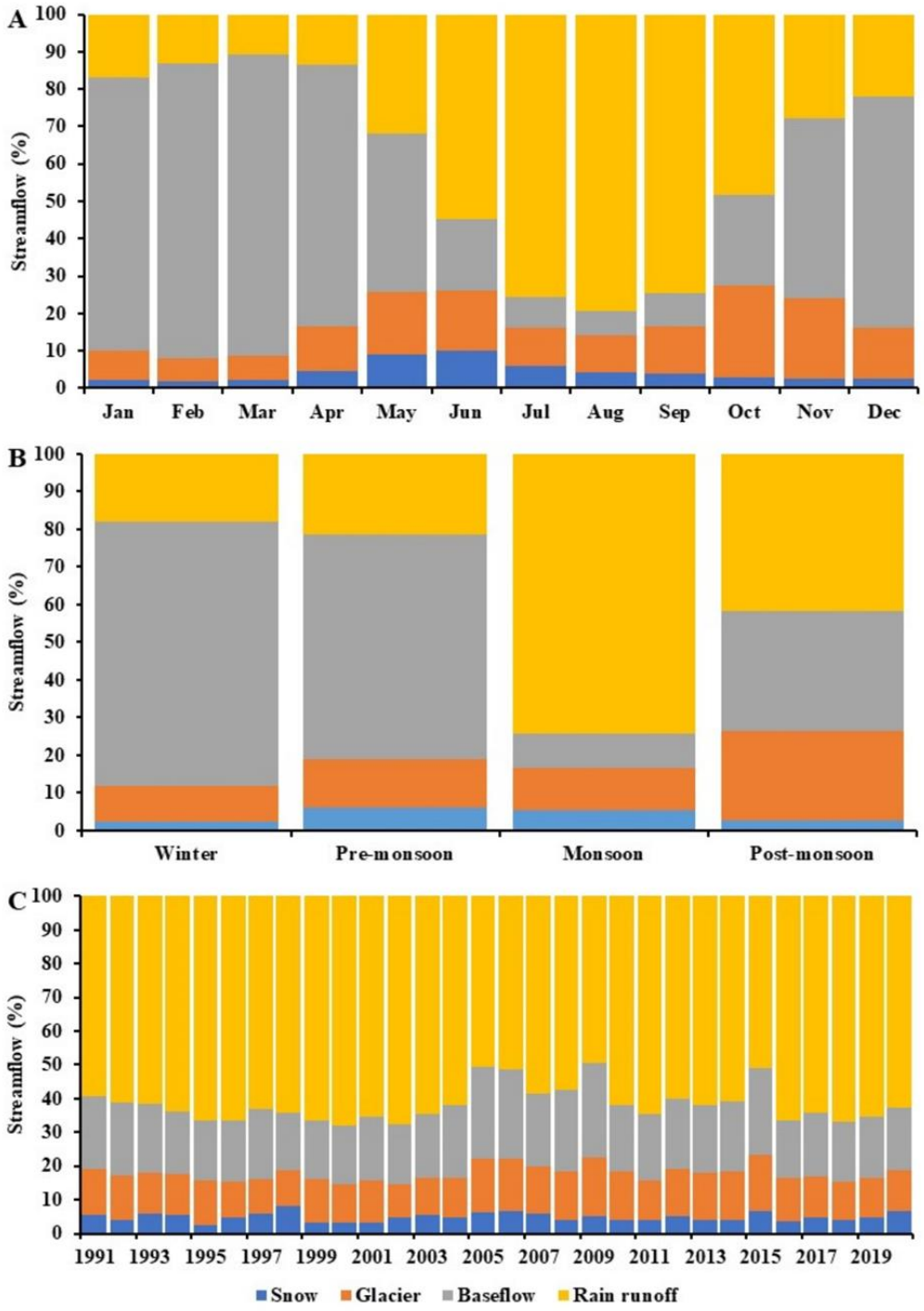

Figure 18: Relative contribution of runoff components to streamflows at the monthly (A), seasonal (B) and annual (C) time scales.

An annual water balance for the Busti gauging station shows variable contributions from several sources. The greatest portion, 1448.10 mm, is accounted for by runoff from rain, groundwater, glacier melt, and snow melt, with respective amounts of 465.03 mm, 111.95 mm, and 295.88 mm. Certain percentages of the cumulative streamflow, as shown in Figure 17A, can be credited with these contributions. Contributions from snow

melt (5%), baseflow (20%), glacier melt (13%), and rain runoff (62%), are the most special.

The annual contribution of these elements varies. The melting of glaciers peaked in 2016 and lowered to its lowest point in 1997. The impact of snow melt on streamflow peaked in 1998 and peaked in 1995. While baseflow peaked in 2020 and fell to its lowest point in 1991, rain runoff reached its highest point in 2000 and fell to its lowest point in 2009. At Busti, the overall runoff contribution fluctuated, reaching its highest point in 2016 and its lowest point in 2009.

Glacier melt ranges from 358.05 mm to 217.076 mm, snow melt contributions range from 210.99 mm to 62.88 mm, baseflow varies from 494.28 mm to 424.26 mm, and rain runoff varies from 1845.51 mm to 836.1 mm annually. These variations are represented in the simulated streamflow contributions Figure 18C and 19c has further information on the yearly streamflow contributions from various components. Figure 17B describes these streamflow components schematically.

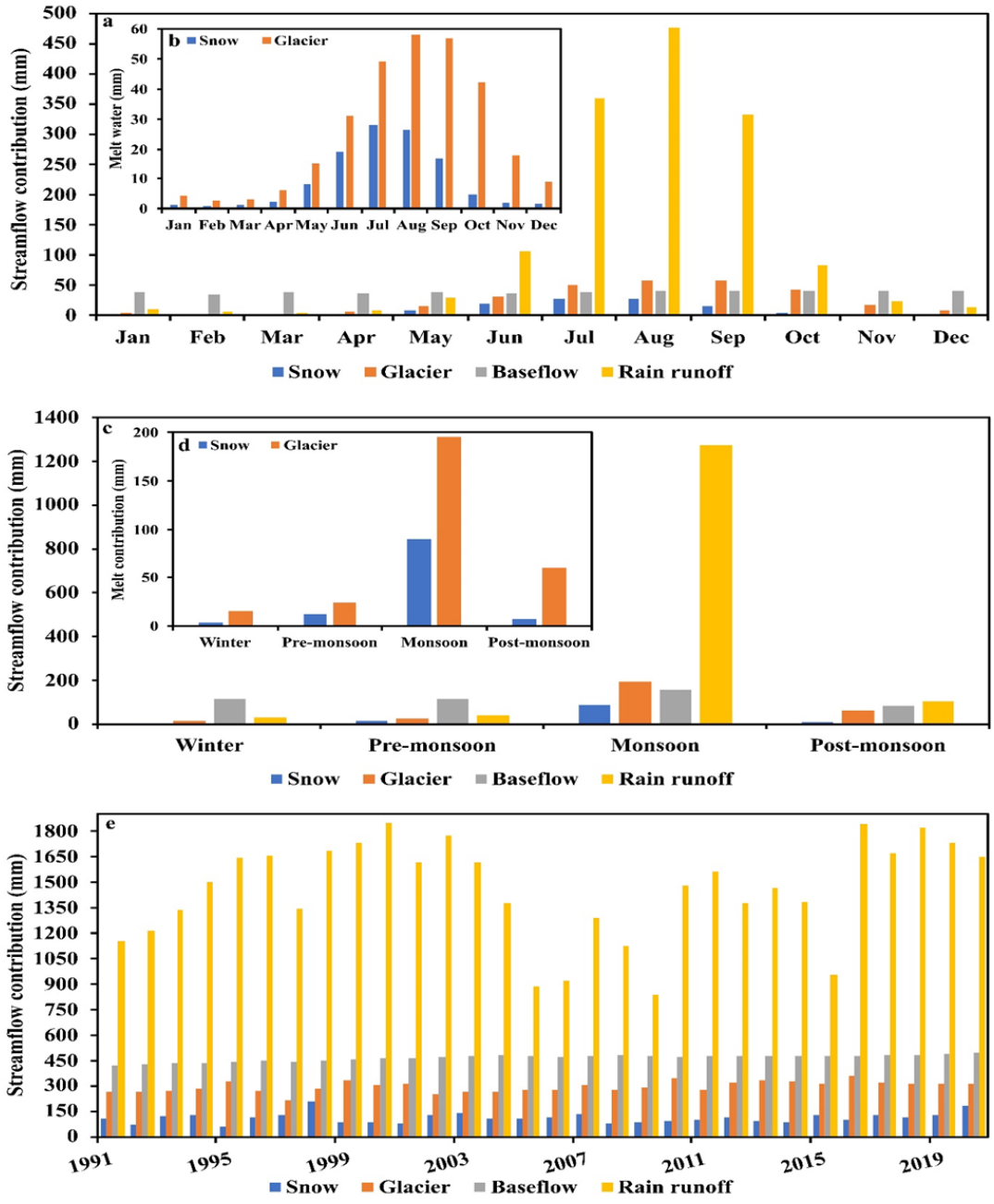

Figure 19: Annual e), Seasonal c & d) a and Monthly a & b) streamflow contribution components.

4.5 Water balance storage

In order to evaluate the water components' availability in the hydrological cycle using model simulations, it is crucial to make sure the outcomes make sense. However, differences between the simulated and observed discharge could occur for a number of reasons, such as the restrictions placed by the standard meteorological network of the World Meteorological Organisation (WMO), the availability of real-time data, the complexity of the geographical terrain, and the difficulties involved in gathering data and rating estimation.

The Busti gauging station's estimation of changes in water balance storage is based on a rather short 30-year period, from 1991 to 2020. Incoming water must equal departing water, which is the basic idea driving these variations in water balance storage. Here, "incoming water" refers to precipitation, and "outgoing water" refers to discharge and water body evaporation. Equation 13 illustrates how this theory, which is in line with the idea of mass conservation, helps to explain the variations in water storage in the Tamakoshi river basin, particularly at the Busti gauging station.

Precipitation, evaporation, the total discharge from rain runoff, baseflow, snow melt runoff, and glacier melt runoff are some of the several elements that affect streamflow dynamics. Together, these elements have an impact on how much water is stored over time. These temporal variations take place on a variety of time ranges, from seasonal and annual variations to daily and monthly changes.

From April to August, the water balance storage showed a positive trend; the subsequent months had negative changes. The main cause of the negative water balance storage was precipitation events. Significantly, the water balance of the basin peaked in October and declined to its lowest point in July. The monthly storage of water balance was enhanced from September to March by streamflow, which was reinforced by groundwater recharge from precipitation and the activities of snow-glaciers. Groundwater resources were refilled during this time. As a result, the basin's water storage reached its maximum levels between April and August, then began to decrease between September and December. Please see Figure 20a for a graphic depiction of these monthly fluctuations in water balance storage.

Figure 20b illustrates the different patterns that the basin's seasonal changes in water storage follow. Water storage rises most significantly during the monsoon season and decreases least during the post-monsoon season. This seasonal disparity is further demonstrated by the distribution of precipitation over the course of the year. Summer precipitation makes up a significant 80.47% of the yearly total, with 14.15% occurring in the pre-monsoon season, 3.15% in the post-monsoon season, and 2.21% in the winter.

These patterns are reflected in the basin's water release, with the monsoon season accounting for a resounding 74% of the total release. On the other hand, the post-monsoon season contributes just 11%, and the winter and pre-monsoon seasons

contribute 7% and 8% of the discharge, respectively. The total water balance and storage dynamics in the area are significantly shaped by this discharge pattern.

Furthermore, there is seasonal variation in the behavior of evapotranspiration. During the monsoon season, a substantial 40% of evapotranspiration occurs. This is followed by 20% during the post-monsoon season, 14% during the winter season, and 25% during the pre-monsoon season. The water balance and storage fluctuations in the basin are directly impacted by these evapotranspiration patterns.

The fluctuations in water storage in the basin are influenced by seasonal variations in precipitation, discharge, and evapotranspiration, as illustrated in Figure 19b. The monsoon season contributes the most to the rise in storage, while the post-monsoon season contributes the least. The general water management of the area is greatly influenced by this seasonal pattern of water balance.

The water storage varied annually, averaging 148.39 mm. The amplitude of these variations varied from 447.35 mm in 2002 to -122.81 mm in 2012. The water balance reserve was always measured at 148.39 mm. A yearly precipitation of 2905.52 mm, an actual evapotranspiration of 434.58 mm, and a simulated discharge of 2322.66 mm are used to maintain that balance.

The elements of the yearly water balance simulation showed fluctuations. The amount of snow melt varied between 210.99 mm and 62.88 mm, whilst the contribution of glacier melt ranged from 358.05 mm to 217.08 mm. Rainfall-runoff varied from 1845.51 mm to 836.09 mm, while baseflow fluctuated between 494.26 mm and 424.28 mm. The range of annual precipitation was 3494.80 mm to 2068 mm. Evapotranspiration varied between 488 mm and 374.98 mm, whereas cumulative discharge varied between 2777.11 mm and 1690.17 mm.

The water balance components, namely total discharge, evaporation, precipitation, rain runoff, baseflow, snow melt, and glacier melt, showed increasing trends over the course of a year. On the other hand, the trend for changes in water storage was declining.

Figure 20 illustrates the water balance trends in the Tamakoshi river basin during various time periods, shedding light on the changing dynamics of water storage. These findings are crucial for estimating downstream water availability and guiding future research in other basins as necessary.

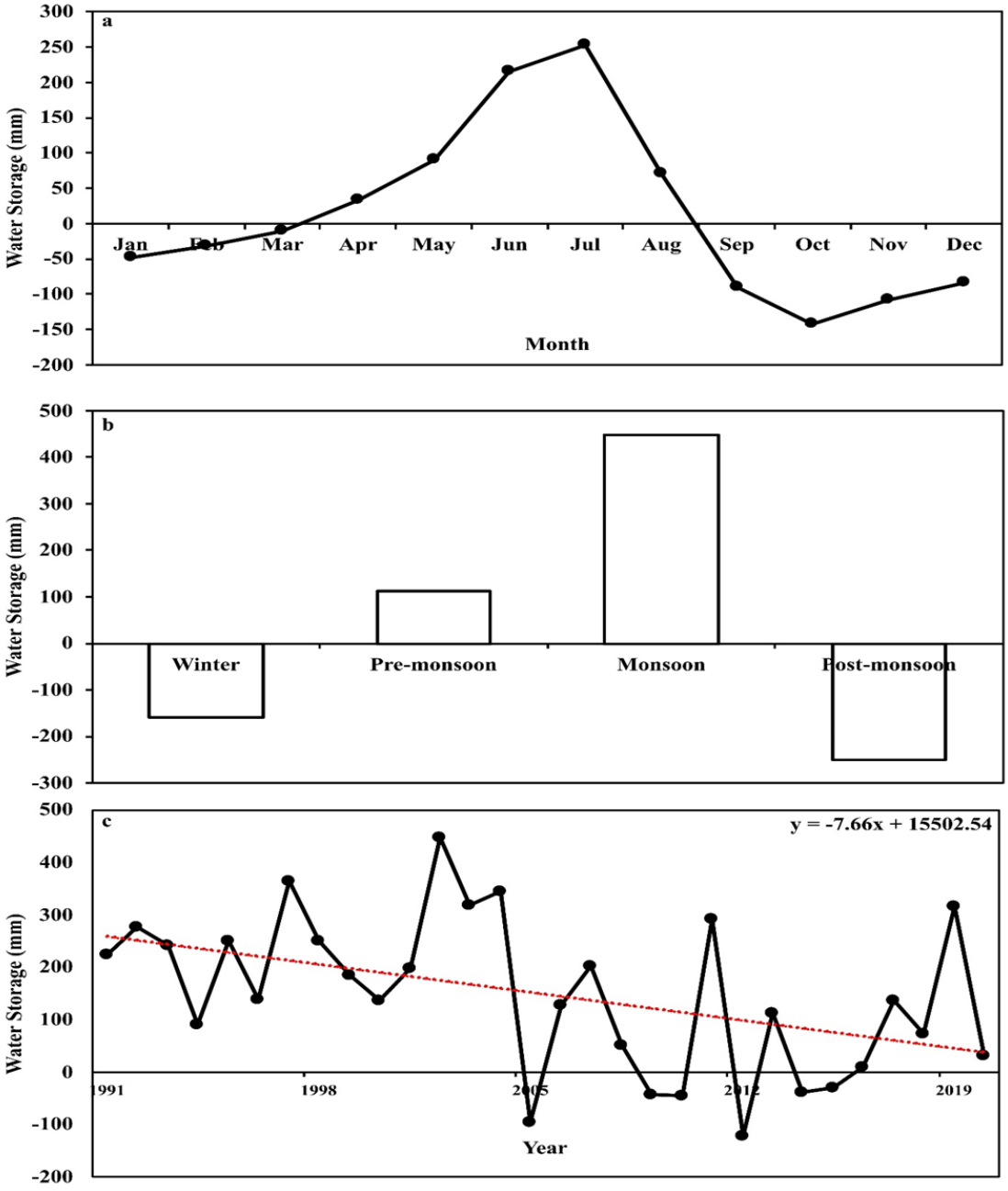

Figure 20: Monthly (a), seasonal (b) and annual (c) water balance storage.

This study explores the temporal variation of the Water balance component's contribution to streamflow and water storage changes in the Tamakoshi river basin by using the HBV model. Previously limited research was done in the same basin by using the SWAT model to investigate the climate change impacts on hydropower development (Shrestha *et al.*, 2016) and climate change impact analysis on glacier and snow melt contribution by using the SRM model (Khadka *et al.*, 2014).

It's important to note that, despite its usefulness, the SWAT model is unable to account for glacier inputs, which makes it more difficult to calculate glacier melt runoff in hydropower impact calculations. Nevertheless, SWAT has been able to quantify meltwater contributions from both snow and glaciers in the Dhudhkoshi River basin by using the T-index approach (Thakuri and Salerno, 2016). This is very important to know in order to comprehend how changes in the components of the water balance affect streamflow, particularly in the winter and monsoon seasons.

The present study aims to examine the many components of streamflow, including baseflow, snow and glacier melt, rain runoff, and their contributions to variations in water storage and balance, particularly at the Busti gauging station. Especially, no prior research has been conducted in the Tamakoshi river basin using this particular combination of research strategies, adding to the body of knowledge.

The reaction of runoff components in the glacierized area of the High Mountain Asia (HMA) upstream river basin at Devghat, Narayani River, was simulated using the SPHY model. Four components of runoff were successfully simulated by the model: baseflow, snow melt, glacier melt runoff, and rain runoff. The primary source of streamflow, rain runoff, made up between 63% and 65% of the total, with slow baseflow contributing 21%. Glacier melt contributed 3–4% of the total, and snow melt contributed 9%–12% (Khanal *et al.*, 2021, Wijngaard *et al.*, 2017). It is noteworthy that although the Tamakoshi river basin is much smaller than the Narayani Basin in terms of area covered, the overall melting contribution is still the same.

Rain runoff constituted the predominant component at downstream stations of total streamflow (Zhang *et al.*, 2022), however, snow and glacier melt had a greater influence at upstream locations in the Himalayan areas (Mukhopadhyay and Khan, 2015). This demonstrates how the components of runoff are not distributed uniformly in various places.

According to Adnan *et al.*'s observations in 2022, glacier melting contributed 45% of the streamflow in the Gilgit river basin, whereas slow baseflow contributed 27%, snow melt contributed 24%, and rain runoff contributed just 5%. On the other hand, our findings for the Tamakoshi river basin indicated that 62% of the total streamflow was contributed by rain runoff, 20% by baseflow, 5% by snow melt, and 13% by glacier melt.

Most streamflow components contribute in the summer season but relatively snow melt contribution is pre-monsoon season and glacier melt contribution is post-monsoon season. The snow and ice melting contribution was annually 17.7%, seasonally in the spring season 24.7%, summer season 17%, autumn season 16.4% and winter season 30.9% on streamflow in the same basin area (Khadka *et al., 2014*), where streamflow contribution by melting snow and glacier in winter is minimum on total streamflow and maximum in post monsoon season in our results but same as total streamflow contribution by melting although differed in seasonal melting contribution on total streamflow main cause there is two processes of runoff as surface and subsurface as a different runoff contributor viz glacier melting, baseflow and rain runoff were not categorized only snow and ice melting contribution were estimated by (Khadka *et al.*, 2014). Snow is not directly converted to surface runoff there is transformed to store glacier and groundwater recharge. Snow and glacier-fed river basin melting process depend on heat energy to surface runoff and sub-surface runoff contribution to streamflow (Lang, 1987). The model simulation period was 10 years but our simulation duration was 30 years. Observed baseflow is the dominant flow during DJF and MAM of total streamflow, Rain runoff is the dominant flow during JJAS and ON of the total flow. Results show that Rain runoff is dominant in May- October and in the remaining months, November-April baseflow is dominant in total streamflow. Maximum snow melt was observed during MAM and glacier melt contribution was ON of total streamflow. The river basin most of the precipitation occurs in the summer season in the HMA Ganga river basin 71% it states that precipitation is dominant in the summer season which is similar to our results but amount of rainfall received quietly differed from our results because area coverage of Ganga River basin at Devghat station is 37 times greater than Tamakoshi river. Tamakoshi river basin receives in monsoon season (JJAS) that is 80% (Khadka *et al.*, 2014). Similarly, which is closely correlated with our results also shows 80 % of rainfall receives in monsoon season. April-August water storage change is positive and September -March shows the negative water storage change simulated by using the same modeling approach with the other two models SWAT and BTOPMC model in the KV watershed (Thapa *et al.,* 2017, Shrestha *et al.*, 2016). Our result is completely similar to that result. Streamflow is dominant in the summer season compared with the dry season because the maximum precipitation occurs in summer season (Shrestha *et al.*, 2016). Our results show that 78% of streamflow occurred in the summer season. It is clear that most streamflow occurred in

summer season. Hence runoff component's contribution to streamflow and water balance storage change varies according to basin characteristics.

4.6 Climate change analysis

In the Tamakoshi river basin, we employed General Circulation Models (GCMs) that have been meticulously adjusted for biases using observed datasets. These models were utilized to make future projections concerning precipitation and temperature. The specific GCMs selected for this purpose include ACCESS CM2, CanESM5, MPI ESM1 2HR and, NorESM2 MM. Two distinct projection scenarios were considered: one involving stabilization without overshoot, denoted as SSP245, and the other focusing on the radiative forcing scenario associated with fossil fuel development, referred to as SSP585.

To ensure the accuracy of the GCMs, they were meticulously bias-corrected using historical periods as references. The analysis of climate change and future projections was divided into distinct time frames: historical (1991-2014), near future (2025-2049), mid future (2050-2074) and far future (2075-2099) perspective.

4.7 Bias correction

The downscale Global Climate Models (GCMs) ACCESS CM2, CanESM5, MPI ESM1 2HR, and NorESM2 projected datasets needed bias adjustment for bias correction factors for temperature Appendix (Table A7) and precipitation Appendix (Table A8) both data in the Tamakoshi river basin. Because of their coarse geographical resolution and the spatial disparities in the data products, GCMs generally display biases.

The air temperature data was adjusted using Jiri's station 1103 data in order to remove these biases. For precipitation data, bias adjustment was performed using the historical period's observed average precipitation data, which ran from 1991 to 2014. The bias correction technique used was compliant with the 2013 methodology reported by Mahmood and Babel.

The resulting monthly average mean bias-corrected temperature and precipitation data show a notable increase in bias reduction. An obvious indicator of the bias correction method's efficacy was obtained by comparing these bias-corrected datasets before and after the correction procedure.

Please see Figure 21, which shows the bias correction of precipitation, for a visual depiction of the bias correction results. Sections A) ACCESS CM2 bias correction, B) CanESM5 bias correction, C) MPI ESM1 2HR bias correction, and D) NorESM2 MM bias correction comprise its division. The bias correction of temperature is shown in Figure 22, where sections A) exhibit the bias correction of ACCESS CM2, B) show the bias correction of CanESM5, C) show the bias correction of MPI ESM1 2HR, and D) presents NorESM2 MM bias correction comprise its division of temperature. The efficiency of the bias correction procedure for temperature and precipitation data is shown graphically in these graphs.

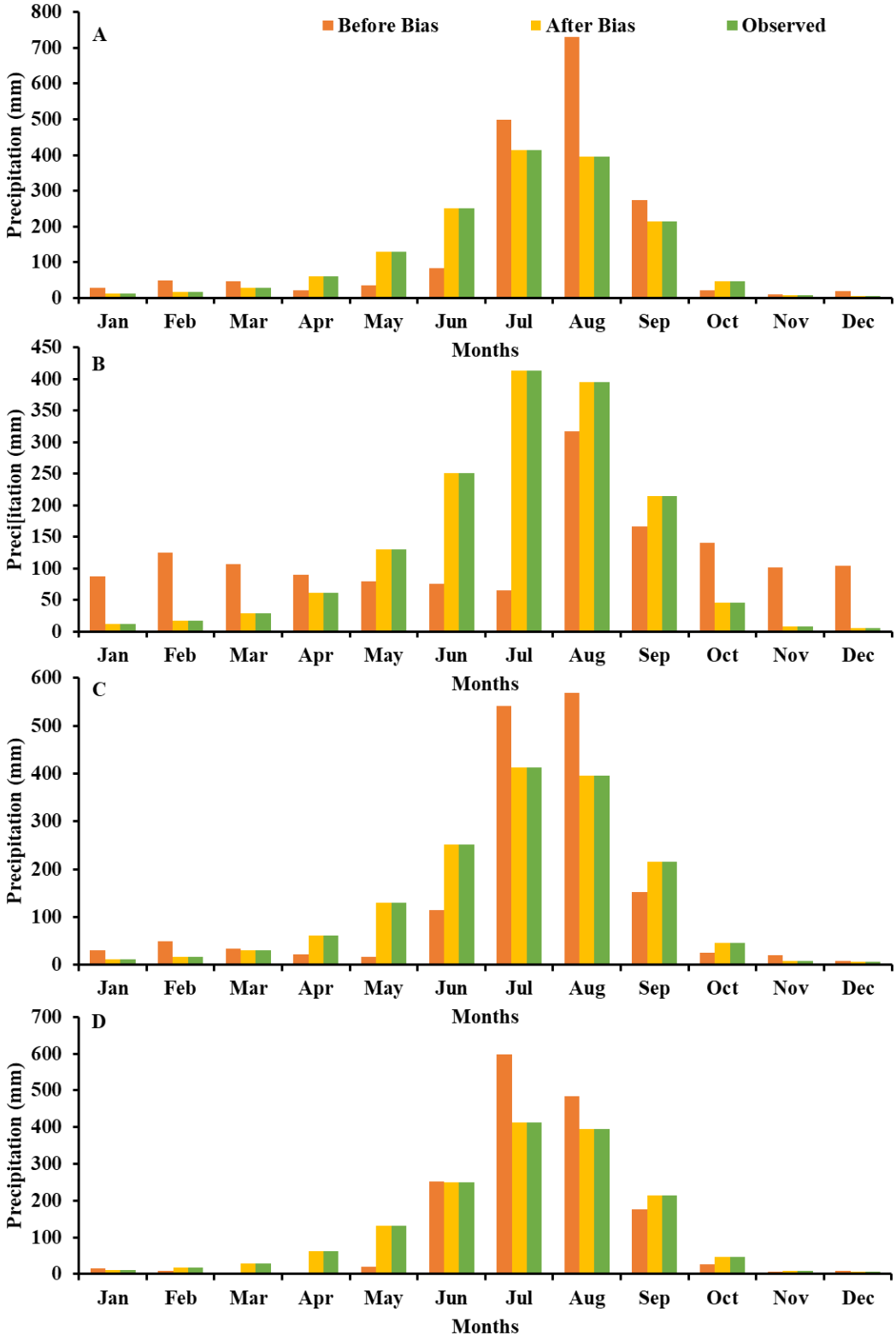

Figure 21: Bias correction of precipitation A) Bias correction of ACCESS CM2 B) Bias correction of CanESM5 C) Bias correction of MPI ESM1 2HR D) Bias correction of NorESM2 MM.

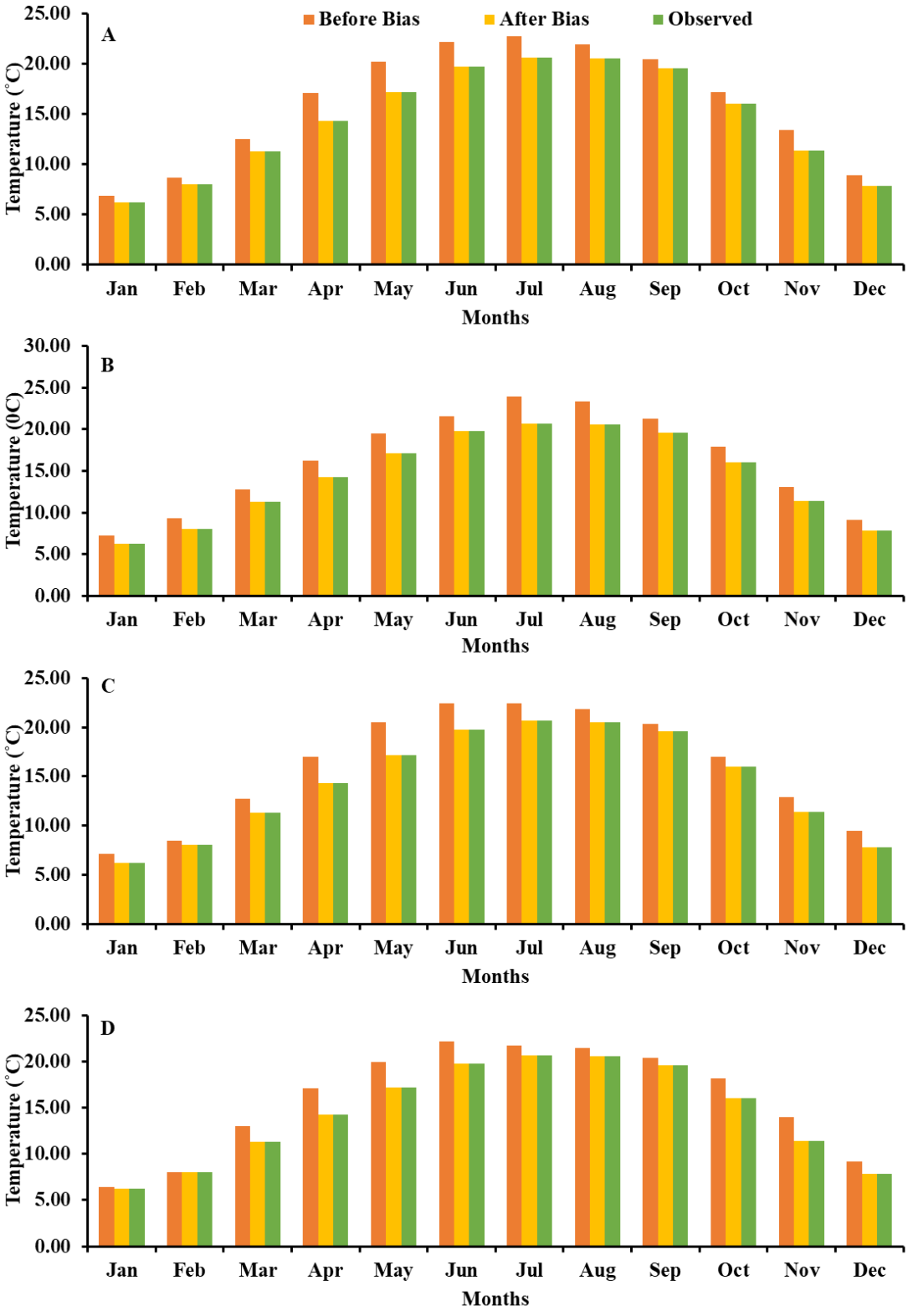

Figure 22: Bias correction of temperature A) Bias correction of ACCESS CM2 B) Bias correction of CanESM5 C) Bias correction of MPI ESM1 2HR D) Bias correction of NorESM2 MM.

4.8 Projected impacts of GCMs

The projected impacts of selected GCMs: ACCESS CM2, CanESM5, MPI ESM1 2HR and NorESM2 MM were individually analyzed. Projected impacts of precipitation and temperature were analyzed in SSP245 and SSP585 scenarios.

4.8.1 Projected precipitation

It is clear that the ACCESS CM2 model forecasts higher precipitation for both the SSP245 and SSP585 scenarios across all time periods after evaluating the bias-corrected precipitation data from the General Circulation Models in the Tamakoshi river basin. The initially recorded precipitation amount of 1584 mm was used as the baseline for these results. For the SSP245 scenario, we found significant increases in precipitation throughout various time intervals. More specifically, precipitation increased by 44% during the Near Future (NF) period, 34% during the Middle Future (MF) period, 22% during the Far Future (FF) period towards the end of the 21st century. On the other hand, the pattern of precipitation variations under the more extreme SSP585 scenario was different. In this scenario, precipitation increased by a more moderate 2% during the Near Future (NF) period and by a considerable 24% during the Middle Future (MF) period. Precipitation increased by an astounding 65% throughout the Far Future (FF) period with the end of the 21st century, marking the most notable development. It is important to note that the changes in precipitation between the SSP245 and SSP585 scenarios differ significantly. The Near Future time period in the SSP245 scenario shows the most rise in precipitation, while the Far Future timeframe shows the least amount of change. Conversely, the SSP585 scenario indicates the least significant change in precipitation during the Near Future period and the largest rise during the Far Future period.

The NorESM2 MM model indicates varying precipitation scenarios for different Shared Socioeconomic Pathways (SSP) in all time periods. The baseline precipitation level was observed to be 1584 mm. Under the SSP245 scenario, the Near Future (NF) precipitation is projected to decrease by 7%, Middle Future (MF) precipitation by 6%, Far Future (FF) precipitation by 11%, the end of the 21st century. Conversely, in the more extreme SSP585 scenario, the NF precipitation is expected to increase by 5%, MF precipitation by 20%, FF the end-of the 21st century precipitation by 1%. Notably, the most significant decrease in precipitation is anticipated in the Far Future time period under the SSP245 scenario, while the least decrease is projected for the Middle Future.

In contrast, under the SSP585 scenario, the greatest increase in precipitation is expected in the Middle Future, and the smallest increase is projected for the Far Future time period.

For both the SSP245 and SSP585 scenarios, the CanESM5 model shows a significant increase in precipitation over all time periods. There was 1584 mm of precipitation recorded as the baseline. The Near Future (NF) precipitation is expected to rise by 39%, the Middle Future (MF) by 70%, the Far Future (FF) by 85%, by the end of the 21st century, precipitation is expected to rise under the SSP245 scenario. On the other hand, even higher increases in precipitation are predicted by the more extreme SSP585 scenario. Precipitation is predicted to increase by 73% in the Near Future (NF), 110% in the Middle Future (MF), a significant 199% in the Far Future (FF), the end of the twenty first century. It is interesting to observe that for both scenarios, the minimum increase in precipitation happens in the Near Future time period, while the highest rise occurs during the Far Future time period.

For the SSP245 and SSP585 scenarios, the MPI ESM1 2HR model shows a significant rise in precipitation levels over all time periods. At 1584 mm, the first baseline measurement of precipitation was made. In the context of the SSP245 scenario, precipitation increased by 5% in the Near Future (NF) time windows, 4% in the Middle Future (MF) time windows, 5% in the Far Future (FF) time windows that end of the twenty first century. On the other hand, the more extreme SSP585 scenario predicted that by the end of the twenty first century, precipitation would have increased by 2% for the Near Future (NF) time windows, 1% for the Middle Future (MF) time windows, a significant 11% increase for the Far Future (FF) time windows. Under the SSP245 scenario, the least rise in precipitation is shown in the Middle Future time period, but there is a notable difference in the highest increase in precipitation that occurs in the Near Future and Far Future time periods. The SSP585 scenario shows that the Far Future time period experiences the highest rise in precipitation, while the Middle Future time period experiences the lowest increase.

For both the SSP245 and SSP585 scenarios, the ensemble of four General Circulation Models (GCMs) shows a rise in precipitation over all time periods. The baseline precipitation, which was first measured at 1584 mm, has increased noticeably. The Near Future (NF) period saw a 20% increase in precipitation under the SSP245 scenario,

whereas the Middle Future (MF) observed a 25% increase. Similarly, precipitation increased by 25% over the Far Future (FF) era increased by the end of the 21st century. On the other hand, the more extreme SSP585 scenario predicted that precipitation would increase by 21% in the near future, 39% in the middle future, a significant 69% in the far future with the end of the 21st century. In the SSP245 scenario, it is noteworthy that the greatest increases in precipitation were recorded in the Middle and Far Future time periods, whereas the least notable increases were recorded in the Near Future time periods. Conversely, for the Far Future time period, the SSP585 scenario demonstrated the highest increase in precipitation, while the Near Future time period saw the least increase. Notably, under the SSP245 scenario, the CanESM5 projection showed the largest increase in precipitation throughout all time periods, but the NorESM2 MM prediction showed a drop in precipitation. With CanESM5 representing the highest increase in precipitation over all time periods and MPI ESM1 2HR reflecting the minimal precipitation projection for the Near Future and Middle Future time periods, (Figures 23A and 23B) visually show these projections. In the SSP585 scenario, NorESM2 MM predicted negligible precipitation during the Far Future time frame. An annual graphical representation of precipitation from the four GCMs, each of which corresponds to a different scenario, is shown in Figure 23.

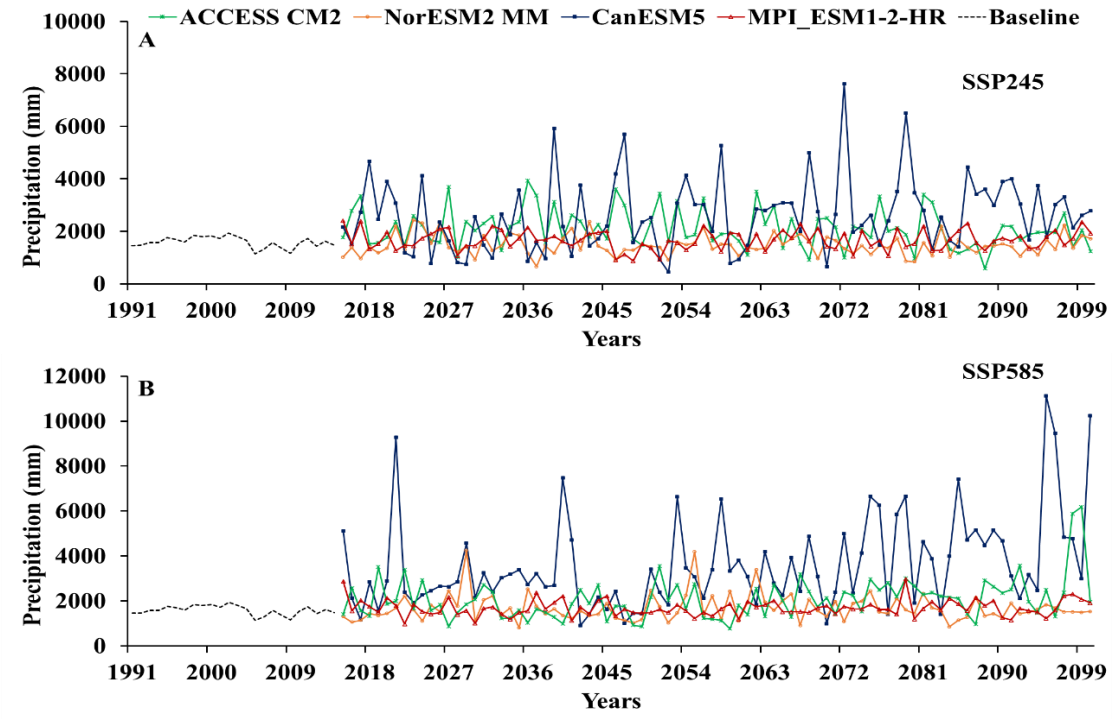

Figure 23: Historical with projected precipitation of four GCMs A) SSP245 B) SSP585.

4.8.2 Projected temperature

After applying the General Circulation Models (GCMs) to the bias-corrected temperature data of the Tamakoshi river basin, it was found that the ACCESS CM2 model predicts a rise in temperature for the SSP245 and SSP585 scenarios over the course of all time periods. This region's baseline temperature was 14.43˚C. Under the SSP245 scenario, the temperature is expected to rise by the end of the twenty-first century, by 1.54 ˚C for the Near Future (NF) time window, 3.11 ˚C for the Middle Future (MF) time window, and 3.97 ˚C for the Far Future (FF) time window. The temperature estimates are considerably more important for the more extreme SSP585 scenario. A temperature increase of 1.88 ˚C is predicted for the Near Future (NF) time window, 4.33 ˚C is predicted for the Middle Future (MF) time window, 6.80 ˚C is predicted for the Far Future (FF) time window is predicted for the end of the 21st century. Notably, in both scenarios, there is a significant difference in temperature increase between the windows for the Far Future and the Near Future time periods.

The NorESM2 MM model demonstrates differing temperature trends across two scenarios: SSP245 and SSP585, spanning various time periods. The baseline temperature is established at 14.43 °C. Under the SSP245 scenario, the Near Future (NF) time frame experiences a increase of 1.31 °C in temperature, while the Middle Future (MF) sees an increase of 2.38 °C. The Far Future (FF) timeframe witnesses a more substantial temperature rise of 2.89 °C by the end of the 21st century. In contrast, the more extreme SSP585 scenario projects a temperature increase in the Near Future (NF) by 1.50 °C, a more significant increase of 3.17 °C in the Middle Future (MF), and a substantial rise of 5.32 °C in the Far Future (FF) by the end of the 21st century, temperatures under SSP585. It is noteworthy that the most substantial temperature increase occurs in the Far Future time period window in both scenarios, while the minimum temperature increase is observed in the Near Future time period window.

The CanESM5 model demonstrates an elevation in temperature for both the SSP245 and SSP585 scenarios across all time periods. The baseline temperature stands at 14.43°C. Under the SSP245 scenario, the temperature in the Near Future (NF) time frame increases by 1.73°C, the Middle Future (MF) experiences a 3.12°C increase, the Far Future (FF) sees a rise of 3.80°C, and by the end of the 21st century, the temperature elevates. In contrast, the more extreme SSP585 scenario projects a 2.28°C increase in the Near Future (NF), a substantial 4.69°C rise in the Middle Future (MF), a significant

7.76°C increase in the Far Future (FF), the temperature surge by the end of the 21st century. Notably, there is a marked disparity in temperature escalation, with the Far Future period experiencing the highest increase and the Near Future period showing the least significant temperature rise in both scenarios.

In comparison to the baseline temperature of 14.43 °C, the MPI ESM1 2HR model shows a steady increase in temperature for both the SSP245 and SSP585 scenarios over all time periods. In the SSP245 scenario, the Near Future (NF) temperature is projected to increase by 0.90 °C, the Middle Future (MF) temperature by 1.85 °C, the Far Future (FF) temperature by 2.41 °C, the end of the 21st century, there is a predicted increase. The temperature forecasts are much greater in the more extreme SSP585 scenario: an increase of 0.94 °C is predicted for the NF, 2.57 °C for the MF, 4.63 °C for the FF by the end of the century. It's important to note that in both scenarios, the temperature rises most significantly in the Far Future time period and least in the Near Future time period.

For both the SSP245 and SSP585 scenarios, the combined model of four Global Climate Models (GCMs) shows a steady increasing trend in temperature throughout a range of time periods. 14.43°C is the starting benchmark temperature. Within the Near Future (NF) time range of the SSP245 scenario, there is a significant 1.37°C increase in temperature. Moreover, the temperature rises by 2.61°C more significantly during the Middle Future (MF) period and by 3.27°C more significantly within the Far Future (FF) time range. On the other hand, the extreme SSP585 scenario predicts a significantly more severe rise in temperature over time. The temperature is expected to rise by 1.65°C in the Near Future (NF) timeframe and by a significant 3.69°C in the Middle Future (MF) period. The anticipated temperature increase in the Far Future (FF) time span is 6.13°C. By the end of the twenty-first century, more warming is predicted. It is noteworthy that, for both scenarios, the largest temperature increase is recorded in the Near Future time period, while the smallest increase occurs in the Far Future time period. The CanESM5 projection is shown in Figure 24, with subfigures (A) and (B) displaying the pattern of significant temperature rises for both the SSP245 and SSP585 scenarios over all time frames. In a similar vein, Figures 24A) and (B) show the MPI ESM1 2HR projection and highlight the minimum temperature projection for each scenario over the course of all time periods. Figure 24 Shows an annual graphical representation of selected GCMs.

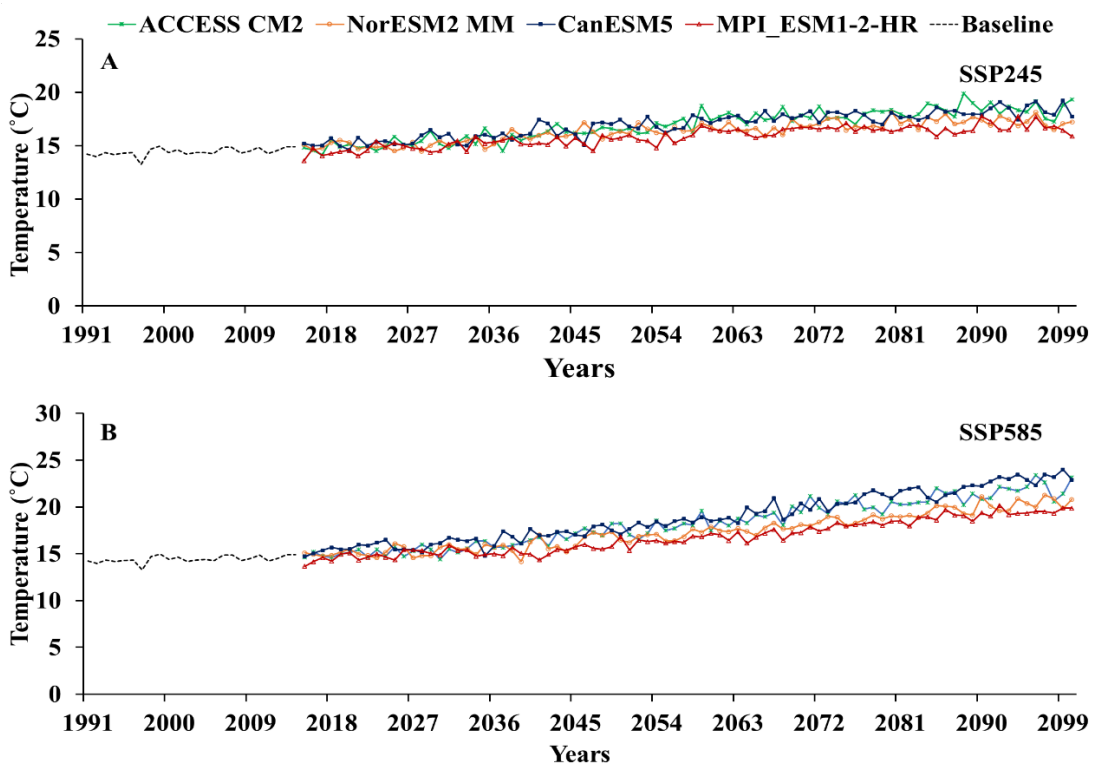

Figure 24: Historical with projected temperature of four GCMs A) SSP245 B) SSP585.

4.9 Climate change impacts on water balance components

Climate change impacts on precipitation, discharge, evapotranspiration, rainfall runoff, baseflow runoff, glacier melt runoff, and snow melt runoff included in the following sections. A calibrated HBV light 4.0 hydrological model was used to simulate these components of the streamflow that make up the water balance. The chosen ensembled GCMs, MPI ESM1 2HR and NorESM2 MM were used to simulate the chosen hydrological model. When it comes to simulating glaciers, the chosen hydrological models outperform the other two, and the chosen GCMs exhibit reduced divergence in extreme annual precipitation occurrences when compared to historical precipitation data. The yearly variations in the streamflow components of the water balance are displayed in Figure (25A and 25B) for all time periods considered in both scenarios.

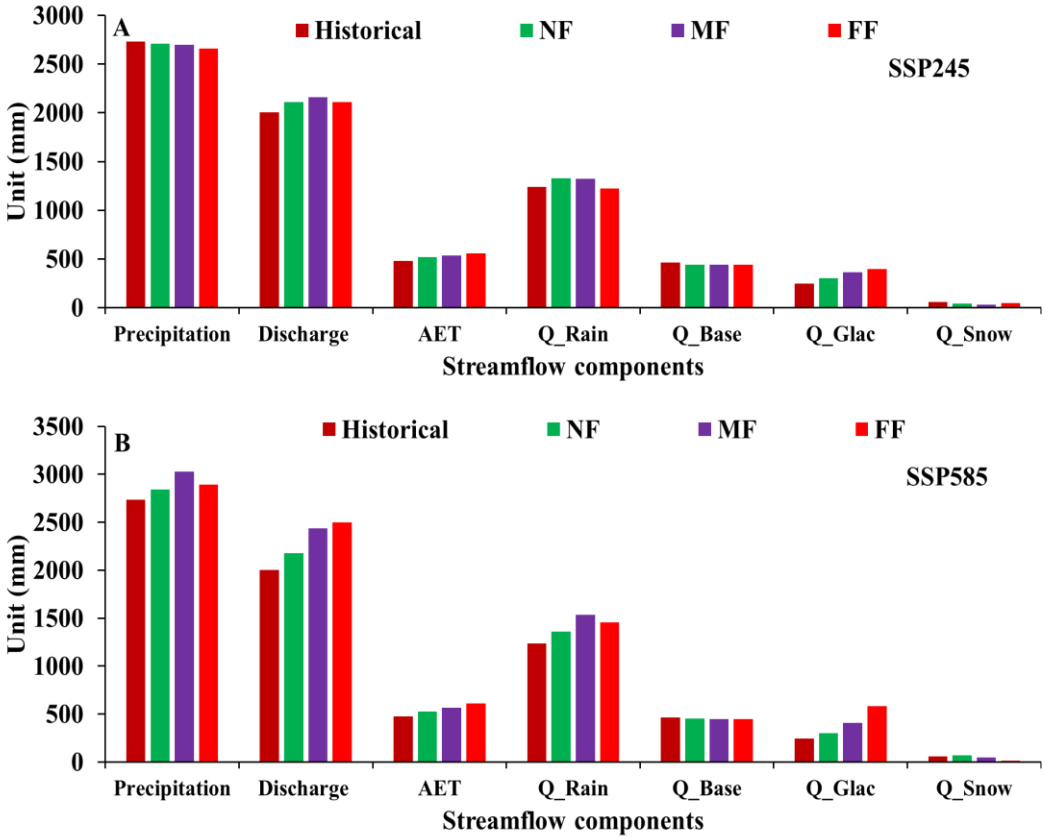

Figure 25: Climate change impacts on streamflow components during the Historical, NF, MF and FF under SSP245 (top) and SSP585 (bottom) scenarios**.**

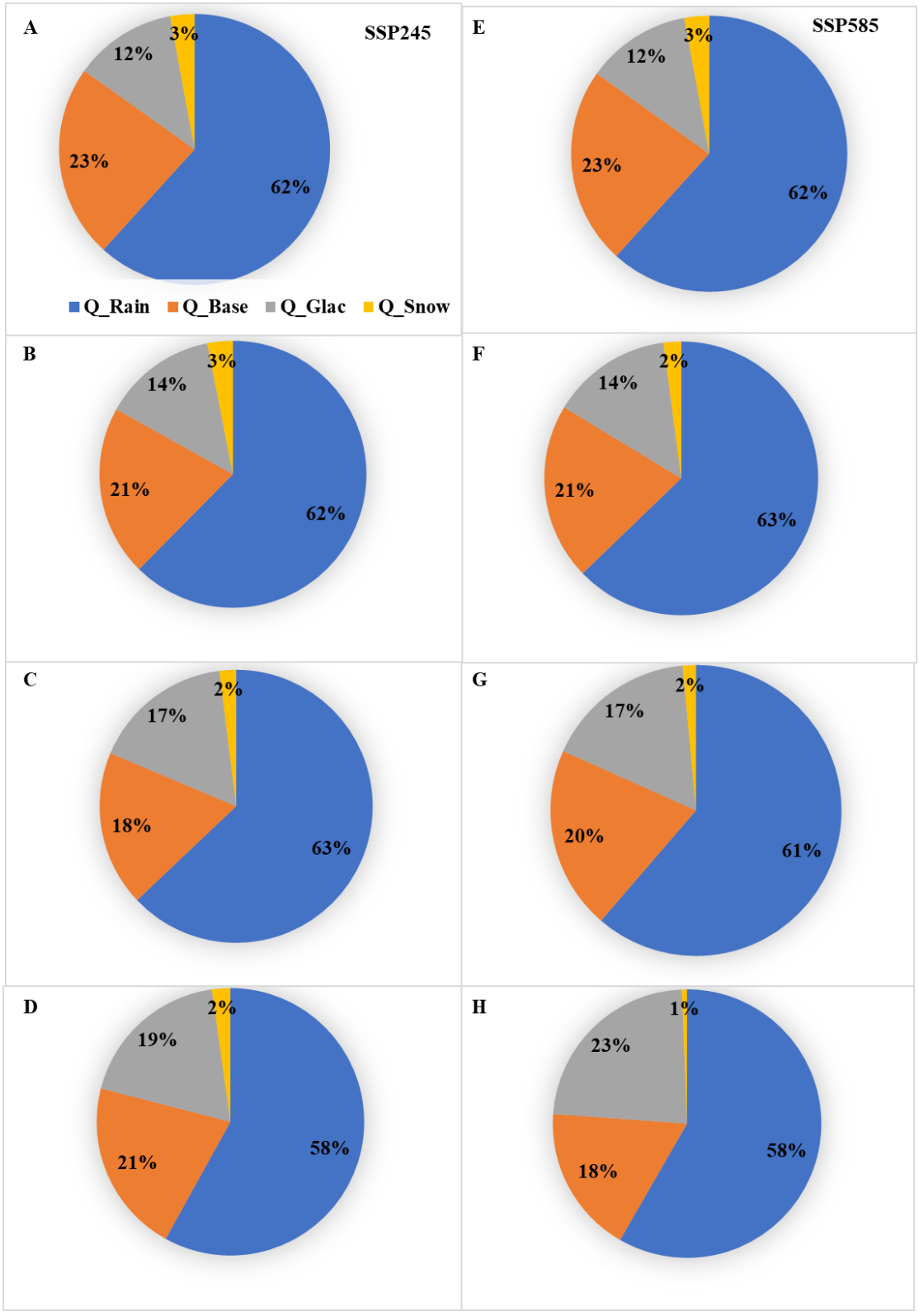

Figure 26: Relative contribution of water balance components during Historical (A, E), NF (B, F), MF (C, G) and FF (D, H) under SSP245 (left) and SSP585 (right) scenarios.

4.9.1. Climate change impact on precipitation

The hydrological cycle is largely regulated by precipitation, especially in terms of how streamflow is affected. Significantly, precipitation is more common in the wet months, which is mainly due to the summer monsoon's dominance in the river basin. Significant seasonal fluctuations in the precipitation pattern are caused by this climatic phenomenon. The season with the most rainfall, or wettest season, usually runs from June to September. The season with the least amount of rainfall, or driest season, usually runs from December to February in Figure 27A and 27C. This precipitation pattern continues till the end of the century and remains constant throughout historical eras and all-time windows.

There is some uncertainty in the predicted range of precipitation, which, depending on the particular scenario, can range from 80% to 84% during the monsoon season and from a tighter range of 2% to 3% in the dry season in Appendix (Table A9). SSP245 projects somewhat different values than SSP585 ranging from 75%-84% in monsoon in Appendix (Table A10). Nonetheless, a little decrease in the rate of precipitation is a general pattern seen in both situations showed by Figure 27B and 27D.

Comparing projected variations in precipitation amounts over different months to historical data, Figure 25 shows how this will likely happen. It is noteworthy that the summer season shows the strongest departures from the historical average, with increased precipitation levels.

In the past, 2733 mm of precipitation served as the baseline. Figure 25A shows precipitation is predicted to drop under the SSP245 scenario over a range of time windows: there will be 1% in the Near Future (NF), 1% in the Middle Future (MF), and 3% in the Far Future (FF) by the end of the 21st century. The SSP585 scenario, on the other hand Figure 25B predicts an increase in precipitation, with a rise of 4% in the Near Future, 11% in the Middle Future, 6% in the Far Future by the end of the 21st century. Notably, the SSP585 scenario predicts that precipitation will increase most significantly in the Middle Future time period and least in the Near Future time period.

In contrast, the SSP245 scenario shows the greatest precipitation decrease in the Far Future time frame, with very minor decreases in the Near Future and Middle Future time frames.

Overall, the findings highlight that, in comparison to the SSP245 scenario, the SSP585 scenario predicts higher precipitation impacts throughout the basin over all time periods.

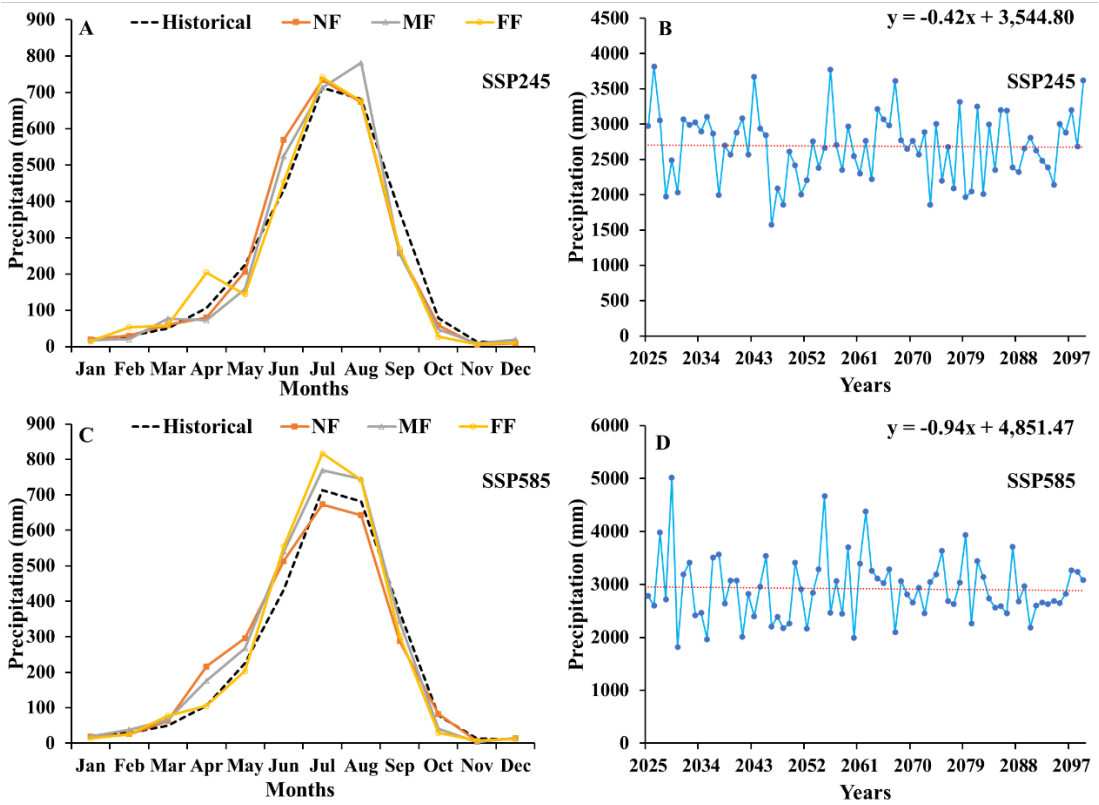

Figure 27: Monthly climate change impacts on the precipitation A) & C) during the Historical, NF, MF, FF and annual linear trend of projected precipitation B) & D) under SSP245 (top) and SSP585 (bottom) scenarios.

4.9.2. Climate change impact on river discharge

Summer rainfall produces monsoon precipitation, which largely affects river discharge in the basin. Rain runoff, baseflow runoff, and runoff from snow and glacier melt all byproducts of different hydrological processes combine to produce this discharge. In both the SSP245 and SSP585 scenarios, the majority between 73% and 76% is anticipated to come from the estimated river flow during the monsoon season, which runs from June to September in Appendix (Table A9). According to the SSP585 scenario, the basin's discharge is expected to rise by 71% to 73% during the monsoon season in Appendix (Table A10).

Baseflow and the contribution from snow and glacier melt are responsible for the river's low flow, which reaches its lowest point in the winter months of December through

February in Figure 28A and 28C. In all scenarios and time frames, this low flow accounts for 6% to 7% of the total flow. The overall river flow is influenced by a number of streamflow components, which are discussed in more detail in the dissertation's section on water balance components.

For both scenarios, the hydrograph at the gauging station shows a continuous pattern of rise and recession over historical data, all time periods, and at the end of the century (28B and 28D). In both cases, projected discharge rates indicate a general increase. In comparison to the historical period, Figure 28 shows that the rate of anticipated discharge can vary based on precipitation levels in all months; however, summertime river flow is consistently higher.

The baseline discharge for the historical era was found to be 2004 mm. With a 5% rise in discharge for the Near Future (NF), 8% increase for the Middle Future (MF), 5% increase for the Far Future (FF) at the end of the 21st century, the anticipated discharge in Figure 25A the SSP245 scenario is predicted to drop. On the other hand, the SSP585 scenario Figure 25B exhibits an increase in the predicted discharge, with increases of 9% for the Near Future (NF), 22% for the Middle Future (MF), 25% for the Far Future (FF) by the end of the 21st century. Notably, in the SSP245 scenario, the largest increase in discharge occurs during the Middle Future time, but in the SSP585 scenario, the largest increase occurs during the Far Future period.

The findings show that, for all time period windows and through the end of the century, the SSP585 scenario predicts a larger discharge in the basin than the SSP245 scenario.

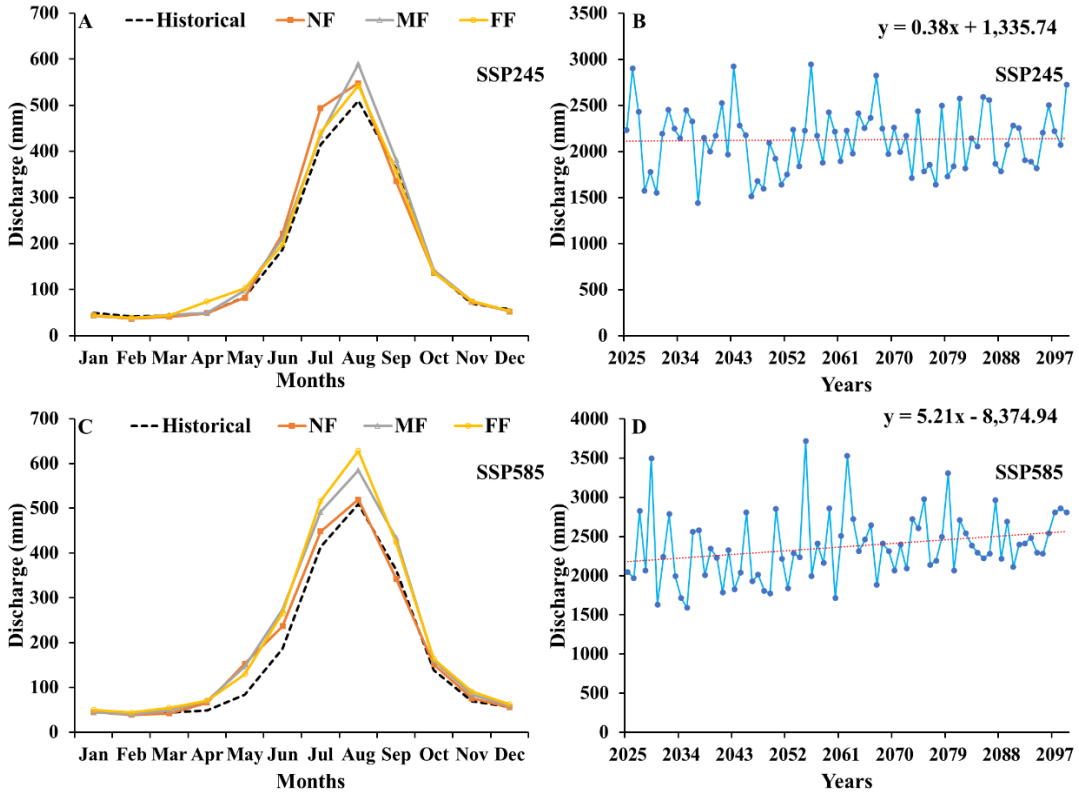

Figure 28: Monthly climate change impacts on the discharge A) & C) during the Historical, NF, MF, FF B) & D) annual linear trend of projected discharge under SSP245 (top) and SSP585 (bottom) scenarios.

4.9.3. Climate change impact on rain runoff

One of the most important factors influencing the overall streamflow in a given area is rain runoff. It is largely dependent on the amount of rainfall; more rainfall causes more rain runoff, whereas less rainfall causes less rain runoff during a certain period of time. Remarkably, rainfall-runoff is highest during the wet season, primarily due to the summer monsoon's predominance in the basin.

In this basin, rain runoff stands out as a significant factor, accounting for approximately 60% of the total discharge. Looking (Figure 26A-H) at two prominent scenarios, SSP245 and SSP585, historical data reveals that rain runoff contributed around 62% of the total discharge in the past. In the near future (NF), this contribution slightly increases to 63% for SSP245 and remains at 62% for SSP585. In the mid-term future (MF), rain runoff's influence remains substantial, with a 61% contribution for SSP245 and 63% for SSP585. However, in the far future (FF), there is a decline in rain runoff's impact, with both scenarios showing a decrease to 58% of total discharge.

Looking further out, particularly near the end of the century, both SSP245 and SSP585 scenarios exhibit a more consistent contribution from rain runoff, stabilizing at the total flow. Remarkably, rain runoff maintains its dominance in the near future (NF) and mid-term future (MF), but in the far future (FF), it becomes less significant in both scenarios. As a result, by century's end, the scenarios come closer together, showing rain runoff's constant and equal contribution to streamflow.

Two possibilities had significant impacts on rain runoff in both historical and end-of-century time frames. The August maximum and the February and March low rainfall were impacted by these situations (Figure 29A and Figure 29C). The measured baseline precipitation total was 1237.18mm.

First, because of the significant effect of decreasing precipitation, there was a decrease in expected rain runoff in the SSP245 scenario (Figure 29B). In particular, Figure 25A showed the rain runoff increased by 7%, and 7%, in the Near Future (NF), Middle Future (MF), respectively. On the other hand, rain runoff decreased by 1% in the Far Future (FF) with the end of the 21st century.

On the other hand, Figure 29D the SSP585 scenario had a rise in anticipated precipitation runoff, mainly due to the noteworthy influence of decreased snow formation brought on by higher temperatures. In this scenario, Figure 25B there would be an increase in rain runoff of 10% in the Near Future (NF), 24% in the Middle Future (MF), 18% in the Far Future (FF), near the end of the 21st century. Remarkably, the Near Future and Middle Future periods witnessed the largest increases in rain runoff, while the Far Future period saw the least.

Overall, the findings show that, in comparison to the SSP245 scenario, the SSP585 scenario in the basin produced more rainfall runoff at the end of the century and throughout all time periods.

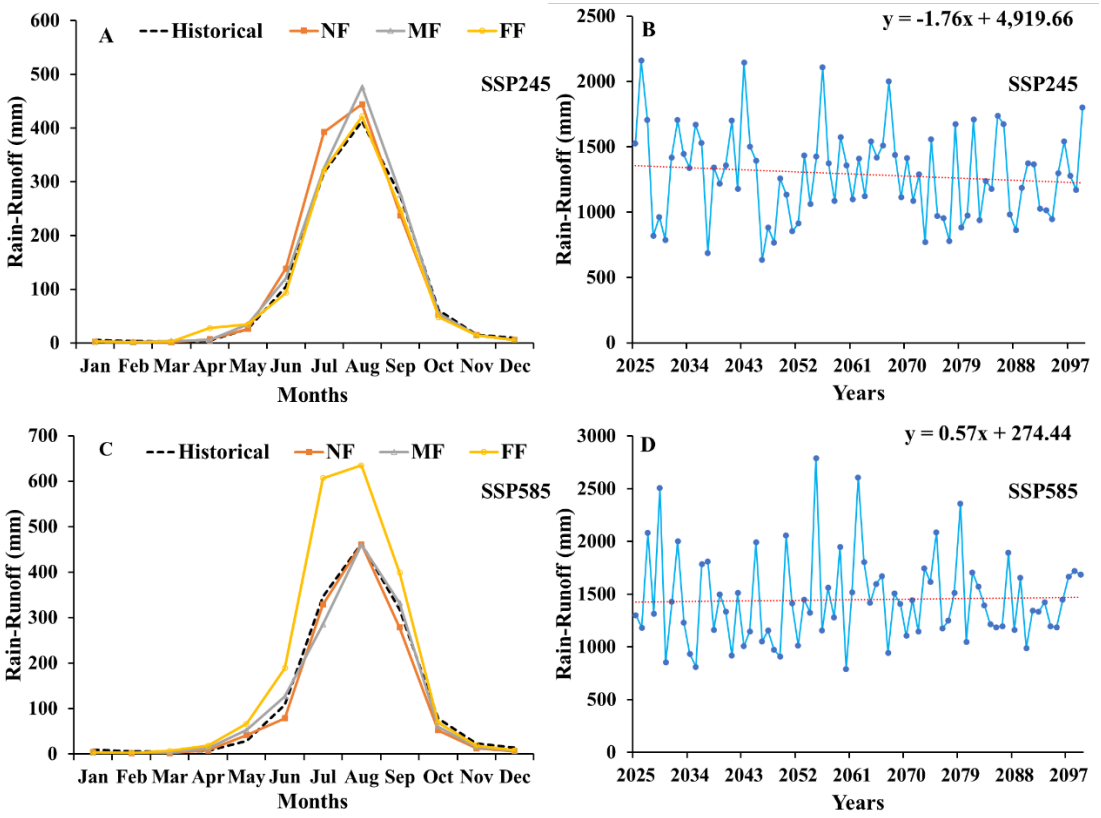

Figure 29: Monthly climate change impacts on the rain runoff A) & C) during the Historical, NF, MF, FF and annual linear trend of projected rain runoff B) & D) under SSP245 (top) and SSP585 (bottom) scenarios.

4.9.4. Climate change impact on baseflow runoff

Baseflow runoff is a continuous streamflow component that contributes significantly to a water basin's overall discharge. This hydrological phenomenon is a significant aspect of the flow regime because of its consistent behavior, particularly during the driest months. Baseflow runoff is dependent on groundwater replenishment during the wet seasons. More notably, (Figure 30A and 30C) it is more noticeable from December to May than runoff from snow and glacier melt in the basin and from rain.

Among the several components of streamflow, baseflow runoff is the second most significant contribution to overall discharge, usually making up around 20% of the total. As seen in scenarios SSP245 and SSP585, the baseflow runoff's contribution to the overall discharge changes over different times (Figure 26A-H).

According to historical data, baseflow runoff has historically made up 23% of the basin's total discharge under the SSP245 scenario. The contribution levels are predicted

to be 21%, 18%, and 21%, respectively, for the Near Future (NF), Mid Future (MF), Far Future (FF) with end of the Century.

The historical baseflow runoff contribution to the overall discharge in the SSP585 scenario stays at 23%. The future predictions, however, indicate differences: the contributions during the Near Future (NF) and Far Future (FF) periods are larger, at 21% and 18%, respectively, while the contributions during the Mid Future (MF) era are lower, at 20%.

It is noteworthy that in SSP245 and SSP585, baseflow runoff dominates in both the Near Future (NF) and Far Future scenarios. But in the SSP245 and SSP585 scenarios, it contributes very little during the Mid Future (MF), suggesting a more dynamic behavior at this time. These patterns offer vital information on the dynamics of baseflow runoff and how it contributes to the basin's overall discharge.

Both scenarios led to an increase in the maximum baseflow runoff in October and the minimum baseflow runoff in February during both historical, all-time period windows (Figure 30A and 30C), and the end of the century. The projected baseflow runoff exhibited an accelerated increase rate due to the significant influence of groundwater recharge resulting from precipitation in both scenarios (Figure 30B). The initial rainfall runoff measurement recorded 463 mm.

In the context of the SSP245 scenario, the projected baseflow runoff is expected to decrease. Specifically, (Figure 25A)in the time windows for the Near Future (NF), Middle Future (MF), Far Future (FF), and at the end of the 21st century, the baseflow runoff is projected to decrease. Conversely, under the SSP585 scenario, (Figure 25B) the baseflow runoff for the Near Future (NF), Middle Future (MF), and Far Future (FF) is anticipated to decrease by 3%, while at the end of the 21st century, it is projected to decrease.

Notably, both scenarios predict a reduction in baseflow runoff across all time windows and at the end of the century, but the SSP585 scenario indicates a more substantial reduction in baseflow runoff, particularly in the Far Future time period window. In all other time frames, the reduction is similar between the two scenarios.

The results indicate that the projected impact of the SSP585 scenario will result in a more pronounced decrease in baseflow runoff compared to the SSP245 scenario throughout all time period windows at the end of the century.

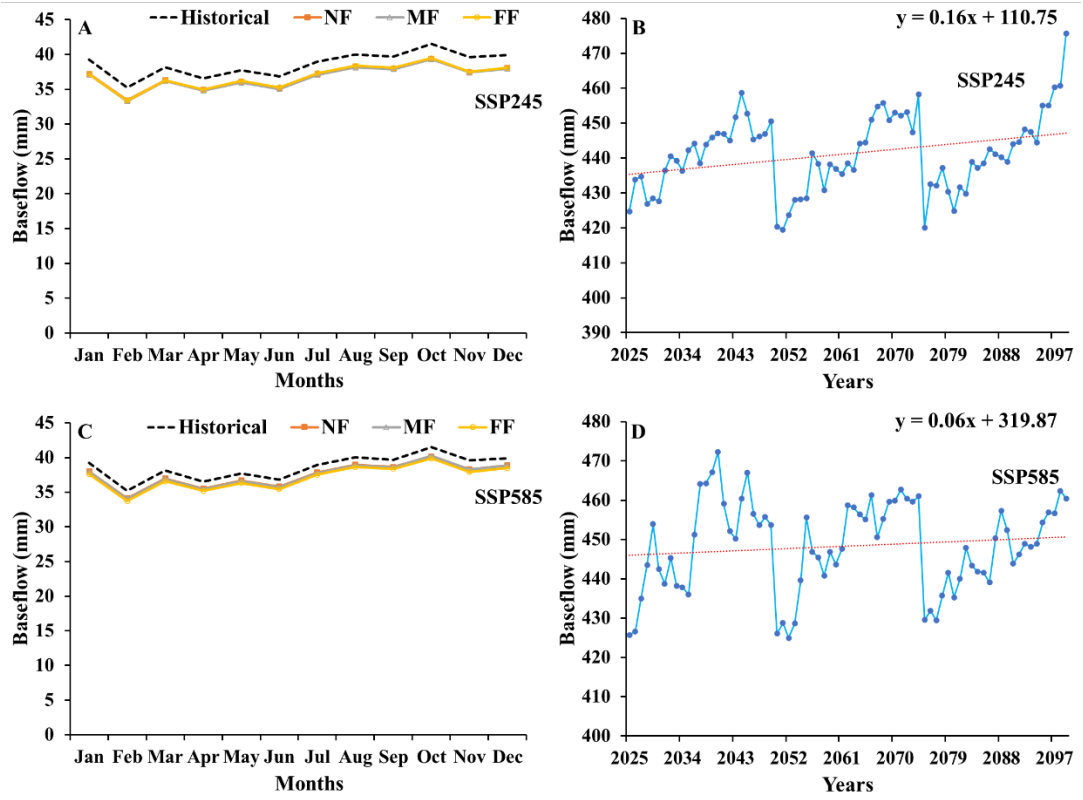

Figure 30: Monthly climate change impacts on the baseflow A) & C) during the Historical, NF, MF, FF and annual linear trend of projected baseflow B) & D) under SSP245 (top) and SSP585 (bottom) scenarios.

4.9.5. Climate change impact on glacier melt runoff

The changing climate poses a significant concern, particularly in relation to the runoff of glacier melt, which constitutes a major component of total discharge accumulation in streamflow. The extent of glacier melt runoff is closely tied to prevailing temperatures, where rising temperatures result in increased runoff, while minimum temperatures lead to reduced melt runoff over time.

Historically, glacier melt runoff has dominated the basin, contributing to approximately 17% of the total discharge. Under the SSP245 scenario, this contribution was 12% in the past, 14% in the Near Future (NF), 17% in the Middle Future (MF), 19% in the Far Future (FF) in the end of the Century. In the SSP585 scenario, the historical glacier melt runoff contribution was also 12%, but it increased to 14% in the Near Future (NF), 17%

in the Middle Future (MF), 23% in the Far Future (FF), at the end of the Century. Notably, glacier melt runoff dominates in the Far Future (FF) for both scenarios, while the minimum contribution occurs in the Near Future (NF) for both scenarios (Figure 26A-H).

Both scenarios exhibit an increase in maximum glacier melt runoff in August and a decrease in minimum glacier melt runoff in February across historical, all-time period windows, and at the end of the century (Figure 31A and 31C). Projected glacier melt runoff displays an escalating trend due to the rising temperatures in both scenarios. The baseline glacier melt runoff, which was observed to be 245 mm, is projected to increase. According to the SSP245 scenario (Figure 25A), during the Near Future (NF), glacier melt runoff is expected to increase by 23%, while in the Middle Future (MF), it is projected to increase by 48%, and in the Far Future (FF), it is expected to increase by 61%. At the end of the 21st century, glacier melt runoff is projected to increase. In the SSP585 scenario (Figure 25B), glacier melt runoff during the Near Future (NF) is expected to increase by 22%, in the Middle Future (MF) by 66%, in the Far Future (FF) by 136%, and at the end of the 21st century, it is projected to increase.

Overall, there is a notable contrast between the minimum increase in glacier melt runoff during the Near Future time period window and the maximum increase in the Far Future time period window for both scenarios. Nevertheless, it's important to emphasize that the minimum glacier melt runoff increase is anticipated during the Near Future time windows for both scenarios.

The results indicate that the SSP585 scenario has a more pronounced impact on glacier runoff (Figure 31D) than the SSP245 scenario (Figure 31B) across all time period windows at the end of the century in the basin.

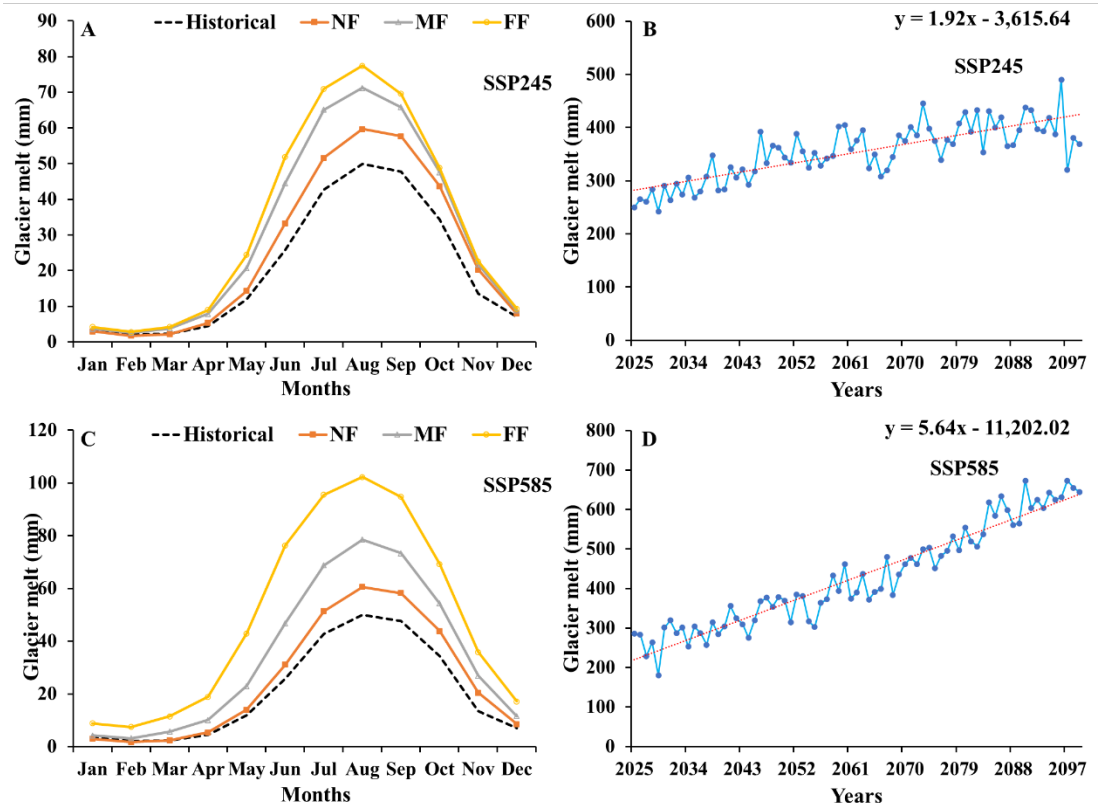

Figure 31: Monthly climate change impacts on the glacier melt A) & C) during the Historical, NF, MF, FF and annual linear trend of projected glacier melt B) & D) under SSP245 (top) and SSP585 (bottom) scenarios.

4.9.6. Climate change impact on snow melt runoff

Snow melt runoff is a crucial component contributing to the total discharge accumulation in a basin. The magnitude of snow melt runoff is contingent upon the interplay of precipitation and temperature. Notably, this runoff is more prominent during the rainy months, primarily due to the basin's dominance by summer monsoons and the concurrent rise in temperatures. However, its contribution to the overall discharge in the basin is relatively modest, accounting for approximately 3% of the total.

When considering two different scenarios, SSP245 and SSP585, we observe variations in the historical and projected contributions of snow melt runoff to the basin's streamflow. Under the SSP245 scenario, historical contributions have remained at 3%, while in the near future (NF), mid future (MF), far future (FF) by the end of the century, these contributions are projected to be 2% of the total discharge.

Conversely, the SSP585 scenario depicts historical contributions at 3%, but with differing projections. In the near future (NF), snow melt runoff is projected to rise to 3%, but then decline to 2% in the mid future (MF), 1% in the far future (FF) ultimately return the end of the century. Notably, snow melt runoff assumes a prominent role in the near future under both scenarios, but its contribution diminishes significantly in the far future (Figure 26A-H).

Both scenarios indicate an increase in maximum snow melt runoff during June and a decrease in minimum rain runoff in February across historical, all-time periods, and the end of the century (Figure 32A and 32B). These changes are attributed to the influence of temperature and precipitation patterns in the SSP245 scenario, where temperature fluctuations play a vital role. In contrast, the SSP585 scenario results in a decline in snow formation due to increasing temperature.

The baseline measurement of snow melt runoff is 58 mm. According to the SSP245 scenario, (Figure 25A) the projected snow melt runoff is expected to decrease over time. Specifically, in the near future (NF), it is anticipated to decrease by 24%, in the mid future (MF) by 45%, in the far future (FF) by 19%, at the end of the 21st century.

Under the SSP585 scenario, (Figure 25B) there is a different trend. In the near future (NF), snow melt runoff is projected to increase by 16%. In the mid future (MF), snow melt runoff is expected to decrease by 17%, while in the far future (FF), it will experience a substantial decline of 73%. Temperature is also anticipated to decrease snow melt contribution by the end of the 21st century under this scenario. Importantly, there is a contrast in the snow melt runoff pattern between the scenarios, with maximum runoff occurring in the far future in SSP585 and minimum runoff increasing in the mid future.

In summary, the results indicate that the SSP585 scenario leads to a greater snow melt runoff impact on the basin in all time periods and at the end of the century compared to the SSP245 scenario (Figure 32B and 32D).

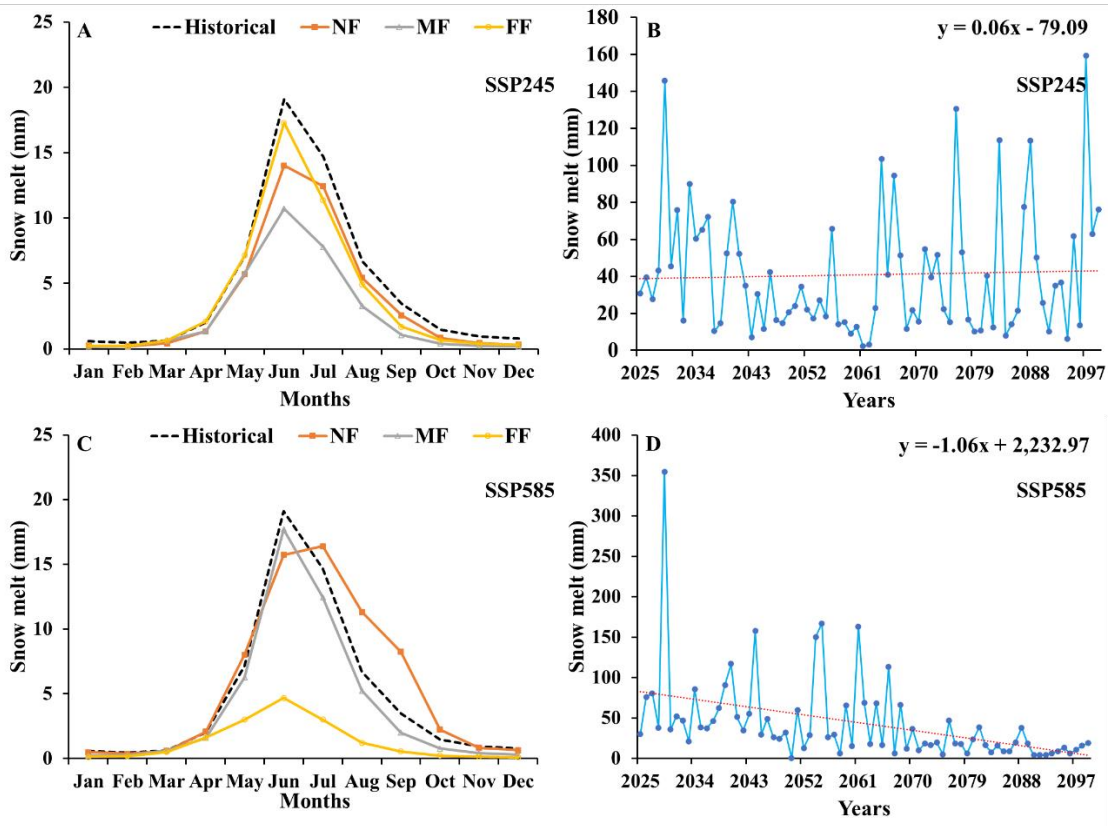

Figure 32: Monthly climate change impacts on the snow melt A) & C) during the Historical, NF, MF, FF and annual linear trend of projected snow melt B) & D) under SSP245 (top) and SSP585 (bottom) scenarios.

4.9.7. Climate change impact on actual evapotranspiration

Evapotranspiration is influenced by both temperature and the availability of water resources, with variations occurring at different temporal scales. Temperature, in turn, is contingent upon the duration of sunshine within a given basin. Evapotranspiration exhibits more significant levels during months characterized by higher rainfall, owing to increased water availability. Notably, in historical records, both scenarios indicate a rise in maximum evapotranspiration levels during October and a decrease in minimum evapotranspiration levels in February (Figure 33A and 3C). Projected evapotranspiration rates show a discernible increase, primarily due to the substantial impact of rising temperatures in both scenarios.

Figure (Figure 33B and 33D) illustrates the projected evapotranspiration's upward trend across all months when compared to the historical period, particularly in the SSP585 scenario. In contrast, the SSP245 scenario forecasts an increase in evapotranspiration only from January to May, with marginal deviations in other months when compared to historical data. This trend is primarily attributable to the projected increases in

temperature, precipitation, and contributions from melting ice to local water bodies, all of which stimulate evapotranspiration.

The altering precipitation patterns and temperature fluctuations have a profound impact on evapotranspiration within the basin area. A baseline evapotranspiration rate of 478 mm was recorded. According to the SSP245 scenario, Figire 25A future evapotranspiration levels are anticipated to increase. In the Near Future (NF), evapotranspiration is projected to rise by 8%, in the Middle Future (MF) by 13%, in the Far Future (FF) by 17%, by the end of the 21st century. Conversely, under the SSP585 scenario, Figure 25B evapotranspiration is expected to increase even further, with a 10% rise in the Near Future (NF), a 19% increase in the Middle Future (MF), a 27% increase in the Far Future (FF) by the end of the 21st century. Notably, the most significant surge in evapotranspiration occurs in the Far Future timeframe, while the least significant increase is observed in the Near Future across both scenarios.

These findings underscore the substantial impact of the SSP585 scenario, which results in greater evapotranspiration levels when compared to the SSP245 scenario across all time period windows, including the end of the century.

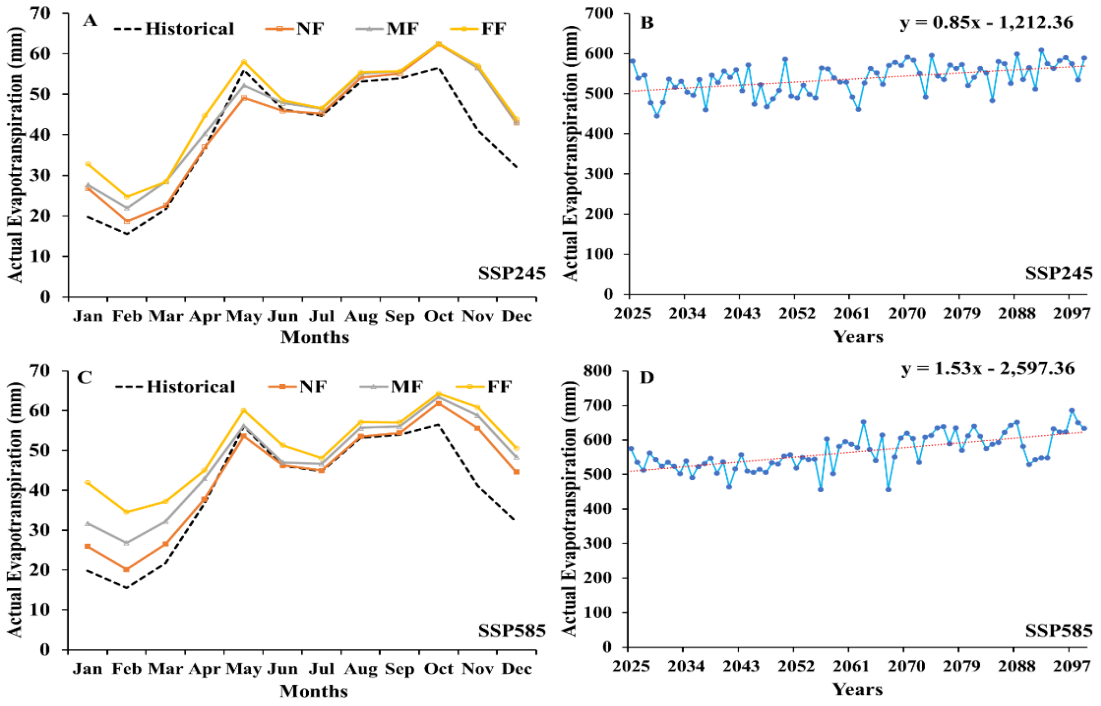

Figure 33: Monthly climate change impacts on the actual evapotranspiration A) & C) during the Historical, NF, MF, FF and annual linear trend of projected actual evapotranspiration B) & D) under SSP245 (top) and SSP585 (bottom) scenarios.

4.9.8. Climate change impact on water balance storage change

This section presents an assessment of water storage fluctuations over different time periods. The analysis reveals positive changes during rainy months, with negative changes observed in the remaining months. Subsequently, we provide estimates of annual water storage variations. It is important to note that the hydrological cycle's water components, as determined by model simulations, are generally reasonable. Nevertheless, disparities between observed and simulated discharge exist due to several factors, including limitations in the availability of data from the WMO standard meteorological network, real-time data, complexities associated with the geographical terrain, data collection procedures, and rating estimation.

The evaluation of water balance storage at the Busti station encompasses different time frames: a historical period spanning from 1991 to 2014, a Near Future time window from 2025 to 2049, a Mid Future period between 2050 to 2074, a Far Future outlook from 2075 to 2099, and an analysis extending until the end of the century. The fundamental principle guiding this assessment is the conservation of mass, where the quantity of incoming water (primarily precipitation) equals the quantity of outgoing water (comprising discharge and water body evaporation). Equation 8 is employed to calculate the changing water storage in the Tamakoshi river basin at the Busti gauging station.

During the historical period, the water balance in the basin exhibited a positive trend, with water storage increasing by 251 mm. SSP245 scenario Figire 34A in the Near Future time period, there was a notable increase of 79 mm in water storage, indicating a positive balance. However, in the Mid Future, the water balance shifted to a negative value of -0.6 mm, and in the Far Future, it dropped further to -5 mm, suggesting decreasing water storage. By the end of this century, the water balance rebounded to a positive 24 mm in the basin (Figure 34A).

When considering the different greenhouse gas emission scenarios, the results diverge. According to SSP585, (Figure 34B) the water balance remained positive during the Near Future, with an increase of 140 mm in water storage, and the Mid Future, with an increase of 23 mm. However, in the Far Future, there was a substantial negative balance of -214 mm, and by the end of the century, the basin's water balance was still negative.

It is worth noting that, for both scenarios, the Far Future time periods consistently displayed the lowest and most negative water storage changes, while the Near Future

time period consistently showed the highest positive water storage changes. These findings underscore the temporal variations in simulated water balance components and their contributions to streamflow in the Tamakoshi river basin, emphasizing the importance of these factors for downstream water availability. This research aims to provide critical insights into the dynamics of water storage in the face of future environmental changes and offers valuable guidance for further investigations in similar river basins.

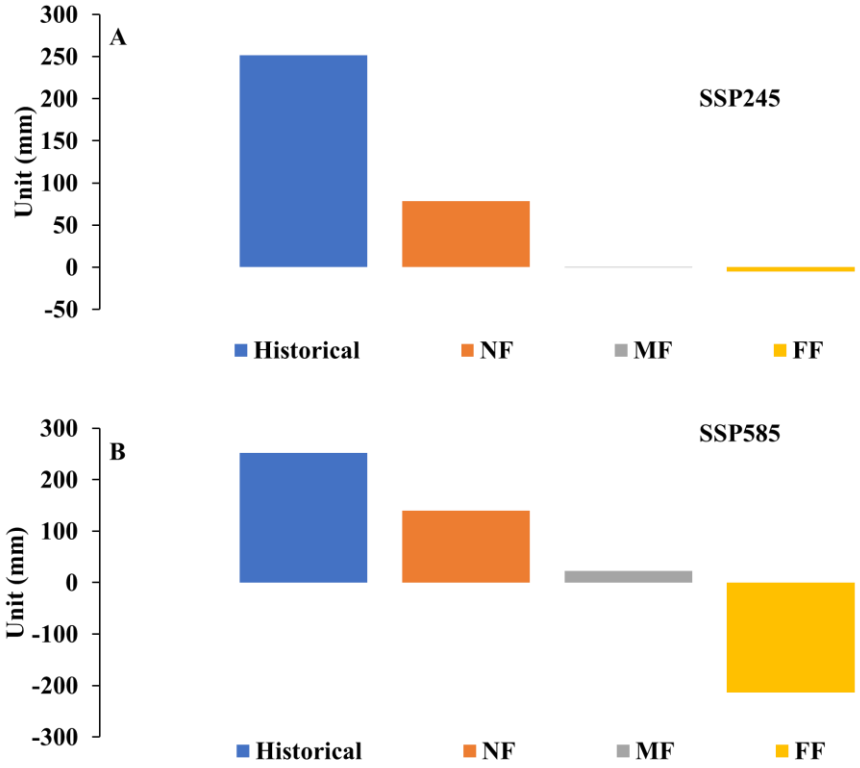

Figure 34 Climate change impacts on water balance storage change during Historical, NF, MF, FF under SSP245 (top) and SSP585 (bottom) scenarios

The model simulation period was 10 years but our simulation duration was 30 years. Observed baseflow is dominant flow during DJF and MAM of total streamflow, Rain runoff is dominant flow during JJAS and ON of the total flow. Results show that Rain runoff is dominant in May- October and in the remaining months, November-April baseflow is dominant in total streamflow. Maximum snow melt was observed during MAM and glacier melt contribution was ON of total streamflow. The river basin most of the precipitation occurs in the summer season in the HMA Ganga river basin 71% it states that precipitation is dominant in the summer season which is similar to our results but amount of rainfall received quietly differed from our results because area coverage

of Ganga River basin at Devghat station is 37 times greater than Tamakoshi river. Tamakoshi river basin receives in monsoon season (JJAS) that is 80% (Khadka *et al.*, 2014). Similarly, which is closely correlated with our results also shows 80 % of rainfall receives in monsoon season. April-August water storage change is positive and September -March shows the negative water storage change simulated by using the same modeling approach with the other two models SWAT and BTOPMC model in the KV watershed (Thapa *et al.*, 2017, Shrestha *et al.*, 2016). Our result is completely similar to that result. Streamflow is dominant in the summer season compared with the dry season because the maximum precipitation occurs in summer season (Shrestha *et al.*, 2016). Our results show that 78% of streamflow occurred in the summer season. It is clear that most streamflow occurred in summer season. Hence runoff component's contribution to streamflow and water balance storage change varies according to basin characteristics.

Multiple studies have demonstrated the increasing impact of projected climate change in the Himalayas region, according to various scenarios such as SRES, RCPs, and SSPs, using General Circulation Models (GCMs) and Regional Climate Models (RCMs) within different timeframes. Previous research has utilized varying timeframes, GCMs, and scenarios to project future climate changes in an upstream basin of the Himalayas. These projections are contingent upon the original model resolution biases inherent in the GCMs' datasets due to spatially heterogeneous lapse rates.

The investigation encompassed water balance components during historical periods with baseline data, Near Future (NF), Middle Future (MF), and Far Future (FF), examining annual, monthly, and seasonal timeframes. Our findings indicate that streamflow is primarily influenced by mid future (MF) projections. Precipitation, discharge, actual evapotranspiration, rain-runoff, and glacier melt all exhibit an increase, whereas baseflow and snow melt runoff decrease with varying timeframes, particularly toward the end of the 21st century. Among these components, glacier melt runoff is anticipated to increase substantially due to the changing climate, while snow melt runoff is expected to decrease.

It is worth noting that previous studies predominantly employed SRES and RCPs scenarios within different timeframes compared to our study in the upstream Himalayas river basin, as outlined by Khadka *et al.* (2014). This earlier research suggested that mean temperature, annual precipitation, and discharge would increase in the future, utilizing SRES scenarios over a decadal scale in the same river basin. However, it

contradicts our findings as snow cover is expected to decrease while snow melt runoff increases. Previous studies did not differentiate discharge into rain runoff, baseflow, glacier melt runoff, and snow melt runoff within this region. Precipitation in the soil partitions water into runoff and evaporation (Lian *et al.*, 2021, Porporato *et al.*, 2004, Porporato and Yin, 2022).

Similarly, Bharati *et al.* (2014) projected that average flow and precipitation would increase in all seasons in trans-mountain regions but decrease baseflow. Future discharge is anticipated to increase in the Koshi River (Nepal, 2016, Nepal *et al.*, 2014, Kaini *et al.*, 2020). Nepal (2016) highlighted that mean temperature, maximum, and minimum temperature would rise in the Himalayas basin due to climate change. Evapotranspiration is expected to increase, while snowfall decreases due to rising temperatures, resulting in reduced snow storage capacity and diminished snow melt runoff in the future. The future glacier melt runoff remains uncertain, although various studies suggest that glacier melt is accelerating in Himalayan regions (Immerzeel *et al.*, 2010, Lutz *et al.*, 2014).

In the same basin, Shrestha *et al.* (2016) projected higher streamflow toward the latter part of the century. The climate change impact over High Mountain Asia (HMA), including the Tibetan Plateau, has been studied under historical periods (1979-2014) and projected under four Shared Socioeconomic Pathways: SSP1-2.6, SSP2-4.5, SSP3-7.0, and SSP5-8.5, using CMIP6 datasets. These investigations revealed a general trend of decreasing snow cover and increasing precipitation associated with warming (Lalande *et al.*, 2021).

Climate change presents numerous challenges for water resources, infrastructure development, agriculture, and the livelihoods of South Asian regions. These challenges have been evaluated using CMIP6 datasets, which project a warmer climate by 3-5°C and increased precipitation by 13-30% by the end of the 21st century (Mishra *et al.*, 2020). It is important to note that the rate of climate change impact analysis depends significantly on the choice of GCMs, scenarios, timeframes, study areas, and methodologies. Differences in these factors account for variations in changing rates when compared to previous climate change studies, even though our results align with the overall trends of increasing temperature, precipitation, discharge, evaporation, and melting ice. In summary, our findings are consistent with previous research conducted in the Himalayas region and High Mountain Asia, including the Tibetan Plateau.

CHAPTER 5

5. CONCLUSION AND RECOMMENDATIONS

5.1 Conclusion

The model performance of the fully distributed SPHY model and semi-distributed HBV and HEC HMS models was examined with daily observed discharge at Busti station with daily inputs. All three models performed according to their features having limitations and advantages successfully applied in the Tamakoshi river basin using the same hydrological and meteorological data. The performance of hydrological models was evaluated through a comprehensive analysis using both graphical and statistical methods. All three hydrological models effectively simulated the discharge of the Tamakoshi river basin. The calibrated results were similar although the features, concept and spatial distribution of models. Both SPHY and HBV models incorporate glacier modules based on the degree day method for the snow and glacier melt. The calibration process used five years of daily data records from the Busti station, with the same period employed for SPHY validation due to its physically based spatially distributed nature. In contrast, HBV and HEC HMS models underwent validation using a two-year timeframe. This study intentionally focused on these three hydrological models as an independent choice. However, it is emphasized that a multiple model evaluation approach offers a more robust selection process for achieving accurate results, thereby facilitating the informed choice of the most suitable hydrological model. Future studies are encouraged to explore numerous models within the same timeframe or available data, thus enhancing the overall understanding and selection criteria for hydrological modeling.

In transboundary Himalaya River basins within developing countries, the scarcity of hydrological gauging stations and observational data arises from challenges related to monitoring, maintenance, and cost. Hydrological information at ungauged basins is important to water resources projects. The comparison of fully distributed and semi-distributed hydrological models i.e. SPHY, HBV, HEC HMS is a robust approach to estimate discharge at ungauged sites. In the overall comparison of Nash Sutcliffe Efficiency, coefficient of determination and volume differences of hydrological models' simulation, the coefficient of determination showed almost similar

performance. The SPHY model, characterized by its spatially distributed features, demonstrated a highly correlated estimation of ungauged discharge, particularly when transferred from two distinct gauged stations. Especially, the SPHY model exhibited superior performance at the Rasnalu gauge station (650) compared to the Busti gauge station (647). The ungauged discharge was estimated on a daily, monthly and annual basis from upstream to downstream. The low flow was a better match in prediction than the high flow, with deviations primarily observed during high flow periods. However, hydrological models, despite variations in flow simulation, remained independent due to their inherent feature availability. The spatial and temporal coverage of climatological station data is limited at the upstream site from Busti gauge station 647 which covered 71% of the area of total basin area up to Benighat. Although there is one rainfall station and two additional stations around the Busti gauging station, the deficiency in station data upstream of Busti necessitates further studies. Enhancing hydrological simulation capability in ungauged sites can be achieved through the incorporation of satellite and reanalysis data. In conclusion, the comparative method emerged as a more reliable approach for discharge estimation at ungauged sites within the transboundary Himalaya River basin, surpassing the capability of individual methods. In such complex and data-limited environments, this emphasises the significance continuous simulation and the possible incorporation of alternate data sources to further hydrological modelling.

In this study, water balance, streamflow components, water storage change and their trend have been evaluated in Tamakoshi river basin (TRB). The hydrological simulation in the basin was effectively conducted using the HBV model, which demonstrated good performance. The model performance indicators, including Nash Sutcliffe Efficiency (NSE), Determination (R^2), and volume difference (Pbias), were employed to assess the accuracy of the model's simulations across various time durations. While the model slightly underestimated peak flow, the overall performance remained satisfactory, with minimal differences observed between simulated and observed discharge during the calibrated 5 year period. The investigation extended to a comprehensive 30 year estimation of water balance, water storage changes, and streamflow components at the Busti gauging station. The model simulated discharge amounted to 2198 mm, with precipitation reaching 2905.64 mm over the basin area. It is worth to note that the TRB is monsoon dominant precipitation pattern, with 80% of rainfall occurring during this

season, contributing to 74% of the total discharge. The model indicated that streamflow contribution was maximum in the summer season and minimum in winter, while baseflow contributes in the pre-monsoon season. The water storage changes are positive in the water balance at Busti gauging station. In streamflow contribution, rain runoff is maximum, whereas snow melt runoff is minimum. The maximum flow occurred in August, while the minimum flow occurred in February. Results showed an increase in water storage during rainy months and a decreased during the driest months. Therefore, the implications of these findings underscore the importance of considering temporal fluctuations in water availability and understanding water balance contribution components for sustainable development in water resources projects. This study used meteorological observations from DHM stations to estimate water balance components and water storage changes at the Busti gauging station. Considering the limitations of the meteorological station network, satellite and reanalysis meteorological data products are suggested for potentially enhanced results. Additionally, future studies should explore the potential impacts of climate change on streamflow components and their implications for water balance.

The ensemble of 4 GCMs model shows an increase in precipitation for both the SSP245 and SSP585 scenarios across all time periods. Under the SSP245 scenario, Near Future (NF) precipitation is projected to rise by 20%, Middle Future (MF) precipitation by 25%, Far Future (FF) precipitation by 25%, with end of the 21st century. In the more extreme SSP585 scenario, NF precipitation is expected to increase by 21%, MF precipitation by 39%, FF precipitation by 69% by end of the 21st century. Similarly, the ensemble GCMs model indicates a temperature increase for both SSP245 and SSP585 scenarios across all time periods. Under SSP245, NF temperature is projected to increase by 1.37 ˚C, MF temperature by 2.61 ˚C, FF temperature by 3.27 ˚C with end of the 21st century. In the more extreme SSP585 scenario, NF temperature is anticipated to rise by 1.65 ˚C, MF temperature by 3.69 ˚C, FF temperature by 6.13 ˚C with end of the 21st century. Projections for discharge follow a similar pattern, with an increase expected under both SSP245 and SSP585 scenarios. For SSP245, NF discharge is projected to increase by 5%, MF discharge by 8%, FF discharge by 5% with end of the 21st century. Under SSP585, NF discharge is anticipated to rise by 9%, MF discharge by 22%, FF discharge by 25%, by end of the 21st century. This climate foresight contributes to planning, development and management to effectively operate water

resource projects downstream of the Tamakoshi river basin. Numerous hydropower projects, lift drinking water projects, irrigation projects and hydraulic structures may be beneficial through a better understanding of this study. This study focused on future hydro-climatic variability which is significant to designing hydraulic infrastructure in the Tamakoshi river basin.

5.2 Recommendations

This study adopts the SPHY, HBV light and HEC HMS models for hydrological simulation within the Tamakoshi river basin. To ensure the applicability of these models for further studies, a crucial step involves their calibration and validation against glacier mass balance, snow cover and long-term discharge data. For simulating streamflow at ungauged basin, it is recommended to complement these methods with multiple approaches, using reanalysis and satellite datasets. Mainly, the conceptual semi-distributed HBV model demonstrates optimal performance, particularly with its glacier module features. The selected HBV light model is utilized to simulate water balance components within the Tamakoshi river basin, incorporating projections from selected General Circulation Models (GCMs). Downscaled datasets from GCMs such as CanESM5, NorESM2, MPI ESM1 2HR, and ACCESS CM2 are employed for future projections. The study focuses on future streamflow forcing using NorESM2 and MPI ESM1 2HR under the SSP245 and SSP585 scenarios. To comprehensively assess future climate change impacts, the recommendation is to expand the analysis by incorporating more GCMs and considering all available climate change scenarios. This approach allows for a more robust evaluation of potential variations in hydrological responses to diverse climatic conditions in the Tamakoshi river basin.

CHAPTER 6

6. SUMMARY

Water resources play a significant role in the country's economy. The hydrological information required to plan water resources projects is evaluated using hydrological models to calibrate and generate streamflow data. The performance of fully distributed and semi-distributed hydrological models are Spatial Process in HYdrology (SPHY) model, HBV model and HEC HMS model evaluated by using Nash Sutcliffe Efficiency (NSE), Coefficient of Determination (R^2), Root Mean Square Error (RMSE), RMSE-observations Standard deviation Ratio (RSR) and Volume difference (P-Bias). The NSE for the SPHY model at Busti was 0.62, at Rasnalu was 0,79, NSE for HEC HMS at Busti was 0.78 and HBV at Busti was 0.77. All three hydrological models were calibrated and validated daily and monthly basis successfully with daily observed discharge of the Tamakoshi river basin at Busti station and Rasnalu station. The simulated discharge during the calibration period is more fit than the validated period. Among the statistical parameters during the simulation period coefficient of determination is closely matched comparatively. The comparative calibrated and validated models will be useful in filling the hydrological data records gap and appropriate selection of hydrological models for planning, management and development of water resource projects in the Tamakoshi river basin.

Continuous hydrological records at the desired site with spatial and temporal coverage are required for the planning, development and management of applications of water. The hydrological simulation used a fully distributed Spatial Process of HYdrology (SPHY) model and a semi-distributed HBV light and HEC HMS hydrological model in Tamakoshi river basin. The SPHY, HBV light and HEC HMS models were calibrated and validated at Busti station and Rasnalu station and were done successfully. The ungauged discharge predicted at Benighat using SPHY, HEC HMS and HBV light hydrological models were estimated from donor catchments. The ungauged discharge is estimated on a daily, monthly and annual basis from upstream gauged stations. The low flow prediction is more reliable than the high flow prediction. The deviation between predicted flow mostly appeared in high flow periods. All the hydrological models simulated ungauged streamflow were similar in flow pattern and discharge at

the ungauged receiver site was greater than donor site. The comparative method is a better alternative method to ungauged discharge estimation than the individual method. This research will support future reference to generate streamflow data at the ungauged site and fill missing data records for planning, management and development of water resource projects up to gauged stations to outlet at Benighat of Tamakoshi river basin.

Continuous hydrological modeling is significant in estimating the water balance component's contribution to streamflow in developing countries. Tamakoshi river is a transboundary Himalaya River which is a complex river system due to glacier-fed and rain-fed system catchment. The HBV light, the conceptual semi-distributed hydrological model is set to simulate daily input parameters in the Tamakoshi river basin. The model parameters are calibrated with the lumped system over the basin. Change in streamflow depends on their components in temporal variation. However, rain runoff is dominant in streamflow was observed. The streamflow contribution of HBV light 4.0.0.25 model simulated 62% rain runoff, 20% baseflow runoff, 5% snow melt runoff and 13% glacier melt runoff at Busti gauge station in Tamakoshi river basin. Seasonally all streamflow components showed maximum contributed in streamflow monsoon season (JJAS) and minimum in Winter (DJF) but baseflow was observed in Pre-monsoon (MAM). Maximum flow was observed in July and August but baseflow was observed in October and minimum flow was observed in February for all streamflow contribution components. Maximum water storage change was during monsoon season and minimum water storage changed during post-monsoon season. The storage was changed with a positive water balance during the simulation period. The calibrated and validated model can used for water resource projects and water-induced disaster management and climate change studies in the future.

Changing climate directly affects streamflow components on the hydrological cycle via changing precipitation and temperature on a global to local scale. The baseline and projected streamflow components are affected by changing precipitation and temperature in this region. In this study, four General Circulation Models (GCMs) of Coupled model Intercomparison Projects (CMIP 6) Assessment Report 6 were used with two scenarios for the projection of temperature and precipitation of the Tamakoshi river basin. The calibrated HBV conceptual semi-distributed model investigated hydrological regimes based on the bias-corrected in study area Shared Socio-economic Pathways scenarios SSP245 and SSP585 of ensembled two General Circulation Models

(GCMs) of Coupled model Intercomparison Projects (CMIP 6) Assessment Report 6. All GCMs showed temperature and precipitation of both scenarios increased but NorESM2 MM scenario SSP245 showed decreasing precipitation. The streamflow components are evaluated on the baseline, Near future (NF), Middle Future (MF), Far Future (FF), annual, monthly and seasonal basis. Streamflow leads the mostly mid future (MF) projections. The streamflow components precipitation, discharge, actual evapotranspiration, rain-runoff, and glacier melt increased but snow melt and baseflow runoff decreased with the end of the 21st century. Among the streamflow components, glacier melt runoff is heavily affected by changing climate. Precipitation is monsoon-dominated and governs the river discharge during the summer season.

7. References

Abbaspour, K., Vaghefi, S. A., Yang, H., & Srinivasan, R. (2019). Global soil, landuse, evapotranspiration, historical and future weather databases for SWAT Applications. *Scientific data*, **6**(1): 263. https://doi.org/10.1038/s41597-019-0282-4

Adhikari, T. R. (2014). *Impact of climate change on flow regime in Himalayan basins, Nepal.* (PhD). Central Department of Hydrology and Meteorology,

Adhikari, T. R., Baniya, B., Tang, Q., Talchabhadel, R., Gouli, M. R., Budhathoki, B. R., & Awasthi, R. P. (2023). Evaluation of post extreme floods in high mountain region: A case study of the Melamchi flood 2021 at the Koshi River Basin in Nepal. *Natural Hazards Research*. https://doi.org/10.1016/j.nhres.2023.07.001

Adhikari, T. R., Talchabhadel, R., Shrestha, S., Sharma, S., Aryal, D., & Pradhanang, S. M. (2022). The evaluation of climate change impact on hydrologic processes of a mountain river basin. *Theoretical and applied climatology*, **150**(1): 749-762. https://doi.org/10.1007/s00704-022-04204-3

Adnan, M., Liu, S., Saifullah, M., Iqbal, M., Ali, A. F., & Mukhtar, M. A. (2022). Spatiotemporal variations in runoff and runoff components in response to climate change in a glacierized subbasin of the Upper Indus Basin, Pakistan. *Frontiers in Earth Science*: 1516. https://doi.org/10.3389/feart.2022.970349

Arnold, J. G., Srinivasan, R., Muttiah, R. S., & Williams, J. R. (1998). Large area hydrologic modeling and assessment part I: model development 1. *JAWRA Journal of the American Water Resources Association*, **34**(1): 73-89. https://doi.org/10.1111/j.1752-1688.1998.tb05961.x

Bajracharya, A. R., Bajracharya, S. R., Shrestha, A. B., & Maharjan, S. B. (2018). Climate change impact assessment on the hydrological regime of the Kaligandaki Basin, Nepal. *Science of the Total Environment*, **625**: 837-848. https://doi.org/10.1016/j.scitotenv.2017.12.332

Balu, A., Ramasamy, S., & Sankar, G. (2023). Assessment of climate change impact on hydrological components of Ponnaiyar river basin, Tamil Nadu using CMIP6 models. *Journal of Water and Climate Change*, **14**(3): 730-747. https://doi.org/10.2166/wcc.2023.354

Bartlett, R., Bharati, L., Pant, D., Hosterman, H., & McCornick, P. G. (2010). *Climate change impacts and adaptation in Nepal* (Vol. 139): IWMI.

Bergstrom, S. (1992). The HBV model-its structure and applications.

Bergstrom, S. (2006). Experience from applications of the HBV hydrological model from the perspective of prediction in ungauged basins. *IAHS publication*, **307**: 97.

Bergström, S. (1976). *Development and application of a conceptual runoff model for Scandinavian catchments*.

Beven, K. (2009). Environmental modelling: an uncertain future?, CRC Press.

Bharati, L., Gurung, P., Jayakody, P., Smakhtin, V., & Bhattarai, U. (2014). The projected impact of climate change on water availability and development in the Koshi Basin, Nepal. *Mountain Research and Development*, **34**(2): 118-130. https://doi.org/10.1659/MRD-JOURNAL-D-13-00096.1

Bhatta, B., Shrestha, S., Shrestha, P. K., & Talchabhadel, R. (2019). Evaluation and application of a SWAT model to assess the climate change impact on the hydrology of the Himalayan River Basin. *Catena*, **181**: 104082. https://doi.org/10.1016/j.catena.2019.104082

Bhattarai, S., Zhou, Y., Shakya, N. M., & Zhao, C. (2018). Hydrological modelling and climate change impact assessment using HBV light model: a case study of Narayani River Basin, Nepal. *Nature Environment and Pollution Technology*, **17**(3): 691-702.

Birkinshaw, S., Moore, P., Kilsby, C., O'donnell, G., Hardy, A. J., & Berry, P. (2014). Daily discharge estimation at ungauged river sites using remote sensing. *Hydrological processes*, **28**(3): 1043-1054. http://dx.doi.org/10.1002/hyp.9647

Budhathoki, A., Babel, M. S., Shrestha, S., Meon, G., & Kamalamma, A. G. (2021). Climate change impact on water balance and hydrological extremes in different physiographic regions of the West Seti River Basin, Nepal. *Ecohydrology & Hydrobiology*, **21**(1): 79-95. https://doi.org/10.1016/j.ecohyd.2020.07.001

Castellarin, A., Galeati, G., Brandimarte, L., Montanari, A., & Brath, A. (2004). Regional flow-duration curves: reliability for ungauged basins. *Advances in Water Resources*, **27**(10): 953-965. https://doi.org/10.1016/j.advwatres.2004.08.005

Célleri, R., Timbe, L., Vázquez, R., & Feyen, J. (2003). Assessment of the relation between the NAM rainfall-runoff model parameters and the physical catchment properties. *HIP-VI UNESCO Technical Documents in Hydrology*, **66**: 9-16.

Chen, J., Brissette, F. P., & Leconte, R. (2011). Uncertainty of downscaling method in quantifying the impact of climate change on hydrology. *Journal of Hydrology*, **401**(3-4): 190-202. https://doi.org/10.1016/j.jhydrol.2011.02.020

Christensen, N. S., & Lettenmaier, D. P. (2007). A multimodel ensemble approach to assessment of climate change impacts on the hydrology and water resources of the Colorado River Basin. *Hydrology and Earth System Sciences*, **11**(4): 1417-1434. https://doi.org/10.5194/hess-11-1417-2007

Cole, S. J., & Moore, R. J. (2009). Distributed hydrological modelling using weather radar in gauged and ungauged basins. *Advances in Water Resources*, **32**(7): 1107-1120. https://doi.org/10.1016/j.advwatres.2009.01.006

Cong, Z., Yang, D., Gao, B., Yang, H., & Hu, H. (2009). Hydrological trend analysis in the Yellow River basin using a distributed hydrological model. *Water resources research*, **45**(7).

Consortium, R. (2017). Randolph Glacier Inventory—a dataset of global glacier outlines. In: Version. https://www.glims.org/RGI/

Cunderlik, J. (2003). *Hydrologic model selection for the CFCAS project: assessment of water resources risk and vulnerability to changing climatic conditions*: Department of Civil and Environmental Engineering, The University of Western Ontario. https://ir.lib.uwo.ca/wrrr/9/

Dahal, N., Shrestha, U. B., Tuitui, A., & Ojha, H. R. (2018). Temporal changes in precipitation and temperature and their implications on the streamflow of Rosi River, Central Nepal. *Climate*, *7*(1), 3. https://doi.org/10.3390/cli7010003

Dahal, P., Shrestha, M. L., Panthi, J., & Pradhananga, D. (2020). Modeling the future impacts of climate change on water availability in the Karnali River Basin of Nepal Himalaya. *Environmental Research*, **185**: 109430. https://doi.org/10.1016/j.envres.2020.109430

Dahri, Z. H., Ludwig, F., Moors, E., Ahmad, S., Ahmad, B., Ahmad, S., . . . Kabat, P. (2021). Climate change and hydrological regime of the high-altitude Indus basin under extreme climate scenarios. *Science of the Total Environment*, **768**: 144467. https://doi.org/10.1016/j.scitotenv.2020.144467

Das, T., Bárdossy, A., Zehe, E., & He, Y. (2008). Comparison of conceptual model performance using different representations of spatial variability. *Journal of Hydrology*, *356*(1-2), 106-118. https://doi.org/10.1016/j.jhydrol.2008.04.008

Dembélé, M., Hrachowitz, M., Savenije, H. H., Mariéthoz, G., & Schaefli, B. (2020). Improving the predictive skill of a distributed hydrological model by calibration on spatial patterns with multiple satellite data sets. *Water resources research*, **56**(1): e2019WR026085. https://doi.org/10.1029/2019WR026085

Devkota, L. P., & Gyawali, D. R. (2015). Impacts of climate change on hydrological regime and water resources management of the Koshi River Basin, Nepal. *Journal of Hydrology: Regional Studies*, **4**: 502-515. https://doi.org/10.1016/j.ejrh.2015.06.023

DHM. (2004). *Hydrological Estimation in Nepal*. Retrieved from Kathmandu, Nepal.

DHM. (2017). *Observed Climate Trend Analysis in the Districts and Physiographic Regions of Nepal (1971-2014)*. Retrieved from Kathmandu, Nepal.

Dibike, Y. B., & Coulibaly, P. (2005). Hydrologic impact of climate change in the Saguenay watershed: comparison of downscaling methods and hydrologic models. *Journal of Hydrology*, **307**(1-4): 145-163. https://doi.org/10.1016/j.jhydrol.2004.10.012

Eeckman, J., Nepal, S., Chevallier, P., Camensuli, G., Delclaux, F., Boone, A., & De Rouw, A. (2017). Assessing reliability of hydrological simulations through model intercomparison at the local scale in the Everest region. *Hydrology and Earth System Sciences Discussions, 2017*, 1-25. https://doi.org/10.5194/hess-2017-401

Eyring, V., Bony, S., Meehl, G. A., Senior, C. A., Stevens, B., Stouffer, R. J., & Taylor, K. E. (2016). Overview of the Coupled Model Intercomparison Project Phase 6 (CMIP6) experimental design and organization. *Geoscientific Model Development*, **9**(5): 1937-1958. https://doi.org/10.5194/gmd-9-1937-2016

Feldman, A. D. (2000). *Hydrologic Modeling System HEC HMS : Technical Reference Manual*. US Army Corps of Engineers, Hydrologic Engineering Center.

Foglia, L., Hill, M. C., Mehl, S. W., & Burlando, P. (2009). Sensitivity analysis, calibration, and testing of a distributed hydrological model using error-based weighting and one objective function. *Water resources research*, **45**(6). https://doi.org/10.1029/2008WR007255

Ghosh, S., & Mujumdar, P. (2007). Nonparametric methods for modeling GCM and scenario uncertainty in drought assessment. *Water resources research*, **43**(7). https://doi.org/10.1029/2006WR005351

Golmohammadi, G., Prasher, S., Madani, A., & Rudra, R. (2014). Evaluating three hydrological distributed watershed models: MIKE-SHE, APEX, SWAT. *Hydrology*, **1**(1): 20-39. https://doi.org/10.3390/hydrology1010020

Gonzalez, P., Neilson, R. P., Lenihan, J. M., & Drapek, R. J. (2010). Global patterns in the vulnerability of ecosystems to vegetation shifts due to climate change. *Global Ecology and Biogeography*, **19**(6): 755-768. https://doi.org/10.1111/j.1466-8238.2010.00558.x

Grimaldi, S., Nardi, F., Piscopia, R., Petroselli, A., & Apollonio, C. (2021). Continuous hydrologic modelling for design simulation in small and ungauged basins: A step forward and some tests for its practical use. *Journal of Hydrology*, **595**: 125664. https://doi.org/10.1016/j.jhydrol.2020.125664

Gulakhmadov, A., Chen, X., Gulahmadov, N., Liu, T., Anjum, M. N., & Rizwan, M. (2020). Simulation of the potential impacts of projected climate change on streamflow in the Vakhsh river basin in central Asia under CMIP5 RCP scenarios. *Water*, **12**(5): 1426. https://doi.org/10.3390/w12051426

Hu, Y., Maskey, S., & Uhlenbrook, S. (2012). Trends in temperature and rainfall extremes in the Yellow River source region, China. *Climatic change*, **110**(1-2): 403-429. https://doi.org/10.1007/s10584-011-0056-2

Huang, J., Su, F., Yao, T., & Sun, H. (2022). Runoff regime, change, and attribution in the upper Syr Darya and Amu Darya, central Asia. *Journal of Hydrometeorology*, **23**(10): 1563-1585. https://doi.org/10.1175/JHM-D-22-0036.1

Huang, Q., Long, D., Du, M., Han, Z., & Han, P. (2020). Daily continuous river discharge estimation for ungauged basins using a hydrologic model calibrated by satellite altimetry: Implications for the SWOT mission. *Water resources research*, **56**(7): e2020WR027309. https://doi.org/10.1029/2020WR027309

Huang, Q., Qin, G., Zhang, Y., Tang, Q., Liu, C., Xia, J., . . . Post, D. (2020). Using remote sensing data-based hydrological model calibrations for predicting runoff in ungauged or poorly gauged catchments. *Water resources research*, **56**(8): e2020WR028205. https://doi.org/10.1029/2020WR028205

Hugonnet, R., McNabb, R., Berthier, E., Menounos, B., Nuth, C., Girod, L., Farinotti D., Huss M., Dussaillant I., Brun F., & Kääb A. (2021). Accelerated global glacier mass loss in the early twenty-first century. *Nature*, **592**(7856): 726-731. https://doi.org/10.1038/s41586-021-03436-z

Huss, M., & Hock, R. (2018). Global-scale hydrological response to future glacier mass loss. *Nature Climate Change*, **8**(2): 135-140. https://doi.org/10.1038/s41558-017-0049-x

Huss, M., Jouvet, G., Farinotti, D., & Bauder, A. (2010). Future high-mountain hydrology: a new parameterization of glacier retreat. *Hydrology and Earth System Sciences*, **14**(5): 815-829. https://doi.org/10.5194/hess-14-815-2010

ICIMOD. (1996). CLIMATIC AND HYDROLOGICAL ATLAS OF NEPAL. Retrieved from Kathmandu:

Immerzeel, W., and, & Droogers, P. (2008). Calibration of a distributed hydrological model based on satellite evapotranspiration. *Journal of Hydrology*, **349**(3-4): 411-424. https://doi.org/10.1016/j.jhydrol.2007.11.017

Immerzeel, W., Pellicciotti, F., & Bierkens, M. (2013). Rising river flows throughout the twenty-first century in two Himalayan glacierized watersheds. *Nature geoscience*, **6**(9): 742-745. https://doi.org/10.1038/ngeo1896

Immerzeel, W. W., Lutz, A. F., Andrade, M., Bahl, A., Biemans, H., Bolch, T., Hyde, S., Brumby, S., Davies, B.J., Elmore, A.C. & Elmore, A. (2020). Importance and vulnerability of the world's water towers. *Nature*, **577**(7790): 364-369. https://doi.org/10.1038/s41586-019-1822-y

Immerzeel, W. W., Van Beek, L. P., & Bierkens, M. F. (2010). Climate change will affect the Asian water towers. *science*, **328**(5984): 1382-1385. https://doi.org/10.1126/science.1183188

IPCC. (2000). *IPCC Special Report Emissions Scenarios. Intergovernmental Panel on Climate Change. Contribution of Working Groups Working Group III.* Retrieved from United Kingdom and New York, NY, USA:

IPCC. (2001). *Mitigation of Climate Change, Contribution of Working Group III to the Third Assessment Report of the Intergovernmental Panel on Climate Change.* Retrieved from United Kingdom and New York, NY, USA.

IPCC. (2007a). *Impacts, Adaptation and Vulnerability: Contribution of Working Group II to the Fourth Assessment Report of the Intergovernmental Panel on Climate Change, Cambridge.* Retrieved from United Kingdom and New York, NY, USA.

IPCC. (2007b). *Mitigation of Climate Change, Contribution of Working Group III to the Fourth Assessment Report of the Intergovernmental Panel on Climate Change.* Retrieved from United Kingdom and New York, NY, USA.

IPCC. (2007c). *The physical science basis: Contribution of Working Group I to the Fourth Assessment Report of the Intergovernmental Panel on Climate Change*. Retrieved from United Kingdom and New York, NY, USA.

IPCC. (2013). *The Physical Science Basis, Contribution of Working Group I to the Fifth Assessment Report of the Intergovernmental Panel on Climate Change*. Retrieved from United Kingdom and New York, NY, USA.

IPCC. (2014a). *Impacts, Adaptation, and Vulnerability. Part A: Global and Sectoral Aspects. Contribution of working Group II to the Fifth Assessment Report of the Intergovernmental Panel on Climate Change*. Retrieved from United Kingdom and New York, NY, USA.

IPCC. (2014b). *Impacts, Adaptation, and Vulnerability. Part B: Regional Aspects. Contribution of Working Group II to the Fifth Assessment Report of the Intergovernmental Panel on Climate Change.* Retrieved from United Kingdom and New York, NY, USA.

IPCC. (2014c). *Mitigation of Climate Change. Contribution of Working Group III to the Fifth Assessment Report of the Intergovernmental Panel on Climate Change* . Retrieved from United Kingdom and New York, NY, USA.

IPCC. (2021). *Summary for Policymakers. In: Climate Change 2021: The Physical Science Basis. Contribution of Working Group I to the Sixth Assessment Report of the Intergovernmental Panel on Climate Change*. Retrieved from United Kingdom and New York, NY, USA.

IPCC. (2022a). *Climate Change 2022 - Impacts, Adaptation and Vulnerability – Summary for Policymakers. In Ipcc.*

IPCC. (2022b). *Technical Summary. The Ocean and Cryosphere in a Changing Climate.*

IPCC. (2023). *Summary for Policymakers. In: Climate Change 2023: Synthesis Report. Contribution of Working Groups I, II and III to the Sixth Assessment Report of the Intergovernmental Panel on Climate Change*. Retrieved from Geneva, Switzerland.

Jansen, K. F., Teuling, A. J., Craig, J. R., Dal Molin, M., Knoben, W. J., Parajka, J., Vis, M. & Melsen, L. A. (2021). Mimicry of a Conceptual Hydrological Model (HBV): What's in a Name? *Water resources research*, **57**(5): e2020WR029143. https://doi.org/10.1029/2020WR029143

Johnson, F., & Sharma, A. (2012). A nesting model for bias correction of variability at multiple time scales in general circulation model precipitation simulations. *Water resources research*, **48**(1). https://doi.org/10.1029/2011WR010464

Kaini, S., Nepal, S., Pradhananga, S., Gardner, T., & Sharma, A. K. (2020). Representative general circulation models selection and downscaling of climate data for the transboundary Koshi river basin in China and Nepal. *International Journal of Climatology*, **40**(9): 4131-4149. https://doi.org/10.1002/joc.6447

Kaini, S., Nepal, S., Pradhananga, S., Gardner, T., & Sharma, A. K. (2021). Impacts of climate change on the flow of the transboundary Koshi River, with implications for local irrigation. *International Journal of Water Resources Development*, **37**(6): 929-954. https://doi.org/10.1080/07900627.2020.1826292

Kandel, P., Chettri, N., Chaudhary, S., Sharma, P., & Uddin, K. (2021). Ecosystem services research trends in the water tower of Asia: A bibliometric analysis from the Hindu Kush Himalaya. *Ecological Indicators*, **121**: 107152. https://doi.org/10.1016/j.ecolind.2020.107152

Karki, R., Hasson, S. u., Schickhoff, U., Scholten, T., & Böhner, J. (2017). Rising precipitation extremes across Nepal. *Climate*, **5**(1): 4. https://doi.org/10.3390/cli5010004

Karki, R., Talchabhadel, R., Aalto, J., & Baidya, S. K. (2016). New climatic classification of Nepal. *Theoretical and applied climatology*, **125**(3): 799-808. https://doi.org/10.1007/s00704-015-1549-0

Kayastha, R. B., Steiner, N., Kayastha, R., Mishra, S. K., & McDonald, K. (2020). Comparative study of hydrology and icemelt in three Nepal river basins using the Glacio-Hydrological Degree-Day Model (GDM) and observations from the Advanced Scatterometer (ASCAT). *Frontiers in Earth Science*, **7**: 354. https://doi.org/10.3389/feart.2019.00354

Khadka, D., Babel, M. S., Shrestha, S., & Tripathi, N. K. (2014). Climate change impact on glacier and snow melt and runoff in Tamakoshi basin in the Hindu Kush Himalayan (HKH) region. *Journal of Hydrology*, **511**: 49-60. https://doi.org/10.1016/j.jhydrol.2014.01.005

Khanal, S., Lutz, A. F., Kraaijenbrink, P. D., van den Hurk, B., Yao, T., & Immerzeel, W. W. (2021). Variable 21st century climate change response for rivers in High Mountain Asia at seasonal to decadal time scales. *Water resources research*, **57**(5): e2020WR029266. https://doi.org/10.1029/2020WR029266

Kim, U., & Kaluarachchi, J. J. (2008). Application of parameter estimation and regionalization methodologies to ungauged basins of the Upper Blue Nile River Basin, Ethiopia. *Journal of Hydrology*, **362**(1-2): 39-56. https://doi.org/10.1016/j.jhydrol.2008.08.016

Kite, G., & Pietroniro, A. (1996). Remote sensing applications in hydrological modelling. *Hydrological Sciences Journal*, **41**(4): 563-591. https://doi.org/10.1080/02626669609491526

Kraaijenbrink, P. D., Bierkens, M. F., Lutz, A. F., & Immerzeel, W. (2017). Impact of a global temperature rise of 1.5 degrees Celsius on Asia's glaciers. *Nature*, **549**(7671): 257-260. https://doi.org/10.1038/nature23878

Krause, P. (2002). Quantifying the impact of land use changes on the water balance of large catchments using the J2000 model. *Physics and Chemistry of the Earth, Parts A/B/C*, **27**(9-10): 663-673. https://doi.org/10.1016/S1474-7065(02)00051-7

Lalande, M., Ménégoz, M., Krinner, G., Naegeli, K., & Wunderle, S. (2021). Climate change in the High Mountain Asia in CMIP6. *Earth system dynamics*, **12**(4): 1061-1098. https://doi.org/10.5194/esd-12-1061-2021

Lamichhane, M., Phuyal, S., Mahato, R., Shrestha, A., Pudasaini, U., Lama, S. D., ... & Neupane, D. (2024). Assessing Climate Change Impacts on Streamflow and Baseflow in the Karnali River Basin, Nepal: A CMIP6 Multi-Model Ensemble Approach Using SWAT and Web-Based Hydrograph Analysis Tool. Sustainability, 16(8), 3262. https://doi.org/10.3390/su16083262

Lang, H. (1986). Forecasting meltwater runoff from snow-covered areas and from glacier basins. *River flow modelling and forecasting*, 99-127. https://doi.org/10.1007/978-94-009-4536-4_5

Lenderink, G., Buishand, A., & Van Deursen, W. (2007). Estimates of future discharges of the river Rhine using two scenario methodologies: direct versus delta approach. *Hydrology and Earth System Sciences*, **11**(3): 1145-1159. https://doi.org/10.5194/hess-11-1145-2007

Li, Q., Peng, Y., Wang, G., Wang, H., Xue, B., & Hu, X. (2019). A combined method for estimating continuous runoff by parameter transfer and drainage area ratio method in ungauged catchments. *Water*, **11**(5): 1104. http://dx.doi.org/10.3390/w11051104

Li, Z., Chen, Y., Li, Y., & Wang, Y. (2020). Declining snowfall fraction in the alpine regions, Central Asia. *Scientific reports*, **10**(1): 3476. https://doi.org/10.1038/s41598-020-60303-z

Lian, X., Piao, S., Chen, A., Huntingford, C., Fu, B., Li, L. Z., Huang, J., Sheffield, J., Berg, A.M., Keenan, T.F. & McVicar, T.R. (2021). Multifaceted characteristics of dryland aridity changes in a warming world. *Nature Reviews Earth & Environment*, **2**(4): 232-250. https://doi.org/10.1038/s43017-021-00144-0

Lutz, A., & Immerzeel, W. (2013). Water availability analysis for the upper Indus, Ganges, Brahmaputra, Salween and Mekong river basins. *Final Report to ICIMOD, September*.

Lutz, A., Immerzeel, W., Shrestha, A., & Bierkens, M. (2014). Consistent increase in High Asia's runoff due to increasing glacier melt and precipitation. *Nature Climate Change*, **4**(7): 587-592. https://doi.org/10.1038/nclimate2237

Lutz, A. F., Immerzeel, W. W., Kraaijenbrink, P. D., Shrestha, A. B., & Bierkens, M. F. (2016). Climate change impacts on the upper indus hydrology: Sources, shifts and extremes. *PloS one*, **11**(11): e0165630. https://doi.org/10.1371/journal.pone.0165630

Madsen, H., Wilson, G., & Ammentorp, H. C. (2002). Comparison of different automated strategies for calibration of rainfall-runoff models. *Journal of Hydrology*, **261**(1-4): 48-59. https://doi.org/10.1016/S0022-1694(01)00619-9

Mahmood, R., & Babel, M. S. (2013). Evaluation of SDSM developed by annual and monthly sub-models for downscaling temperature and precipitation in the Jhelum basin, Pakistan and India. *Theoretical and applied climatology*, **113**: 27-44. http://dx.doi.org/10.1007/s00704-012-0765-0

Manabe, S., Milly, P., & Wetherald, R. (2004). Simulated long-term changes in river discharge and soil moisture due to global warming/Simulations à long terme de changements d'écoulement fluvial et d'humidité du sol causés par le réchauffement global. *Hydrological Sciences Journal*, **49**(4). https://doi.org/10.1623/hysj.49.4.625.54429

Marahatta, S., Aryal, D., Devkota, L. P., Bhattarai, U., & Shrestha, D. (2021). Application of SWAT in hydrological simulation of complex mountainous river basin (Part II: climate change impact assessment). *Water*, **13**(11): 1548. https://doi.org/10.3390/w13111548

Maraun, D. (2016). Bias correcting climate change simulations-a critical review. *Current Climate Change Reports*, **2**: 211-220. https://doi.org/10.1007/s40641-016-0050-x

Maraun, D., & Widmann, M. (2018). Cross-validation of bias-corrected climate simulations is misleading. *Hydrology and Earth System Sciences*, **22**(9): 4867-4873. https://doi.org/10.5194/hess-22-4867-2018

Maskey, S., Uhlenbrook, S., & Ojha, S. (2011). An analysis of snow cover changes in the Himalayan region using MODIS snow products and in-situ temperature data. *Climatic change*, **108**(1-2): 391-400. http://dx.doi.org/10.1007/s10584-011-0181-y

McDonnell, J., Sivapalan, M., Vaché, K., Dunn, S., Grant, G., Haggerty, R., Hinz, C., Hooper, R., Kirchner, J., Roderick, M.L. & Selker, J. (2007). Moving beyond heterogeneity and process complexity: A new vision for watershed hydrology. *Water resources research*, **43**(7). https://doi.org/10.1029/2006WR005467

Meehl, G. A., Covey, C., Delworth, T., Latif, M., McAvaney, B., Mitchell, J. F., Stouffer, R.J. & Taylor, K. E. (2007). The WCRP CMIP3 multimodel dataset: A new era in climate change research. *Bulletin of the American Meteorological society*, **88**(9): 1383-1394. https://doi.org/10.1175/BAMS-88-9-1383

Meehl, G. A., Moss, R., Taylor, K. E., Eyring, V., Stouffer, R. J., Bony, S., & Stevens, B. (2014). Climate model intercomparisons: Preparing for the next phase. *Eos, Transactions American Geophysical Union*, **95**(9): 77-78. https://doi.org/10.1002/2014EO090001

Meinshausen, M., Smith, S. J., Calvin, K., Daniel, J. S., Kainuma, M. L., Lamarque, J.-F., . . . Riahi, K. (2011). The RCP greenhouse gas concentrations and their extensions from 1765 to 2300. *Climatic change*, **109**: 213-241. https://doi.org/10.1007/s10584-011-0156-z

Milly, P. (1994). Climate, interseasonal storage of soil water, and the annual water balance. *Advances in Water Resources*, **17**(1-2): 19-24. https://doi.org/10.1016/0309-1708(94)90020-5

Mishra, V., Bhatia, U., & Tiwari, A. D. (2020). Bias-corrected climate projections for South Asia from coupled model intercomparison project-6. *Scientific data*, **7**(1): 338. https://doi.org/10.1038/s41597-020-00681-1

MoFE. (2019). *Climate change scenarios for Nepal for National Adaptation Plan (NAP)*. Retrieved from https://lib.icimod.org/record/34554

Moss, R. H., Babiker, M., Brinkman, S., Calvo, E., Carter, T., Edmonds, J. A., Elgizouli, I., Emori, S., Lin, E., Hibbard, K. & Jones, R. (2008). *Towards new scenarios for analysis of emissions, climate change, impacts, and response strategies*. (No. PNNL-SA-63186). Pacific Northwest National Lab.(PNNL), Richland, WA (United States).

Moss, R. H., Edmonds, J. A., Hibbard, K. A., Manning, M. R., Rose, S. K., Van Vuuren, D. P., Carter, T.R., Emori, S., Kainuma, M., Kram, T. & Meehl, G.A. (2010). The next generation of scenarios for climate change research and assessment. *Nature*, **463**(7282): 747-756. https://doi.org/10.1038/nature08823

Mukhopadhyay, B., & Khan, A. (2015). A reevaluation of the snow melt and glacial melt in river flows within Upper Indus Basin and its significance in a changing climate. *Journal of Hydrology*, **527**: 119-132. https://doi.org/10.1016/j.jhydrol.2015.04.045

Nakicenovic, N., & Swart, R. (2000). Emissions scenarios-special report of the Intergovernmental Panel on Climate Change.

Nash, J. E., & Sutcliffe, J. V. (1970). River flow forecasting through conceptual models part I-A discussion of principles. *Journal of Hydrology*, **10**(3): 282-290. https://doi.org/10.1016/0022-1694(70)90255-6

Nepal, S. (2016). Impacts of climate change on the hydrological regime of the Koshi river basin in the Himalayan region. *Journal of Hydro-Environment Research*, **10**: 76-89. https://doi.org/10.1016/j.jher.2015.12.001

Nepal, S., Flügel, W. A., Krause, P., Fink, M., & Fischer, C. (2017). Assessment of spatial transferability of process-based hydrological model parameters in two neighbouring catchments in the Himalayan Region. Hydrological Processes, 31(16), 2812-2826. https://doi.org/10.1002/hyp.11199

Nepal, S., Krause, P., Flügel, W. A., Fink, M., & Fischer, C. (2014). Understanding the hydrological system dynamics of a glaciated alpine catchment in the Himalayan region using the J2000 hydrological model. *Hydrological processes*, **28**(3): 1329-1344. https://doi.org/10.1002/hyp.9627

Nepal, S., & Shrestha, A. B. (2015). Impact of climate change on the hydrological regime of the Indus, Ganges and Brahmaputra river basins: a review of the literature. *International Journal of Water Resources Development*, **31**(2): 201-218. https://doi.org/10.1080/07900627.2015.1030494

Nepal, S., Zheng, H., Penton, D. J., & Neumann, L. E. (2015). Comparative performance of GR4JSG and J2000 hydrological models in the Dudh Koshi catchment of the Himalayan region. MODSIM2015. MSSANZ, 2395-2401. DOI:10.36334/modsim.2015.l13.nepal

Neupane, P., Shrestha, S., & Ghimire, S. (2022). Climate Change Impact on the Hydrological Extremes of a River Basin in the Hindu Kush Himalayan Region: A Case Study of the Marsyangdi River Basin, Nepal. In Handbook of Himalayan Ecosystems and Sustainability, Volume 2 (pp. 111-136). CRC Press.

Neupane, R. P., White, J. D., & Alexander, S. E. (2015). Projected hydrologic changes in monsoon-dominated Himalaya Mountain basins with changing climate and deforestation. Journal of Hydrology, 525, 216-230. https://doi.org/10.1016/j.jhydrol.2015.03.048

Neupane, R. P., Yao, J., & White, J. D. (2014). Estimating the effects of climate change on the intensification of monsoonal-driven stream discharge in a Himalayan watershed. Hydrological Processes, 28(26), 6236-6250. DOI: 10.1002/hyp.10115

Neupane, S. N., & Pandey, A. (2021). Hydrological Modeling of West Rapti River Basin of Nepal Using SWAT Model. Water Management and Water Governance: Hydrological Modeling, 279-302. https://doi.org/10.1007/978-3-030-58051-3_19

Nguyen, T. V., Dietrich, J., Dang, T. D., Tran, D. A., Van Doan, B., Sarrazin, F. J., Abbaspour, K. & Srinivasan, R. (2022). An interactive graphical interface tool for parameter calibration, sensitivity analysis, uncertainty analysis, and visualization for the Soil and Water Assessment Tool. *Environmental Modelling & Software*, **156**: 105497. https://doi.org/10.1016/j.envsoft.2022.105497

Nóbrega, M. T., Collischonn, W., Tucci, C. E. M., & Paz, A. R. d. (2011). Uncertainty in climate change impacts on water resources in the Rio Grande Basin, Brazil. *Hydrology and Earth System Sciences*, **15**(2): 585-595. https://doi.org/10.5194/hess-15-585-2011

Nonki, R. M., Amoussou, E., Lenouo, A., Tshimanga, R. M., & Houndenou, C. (2023). Sensitivity and identifiability analysis of a conceptual-lumped model in the headwaters of the Benue River Basin, Cameroon: implications for uncertainty quantification and parameter optimization. *Hydrology Research*, ***54***(9), 1036-1054. https://doi.org/10.2166/nh.2023.243

Nonki, R. M., Lenouo, A., Tshimanga, R. M., Donfack, F. C., & Tchawoua, C. (2021). Performance assessment and uncertainty prediction of a daily time-step HBV - Light rainfall-runoff model for the Upper Benue River Basin, Northern Cameroon. *Journal of Hydrology: Regional Studies, 36*, 100849. http://dx.doi.org/10.1016/j.ejrh.2021.100849

Normand, S., Konz, M., & Merz, J. (2010). An application of the HBV model to the Tamor Basin in Eastern Nepal. *Journal of Hydrology and Meteorology*, **7**(1): 49-58.

O'Neill, B. C., Tebaldi, C., Van Vuuren, D. P., Eyring, V., Friedlingstein, P., Hurtt, G., Knutti, R., Kriegler, E., Lamarque, J.F., Lowe, J. & Meehl, G.A. (2016). The scenario model intercomparison project (ScenarioMIP) for CMIP6. *Geoscientific Model Development*, **9**(9): 3461-3482. https://doi.org/10.5194/gmd-9-3461-201

Orlandini, S., & Rosso, R. (1998). Parameterization of stream channel geometry in the distributed modeling of catchment dynamics. *Water resources research*, **34**(8): 1971-1985. https://doi.org/10.1029/98WR00257

Ouyang, S., Puhlmann, H., Wang, S., von Wilpert, K., & Sun, O. J. (2014). Parameter uncertainty and identifiability of a conceptual semi-distributed model to simulate hydrological processes in a small headwater catchment in Northwest China. *Ecological Processes*, *3*, 1-17. https://doi.org/10.1186/s13717-014-0014-9

Pandey, V. P., Dhaubanjar, S., Bharati, L., & Thapa, B. R. (2020). Spatio-temporal distribution of water availability in Karnali-Mohana Basin, Western Nepal: Climate change impact assessment (Part-B). *Journal of Hydrology: Regional Studies*, **29**: 100691. https://doi.org/10.1016/j.ejrh.2020.100690

Panthi, J., Talchabhadel, R., Ghimire, G. R., Sharma, S., Dahal, P., Baniya, R., Boving, T., Pradhanang, S.M. & Parajuli, B. (2021). Hydrologic regionalization under data scarcity: Implications for streamflow prediction. *Journal of Hydrologic Engineering*, **26**(9): 05021022. https://doi.org/10.1061/(ASCE)HE.1943-5584.0002121

Parajuli, A., Devkota, L. P., Adhikari, T. R., Dhakal, S., & Kayastha, R. B. (2015). Impact of Climate change on river discharge and rainfall pattern: a case study

from Marshyangdi River basin, Nepal. *Journal of Hydrology and Meteorology*, **9**(1): 60-73.

Pechlivanidis, I., Jackson, B., Mcintyre, N., & Wheater, H. (2011). Catchment scale hydrological modelling: a review of model types, calibration approaches and uncertainty analysis methods in the context of recent developments in technology and applications. *Global NEST journal,* **13**(3): 193-214. https://doi.org/10.30955/gnj.000778

Peterson, B. J., Holmes, R. M., McClelland, J. W., Vorosmarty, C. J., Lammers, R. B., Shiklomanov, A. I., Shiklomanov, I.A. & Rahmstorf, S. (2002). Increasing river discharge to the Arctic Ocean. *science,* **298**(5601): 2171-2173. https://doi.org/10.1126/science.1077445

Piani, C., Weedon, G., Best, M., Gomes, S., Viterbo, P., Hagemann, S., & Haerter, J. (2010). Statistical bias correction of global simulated daily precipitation and temperature for the application of hydrological models. *Journal of Hydrology,* **395**(3-4): 199-215. https://doi.org/10.1016/j.jhydrol.2010.10.024

Pierce, D. W., Barnett, T. P., Santer, B. D., & Gleckler, P. J. (2009). Selecting global climate models for regional climate change studies. *Proceedings of the National Academy of Sciences*, ***106***(21), 8441-8446. http://dx.doi.org/10.1073/pnas.0900094106

Porporato, A., Daly, E., & Rodriguez-Iturbe, I. (2004). Soil water balance and ecosystem response to climate change. *The American Naturalist,* **164**(5): 625-632. http://dx.doi.org/10.1086/424970

Porporato, A., & Yin, J. (2022). *Ecohydrology: Dynamics of life and water in the critical zone*: Cambridge University Press.

Qi, W., Zhang, Y., Gao, J., Yang, X., Liu, L., & Khanal, N. R. (2013). Climate change on the southern slope of Mt. Qomolangma (Everest) Region in Nepal since 1971. *Journal of Geographical Sciences,* **23**: 595-611. https://doi.org/10.1007/s11442-013-1031-9

Raghunath, H. M. (2006). *Hydrology: principles, analysis and design*: New Age International.

Rajbhandari, R., Shrestha, A. B., Nepal, S., & Wahid, S. (2016). Projection of future climate over the Koshi River basin based on CMIP5 GCMs. *Atmospheric and Climate Sciences,* **6**(2): 190-204. http://dx.doi.org/10.4236/acs.2016.62017

Rajib, A., Merwade, V., & Yu, Z. (2018). Rationale and efficacy of assimilating remotely sensed potential evapotranspiration for reduced uncertainty of hydrologic models. *Water resources research*, **54**(7): 4615-4637. https://doi.org/10.1029/2017WR021147

Razavi, T., & Coulibaly, P. (2016). Improving streamflow estimation in ungauged basins using a multi-modelling approach. *Hydrological Sciences Journal*, **61**(15): 2668-2679. https://doi.org/10.1080/02626667.2016.1154558

Riahi, K., Van Vuuren, D. P., Kriegler, E., Edmonds, J., O'neill, B. C., Fujimori, S., Bauer, N., Calvin, K., Dellink, R., Fricko, O. & Lutz, W. (2017). The Shared Socioeconomic Pathways and their energy, land use, and greenhouse gas emissions implications: An overview. *Global environmental change*, **42**: 153-168. https://doi.org/10.1016/j.gloenvcha.2016.05.009

Rounce, D. R., Hock, R., & Shean, D. E. (2020). Glacier mass change in High Mountain Asia through 2100 using the open-source python glacier evolution model (PyGEM). *Frontiers in Earth Science*, **7**: 331. https://doi.org/10.3389/feart.2019.00331

Seibert, J. (1997). Estimation of parameter uncertainty in the HBV model: Paper presented at the Nordic Hydrological Conference (Akureyri, Iceland-August 1996). *Hydrology Research*, **28**(4-5): 247-262. https://doi.org/10.2166/nh.1998.15

Seibert, J. (2005). HBV light version 2. User's manual. Department of Earth Sciences, Uppsala University, Uppsala.

Seibert, J., & Bergström, S. (2022). A retrospective on hydrological catchment modelling based on half a century with the HBV model. *Hydrology and Earth System Sciences*, **26**(5): 1371-1388. https://doi.org/10.5194/hess-26-1371-2022

Seibert, J., & Beven, K. J. (2009). Gauging the ungauged basin: how many discharge measurements are needed? *Hydrology and Earth System Sciences*, **13**(6): 883-892. https://doi.org/10.5194/hess-13-883-2009

Seibert, J., & Vis, M. J. (2012). Teaching hydrological modeling with a user-friendly catchment-runoff-model software package. *Hydrology and Earth System Sciences*, **16**(9): 3315-3325. https://doi.org/10.5194/hess-16-3315-2012

Seibert, J., Vis, M. J., Kohn, I., Weiler, M., & Stahl, K. (2018). Representing glacier geometry changes in a semi-distributed hydrological model. *Hydrology and*

Earth System Sciences, **22**(4): 2211-2224. https://doi.org/10.5194/hess-22-2211-2018

Shah, S., Duan, Z., Song, X., Li, R., Mao, H., Liu, J., Ma, T. & Wang, M. (2021). Evaluating the added value of multi-variable calibration of SWAT with remotely sensed evapotranspiration data for improving hydrological modeling. *Journal of Hydrology*, **603**: 127046. https://doi.org/10.1016/j.jhydrol.2021.127046

Shiklomanov, A. I., Yakovleva, T. I., Lammers, R. B., Karasev, I. P., Vörösmarty, C. J., & Linder, E. (2006). Cold region river discharge uncertainty-Estimates from large Russian rivers. *Journal of Hydrology*, **326**(1-4): 231-256. https://doi.org/10.1016/j.jhydrol.2005.10.037

Shrestha, A. B., Wake, C. P., Mayewski, P. A., & Dibb, J. E. (1999). Maximum temperature trends in the Himalaya and its vicinity: an analysis based on temperature records from Nepal for the period 1971–94. *Journal of climate*, **12**(9): 2775-2786. https://doi.org/10.1175/1520-0442(1999)012%3C2775:MTTITH%3E2.0.CO;2

Shrestha, M., Acharya, S. C., & Shrestha, P. K. (2017). Bias correction of climate models for hydrological modelling–are simple methods still useful?. Meteorological Applications, 24(3), 531-539. https://doi.org/10.1002/met.1655

Shrestha, S., & Alfredsen, K. (2011). Application of HBV model in hydrological studies of Nepali river basins: A case study. *Hydro Nepal: Journal of Water, Energy and Environment*, **8**: 38-43. http://dx.doi.org/10.3126/hn.v8i0.4910

Shrestha, S., Bajracharya, A. R., & Babel, M. S. (2016). Assessment of risks due to climate change for the Upper Tamakoshi Hydropower Project in Nepal. *Climate Risk Management*, **14**: 27-41. https://doi.org/10.1016/j.crm.2016.08.002

Shrestha, S., Yao, T., & Adhikari, T. R. (2019). Analysis of rainfall trends of two complex mountain river basins on the southern slopes of the Central Himalayas. *Atmospheric Research*, **215**: 99-115. https://doi.org/10.1016/j.atmosres.2018.08.027

Shrestha, S., Yao, T., Kattel, D. B., & Devkota, L. P. (2019). Precipitation characteristics of two complex mountain river basins on the southern slopes of the central Himalayas. *Theoretical and applied climatology*, **138**(1): 1159-1178. https://doi.org/10.1007/s00704-019-02897-7

Sichangi, A. W., Wang, L., & Hu, Z. (2018). Estimation of river discharge solely from remote-sensing derived data: an initial study over the Yangtze river. *Remote Sensing*, **10**(9): 1385. https://doi.org/10.3390/rs10091385

Siegfried, T., Bernauer, T., Guiennet, R., Sellars, S., Robertson, A. W., Mankin, J., Bauer-Gottwein, P. & Yakovlev, A. (2012). Will climate change exacerbate water stress in Central Asia? *Climatic change*, **112**: 881-899. https://doi.org/10.1007/s10584-011-0253-z

Siegfried, T., Mujahid, A. U. H., Marti, B. S., Molnar, P., Karger, D. N., & Yakovlev, A. (2023). Assessing Future Hydrological Impacts of Climate Change on High-Mountain Central Asia: Insights from a Stochastic Soil Moisture Water Balance Model. *EGUsphere, 2023*, **1**-43. https://doi.org/10.5194/egusphere-2023-520

Singh, V., Jain, S. K., & Shukla, S. (2021). Glacier change and glacier runoff variation in the Himalayan Baspa river basin. *Journal of Hydrology*, **593**: 125918. https://doi.org/10.1016/j.jhydrol.2020.125918

Sorg, A., Bolch, T., Stoffel, M., Solomina, O., & Beniston, M. (2012). Climate change impacts on glaciers and runoff in Tien Shan (Central Asia). *Nature Climate Change*, **2**(10): 725-731. https://doi.org/10.1038/nclimate1592

Souffront Alcantara, M. A., Nelson, E. J., Shakya, K., Edwards, C., Roberts, W., Krewson, C., Ames, D.P., Jones, N.L. & Gutierrez, A. (2019). Hydrologic modeling as a service (HMaaS): a new approach to address hydroinformatic challenges in developing countries. *Frontiers in Environmental Science*, **7**: 158. https://doi.org/10.3389/fenvs.2019.00158

Spencer, J. E., Thomas, W. L., & Winter, R. E. (1978). *Introducing cultural geography*: Wiley New York.

Stahl, K., Moore, R., Shea, J., Hutchinson, D., & Cannon, A. (2008). Coupled modelling of glacier and streamflow response to future climate scenarios. *Water resources research*, **44**(2). https://doi.org/10.1029/2007WR005956

Su, F., Pritchard, H. D., Yao, T., Huang, J., Ou, T., Meng, F., Sun, H., Li, Y., Xu, B., Zhu, M. & Chen, D. (2022). Contrasting fate of western Third Pole's water resources under 21st century climate change. *Earth's Future*, **10**(9): e2022EF002776. https://doi.org/10.1029/2022EF002776

Swain, J. B., & Patra, K. C. (2017). Streamflow estimation in ungauged catchments using regional flow duration curve: comparative study. *Journal of Hydrologic*

Engineering, **22**(7): 04017010. https://doi.org/10.1061/(ASCE)HE.1943-5584.0001509

Talchabhadel, R., Maskey, S., Gouli, M. R., Dahal, K., Thapa, A., Sharma, S., Dixit, A.M. & Kumar, S. (2023). Multimodal multiscale characterization of cascading hazard on mountain terrain. *Geomatics, Natural Hazards and Risk*, **14**(1): 2162443. https://doi.org/10.1080/19475705.2022.2162443

Talchabhadel, R., Chhetri, R. (2024) Evaluation of long-term changes in water balances in the Nepal Himalayas. *Theor Appl Climatol* **155**, 439–450 https://doi.org/10.1007/s00704-023-04646-3

Talchabhadel, R., Nakagawa, H., Kawaike, K., Yamanoi, K., Musumari, H., Adhikari, T. R., & Prajapati, R. (2021). Appraising the potential of using satellite-based rainfall estimates for evaluating extreme precipitation: A case study of august 2014 event across the west rapti river basin, Nepal. *Earth and Space Science*, **8**(8): e2020EA001518. https://doi.org/10.1029/2020EA001518

Taylor, K. E., Stouffer, R. J., & Meehl, G. A. (2012). An overview of CMIP5 and the experiment design. *Bulletin of the American Meteorological society*, **93**(4): 485-498. https://doi.org/10.1175/BAMS-D-11-00094.1

Teng, F., Huang, W., Cai, Y., Zheng, C., & Zou, S. (2017). Application of hydrological model PRMS to simulate daily rainfall runoff in Zamask-Yingluoxia subbasin of the Heihe River Basin. *Water*, **9**(10): 769. https://doi.org/10.3390/w9100769

Terink, W., Immerzeel, W., Lutz, A., Droogers, P., Khanal, S., Nepal, S., & Shrestha, A. (2017). Hydrological and Climate Change Assessment for Hydropower development in the Tamakoshi river basin. *Nepal, Wageningen, the Netherlands*.

Terink, W., Lutz, A. F., Simons, G. W. H., Immerzeel, W. W., & Droogers, P. (2015). SPHY v2. 0: Spatial processes in hydrology. *Geoscientific Model Development*, **8**(7): 2009-2034. https://doi.org/10.5194/gmd-8-2009-2015

Teutschbein, C., & Seibert, J. (2010). Regional climate models for hydrological impact studies at the catchment scale: a review of recent modeling strategies. *Geography Compass*, **4**(7): 834-860. https://doi.org/10.1111/j.1749-8198.2010.00357.x

Teutschbein, C., & Seibert, J. (2013). Is bias correction of regional climate model (RCM) simulations possible for non-stationary conditions? *Hydrology and*

Earth System Sciences, **17**(12): 5061-5077. https://doi.org/10.5194/hess-17-5061-2013

Thakuri, S., & Salerno, F. (2016). Glacio-Hydrological Simulation in Dudh Koshi River Basin, Nepal. *International Journal of Scientific Development and Research*, **1**: 72-78. https://mail.ijsdr.org/papers/IJSDR1602013.pdf

Thakuri, S., Dahal, S., Shrestha, D., Guyennon, N., Romano, E., Colombo, N., & Salerno, F. (2019). Elevation-dependent warming of maximum air temperature in Nepal during 1976–2015. Atmospheric Research, 228, 261-269. https://doi.org/10.1016/j.atmosres.2019.06.006

Thapa, B. R., Ishidaira, H., Pandey, V. P., & Shakya, N. M. (2017). A multi-model approach for analyzing water balance dynamics in Kathmandu Valley, Nepal. *Journal of Hydrology: Regional Studies*, **9**: 149-162. https://doi.org/10.1016/j.ejrh.2016.12.080

Themeßl, M. J., Gobiet, A., & Heinrich, G. (2012). Empirical-statistical downscaling and error correction of regional climate models and its impact on the climate change signal. *Climatic change*, **112**: 449-468. https://doi.org/10.1007/s10584-011-0224-4

Thornthwaite, C., & Mather, J. (1955). The water balance. Laboratory of Climatology, Drexel Institute of Technology: Centerton, AR. Publications in Climatology, **8**.

Tian, B., & Dong, X. (2020). The double-ITCZ bias in CMIP3, CMIP5, and CMIP6 models based on annual mean precipitation. *Geophysical Research Letters*, **47**(8): e2020GL087232. https://doi.org/10.1029/2020GL087232

Tigabu, T. B., Wagner, P. D., Narasimhan, B., & Fohrer, N. (2023). Pitfalls in hydrologic model calibration in a data scarce environment with a strong seasonality: experience from the Adyar catchment, India. *Environmental Earth Sciences*, **82**(15): 367. https://doi.org/10.1007/s12665-023-11047-2

Tran, Q. Q., De Niel, J., & Willems, P. (2018). Spatially distributed conceptual hydrological model building: A generic top-down approach starting from lumped models. *Water Resources Research*, *54*(10), 8064-8085. https://doi.org/10.1029/2018WR023566

Unger-Shayesteh, K., Vorogushyn, S., Farinotti, D., Gafurov, A., Duethmann, D., Mandychev, A., & Merz, B. (2013). What do we know about past changes in

the water cycle of Central Asian headwaters? A review. *Global and Planetary Change*, **110**: 4-25. https://doi.org/10.1016/j.gloplacha.2013.02.004

Van Liew, M. W., & Mittelstet, A. R. (2018). Comparison of three regionalization techniques for predicting streamflow in ungaged watersheds in Nebraska, USA using SWAT model. https://doi.org/10.25165/j.ijabe.20181103.3528

Van Vuuren, D. P., Edmonds, J., Kainuma, M., Riahi, K., Thomson, A., Hibbard, K., Hurtt, G.C., Kram, T., Krey, V., Lamarque, J.F. & Masui, T. (2011). The representative concentration pathways: an overview. *Climatic change*, **109**: 5-31. https://doi.org/10.1007/s10584-011-0148-z

Vormoor, K., Heistermann, M., Bronstert, A., & Lawrence, D. (2018). Hydrological model parameter (in) stability–"crash testing" the HBV model under contrasting flood seasonality conditions. *Hydrological Sciences Journal*, **63**(7): 991-1007. https://doi.org/10.1080/02626667.2018.1466056

Walling, D., & Fang, D. (2003). Recent trends in the suspended sediment loads of the world's rivers. *Global and Planetary Change*, **39**(1-2): 111-126. https://doi.org/10.1016/S0921-8181(03)00020-1

Wang, J., Zhou, L., Ma, C., & Sun, W. (2023). How Remote-Sensing Evapotranspiration Data Improve Hydrological Model Calibration in a Typical Basin of Qinghai-Tibetan Plateau Region. *Hydrology and Earth System Sciences Discussions*, **2023**: 1-26. https://doi.org/10.5194/hess-2023-200

Waseem, M., Ajmal, M., & Kim, T.-W. (2015). Ensemble hydrological prediction of streamflow percentile at ungauged basins in Pakistan. *Journal of Hydrology*, **525**: 130-137. https://doi.org/10.1016/j.jhydrol.2015.03.042

WECS. (2011). *Water Resources of Nepal in the Context of Climate Change.* Retrieved from Singha Durbar, Kathmandu, Nepal.

WECS/DHM. (1990). *Methodologies for Estimating Hydrologic Characteristics of Ungauged Locations in Nepal*, *His majesty's government of Nepal*. Ministry of Water Resources, Water and Energy Commission Secretariat and Department of Hydrology and Meteorology, Kathmandu.

Wijngaard, R. R., Lutz, A. F., Nepal, S., Khanal, S., Pradhananga, S., Shrestha, A. B., & Immerzeel, W. W. (2017). Future changes in hydro-climatic extremes in the Upper Indus, Ganges, and Brahmaputra River basins. *PloS one*, **12**(12): e0190224. https://doi.org/10.1371/journal.pone.0190224

Wilby, R. L., & Harris, I. (2006). A framework for assessing uncertainties in climate change impacts: Low-flow scenarios for the River Thames, UK. *Water resources research*, **42**(2). https://doi.org/10.1029/2005WR004065

WMO. (2008). Guide to hydrological practices. Volume I: Hydrology—From measurement to hydrological information. *WMO Report No. 168*: 296.

Wongchuig-Correa, S., de Paiva, R. C. D., Biancamaria, S., & Collischonn, W. (2020). Assimilation of future SWOT-based river elevations, surface extent observations and discharge estimations into uncertain global hydrological models. *Journal of Hydrology*, **590**: 125473. https://doi.org/10.1016/j.jhydrol.2020.125473

Wu, J., Li, H., Zhou, J., Tai, S., & Wang, X. (2021). Variation of runoff and runoff components of the upper Shule River in the northeastern qinghai–tibet plateau under climate change. *Water*, *13*(23), 3357. https://doi.org/10.3390/w13233357

Wu, Y., Guo, L., Zheng, H., Zhang, B., & Li, M. (2019). Hydroclimate assessment of gridded precipitation products for the Tibetan Plateau. *Science of the Total Environment*, **660**: 1555-1564. https://doi.org/10.1016/j.scitotenv.2019.01.119

Yao, T., Thompson, L. G., Mosbrugger, V., Zhang, F., Ma, Y., Luo, T., Xu, B., Yang, X., Joswiak, D.R., Wang, W. & Joswiak, M.E. (2012). Third pole environment (TPE). *Environmental Development*, **3**: 52-64. https://doi.org/10.1016/j.envdev.2012.04.002

Yao, T., Xue, Y., Chen, D., Chen, F., Thompson, L., Cui, P., Koike, T., Lau, W.K.M., Lettenmaier, D., Mosbrugger, V. & Zhang, R. (2019). Recent third pole's rapid warming accompanies cryospheric melt and water cycle intensification and interactions between monsoon and environment: Multidisciplinary approach with observations, modeling, and analysis. *Bulletin of the American Meteorological society*, **100**(3): 423-444. https://doi.org/10.1175/BAMS-D-17-0057.1

Zhang, J., & Han, D. (2017). Catchment morphing (CM): a novel approach for runoff modeling in ungauged catchments. *Water resources research*, **53**(12): 10899-10907. https://doi.org/10.1002/2017WR021403

Zhang, T., Li, D., & Lu, X. (2022). Response of runoff components to climate change in the source-region of the Yellow River on the Tibetan plateau. *Hydrological processes*, **36**(6): e14633. https://doi.org/10.1002/hyp.14633

Zhang, Y., Chiew, F. H., Liu, C., Tang, Q., Xia, J., Tian, J., Kong, D. & Li, C. (2020). Can remotely sensed actual evapotranspiration facilitate hydrological prediction in ungauged regions without runoff calibration? *Water resources research*, **56**(1): e2019WR026236. https://doi.org/10.1029/2019WR026236

Zhang, Y., Zheng, H., Zhang, X., Leung, L. R., Liu, C., Zheng, C., Guo, Y., Chiew, F.H., Post, D., Kong, D. & Beck, H.E. (2023). Future global streamflow declines are probably more severe than previously estimated. *Nature Water*, **1**(3): 261-271. http://dx.doi.org/10.1038/s44221-023-00030-7

APPENDICES

APPENDIX -A: SUPPLEMENTRY TABLE OF THESIS

Table A1: Static Database

S.N.	Static Database
1	Globcover 2009 land use
2	Hi-Hydrosoils
3	Hydrosheds SRTM Dem
4	Latitude
5	RGI6 Glaciers

Table A2: Hydrological and Meteorological stations of study area.

Meteorological Stations

Station ID	Location	Type	Long	Lat	Elevation	Frequency
1115	Nepalthok	Precipitation	85.85	27.42	690	Daily
1123	Manthali	Climatology	86.06	27.39	497	Daily
1027	Bahrabise	Climatology	85.90	27.79	884	Daily
1101	Nagdaha	Precipitation	86.10	27.68	909	Daily
1102	Charikot	Climatology	86.05	27.67	1940	Daily
1103	Jiri	Agrometeorology	86.23	27.63	1877	Daily
1104	Melung	Precipitation	86.05	27.52	1536	Daily
1124	Kavre	Agrometeorology	86.13	27.63	1755	Daily

Hydrological Stations

Station ID	Locations	Types	Long	Lat	Elevation	Frequency
647	Busti	Cable Way	86.08	27.63	849	Daily
650	Rasnalu	Cable Way	86.20	27.58	1520	Daily

Table A3: Spatial resolution of selected GCMs

S. No.	Model name	Latitude resolution (degree)	Longitude resolution (degree)
1	ACCESS CM2	1.25	1.875
2	CanESM5	2.7906	2.8125
3	MPI ESM1 2HR	0.9351	0.9375
4	NorESM2 MM	0.9424	1.25

Table A4: Calibrated parameters of SPHY model in Busti and Rasnalu gauging stations

Descriptions	Calibrated Parameters	Busti	Rasnalu	Units
Routing	Recession Coefficient	0.94	0.96	
Ground water	deltaGW	180	180	
	alphaGW	0.01	0.01	
Glacier	GlacF	0.9	0.9	mm /^{0}C/day
	DDFDG	2	2	mm /^{0}C/day
	DDFG	4	4	mm /^{0}C/day
Snow	SnowSC	0.5	0.5	mm /^{0}C/day
	DDFS	5.5	5.5	mm /^{0}C/day
	Tcrit	0	0	mm /^{0}C/day
Soil	Root Layer	10	1600	mm/day
	Sub Layer	10	1600	mm/day
	Capillary Rise	1	2	mm/day

Table A5: Calibrated parameters of HEC HMS model in Busti gauging stations

Calibrated Parameters	Value	Units
Intial Storage	1	%
Max Storage	2	mm
Crop Coefficient	1	mm
Incial Deficit	2	mm
Maximum storage	3	mm
Constant rate	0.21	mm/hr
Storage Coefficient	6	hr

Table A6: Calibrated parameters of HBV model in Busti gauging stations

Snow Routine			**Glacier Routine**		
Parameters	**Value**	**Units**	**Parameters**	**Value**	**Units**
TT	2.00	˚C	KSI	0.001	1/Δt
CFMAX	3.50	mm/Δt˚C	dKG	0.01	1/Δt
SP	0.00	-	Kgmin	0.02	1/Δt
SFCF	0.70	-	AG	0.9	mm/Δt
CFR	0.05	-	**Response Routine**		
CWH	0.50	-	PERC	4	mm/Δt
CFGlacier	1.00	-	Alpha		-
CFSlope	1.00	-	UZL	10	mm
Soil Moisture Routine			K0	0.06	1/Δt
FC	450.00	-	K1	0.0003	1/Δt
LP	0.30	-	K2	0.00001	1/Δt
BETA	4.00	-	**Routing Routine**		
			MAXBAS	1	Δt

Table A7: Bias correction factors for Temperature

GCMs	Jan	Feb	Mar	Apr	May	Jun	Jul	Aug	Sep	Oct	Nov	Dec
ACCESS CM2	-0.6	-0.6	-1.2	-2.8	-3.1	-2.5	-2.1	-1.4	-0.9	-1.2	-2.0	-1.1
CanESM5	-1.0	-1.3	-1.5	-2.0	-2.3	-1.9	-3.3	-2.8	-1.6	-1.9	-1.7	-1.3
MPI ESM1 2HR	-0.9	-0.4	-1.5	-2.7	-3.4	-2.7	-1.7	-1.3	-0.8	-1.0	-1.5	-1.6
NorESM2 MM	-0.2	0.0	-1.8	-2.8	-2.8	-2.5	-1.1	-0.9	-0.8	-2.2	-2.6	-1.4

Table A8: Bias correction factors for Precipitation

GCMs	Jan	Feb	Mar	Apr	May	Jun	Jul	Aug	Sep	Oct	Nov	Dec
ACCESS CM2	0.4	0.3	0.6	3.0	3.6	3.0	0.8	0.5	0.8	2.2	0.8	0.3
CanESM5	0.1	0.1	0.3	0.7	1.6	3.3	6.3	1.2	1.3	0.3	0.1	0.1
MPI ESM1 2HR	0.4	0.3	0.9	2.9	8.0	2.2	0.8	0.7	1.4	1.8	0.4	0.8
NorESM2 MM	0.8	1.7	9.4	17.1	6.4	1.0	0.7	0.8	1.2	1.7	1.4	0.7

Table A9: Seasonal contribution of Precipitation - Discharge (SSP245 scenario)

Precipitation	**DJF %**	**MAM %**	**JJAS %**	**ON %**
Historical	2	14	80	3
NF	2	13	83	2
MF	2	11	84	2
FF	3	15	81	1
Discharge	**DJF %**	**MAM %**	**JJAS %**	**ON %**
Historical	7	9	73	10
NF	6	8	76	10
MF	6	9	75	10
FF	6	10	73	10

Table A10: Seasonal contribution of Precipitation - Discharge (SSP585 scenario)

Precipitation	**DJF %**	**MAM %**	**JJAS %**	**ON %**
Historical	2	14	80	3
NF	2	20	75	3
MF	2	17	79	2
FF	2	13	84	1
Discharge	**DJF %**	**MAM %**	**JJAS %**	**ON %**
Historical	7	9	73	10
NF	6	12	71	10
MF	6	11	73	10
FF	6	10	73	10

APPENDIX -B: PUBLICATIONS AND CONFERENCE

B1: List of Publications

1 **BR Budhathoki**, TR Adhikari, S Shrestha, RP Awasthi (2023). Application of hydrological model to simulate streamflow contribution on water balance in Himalaya river basin, Nepal, *Frontiers in Earth Science 11, 1128959* https://doi.org/10.3389/feart.2023.1128959 **(SCI-Q_1)**

2 **BR Budhathoki**, TR Adhikari, S Shrestha, RP Awasthi (2023). Flow Transfer through Spatially Distributed Hydrological (SPHY) Model in Tamakoshi river basin of Nepal. *Journal of Hydrology and Meteorology, Vol. 11 SOHAM-Nepal* https://doi.org/10.3126/jhm.v11i1.59662 **(NepJoL)**

3 **BR Budhathoki**, TR Adhikari, S Shrestha, RP Awasthi, B Dawadi, H Gao, YP Dhital (2024). Application of Hydrological models to Streamflow Estimation at Ungauged Trans-boundary Himalaya River Basin, Nepal. (**Accepted**) *Hydrology Research* (**SCI-Q_2**)

4 TR Adhikari, B Baniya, Q Tang, R Talchabhadel, MR Gouli, **BR Budhathoki,** RP Awasthi (2023), Evaluation of post extreme floods in high mountain region: A case study of the Melamchi flood 2021 at the Koshi River Basin in Nepal, *Natural Hazards Research* https://doi.org/10.1016/j.nhres.2023.07.001 **(Scopus Index)**

5 TR Adhikari, B Baniya, Q Tang, R Talchabhadel, S Pradhanga, D Pradhanga, M Sigdel, D Chen, MR Gouli, **BR Budhathoki,** RP Awasthi (2024), Identification Precipitation threshold and resulting river discharge: An IDF based approach in the central Himalya, Nepal. Geografiska Annaler: *Series A, Physical Geography* https://doi.org/10.1080/04353676.2024.2373575 (**SCI-Q_2**)

B2: Conference

1. International Training Program on Theory and Technology for Ecological Restoration of Typical Ecosystems along the Belt and Road regions. Institute Subtropical Agriculture, Chinese Academy of Sciences, 14-30 June 2024, Hunan China
2. 4th International Symposium on Sustainable Agriculture for Subtropical Regions (ISSASR-4). June 22-24, Changsha China

3. 2024 Hunan “One Belt One Road” Morden Agriculture Technology International Transfer and Cooperation Conference. Hunan Province Science and Technology Department, 21 June 2024 Changsha, Hunan China
4. International Conference on Advances Science and Technology for Sustainable Development Goals (IC-ASTSDGs-2024) (**Invited Speaker**), AKS University 9-10 February 2024, Satna, Madhya Pradesh, India
5. International Training on Resource & Environment Scientific Data Sharing along the “Belt and Road”. China Institute of Geographic Sciences and Natural Resources Research, Chinese Academy of Sciences, 4-18 November 2023 Beijing China
6. 1st IOST PhD Festival by Institute of Science and Technology. Tribhuvan University (**Poster**), October 9-10 Kathmandu
7. 9th National Conference on Science and Technology by Nepal Academy of Science and Technology (NAST), Government of Nepal **(Oral)-**2022 June 26-28, Kathmandu
8. HIMALICE Symposium on Climate, Cryosphere, Hazard and Livelihood in the Fourth International Conference on Mountains in the Changing World. By KIAS **(Poster)-**2019 October 18-19, Kathmandu

frontiers | Frontiers in Earth Science

TYPE Original Research
PUBLISHED 22 May 2023
DOI 10.3389/feart.2023.1128959

OPEN ACCESS

EDITED BY
Sudeep Thakuri,
Central Department of Environmental Science, Institute of Science and Technology, Tribhuvan University Kirtipur, Nepal

REVIEWED BY
Achut Parajuli,
University of Alberta, Canada
Suraj Mal,
University of Delhi, India

*CORRESPONDENCE
Suraj Shrestha,
theshrestha.amigo@gmail.com

RECEIVED 21 December 2022
ACCEPTED 11 May 2023
PUBLISHED 22 May 2023

CITATION
Budhathoki BR, Adhikari TR, Shrestha S and Awasthi RP (2023), Application of hydrological model to simulate streamflow contribution on water balance in Himalaya river basin, Nepal. *Front. Earth Sci.* 11:1128959. doi: 10.3389/feart.2023.1128959

Application of hydrological model to simulate streamflow contribution on water balance in Himalaya river basin, Nepal

Bhumi Raj Budhathoki[1], Tirtha Raj Adhikari[1], Suraj Shrestha[1,2,3]* and Ram Prasad Awasthi[4]

[1]Central Department of Hydrology and Meteorology, Tribhuvan University, Kathmandu, Nepal, [2]Kathmandu Center for Research and Education, Chinese Academy of Sciences, Tribhuvan University, Kathmandu, Nepal, [3]Institute of Fundamental Research and Studies, Kathmandu, Nepal, [4]Department of Hydrology and Meteorology, Government of Nepal, Kathmandu, Nepal

Hydrological models are widely used and often regarded as reliable tools for accurately estimating various components of the water balance. In a remote Himalayan catchment, such as Tamakoshi basin, where limited hydrometric dataset is available, such models often provide essential insights that are crucial to water researchers and planners. In this regard, we employed the semi-distributed HBV-light (version 4.0.0.25) hydrological model for glacierized Tamakoshi river basin and attempted to quantify various water balance components. For our model tests, using the daily streamflow records, we selected two distinct periods, i.e., 2004–2008 as a calibration period whilst 2011–2012 for model validation. Based on our findings, the model was able to reasonably predict the streamflow (validation efficiency: Nash-Sutcliffe Efficiency of 0.82 and percent bias −21%). At our site, HBV-light model predicted that the change in streamflow was mostly governed by monsoonal rain (62%) followed by baseflow (20%), glacier melt (13%) and snowmelt (5%). As expected, the streamflow peaked during the month of August where monsoon-induced rain and melting of glaciers significantly contributed to river flow. As a result, monsoon period showcased largest fluctuation in water storage while negligible change was observed during post-monsoon season. Nonetheless, our findings revealed that the baseflow contribution to streamflow was maximum during the month of October and lowest during February. Our findings indicated that the water balance of the Tamakoshi basin is largely influenced by monsoonal rain during June–September window as well as baseflow and glacier melt during the dry season. Runoff components contribution to streamflow was increasing but water storage changes was decreasing in recent decade (2011–2020). We believe our findings are crucial for future initiatives involving water resources, water-induced disaster management, and studies of climate change may benefit from the findings of this study, especially in a region with limited hydrometric data availability.

KEYWORDS

HBV model, flow contribution, Tamakoshi river basin, streamflow components, water balance storage

1 Introduction

Water balance and streamflow depend on the different runoff components of the hydrological cycle and their various forms. Streamflow consists mainly of two parts: surface flow and sub-surface flow, where surface flow consists of direct runoff from rain and snow-glacier melt and sub-surface flow is the infiltration of water from the soil to sub-soil. Firstly, Thornthwaite and Mather (1955) introduced water balance models with revisions. The water balance and hydrological regimes are affected by the changing climate. Due to the changing climate, the water availability downstream is changing continuously, in the past and the future (Bajracharya et al., 2018). Climate change and rising temperatures have an impact on snow and glacier areas, influencing future water availability downstream. Snow and glacier areas that significantly melt contribute to streamflow in snow and glacier-fed river basin systems (Khadka et al., 2014). The changing climate influences the hydrological processes that impact river flow regimes and freshwater availability in catchment-scale hydrology in the Himalayan River basin (Adhikari et al., 2022).

After the 1960s, hydrological modeling systems were launched to simulate hydrological processes. Several hydrological models have been developed in recent years such as HBV model (Bergström, 1976; Bergstrom, 1992), SWAT model (Arnold et al., 1998), JAMS J2000 model (Krause, 2002), SPHY model (Terink et al., 2015), GDM model (Kayastha et al., 2020), etc to estimate water balance and components through model parameterization. The hydrological models simulate the streamflow components, such as the glacier-snow melt and cover, evaporation, precipitation and baseflow over the basin. The classification of streamflow components by different methods includes empirical or statistical methods and hydrological modeling; hydrological modeling is a robust approach to the separation of streamflow components (Wu et al., 2021). Different hydrological processes such as baseflow, snow-glacier runoff, and rain runoff are contained in the streamflow components and contribute to river flow (Khanal et al., 2021). Runoff and its components are responsible for streamflow and the fluctuations in runoff from year to year regulate streamflow (Adnan et al., 2022). Depending on the availability of datasets, snow and glacier melting in Himalayan areas are conceptualized in simple or complex ways (Hock, 2003). The change in glacier melt runoff significantly affects the water availability in the Himalayan River basin (Singh et al., 2021). Snow melt, discharge, evaporation and snowfall are sensitive to climate change in the Himalayan River basin, causing an effect on hydrological regimes (Nepal, 2016). Hydrological phenomena vary in space and time from sub-basin to basin scale, as well as on daily, sub-daily, and decadal scales (Khanal et al., 2021). In recent decades, the Himalayan river basin has observed a rise in the frequency of extreme streamflow occurrences (Gaire et al., 2022). The hydrological extremes and water balance components are changing in different physiographic regions as well as from the river basin scale to the sub-basin scale (Budhathoki et al., 2021). Few researches have quantified the contribution of streamflow to the Himalayan river basin. In a number of these studies, the glacier model SPHY was used to simulate the contribution of streamflow to the HMA upstream rivers. The various streamflow components were included in the SPHY model (Khanal et al., 2021). To close the gaps left by earlier research in the Tamakoshi River Basin, the HBV model simulates the contribution of each component to streamflow.

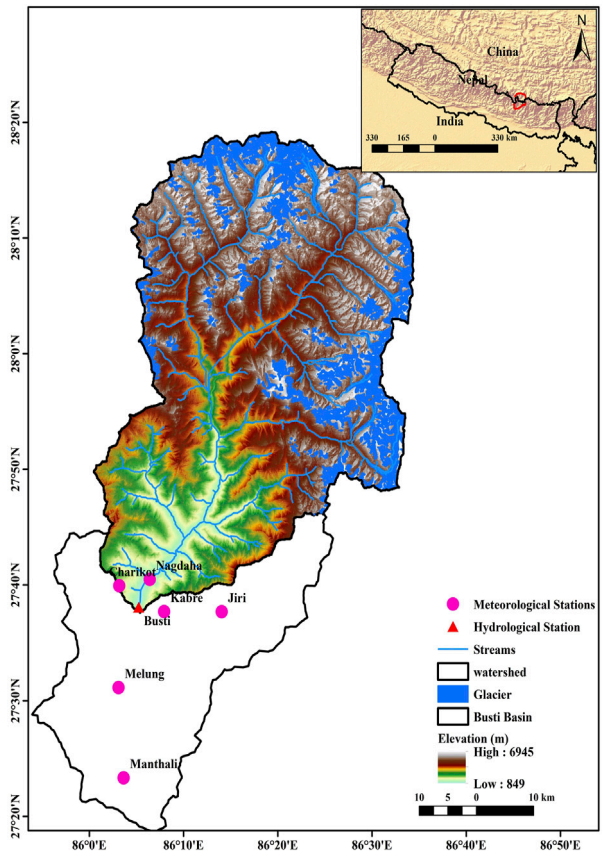

FIGURE 1
Study area (Tamakoshi river basin with black boundary) showing its topographical map along with its locations of streams with gauging stations, climate stations and glacier cover used in this study.

The purpose of this study is to determine the availability of water in the Tamakoshi river basin's hydrological cycle in various forms. However, changes in water storage, total water balance and streamflow contribution components are important to the estimation of water availability. Understanding streamflow processes is crucial for water resource projects. This study looks at how rain runoff, baseflow runoff, snowmelt runoff, and glacier melt runoff affect water balance. The components of streamflow contribution are changing as a result of changes in hydrological processes, which has an impact on changes in water storage. The water balance and its component's contributions to runoff estimation and water availability for hydropower, irrigation, and drinking water planning, development, and management.

2 Study area

The Tamakoshi river is a trans-boundary Himalayan river basin and one of the main tributaries of the Koshi river basin system, located in eastern Nepal on the southern slope of the central Himalayas (Figure 1). The basin is geographically located on

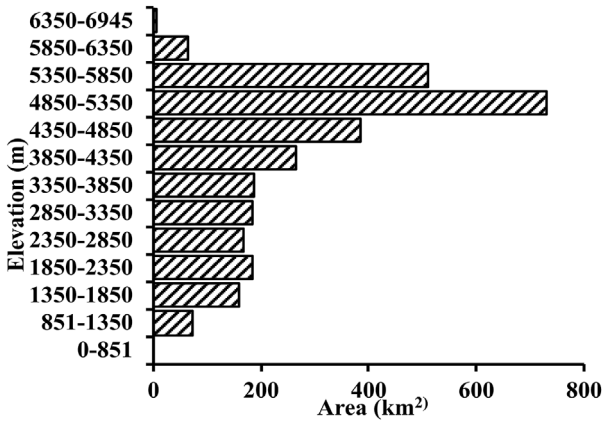

FIGURE 2
Hypsometric distribution of the area of the study basin.

Nepal's political border in the districts of Dolakha and Ramechhap. At the Busti gauging station, the basin covers 2,933.29 km^2, of which 1,444.57 km^2 is on Chinese territory. Tamakoshi river basin is located 27^{0}20$^{'}$ N to 28^{0}20$^{'}$ N and 85^{0}40$^{'}$ E to 86^{0}40$^{'}$ E with elevations ranging from 849 masl to 6,945 masl. The climate of this basin is subtropical at lower elevations and varies to tundra at higher elevations (Karki et al., 2016). This basin's runoff and water balance are dominated by the monsoon rainfall.

2.1 Hypsometric curve (elevation-area distribution)

Regions with and without glaciers need to simulate the area, elevation, and aspect. In the catchment setting, the basin area is divided into 13 elevation zones every 500 m. The height and air temperature both affect precipitation (rain or snow). In order to adjust for temperature and precipitation, PCALT should be set at 10%/100 m and TCALT at −0.65/100 m, respectively, as the elevation rises. The total area to Aspect wise East-west horizontal is 1,327.85 km^2, North oriented area occupied 618.64 km^2 and South oriented area occupied 901.62 km^2 among them 253.59 km^2 area covered by the glacier in Tamakoshi river basin. The curve in Figure 2 depicts the area elevation dispersion.

3 Data and methods

3.1 Input data

For dynamic datasets, observations are precipitation, temperature, evapotranspiration and discharge from ground stations. These datasets are collected from the Department of Hydrology and Meteorology (DHM). The climatic datasets processing in this study using normal ratio method to fill in the rainfall data (Shrestha et al., 2019a; Shrestha et al., 2019b), evaporation data was calculated using Thornwaite method based on the mean monthly temperature and the lapse rate method is used to fill in the temperature data (Adhikari et al., 2022). The dynamic datasets are discharge and climatic stations used in this research in Table 1.

HBV model requires mainly dynamic as well as static datasets. Static datasets are DEM and glacier data. The Digital Elevation Model (DEM) Shuttle Rader Topographic Mission (SRTM) Hydrosheds (http://hydrosheds.cr.usgs.gov/) data was used. The glaciers inventory datasets RGI 6.0 South Asia East is used (RGI 6.0 Consortium 2017).

3.2 HBV model

The Hydrologiska Byrns avdeling for Vattenbalans (HBV), HBV-light version 4.0.0.25 model is a conceptual approach since it incorporates some physical processes and basin structure. Utilizing temperature and precipitation data as inputs, the Precipitation-Runoff Model assesses stream flow and simulates streamflow (Vormoor et al., 2018). By combining evaluations of precipitation, climate, and land use, basin responses to water balance, flow regimes, climate change, flood peaks and volumes, the interaction between soil and water, and sediment yields are assessed (Adhikari et al., 2022). According to Siebert et al. (2012), the HBV light version features a routine for precipitation in snow, soil moisture, reaction, and routing that includes lakes and glaciers (Siebert., 2005). HBV model continuously simulates discharge at glacierized and non-glacierized zone elevation-wise at the desired site within the basin area.

3.3 Streamflow components

HBV model simulates the streamflow contribution parameters in Tamakoshi river basin. The streamflow contribution of the Tamakoshi river basin is primarily made up of four components: baseflow runoff, glacier melt runoff, snowmelt runoff, and rain runoff. The snow formation process depends on critical temperature. The melt contribution by snow and glacier depends upon degree day factor. The streamflow contribution at hydrological station Busti simulated by HBV model is calculated using Eq. 1

$$Q_{Tot} = Q_{rr} + Q_{sm} + Q_{gm} + Q_{bf} \quad (1)$$

where Q_{Tot} is total contributed discharge, Q_{rr} is discharge contributed by rain runoff, Q_{sm} is discharge contributed by snowmelt runoff, Q_{gm} is discharge contributed by glacier melt runoff and Q_{bf} is discharge contributed by baseflow runoff.

3.4 Water balance storage

The water balance was evaluated by hydrological cycle components using HBV model. The water balance estimated at Busti gauging station is based on the principle of water mass conservation, i.e., entering and discharging of water (Milly, 1994). The water availability storage is changing spatially and temporally. The water balance is account for the change in water storage. Water

TABLE 1 List of hydro-meteorological stations used in the study.

Hydro-Meteorological Stations						
Station ID	Location	Type	Long. (DD)	Lat. (DD)	Elevation (m)	Frequency
1115	Nepalthok	Precipitation	85.85	27.42	690	Daily
1123	Manthali	Climatology	86.06	27.39	497	Daily
1027	Bahrabise	Climatology	85.90	27.79	884	Daily
1101	Nagdaha	Precipitation	86.10	27.68	909	Daily
1102	Charikot	Climatology	86.05	27.67	1940	Daily
1103	Jiri	Agrometeorology	86.23	27.63	1877	Daily
1104	Melung	Precipitation	86.05	27.52	1536	Daily
1124	Kabre	Agrometeorology	86.13	27.63	1755	Daily
647	Busti	Discharge	27.63	86.08	849	Daily

balance components simulated by model are discharge (Q_{sim}), observed discharge (Q_{obs}), precipitation, actual evaporation and potential evaporation. The changing of water storage is calculated by using Eq. 2.

$$\Delta S = P - Q - ET \quad (2)$$

where ΔS changes in storage, P is Precipitation, Q is discharge and ET is actual evapotranspiration.

3.5 Calibration and validation

The hydrological model HBV light was set up at Tamakoshi river basin at Busti gauging station (ID 647). With the help of observed daily discharge records, the model was manually calibrated. Trial parametrization served as the basis for manual calibration. The model was calibrated from 2004 to 2008 and validated from 2011 to 2012 and was evaluated with Nash-Sutcliffe Efficiency (NSE) (Nash and Sutcliffe, 1970), Coefficient of Determination (R^2), and Volume Difference (Pbias). Using Eq. 3, NSE can be determined which ranges from infinite ∞ to 1, where closer to 1 is perfect model efficiency. Coefficient of Determination (R^2) is the fitting of the simulated discharge with the observed discharge as measured by Eq. 4. Higher values of R^2, which range from 0 to 1, are optimal for fitting. The volume difference between observed and simulated discharge evaluated by Pbias is less than ±25 calculated using Eq. 5.

$$\mathbf{NSE} = \mathbf{1} - \frac{\sum_{i=1}^{n}(\mathbf{O_i} - \mathbf{S_i})^2}{\sum_{i=1}^{n}(\mathbf{O_i} - \bar{\mathbf{O}})^2} \quad (3)$$

$$R^2 = \left(\frac{\sum_{i=1}^{n}(O_i - \bar{O})(S_i - \bar{S})}{\sqrt{\sum_{i=1}^{n}(O_i - \bar{O})^2}\sqrt{\sum_{i=1}^{n}(S_i - \bar{S})^2}} \right)^2 \quad (4)$$

$$\mathbf{Pbias\ or\ PEV} = \mathbf{100\%} \times \left[\frac{\boldsymbol{O_i} - \boldsymbol{S_i}}{\boldsymbol{O_i}} \right] \quad (5)$$

where O_i is measured observed discharge, S_i is simulated discharge, $\bar{O}$ is observed average discharge and $\bar{S}$ is simulated average discharge. The overall methodology adopted in this study is shown in the flow diagram (Figure 3).

4 Results

4.1 Performance of HBV light model

The HBV light model performed admirably and was successfully implemented in the Tamakoshi river basin. The model was calibrated and validated against observed discharge at the gauging station Busti in daily time step data using a manual approach based on the trial-and-error process (Figure 4). In this research, the only dynamic datasets used were solely observed station data, which was taken from DHM. The model was calibrated at Busti station (ID 647) in 2004–2008 and validated in 2011–2012. The model performance at Busti, the Nash-Sutcliffe Efficiency (NSE) is 0.77, Coefficient of Determination (R^2) estimated simulated discharge is 0.77, and the simulated volume (Pbias) is slightly biased by −3%. Similarly, the model was validated with the same calibrated parameters and values (Table 2). The validated performance of the model NSE is 0.82 and R^2 estimated simulated discharge is 0.87, and the simulating volume difference Pbias is −21%. The validated model performance period is better than the calibration period. The peak flow is overestimated due to the rating estimation by the Department of Hydrology and Meteorology (DHM) and cascading flooding in Himalayan catchments. The river discharge is not uniformly continuous and regular due to extreme events of precipitation and physical processes that block the river and stream at upstream sites. Landslides and debris flow have blocked the river and small streams, with the majority of landslides causing debris flow occurring in the summer. In recent years, most infrastructure has been built without regard for watershed and drainage management. DHM classified discharge as poor, fair, or good, but there is only fair discharge at Busti station (ID 647).

4.2 Water balance components contribution to streamflow

In this study, the streamflow components are primarily classified as rain-snow precipitation, which is determined by the critical temperature,

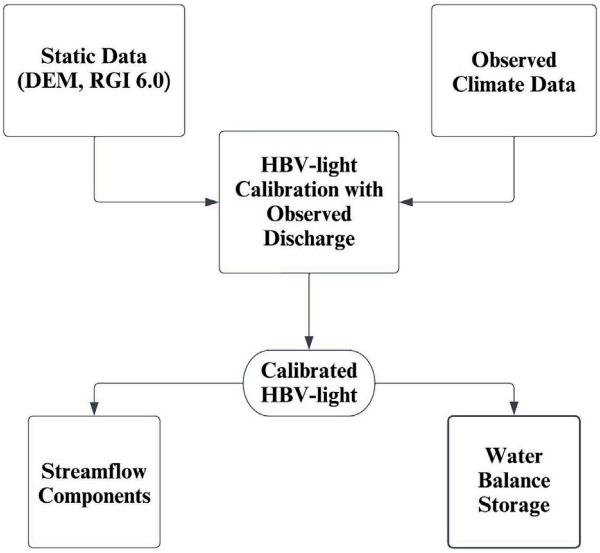

FIGURE 3
Flow chart of methodology.

actual evapotranspiration, rain runoff, snowmelt runoff, and glacier melt runoff. The streamflow components and their contribution to the river flow at Busti Station are estimated for the 30 years 1991–2020. The streamflow components are rain, baseflow and snow-glacier melt that contribute to Busti discharge station in hydrological cyclic processes. These streamflow components influence river discharge at Busti hydrological station in terms of monthly, seasonal, and annual variations.

Figures 5A, B showed that the monthly average streamflow contribution from snow melt ranged from 0.88 mm to 27.78 mm, glacier melt contributions ranged from 2.75 mm to 58.05 mm, baseflow contributions ranged from 35.40 mm to 41.55 mm, and rain runoff contributions ranged from 5.09 mm to 476.41 mm. Depending on streamflow, the total discharge might range from 45.01 mm to 601.05 mm. The results also showed that the rain runoff in August, baseflow in October, snowmelt in July, and glacier melt in August were the monthly factors that had the greatest impact on streamflow. Snowmelt in February, baseflow in February, rain runoff in March and glacier melt in February all contributed to the lowest monthly streamflow. In terms of the total discharge, the highest streamflow occurred in August and the lowest discharge occurred in February. The analysis reveals that from June to October, rain runoff predominates, while from November to May, baseflow predominates in terms of total streamflow.

Figures 5C, D showed that the seasonal streamflow contribution from snow melt ranged from 3.56 mm to 90.12 mm, glacier melt contributions ranged from 15.48 mm to 195.53 mm, baseflow contributions ranged from 81.23 mm to 156.02 mm, and rain runoff contributions ranged from 28.94 mm to 1,272.83 mm. Depending on streamflow, the total discharge might range from 161.66 mm to 1714.49 mm. The results showed that streamflow components

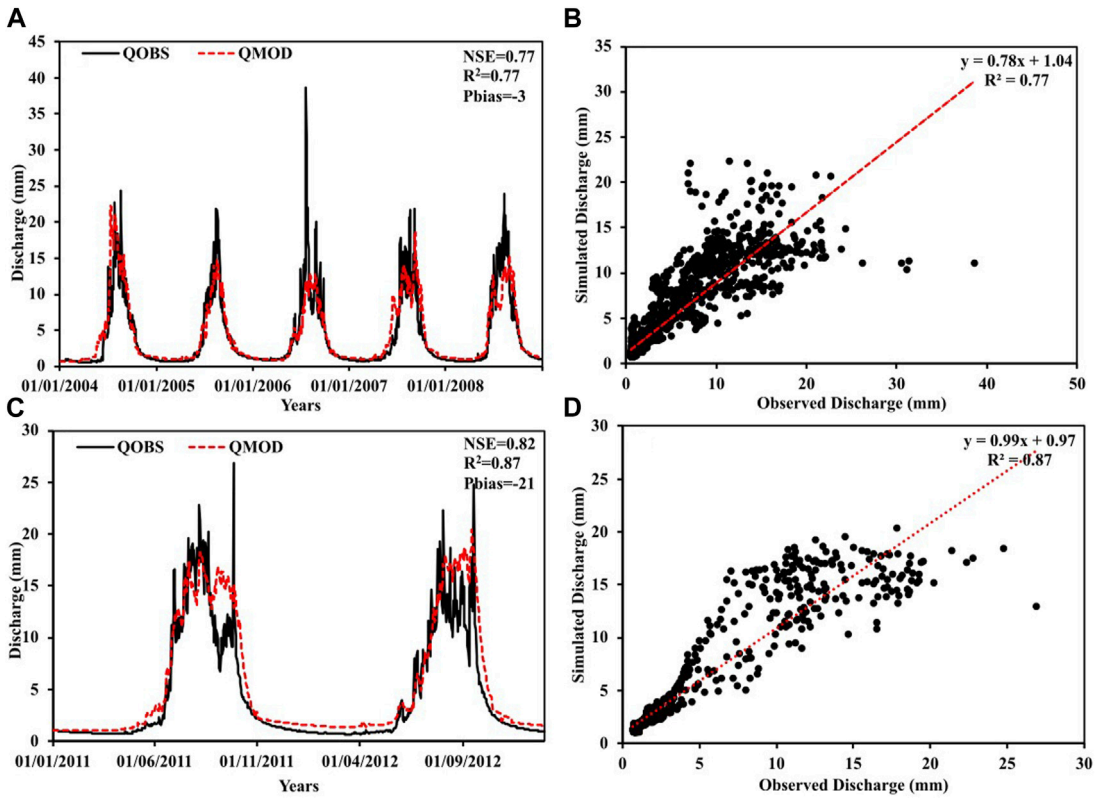

FIGURE 4
Daily observed (black) and HBV-light simulated (red) streamflow during the: calibration (2004–2008, **(A)** and validation (2011–2012, **(C)** for the Tamakoshi river basin. Scatter plots show the fit between the observed and simulated values for the calibration **(B)** and validation **(D)** periods.

TABLE 2 Optimized Values of the different model parameters HBV-light during calibration.

Snow routine			Glacier routine		
Parameters	Value	Units	Parameters	Value	Units
TT	2.00	°C	KSI	0.001	1/Δt
CFMAX	3.50	mm/Δt°C	dKG	0.01	1/Δt
SP	0.00	-	Kgmin	0.02	1/Δt
SFCF	0.70	-	AG	0.9	mm/Δt
CFR	0.05	-	Response Routine		
CWH	0.50	-	PERC	4	mm/Δt
CFGlacier	1.00	-	Alpha		-
CFSlope	1.00	-	UZL	10	mm
Soil Moisture Routine			K0	0.06	1/Δt
FC	450.00	-	K1	0.0003	1/Δt
LP	0.30	-	K2	0.00001	1/Δt
BETA	4.00	-	Routing Routine		
			MAXBAS	1	Δt

contribution is generally maximum during the summer season (JJAS), with minimum streamflow varying according to contribution components in the winter (DJF) and pre-monsoon (MAM) seasons. Similarly, rain runoff contributes the most to total streamflow, while snowmelt contributes the least. Although baseflow contributed during the pre-monsoon season, streamflow contribution peaked during the monsoon season and then declined in winter. The seasonal maximum streamflow contribution in monsoon season 74% and minimum streamflow occurred in winter 7% but baseflow contributed in post-monsoon season (Supplementary Figure S1A).

Figure 5E showed that the snow melt contribution to the annual simulated streamflow varied from 62.88 mm to 211 mm; glacier melt contribution varied from 217.08 mm to 358.05 mm; baseflow varied from 424.26 mm to 494.28 mm, and rain runoff varied from 836.10 mm to 1845.51 mm. Annually, the contributions from the runoff component were as follows: the snowmelt contribution was highest in 1998 and lowest in 1995; the contribution from glacier melt to streamflow was highest in 2016 and lowest in 1997; the contribution from rain runoff was highest in 2000 and lowest in 2009, and the contribution from baseflow to streamflow was highest in 2020 and lowest in 1991. The total runoff contribution to streamflow at Busti was at its maximum in 2016 with a value of 2,777.11 mm and at its minimum in 2009 with a value of 1,690.17 mm. Among the water balance components relatively rain runoff contribution was maximum, i.e., 62%, then gradually baseflow 20%, glacier melt 13% and snowmelt 5% contribute to cumulative streamflow (Supplementary Figure S1B).

The decadal change shows the changes in different water components and variables over the past 3 decades (1991–2020). The Supplementary Table S2 includes the values of glacier melt, snowmelt, baseflow, rain runoff, and total discharge. Firstly, in the recent decade (2011–2020), the maximum contributions were observed from the runoff components, including snowmelt (116.63 mm), glacier melt (317.94 mm), baseflow (479.65 mm), and rain runoff (1,544.88 mm) and total discharge (2,459.11 mm). Secondly, the minimum contributions from the runoff components were snowmelt (107.53 mm), rain runoff (1,292.27 mm) and total discharge (2,161.38 mm), observed in the previous decade (2001–2010) of the past 3 decades. Similarly, the minimum values for glacier melt (282.80 mm), and baseflow (442.45 mm) were observed in the previous decade (1991–2000).

4.3 Water balance storage

The availability of water components in the hydrological cycle estimated by model simulation should be reasonable; however, there are some differences between observed and simulated discharge due to WMO standard meteorological network availability, real-time data, complex territory, data collection, and rating estimation. The change in water balance storage at Busti station is estimated to have occurred over a 30-year period from 1991 to 2020. The principle of mass conservation governs water balance storage: incoming water equals outgoing water, where incoming water is precipitation and outgoing water is discharge and evaporation of water bodies. Eq. 2 is used to compute the changing water storage in the Tamakoshi river basin at the Busti gauging station. The components of streamflow are precipitation, evaporation, total discharge from rain runoff, baseflow, snowmelt, and glacier melt runoff, which are responsible for water storage changes. The water storage varied temporally, as in annually, seasonally, monthly, and decadal.

Figure 6A showed that from April to August, the water balance storage was positive, but the subsequent month's statistics revealed a decrease in the water balance storage. The incidence of precipitation led to a negative water balance storage. In the basin's water balance, maximum water storage was reached in July at 253.49 mm, and minimum water storage was reached in October at −142.89 mm. From September to March, the monthly water balance storage contributed to streamflow supplemented by groundwater, where groundwater is recharged by falling precipitation and snow-glacier processes. Water is mostly stored from April to August, and less water is stored from September to December.

Figure 6B demonstrated that the water balance was positive during the pre-monsoon and monsoon seasons and negative during the post-monsoon and winter seasons. The post-monsoon season has the least amount of water storage with a value of −251.05 mm compared to the monsoon season which has a water storage of 449.26 mm. Precipitation was found 81%, 14%, 3%, and 2% in monsoon, pre-monsoon, post-monsoon and winter season respectively on water balance storage in basin (Table 3). Also, 74% total discharge occurred in monsoon season, 11% in post-monsoon season, 7% in winter season and 8% in pre-monsoon season on streamflow contribution on water balance storage. Similarly, 40% evapotranspiration occurred in monsoon season, 20% in post-monsoon season, 14% in winter season and 25% in pre-monsoon season on water balance storage in basin.

Similarly, Figure 6C showed that the water balance was positive during most of the years with a few exceptions. In the basin's water balance, maximum water storage was reached in the year 2002 with 447.35 mm, and minimum water storage was reached in the year 2012 with −122.81 mm. Decadal maximum changes in water storage (216.29 mm) were observed in the previous dacade (1991–2000) while the minmum changes in water storage (78.09 mm) were observed in the recent decade (2011–2020) of the past 3 decades (Supplementary Table S2).

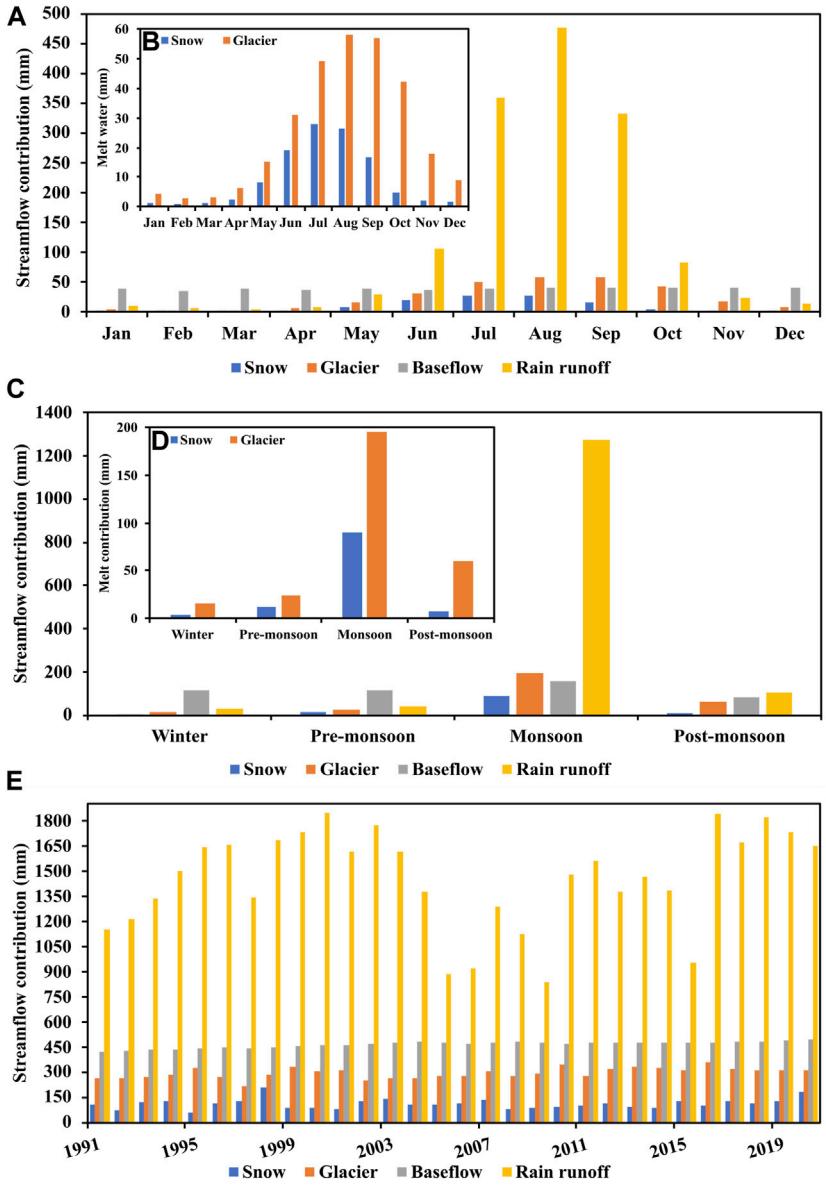

FIGURE 5
Monthly **(A)**, seasonal **(C)** and annual **(E)** variations in simulated streamflow components where snow and glacier melt contribution are shown in monthly **(B)** and seasonal **(D)** variations.

5 Discussion

Using the HBV model, this study investigated the temporal variation of the water balance component's contribution to streamflow and water storage changes in the Tamakoshi river basin. Previously, limited research in the same basin was conducted using the SWAT model to investigate the climate change impacts on hydropower development and the SRM model to analyze the climate change impact on glacier and snowmelt contributions (Shrestha et al., 2016; Khadka et al., 2014). SWAT model didn't include a glacier input feature; therefore, the model didn't simulate the glacier melt runoff during hydropower impact analysis, although SWAT included using the T-index approach to estimate the meltwater contribution from snow and glaciers (Thakuri and Salerno, 2016). Hydrological modeling has been biased to simulate the baseflow and rain runoff flow contributions to streamflow in past studies, which are important to winter and monsoon streamflow. This study investigated the effects of streamflow components (rain runoff, baseflow, snow and glacier melt contribution to water balance and water storage change at Busti gauging station) using the HBV model with station data. There had previously been no research in the Tamakoshi river basin using this combination of research designs.

SPHY model simulations simulated runoff component responses in the glacierized Narayani river basin at Devghat. This model successfully simulated four runoff components: rain runoff, baseflow, snowmelt, and glacier melt runoff. According to Khanal et al. (2021) and Wijngaard et al. (2017), the contribution

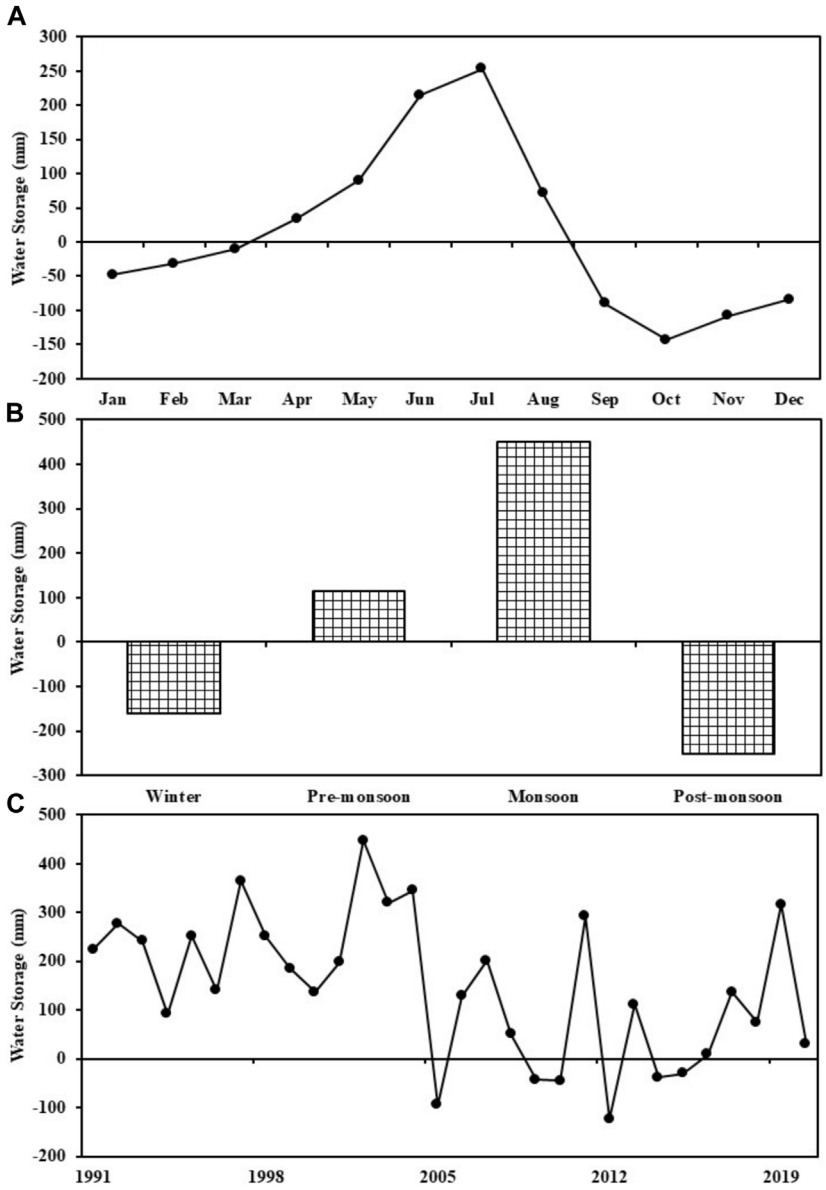

FIGURE 6
Water storage at the monthly **(A)**, seasonal **(B)**, and annual **(C)** time scale.

TABLE 3 Seasonal water balance storage components.

Components	Winter (%)	Pre-monsoon (%)	Monsoon (%)	Post-monsoon (%)
Total Discharge	7	8	74	11
Precipitation	2	14	81	3
Evapotranspiration	14	25	40	20

of rain runoff to streamflow is 63%–65%. Baseflow is approaching 21%, with snowmelt contributing 9%–12% and glacier melt contributing 3%–4%. This study closely matches the contribution of baseflow and rain runoff to streamflow, but the results of the contribution of snow and glacier melt to streamflow varied because the Narayani basin has an area coverage that is approximately 37 times greater than that of the Tamakoshi river basin, even though the total melting contribution is almost certainly similar. According to Zhang et al. (2022), rain runoff dominates total streamflow at

downstream stations, but snow and glacier melt predominate at upstream stations in the Himalayan drainage basins (Mukhopadhyay and Khan, 2015). As a result, the runoff contribution to streamflow by components is not uniform; there are differences. For example, In the Gilgit river basin, glacier melting is at its highest, or 45%, while baseflow gradually drops to 27%, snowmelt to 24%, and rain runoff to 5% (Adnan et al., 2022).

Our findings closely match the pattern of streamflow contribution, but the percentage of contribution varies slightly due to the basin's area coverage. Our results show that rain runoff contributes 62%, baseflow contributes 20%, snowmelt contributes 5%, and glacier melt contributes 13% of total streamflow in the Tamakoshi river basin. The majority of streamflow components contribute during the summer season, but snowmelt contributions are more prevalent during the pre-monsoon season and glacier melt contributions are more prevalent during the post-monsoon season. The contribution of snow and ice melting to streamflow was 17.7% annually while in the spring season (24.7%), summer season (17%), autumn season (16.4%), and winter season (30.9%) (Khadka et al., 2014). Our research, however, revealed that the contribution to overall streamflow made by snow and glacier melting in the winter is minimal and peaks in the post-monsoon season. Our results differed from the melting contribution to streamflow because there are two processes of runoff: surface and subsurface, which are different runoff contributors; glacier melting, baseflow, and rain runoff were not categorized; and Khadka et al. (2014) estimated only snow and ice melting contributions. Snow is not converted directly to surface runoff; instead, it is transformed into glacier and groundwater recharge storage. The melting processes of snow and glacier-fed river basins rely on heat energy for surface runoff and subsurface runoff contribution to streamflow (Lang, 1986). The model simulation period was 10 years, but our simulation duration was 30 years. Observed baseflow is the dominant flow of total streamflow during winter and pre-monsoon, and rain runoff is the dominant flow during monsoon and post-monsoon. The results show that rain runoff dominates total streamflow from May to October, while baseflow dominates total streamflow from November to April. Maximum snowmelt and glacier melt were observed during pre-monsoon and post-monsoon total streamflow. The river basin where most of the precipitation occurred in the summer season, the Ganga river basin, is 71% (Khanal et al., 2021). It states that precipitation is dominant in the summer season, which is similar to our results, but the amount of rainfall received quietly differed from our results because the area coverage of the Ganga river is greater than that of the Tamakoshi river. Tamakoshi river basin receives 80% of its water during the monsoon season (Khadka et al., 2014). Similarly, 80% of rainfall falls during the monsoon season, which is closely related to our findings. April-August water storage change is positive and September-March shows the negative water storage change simulated by using the same modeling approach as the other two models, SWAT and BTOPMC, in the KV watershed (Thapa et al., 2017); our result is completely similar to that result. Streamflow is dominant in the summer season compared with the dry season because the maximum precipitation occurs in summer season (Shrestha et al., 2016). Our results show that 78% of streamflow occurred in the summer season. The majority of streamflow occurred during the summer. Thus, runoff component's contributions to changes in streamflow and water balance storage vary depending on the characteristics of the basin. The river discharge usually increases in the high Himalayan river basin due to an increase in melt and liquid precipitation fraction (Manabe et al., 2004; Khanal et al., 2021). Similarly, our results showed the decadal changes that the water input to the system has been increasing over time. The streamflow components were increasing in the most recent decade than the previous decades. However, water storage changes were observed to decrease throughout the decades. Water storage changes decreasing in the recent decade due to the increase in runoff components contribution to river discharge and evaporation.

This research attempted to determine the temporal variation of the simulated water balance component's relative contributions and water storage changes on streamflow in the Tamakoshi river basin. The response of water balance components and changing water storage is significant for estimating water availability in downstream basins and for further research in other basins as needed.

6 Conclusion

In this research, water balance, streamflow components, water storage change and their trends have been evaluated in the Tamakoshi river basin (TRB). In the basin, the HBV 4.0 model performed well for hydrological simulation. Nash-Sutcliffe Efficiency (NSE), Determination (R^2), and volume difference (Pbias) are employed as the model performance indicators. Overall durations, the flow pattern was almost perfectly replicated by the model. Overall, the model is underappreciated, but it is adequate. There are slight variations between the calibrated period's simulated and observed discharge throughout the course of 5 years. The water balance, water storage change and streamflow components were estimated at gauging station Busti during a 30-year period. The discharge predicted by the model is 2,198 mm, and the basin-wide precipitation total was 2,903.52 mm. Rainfall in the river basin is predominately monsoonal, with an average rate of 80% leading to 74% of the discharge taking place during the monsoon season.

Although baseflow contributes during the pre-monsoon season, the simulated streamflow contribution is maximum in the summer and minimum in the winter. The Busti gauging station's water balance has improved as a result of the storage improvements. Rain runoff contributes the most to streamflow, whereas snowmelt contributes the least. The flow was at its highest in August and its lowest in February. Results showed that water storage increased during rainy months and decreased during dry months.

As a result, water resource project planners and developers should base their decisions on the temporal variability of water availability and its contribution components to sustainable development. This study makes use of meteorological observation from DHM stations to estimate the components of the water balance and the changes in water storage at the Busti gauge station. Since the network of meteorological stations cannot be tolerated, satellite and reanalysis meteorological data products may produce superior results. It is also advised to consider how future climate change may affect the components of streamflow and water balance.

Data availability statement

The original contributions presented in the study are included in the article/Supplementary Material, further inquiries can be directed to the corresponding author.

Author contributions

BRB: conceptualization, formal analysis, methodology, and writing—original draft. TRA: conceptualization, formal analysis, methodology, writing—review and editing, and supervision. SS: conceptualization, formal analysis, writing—review and editing, supervision. RPA: investigation, visualization, validation. All authors listed have made a substantial, direct, and intellectual contribution to the work and approved it for publication.

Funding

The first author is supported by University Grant Commission, Nepal (UGC award no: PhD-076/77 S&T -15) PhD Fellowship.

Acknowledgments

We thank the Department of Hydrology and Meteorology (DHM), Nepal for providing available data.

Conflict of interest

The authors declare that the research was conducted in the absence of any commercial or financial relationships that could be construed as a potential conflict of interest.

The handling editor ST declared a shared affiliation with the author(s) BRB, TRA & SS at the time of review.

Publisher's note

Supplementary material

The Supplementary Material for this article can be found online at: https://www.frontiersin.org/articles/10.3389/feart.2023.1128959/full#supplementary-material

SUPPLEMENTARY FIGURE S1
Relative contribution of runoff components to streamflow's at the seasonal **(A)** and annual **(B)** time scale.

References

Adhikari, T. R., Talchabhadel, R., Shrestha, S., Sharma, S., Aryal, D., and Pradhanang, S. M. (2022). The evaluation of climate change impact on hydrologic processes of a mountain river basin. *Theor. Appl. Climatol.* 150, 749–762. doi:10.1007/s00704-022-04204-3

Adnan, M., Liu, S., Saifullah, M., Iqbal, M., Ali, A. F., and Mukhtar, M. A. (2022). Spatiotemporal variations in runoff and runoff components in response to climate change in a glacierized subbasin of the Upper Indus Basin, Pakistan. *Front. Earth Sci.* 1516. doi:10.3389/feart.2022.970349

Arnold, J. G., Srinivasan, R., Muttiah, R. S., and Williams, J. R. (1998). Large area hydrologic modeling and assessment part I: Model development 1. *JAWRA J. Am. Water Resour. Assoc.* 34, 73–89. doi:10.1111/j.1752-1688.1998.tb05961.x

Bajracharya, A. R., Bajracharya, S. R., Shrestha, A. B., and Maharjan, S. B. (2018). Climate change impact assessment on the hydrological regime of the Kaligandaki Basin, Nepal. *Sci. Total Environ.* 625, 837–848. doi:10.1016/j.scitotenv.2017.12.332

Bergström, S. (1976). *Development and application of a conceptual runoff model for Scandinavian catchments.*

Bergstrom, S. (1992). *The HBV model-its structure and applications.*

Budhathoki, A., Babel, M. S., Shrestha, S., Meon, G., and Kamalamma, A. G. (2021). Climate change impact on water balance and hydrological extremes in different physiographic regions of the West Seti River Basin, Nepal. *Ecohydrol. Hydrobiology* 21, 79–95. doi:10.1016/j.ecohyd.2020.07.001

Hock, R. (2003). Temperature index melt modelling in mountain areas. *J. hydrology* 282, 104–115. doi:10.1016/s0022-1694(03)00257-9

Karki, R., Talchabhadel, R., Aalto, J., and Baidya, S. K. (2016). New climatic classification of Nepal. *Theor. Appl. Climatol.* 125, 799–808. doi:10.1007/s00704-015-1549-0

Kayastha, R. B., Steiner, N., Kayastha, R., Mishra, S. K., and Mcdonald, K. (2020). Comparative study of hydrology and icemelt in three Nepal river basins using the Glacio-Hydrological Degree-Day Model (GDM) and observations from the Advanced Scatterometer (ASCAT). *Front. Earth Sci.* 7, 354. doi:10.3389/feart.2019.00354

Khadka, D., Babel, M. S., Shrestha, S., and Tripathi, N. K. (2014). Climate change impact on glacier and snow melt and runoff in Tamakoshi basin in the Hindu Kush Himalayan (HKH) region. *J. Hydrology* 511, 49–60. doi:10.1016/j.jhydrol.2014.01.005

Khanal, S., Lutz, A. F., Kraaijenbrink, P. D., van Den Hurk, B., Yao, T., and Immerzeel, W. W. (2021). Variable 21st century climate change response for rivers in High Mountain Asia at seasonal to decadal time scales. *Water Resour. Res.* 57, e2020WR029266. doi:10.1029/2020wr029266

Krause, P. (2002). Quantifying the impact of land use changes on the water balance of large catchments using the J2000 model. *Phys. Chem. Earth, Parts A/B/C* 27, 663–673. doi:10.1016/s1474-7065(02)00051-7

Lang, H. (1986). Forecasting meltwater runoff from snow-covered areas and from glacier basins. *River flow Model. Forecast.* 3, 99–127.

Manabe, S., Milly, P., and Wetherald, R. (2004). Simulated long-term changes in river discharge and soil moisture due to global warming/Simulations à long terme de changements d'écoulement fluvial et d'humidité du sol causés par le réchauffement global. *Hydrological Sci. J.* 49. doi:10.1623/hysj.49.4.625.54429

Milly, P. (1994). Climate, interseasonal storage of soil water, and the annual water balance. *Adv. Water Resour.* 17, 19–24. doi:10.1016/0309-1708(94)90020-5

Mukhopadhyay, B., and Khan, A. (2015). A reevaluation of the snowmelt and glacial melt in river flows within Upper Indus Basin and its significance in a changing climate. *J. Hydrology* 527, 119–132. doi:10.1016/j.jhydrol.2015.04.045

Nash, J. E., and Sutcliffe, J. V. (1970). river flow forecasting through conceptual models part I—a discussion of principles. *J. hydrology* 10, 282–290. doi:10.1016/0022-1694(70)90255-6

Nepal, S. (2016). Impacts of climate change on the hydrological regime of the Koshi river basin in the Himalayan region. *J. Hydro-Environment Res.* 10, 76–89. doi:10.1016/j.jher.2015.12.001

Prasad Gaire, N., Zaw, Z., Bräuning, A., Sharma, B., Raj Dhakal, Y., Timilsena, R., et al. (2022). Increasing extreme events in the central Himalaya revealed from a tree-ring based multi-century streamflow reconstruction of Karnali River Basin. *J. Hydrology* 610, 127801. doi:10.1016/j.jhydrol.2022.127801

Seibert, J. (2005). *HBV light version 2, user's manual*. Uppsala: Department of Earth Sciences, Uppsala University.

Seibert, J., and Vis, M. J. (2012). Teaching hydrological modeling with a user-friendly catchment-runoff-model software package. *Hydrology Earth Syst. Sci.* 16, 3315–3325. doi:10.5194/hess-16-3315-2012

Shrestha, S., Bajracharya, A. R., and Babel, M. S. (2016). Assessment of risks due to climate change for the upper Tamakoshi hydropower project in Nepal. *Clim. Risk Manag.* 14, 27–41. doi:10.1016/j.crm.2016.08.002

Shrestha, S., Yao, T., and Adhikari, T. R. (2019a). Analysis of rainfall trends of two complex mountain river basins on the southern slopes of the Central Himalayas. *Atmos. Res.* 215, 99–115. doi:10.1016/j.atmosres.2018.08.027

Shrestha, S., Yao, T., Kattel, D. B., and Devkota, L. P. (2019b). Precipitation characteristics of two complex mountain river basins on the southern slopes of the central Himalayas. *Theor. Appl. Climatol.* 138, 1159–1178. doi:10.1007/s00704-019-02897-7

Singh, V., Jain, S. K., and Shukla, S. (2021). Glacier change and glacier runoff variation in the Himalayan Baspa river basin. *J. Hydrology* 593, 125918. doi:10.1016/j.jhydrol.2020.125918

Terink, W., Lutz, A. F., Simons, G. W. H., Immerzeel, W. W., and Droogers, P. (2015). SPHY v2. 0: Spatial processes in hydrology. *Geosci. Model. Dev.* 8, 2009–2034. doi:10.5194/gmd-8-2009-2015

Thakuri, S., and Salerno, F. (2016). Glacio-hydrological simulation in dudh Koshi River Basin, Nepal. *Int. J. Sci. Dev. Res.* 1, 72–78.

Thapa, B. R., Ishidaira, H., Pandey, V. P., and Shakya, N. M. (2017). A multi-model approach for analyzing water balance dynamics in Kathmandu Valley, Nepal. *J. Hydrology Regional Stud.* 9, 149–162. doi:10.1016/j.ejrh.2016.12.080

Thornthwaite, C., and Mather, J. (1955). *The water balance. Centerton, N. J. Drexel Institute of Technology - laboratory of climatology*. Berlin, Germany: ScienceOpen.

Vormoor, K., Heistermann, M., Bronstert, A., and Lawrence, D. (2018). Hydrological model parameter (in) stability–"crash testing" the HBV model under contrasting flood seasonality conditions. *Hydrological Sci. J.* 63, 991–1007. doi:10.1080/02626667.2018.1466056

Wijngaard, R. R., Lutz, A. F., Nepal, S., Khanal, S., Pradhananga, S., Shrestha, A. B., et al. (2017). Future changes in hydro-climatic extremes in the upper indus, ganges, and brahmaputra river basins. *PloS one* 12, e0190224. doi:10.1371/journal.pone.0190224

Wu, J., Li, H., Zhou, J., Tai, S., and Wang, X. (2021). Variation of runoff and runoff components of the upper shule river in the northeastern qinghai–tibet plateau under climate change. *Water* 13, 3357. doi:10.3390/w13233357

Zhang, T., Li, D., and Lu, X. (2022). Response of runoff components to climate change in the source-region of the Yellow River on the Tibetan plateau. *Hydrol. Process.* 36, e14633. doi:10.1002/hyp.14633

Flow Transfer through Spatially Distributed Hydrological (SPHY) Model in Tamakoshi River Basin of Nepal

Bhumi Raj Budhathoki[1], Tirtha Raj Adhikari[1], Suraj Shrestha[1,2,3]*, and Ram Prasad Awasthi[4]

[1]*Central Department of Hydrology and Meteorology, Tribhuvan University.*
[2]*Kathmandu Centre for Research and Education, Tribhuvan University-Chinese Academy of Sciences.*
[3]*Institute of Fundamental Research and Studies, Kathmandu 44600, Nepal.*
[4]*Department of Hydrology and Meteorology, Government of Nepal.*

(Received 31 August 2023; Accepted 27 September 2023)

ABSTRACT

The availability of continuous hydrological records, both spatially and temporally, is often limited. This research employed a fully distributed Spatial Process in HYdrology (SPHY) model within the Tamakoshi River Basin to address this gap. The SPHY model was calibrated from 2004 to 2008 with NSE 0.62 at Busti station of Tamakoshi [2933.29 km^2] and validated from 2004 to 2008 with NSE 0.76 at Rasnalu station of Khimti [322.58 km^2]. Conversely, SPHY model was calibrated from 2004 to 2008 with NSE 0.79 at Rasnalu station of Khimti and validated from 2004 to 2008 with NSE 0.61 at Busti station of Tamakoshi. The observed annual average discharge at Busti station was 1632 m^3/s and Rasnalu station was 261 m^3/s during the simulation period. The annual average discharges at Benighat [862.09 km^2 downstream] transferred from Busti and Rasnalu models are 1963.1 m^3/s and 1961.32 m^3/s, respectively. Daily streamflow generated at Benighat from Busti and Rasnalu stations, closely aligns and perfectly matches and highly correlates, with the coefficient of determination 0.99. SPHY model is a good technique for prediction of flows in ungauged basins of Himalayan region. The SPHY model emerges as a robust technique for predicting discharge within the Himalayan River basin. This research holds the potential to serve as a valuable reference for generating streamflow data at ungauged locations, that are vital for planning, management and development of water resource projects.

Keywords: SPHY model, Ungauged River, Trans-boundary, Himalayan River Basins.

1. Introduction

Nepal has plentiful water resource coverage with three major perennial river systems (snow-fed), and several medium-sized (non-snow-fed) to small-size river basins along the country. However, several basins in Nepal are currently ungauged and do not match the World Meteorological Organization's (WMO) requirements for station network density (WMO, 2008). For hydrological and meteorological activities in terrains based on temperate Mediterranean and tropical zones, plains of comparable zones, and dry and polar regions, the WMO has established a baseline number of stations. Specifically, these regions should have one station for every 25-100 km^2, 600-900 km^2, and 1500-10,000 km^2 respectively (WMO, 2008). Notably, it is challenging to install and maintain instrumentation for real-time data retrieval from gauged or ungauged sites in data-scarce situations and inaccessible mountainous terrain regions due to the intricate interconnectedness of larger hydrological networks and smaller catchments. As a result, hydrological modeling may be used as a potential replacement strategy (Terink et al., 2015).

For continuous daily and monthly streamflow modeling in ungauged catchments, the combination of parameter transfer and drainage area ratio methods may be more effective than either approach alone in terms of efficiency (Li et al., 2019). Although several techniques have been used in the past to regionalize streamflow in ungauged basins, the physical characteristics of these catchments continue to make it difficult to obtain accurate streamflow data (Waseem et al., 2015). When comparing low flow estimates to high flow estimates in the central Himalayas, regionalization of flow duration curves that takes into account climate conditions and basin peculiarities produces lowered and ordinary persistent streamflow estimates (Panthi et al., 2021). The configuration and support of station networks are hampered by the political complexity of transfrontier river areas in the scenery of the Nepalese river system, which is closely connected to the trans-Himalayan region. Successful water management downstream is hampered by these obstacles. Gaining knowledge of central basin factors such as annual precipitation, slope, channel

*Corresponding author: Suraj Shrestha, theshrestha.amigo@gmail.com

https://doi.org/10.3126/jhm.v11i1.59662

length and elevations is necessary to account for increases in unmeasured streamflow. These factors have a significant impact on enhanced estimating techniques (DHM, 2004; Li et al., 2019; WECS/DHM, 1990).

The use of reliable hydrological models and suitable regionalization approaches is of the utmost importance when dealing with the complex issue of forecasting streamflow, particularly in cases when gauges are absent (Kim and Kaluarachchi, 2008). Despite the fact that a number of hydrological models are easily changeable both within and outside of their normal range (Bergstrom, 2006), inconsistencies may still happen due to the variety of calibration operations and distinguishing features (Van Liew and Mittelstet, 2018). A number of modeling techniques have been enhanced by utilising the regionalization process, which transfers data from gauged areas to those where gauges are absent, in order to improve regular estimates of streamflow in lacking-gauge basins (Razavi and Coulibaly, 2016). Evidently, rather than relying on empirical equations, these methods are predominantly included in hydrological models (Clark et al., 2017). Nevertheless, the SPHY model offers a thorough solution and incorporates dispersed features that are helpful for simulating endless unmeasured discharge states.

In this study, the spatially distributed hydrological model (SPHY), which could transfer continuous streamflow to an ungauged basin, is used to examine the applicability of in-situ data to estimate ungauged discharge from the donor to the target site. The main aim of this study is to use a hydrological modeling system to determine the suitability of ungauged streamflow data.

2. Data and Methods

2.1. Study Area

Tamakoshi River is a transboundary Himalayan river basin, which is one of the main tributaries of the Koshi River basin system of Nepal (Figure 1). Tamakoshi River basin has an elevation range from 455 masl to 6945 masl. Tamakoshi River Basin originated from the Tibetan plateau and merges with Sunkoshi River at Benighat. Tamakoshi River Basin lies in Dolakha and Ramechhap districts of Nepal. The total basin occupies 4117.96 km^2 up to Benighat before merging with Sunkoshi River. There are two discharge gauging stations upstream of Benighat: one in Tamakoshi at Busti having a basin area of 2933.29 km^2 and another in Khimti at Rasnalu having a basin area of 322.58 km^2. The remaining area of 862.09 km^2 downstream of the Tamakoshi River Basin is ungauged up to Benighat before it merged with Sunkoshi River. The Tamakoshi River Basin extends from the high Himalayas to the Silwalik range (Khadka et al., 2014). The climate of the basin typically varies from tundra to tropical (Karki et al., 2016).

2.2. Data Used

SPHY model uses mainly two kinds of data sets: static and dynamic datasets. These are land use/land cover (LULC) map, soil map, digital elevation model and hydrometeorological parameters precipitation, temperature (average, minimum and maximum) and discharge. The Globecover (2009) dataset is open source. Digital Elevation Model (DEM) of Shuttle Rader Topographic Mission (SRTM) 3 arc seconds is hydrologically conditioned. The glaciers inventory outlines RGI 6.0 South Asia East is used (Consortium, 2017).

The dynamic datasets like precipitation, minimum and maximum temperatures and discharges are collected from the Department of Hydrology and Meteorology (DHM). The missing rainfall data are filled using Normal Ratio Method and temperatures using lapse rate of 0.0065 °C/m. The dynamic datasets of discharge and climatic stations used in this research are quantified in Table 1 and their geographical locations are presented in Figure 1.

2.3. Model Description

SPHY model is a spatially distributed cell-by-cell basis leaky bucket type of model. SPHY model simulates large-scale basin-to-catchment scale hydrology. SPHY model is glacier module concept (Terink et al., 2015). For snow processes three steps were involved: snow and rainfall depending on the threshold of temperature, snowmelt, refreezing and storage using the degree day approached and snowmelt runoff when air temperature above the melting point for each grid cell. The glacier processes involved glacier melt used degree day approaches, glacier percolation was ground water and glacier runoff from glacier melting processes from both debris-covered and free zone. Soil water process involved three steps root zone layer, subzone and groundwater layer. During the soil water process involved surface runoff, actual evapotranspiration, lateral flow, percolation, groundwater recharge and baseflow occurred. The total runoff routing is the summation of the flow of these processes. SPHY model simulates the total runoff from each setup from the desired outlet of the basin. Each and every runoff is routed downstream using a simple recession coefficient. The meteorological stations and outlets create in respective locations in delineated watersheds of cloned DEM. The locations of meteorological stations require bilinear interpolation for the interpolation method. Outlets of each subbasin are mandatory to place and must located on the river network. The Accuflux function of SPHY model the determines flow accumulation for total discharge in locations of outlets in the river network.

2.4. Runoff Routing

In streamflow routing is referred to transport of water through an open-channel system network. Since unsteady

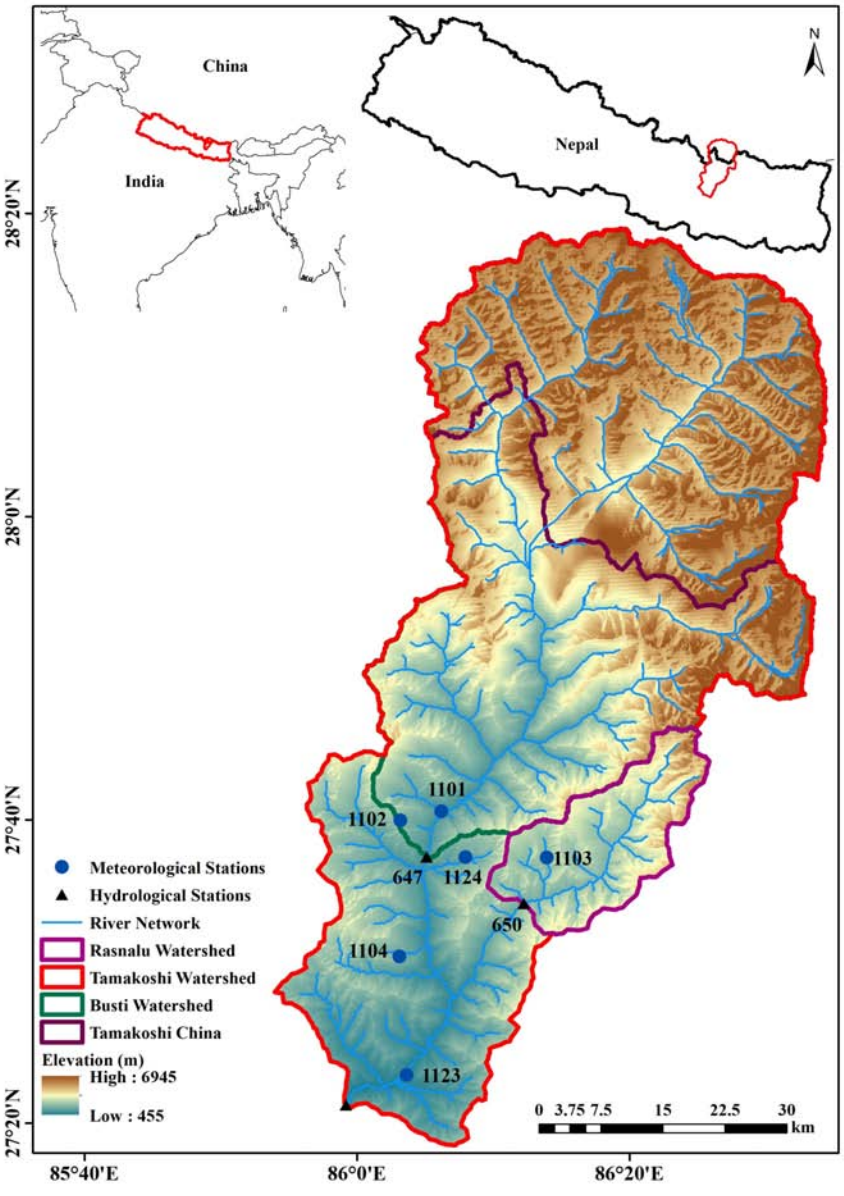

FIG. 1. Hydrological and Meteorological stations of Tamakoshi River Basin.

flow from open channel, streamflow routing often involves complex partial differential equations. SPHY model calculates the accumulated amount of water for each cell that flows out of the cell by cell into downstream cell. The accuflux PCRaster built-in function in SPHY model, which calculates the accumulated runoff from its upstream cells for each cell, including the specific runoff generated within the cell itself. SPHY model implements a flow recession coefficient (kx (–)) that accounts for flow travel time, which can be a result of the channel friction. Using this coefficient Kx, the river flow in SPHY is calculated using the following three equations below.

$$Q_{tot*} = \frac{Q_{Tot}.0.001.A}{24.3600} \quad (1)$$

$$Qaccu,t = accuflux(Fdir,\ Qtot*) \quad (2)$$

$$Qrout,t = (1-Kx)\,.Qaccu,t + kx.Qrout,t-1 \quad (3)$$

where, Q_tot* (m^3/s) the specific runoff on day t, QTot the specific runoff in mm on day t, A (m^2) the grid-cell area, Qaccu,t (m^3/s) the accumulated streamflow on day t

Table 1. Hydrological and Meteorological stations.

Meteorological Stations						
Station ID	Location	Type	Long	Lat	Elevation	Frequency
1115	Nepalthok	Precipitation	85.85	27.42	690	Daily
1123	Manthali	Climatology	86.06	27.39	497	Daily
1027	Bahrabise	Climatology	85.90	27.79	884	Daily
1101	Nagdaha	Precipitation	86.10	27.68	909	Daily
1102	Charikot	Climatology	86.05	27.67	1940	Daily
1103	Jiri	Agrometeorology	86.23	27.63	1877	Daily
1104	Melung	Precipitation	86.05	27.52	1536	Daily
1124	Kavre	Agrometeorology	86.13	27.63	1755	Daily
Hydrological Stations						
Station ID	Locations	Types	Long	Lat	Elevation	Frequency
647	Busti	Cable Way	86.08	27.63	849	Daily
650	Rasnalu	Cable Way	86.20	27.58	1520	Daily

without flow delay taken into account, Qrout,t (m^3/s) the routed streamflow on day t, Qrout,t-1 (m^3/s) the routed streamflow on day t-1, F the flow direction network, and kx (–) the flow recession coefficient. kx has values ranging between 0 and 1, where values close to 0 correspond to a fast-responding catchment, and values approaching 1 correspond to a slow-responding catchment.

2.5. Model Simulation

The SPHY model was calibrated on a manual and trial basis. SPHY model calibrated with observed discharge at Busti station of Tamakoshi river basin and validated at Rasnalu station of Khimti Khola watershed from 2004 to 2008. Similarly, the model was calibrated at Rasnalu station of Khimti Khola watershed and validated at Busti station of Tamakoshi river basin from 2004 to 2008. The same model was calibrated and validated in the same basin with same parameters (Terink et al., 2017).

The continuous flows were transposed by calibrated and validated SPHY model in upstream station Busti and Rasnalu downstream of these stations to Benighat. Busti and Rasnalu is donor basin to Benighat where Benighat is the total stream flow receiver of Tamakoshi river basin.

This study has two approaches to ungauged flow estimation that is the flow simulated from Busti station and another flow simulated from Rasnalu station due to spatial distributed features of SPHY modeling system. On the basis of calibrated gauged stations, streamflow were transposed from both stations model simulated flows at Benighat. SPHY model parameters were calibrated at station for better performance but total runoff at Benighat was estimated without calibration on the basis of calibrated parameters of gauged stations.

The model performance was evaluated by Nash Sutcliffe Efficiency (NSE), simulated discharge was evaluated with observed discharge by statistical parameter through coefficient of determination (R^2) and the volume difference between observed and simulated was evaluated by Pbias.

2.6. Performance of Model Evaluation Methods

The SPHY model is evaluated by the Nash Sutcliffe Efficiency (NSE) (Nash and Sutcliffe, 1970). NSE is ranging from -∞ to 1, the better performance if the model is closer to 1 is an excellent fit.

$$NSE = 1 - \frac{\sum_{i=1}^{n}(O_i - S_i)^2}{\sum_{i=1}^{n}\left(O_i - \bar{O}\right)^2} \tag{4}$$

The variation of simulated and observed discharge by SPHY model was evaluated by the coefficient of determination (R^2). The range of coefficient of determination (R^2) is 0 to 1, closer to 1 is the best fit.

$$R^2 = \left(\frac{\sum_{i=1}^{n}(O_i - \overline{O})(S_i - \overline{S})}{\sqrt{\sum_{i=1}^{n}\left(O_i - \overline{O}\right)^2}\sqrt{\sum_{i=1}^{n}\left(S_i - \overline{S}\right)^2}} \right)^2 \tag{5}$$

The goodness of fit between simulated discharge by SPHY model and observed discharge was calculated using the percent of bias (Pbias).

$$Pbias = 100 \times \left[\frac{O_i - S_i}{O_i} \right] \tag{6}$$

where, Oi is measured observed discharge, Si is simulated discharge, O is observed average discharge and S is simulated average discharge.

3. Results and Discussion

3.1. Gauged Simulation

The SPHY model performed at Busti gauging station efficiency with Nash Sutcliffe Efficiency (NSE) equal to

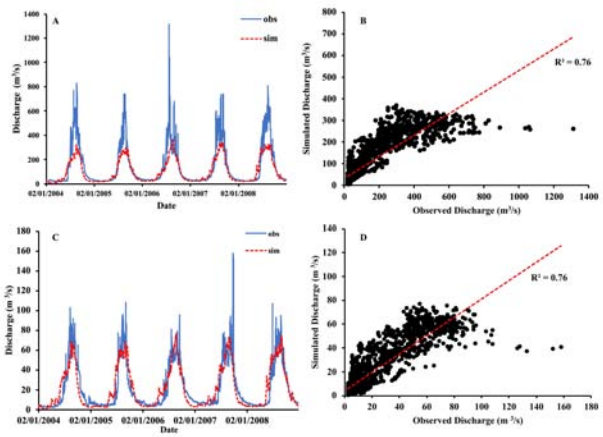

FIG. 2. Hydrograph of calibrated model with observed discharge (A) and Scatter plot (B) at Busti, hydrograph of validated model (C) and Scatter plot (D) at Rasnalu.

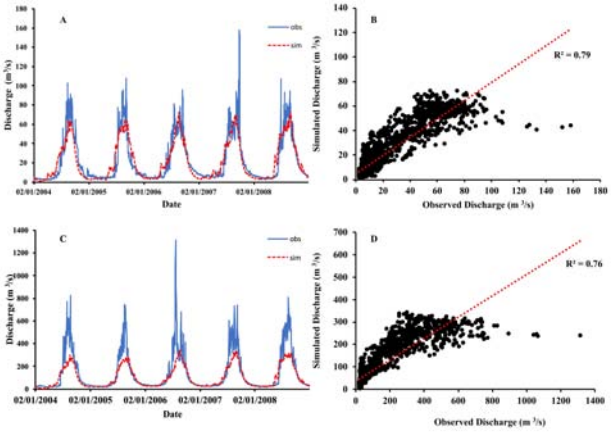

FIG. 3. Hydrograph of calibrated model with observed discharge (A) and Scatter plot (B) at Rasnalu, hydrograph of validated model (C) and Scatter plot (D) at Busti.

0.62, coefficient of determination (R^2) of the observed discharge and simulated discharge equal to 0.76 and simulated volume biases with observed discharge (Pbias) equal to 26%. The validation at Rasnalu station achieved model efficiency of NSE equals to 0.76, R^2 equals to 0.76 and Pbias equals to 4%. The model performance NSE and volume differences Pbias was better results in validated period than calibrated period but R^2 is similar between validated period and calibrated period. The hydrographs of calibrated and validated discharge at both stations underestimated the peak discharge during rainy months. This perhaps be due to the input data quality, model assumptions, local conditions, uncertain input data and insufficient data during extreme events (Tigabu et al., 2023). The calibrated and validated hydrograph with their respective scatter plots of Busti station are presented in Figure 2.

Similarly, SPHY model calibrated at Rasnalu station achieved model performance with NSE equals to 0.79, R^2 equals to 0.79 and Pbias equals to 4%. The validation at Busti station was performed with NSE equals to 0.61, R^2 equals to 0.76 and Pbias equals to 26%. The hydrograph of calibrated and validated discharge at both stations shows the underestimated discharge during rainy months. This might be due to the input data quality, model assumptions, and local conditions (Tigabu et al., 2023; Nguyen et al., 2022; Abbaspour et al., 2019). SPHY model shows better simulation to low flow than high flow. The model efficiency NSE, R^2 and Pbias were better simulated in calibrated period than validated period. The calibrated and validated hydrographs with their respective scatter plots of Rasnalu station are presented in Figure 3. SPHY model was better performed in the Rasnalu gauging station than in the Busti station.

SPHY model underestimated the peak discharge at Busti station. This discrepancy could potentially be attributed to both discharge stations' statistics falling within the 'fair' category based on DHM's assessment of discharge data, categorized as poor, fair, or good. Additionally, the meteorological stations observed in the Busti watershed may not be sufficiently representative of the entire watershed's actual conditions.Furthermore, in the Himalayas basin, the cascading type of hazard has recurrently manifested (Adhikari et al., 2023; Talchabhadel et al., 2023) due to extreme events leading to the obstruction of river network runoff. The parameters were calibrated and validated with values quantified in Table 2. The routing parameter recession coefficient (Kx) and groundwater parameters delta GW and alpha GW were more sensible parameters in the basin during calibration process.

3.2. Ungauged Simulation

The presence of discharge gauging stations is crucial for improving the calibration and validation of hydrological models for ungauged basins. Accurate calibration is difficult to achieve without these stations and because data records have gaps. Even in situations when calibration is not used, hydrological models discover their calibration efficacy within a range of conditions, both inside and outside of that range (Bergstrom, 2006). Here in this study, SPHY model parameters of calibration are independent within range at gauged stations (Table 2). The comparison of streamflow transposed at Benighat from two calibrated gauged stations Busti and Rasnalu showed the highly correlated streamflow records.

Figure 4 showed that daily streamflow generated at Benighat from Busti and Rasnalu SPHY models are closely aligned and perfectly matched. The scatter plot between flow simulation from Busti and Rasnalu highly correlated flow and coefficient of determination by 0.99.

Table 2. Calibrated parameters.

Descriptions	Calibrated Parameters	Busti	Rasnalu	Units
Routing	Recession Coefficient	0.94	0.96	
Ground water	deltaGW	180	180	
	alphaGW	0.01	0.01	
Glacier	GlacF	0.9	0.9	mm /°C/day
	DDFDG	2	2	mm /°C/day
	DDFG	4	4	mm /°C/day
Snow	SnowSC	0.5	0.5	mm /°C/day
	DDFS	5.5	5.5	mm /°C/day
	Tcrit	0	0	mm /°C/day
Soil	Root Layer	10	1600	mm/day
	Sub Layer	10	1600	mm/day
	Capillary Rise	1	2	mm/day

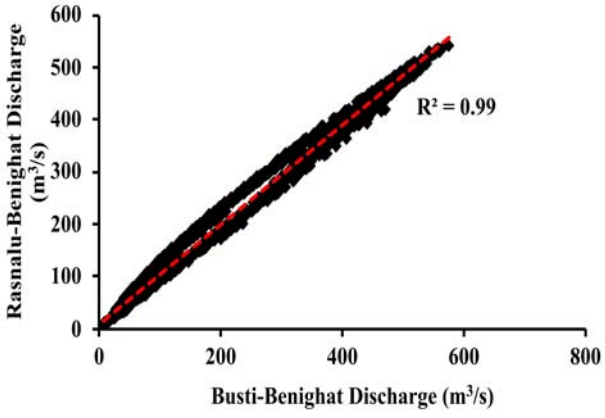

Fig. 4. Scatter diagram of transposed discharge from Busti station and Rasnalu station.

The daily average observed discharges of donor catchments at Busti and Rasnalu stations were 138.72 m^3/s and 21.88 m^3/s respectively. The daily average discharges at receiver Benighat basin transferred by SPHY models of Busti and Rasnalu are 164.35 m^3/s and 164.18 m^3/s respectively. The daily estimated discharges from 2004 to 2008 are plotted in Figure 5a. This figure showed that the daily flow transposed from two calibrated sites to an ungauged site perfectly matched. The flow pattern of the ungauged flow is completely aligned as aforementioned. The continuous daily flow simulation at the ungauged site is complicated due to erratic behavior of rainfall although distributed feature of model is a good approach for ungauged continuous data generation.

Figure 5b showed that the lowest flow was estimated in February and maximum discharge was simulated in August at Benighat for both transposed from both gauging stations. Table 3 showed that rising discharge in May and recession discharge in November transposed from both gauged stations at Benighat. Busti-Benighat transposed streamflow leads discharge in May to August and then Rasnalu-Benighat transposed streamflow data leads September to December. The detail of monthly flow transposed from Busti and Rasnalu gauge station with averaging value at Benighat is presented in Table 3. The observed annual average discharge at Busti station is 138.72 m^3/s and Rasnalu station is 21.88 m^3/s during simulation period. The annual average discharges at Benighat transferred from Busti and Rasnalu models are 163 m^3/s and 164 m^3/s respectively which are very similar shown in Figure 5c and Table 3. SPHY model has simulated a greater amount of discharge at Benighat than a summation of discharges at Busti and Rasnalu gauging stations, which seems logical because discharge downstream is always greater than upstream due to stream network system in large river basins. The streamflow data simulated by SPHY model at the ungauged site from calibrated gauged stations is almost similar in volume due to the spatially based distributed feature of models. The ungauged discharge comparison at Benighat transposed from two different upstream gauged stations shows almost similar discharge on a daily, monthly and annual basis. Model simulation and parameter calibration with gauged to ungauged same basin same input climatic datasets in SPHY model is a good approach for ungauged streamflow estimation. There are numerous methods for ungauged streamflow data generation among them fully distributed model is a very good alternative method for ungauged streamflow information as it requires large numbers of parameters (Patil and Stieglitz, 2014). The comparative discharge transposed from different calibrated stations is a better improvement technique using a fully distributed hydrological model for ungauged flow estimation. The water resource project developers will be beneficial from continuous ungauged streamflow records simulation techniques using this model.

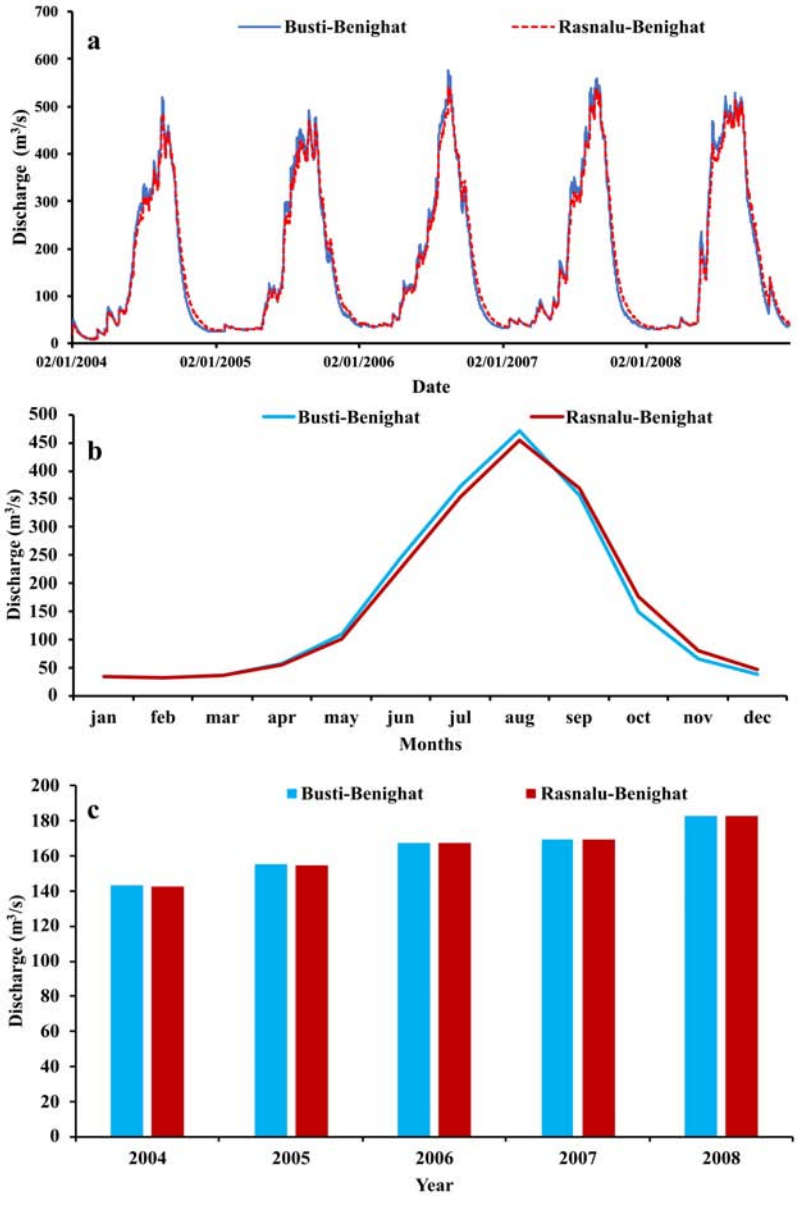

FIG. 5. Ungauged simulation at Benighat (A) Daily discharge, (B) Monthly discharge and (C) Scatter plot of Busti and Rasnalu transpose discharge at Benighat.

TABLE 3. Monthly and annual discharge (m^3/s) of Benighat transposed from Busti and Rasnalu.

Stations	Jan	Feb	Mar	Apr	May	Jun	Jul	Aug	Sep	Oct	Nov	Dec	Annual
Busti-Benighat	33	31	37	56	109	245	373	471	356	149	64	38	163
Rasnalu-Benighat	34	31	36	54	101	225	354	455	369	176	81	46	164
Average	34	31	36	55	105	235	363	463	363	162	72	42	163.5

4. Conclusion and Recommendation

Hydrological estimates at ungauged basins are an important task for the planning and design of water resources projects. SPHY model has simulated the highly matched and correlated discharge at ungauged sites transferred from two different gauging stations. The model performance at

Rasnalu station is better than at Busti station. The ungauged discharges of daily, monthly and annual are estimated from upstream gauged stations to downstream ungauged locations. The low flows are better matched than the high flows in the prediction of stream flows. However hydrological models are independently streamflow simulated. In the upstream catchment of Busti gauge station, spatial and temporal coverage of climatological station data are limited, which cover 71% of the total basin area. Discharge gauging stations and observations are limited at transboundary Himalayan river basins, mainly in least developing countries like Nepal due to difficulties in continuous monitoring, maintenance and high cost. However, the lacking of proper data upstream of Busti gauging station reveals that further studies in ungauged basins may enhance hydrological simulation capability using satellite data.

This study claims that the SPHY model is appropriate for mountain catchments in Nepal. Hence it is recommended for further use in other mountain basins having the presence of snow and glaciers. Similarly, the model should be applied in small basins of hills and plains to verify the results and its applicability.

Funding. The first author is supported by University Grant Commission, Nepal (UGC award no: PhD-076/77 S&T -15) PhD Fellowship.

Acknowledgments. We thank the Department of Hydrology and Meteorology (DHM), Nepal for providing available data.

References

Abbaspour, K., S. A. Vaghefi, H. Yang, and R. Srinivasan, 2019. Global soil, landuse, evapotranspiration, historical and future weather databases for swat applications. *Scientific data*, 6 (1), 263.

Adhikari, T. R., B. Baniya, Q. Tang, R. Talchabhadel, M. R. Gouli, B. R. Budhathoki, and R. P. Awasthi, 2023. Evaluation of post extreme floods in high mountain region: A case study of the melamchi flood 2021 at the koshi river basin in nepal. *Natural Hazards Research*.

Bergstrom, S., 2006. Experience from applications of the hbv hydrological model from the perspective of prediction in ungauged basins. *IAHS publication*, 307, 97.

Clark, G. E., K.-H. Ahn, and R. N. Palmer, 2017. Assessing a regression-based regionalization approach to ungauged sites with various hydrologic models in a forested catchment in the northeastern united states. *Journal of Hydrologic Engineering*, 22 (12), 05017 027.

Consortium, 2017. A dataset of global glacier outlines: Version 6.0. *Global Land Ice Measurements from Space: Boulder, CO, USA*.

DHM, 2004. Hydrological estimation in nepal. *His Majesty's Government of Nepal, Department of Hydrology and Meteorology, Kathmandu, Nepal*.

Karki, R., R. Talchabhadel, J. Aalto, and S. K. Baidya, 2016. New climatic classification of nepal. *Theoretical and applied climatology*, 125 (3-4), 799–808.

Khadka, D., M. S. Babel, S. Shrestha, and N. K. Tripathi, 2014. Climate change impact on glacier and snow melt and runoff in tamakoshi basin in the hindu kush himalayan (hkh) region. *Journal of Hydrology*, 511, 49–60.

Kim, U., and J. J. Kaluarachchi, 2008. Application of parameter estimation and regionalization methodologies to ungauged basins of the upper blue nile river basin, ethiopia. *Journal of Hydrology*, 362 (1-2), 39–56.

Li, Q., Y. Peng, G. Wang, H. Wang, B. Xue, and X. Hu, 2019. A combined method for estimating continuous runoff by parameter transfer and drainage area ratio method in ungauged catchments. *Water*, 11 (5), 1104.

Nash, J. E., and J. V. Sutcliffe, 1970. River flow forecasting through conceptual models part i—a discussion of principles. *Journal of hydrology*, 10 (3), 282–290.

Nguyen, T. V., J. Dietrich, T. D. Dang, D. A. Tran, B. Van Doan, F. J. Sarrazin, K. Abbaspour, and R. Srinivasan, 2022. An interactive graphical interface tool for parameter calibration, sensitivity analysis, uncertainty analysis, and visualization for the soil and water assessment tool. *Environmental Modelling & Software*, 156, 105 497.

Panthi, J., and Coauthors, 2021. Hydrologic regionalization under data scarcity: Implications for streamflow prediction. *Journal of Hydrologic Engineering*, 26 (9), 05021 022.

Patil, S., and M. Stieglitz, 2014. Modelling daily streamflow at ungauged catchments: what information is necessary? *Hydrological Processes*, 28 (3), 1159–1169.

Razavi, T., and P. Coulibaly, 2016. Improving streamflow estimation in ungauged basins using a multi-modelling approach. *Hydrological Sciences Journal*, 61 (15), 2668–2679.

Talchabhadel, R., S. Maskey, M. R. Gouli, K. Dahal, A. Thapa, S. Sharma, A. M. Dixit, and S. Kumar, 2023. Multimodal multiscale characterization of cascading hazard on mountain terrain. *Geomatics, Natural Hazards and Risk*, 14 (1), 2162 443.

Terink, W., W. Immerzeel, A. Lutz, P. Droogers, S. Khanal, S. Nepal, and A. Shrestha, 2017. Hydrological and climate change assessment for hydropower development in the tamakoshi river basin. *Nepal, Wageningen, the Netherlands*.

Terink, W., A. F. Lutz, G. W. H. Simons, W. W. Immerzeel, and P. Droogers, 2015. Sphy v2. 0: Spatial processes in hydrology. *Geoscientific Model Development*, 8 (7), 2009–2034.

Tigabu, T. B., P. D. Wagner, B. Narasimhan, and N. Fohrer, 2023. Pitfalls in hydrologic model calibration in a data scarce environment with a strong seasonality: experience from the adyar catchment, india. *Environmental Earth Sciences*, 82 (15), 367.

Van Liew, M. W., and A. R. Mittelstet, 2018. Comparison of three regionalization techniques for predicting streamflow in ungaged watersheds in nebraska, usa using swat model.

Waseem, M., M. Ajmal, and T.-W. Kim, 2015. Ensemble hydrological prediction of streamflow percentile at ungauged basins in pakistan. *Journal of Hydrology*, 525, 130–137.

WECS/DHM, 1990. Methodologies for estimating hydrologic characteristics of ungauged locations in nepal, his majesty's government of nepal. *Ministry of Water Resources, Water and Energy Commission Secretariat and Department of Hydrology and Meteorology, Kathmandu*.

WMO, 2008. Guide to hydrological practices. *World Meteorological Organization*.